Prediction of Oxygen Uptake and its Dynamics by Wearable Sensors During Activities of Daily Living

by

Thomas Beltrame

A thesis

presented to the University of Waterloo

in fulfillment of the

thesis requirement for the degree of

Doctor of Philosophy

in

Kinesiology

Waterloo, Ontario, Canada 2016

Author's Declaration

This thesis consists of material all of which I authored or co-authored: see Statement of Contributions included in the thesis. This is a true copy of the thesis, including any required final revisions, as accepted by my examiners.

I understand that my thesis may be made electronically available to the public.

Statement of Contributions

The author contributions for each Chapter are described above.

Chapter 1 and 8: Thomas Beltrame wrote the initial draft of the Chapter; Thomas Beltrame and Richard L. Hughson drafted Chapter; Thomas Beltrame and Richard L. Hughson edited and revised Chapter; Thomas Beltrame and Richard L. Hughson approved final version of Chapter.

Chapter 2: Thomas Beltrame and Richard L. Hughson conception and design of research; Thomas Beltrame and Richard L. Hughson performed experiments; Thomas Beltrame and Richard L. Hughson analyzed data; Thomas Beltrame and Richard L. Hughson interpreted results of experiments; Thomas Beltrame and Richard L. Hughson prepared figures; Thomas Beltrame wrote the initial draft of the Chapter; Thomas Beltrame and Richard L. Hughson drafted Chapter; Thomas Beltrame and Richard L. Hughson edited and revised Chapter; Thomas Beltrame and Richard L. Hughson approved final version of Chapter.

Chapter 3: Thomas Beltrame and Richard L. Hughson conception and design of research; Thomas Beltrame and Richard L. Hughson performed experiments; Thomas Beltrame and Richard L. Hughson analyzed data; Thomas Beltrame and Richard L. Hughson interpreted results of experiments; Thomas Beltrame and Richard L. Hughson prepared figures; Thomas Beltrame wrote the initial draft of the Chapter; Thomas Beltrame and Richard L. Hughson drafted Chapter; Thomas Beltrame and Richard L. Hughson edited and revised Chapter; Thomas Beltrame and Richard L. Hughson approved final version of Chapter.

Chapter 4: Thomas Beltrame, Robert Amelard, Rodrigo Villar, Javad M. Shafiee, Alexander Wong, and Richard L. Hughson conception and design of research; Thomas Beltrame, Rodrigo Villar, and Richard L. Hughson performed experiments; Thomas Beltrame, Robert Amelard, Rodrigo Villar, Javad M. Shafiee, Alexander Wong, and Richard L. Hughson analyzed data; Thomas Beltrame, Robert Amelard, Rodrigo Villar, Javad M. Shafiee, Alexander Wong, and

Richard L. Hughson interpreted results of experiments; Thomas Beltrame, Robert Amelard, Rodrigo Villar, and Richard L. Hughson prepared figures; Thomas Beltrame wrote the initial draft of the Chapter; Thomas Beltrame, Robert Amelard, Rodrigo Villar, Javad M. Shafiee, Alexander Wong, and Richard L. Hughson drafted Chapter; Thomas Beltrame, Robert Amelard, Rodrigo Villar, Javad M. Shafiee, Alexander Wong, and Richard L. Hughson edited and revised Chapter; Thomas Beltrame, Robert Amelard, Rodrigo Villar, Javad M. Shafiee, Alexander Wong, and Richard L. Hughson approved final version of Chapter.

Chapter 5: Thomas Beltrame and Richard L. Hughson conception and design of research; Thomas Beltrame and Richard L. Hughson performed experiments; Thomas Beltrame and Richard L. Hughson analyzed data; Thomas Beltrame and Richard L. Hughson interpreted results of experiments; Thomas Beltrame and Richard L. Hughson prepared figures; Thomas Beltrame wrote the initial draft of the Chapter; Thomas Beltrame and Richard L. Hughson drafted Chapter; Thomas Beltrame and Richard L. Hughson edited and revised Chapter; Thomas Beltrame and Richard L. Hughson approved final version of Chapter.

Chapter 6: Thomas Beltrame, Robert Amelard, Alexander Wong, and Richard L. Hughson conception and design of research; Thomas Beltrame and Richard L. Hughson performed experiments; Thomas Beltrame, Robert Amelard, Alexander Wong, and Richard L. Hughson analyzed data; Thomas Beltrame, Robert Amelard, Alexander Wong, and Richard L. Hughson interpreted results of experiments; Thomas Beltrame, Robert Amelard and Richard L. Hughson prepared figures; Thomas Beltrame wrote the initial draft of the Chapter; Thomas Beltrame, Robert Amelard, Alexander Wong, and Richard L. Hughson drafted Chapter; Thomas Beltrame, Robert Amelard, Alexander Wong, and Richard L. Hughson edited and revised Chapter; Thomas Beltrame, Robert Amelard, Alexander Wong, and Richard L. Hughson approved final version of Chapter.

Chapter 7: Thomas Beltrame, Robert Amelard, Alexander Wong, and Richard L. Hughson conception and design of research; Thomas Beltrame and Richard L. Hughson performed experiments; Thomas Beltrame, Robert Amelard, Alexander Wong, and Richard L. Hughson analyzed data; Thomas Beltrame, Robert Amelard, Alexander Wong, and Richard L. Hughson interpreted results of experiments; Thomas Beltrame, Robert Amelard and Richard L. Hughson prepared figures; Thomas Beltrame wrote the initial draft of the Chapter; Thomas Beltrame, Robert Amelard, Alexander Wong, and Richard L. Hughson drafted Chapter; Thomas Beltrame, Robert Amelard, Alexander Wong, and Richard L. Hughson edited and revised Chapter; Thomas Beltrame, Robert Amelard, Alexander Wong, and Richard L. Hughson approved final version of Chapter.

Abstract

The evaluation of the aerobic response to a new energetic demand provides valuable information regarding the functional capabilities of the aerobic system. Abnormal, or impaired aerobic responses may occur before the clinical detection of degenerative disease states, demonstrating a need for the development of tools for the continuous assessment of aerobic system dynamics in real-life scenarios. Current wearable technologies are commonly used to quantify physical activity levels; however, the big data streamed from these devices offer the unique possibility to predict the oxygen uptake ($\dot{V}O_2$) dynamics during unsupervised activities of daily living (ADL) when calorimetry techniques are not accessible. The evaluation of $\dot{V}O_2$ dynamics has been associated with physical fitness and might provide insight into changes in health status. The main objective of this thesis was to predict and evaluate the temporal dynamics of the aerobic response during realistic activities. To accomplish this, a series of seven studies that began with observations of $\dot{V}O_2$ dynamics under standard laboratory conditions, progressed to specified patterns of over-ground walking, and concluded with unsupervised ADL facilitated the development of novel techniques for aerobic system analysis during walking and ADL based on wearable sensors. The variables derived from the wearable sensors were used to create a $\dot{V}O_2$ predictor based on different machine learning approaches. Predicted $\dot{V}O_2$was individually validated by Bland-Altman plot and Pearson's linear correlation coefficient (r). The $\dot{V}O_2$ dynamic analysis included Fourier transformations, exponential data modeling, and a novel approach derived from the mean normalized gain amplitude (MNG in %). This new indicator of $\dot{V}O_2$ dynamics correlated strongly with the standard method obtained, in the same subjects, from a step change in work rate on the cycle ergometer, and with the classical indicator of fitness, maximal $\dot{V}O_2$. The results showed the strong ability of the proposed algorithms to predict $\dot{V}O_2$ during ADL based on wearable sensors

allowing for not only overall assessment of metabolic rate but also for successful prediction of $\dot{V}O_2$ dynamics. Thus, the proposed $\dot{V}O_2$ predictor in conjunction with MNG can be used to investigate aerobic fitness during ADL with direct applicability for the general population. This new technology provides a significant advance in ambulatory and continuous assessment of aerobic fitness with potential for future applications such as the early detection of deterioration in physical health.

Acknowledgments

I would like to thank the people who have dedicated their time to the completion of this work. Mainly, the participants that kindly volunteered to be monitored during their daily routine and during the laboratory tests.

To my advisor and mentor, Dr. Richard Hughson, who always supported my ideas and provided everything that was needed for my evolution as student, researcher and science enthusiastic. It will be my honor to carry with me his teaching on different aspects of our field. Also, for his patience and understanding with me. Thanks for all opportunities, Rich!

To my committee, Russ Tupling, Alex Wong, Bill McIlroy, Thomas J. Barstow and Jennifer Boger. The support and advice offered throughout this work was essential. It was enjoyable to learn from cellular control to machine learning and how to connect both thorough wearable sensors.

To my lovely wife, Juliana, that always supported me with her love and understanding. At her side, my life gains more meaning. To my quasi-daughter, Belinha, for reminding me that life is sometimes very simple.

To my family, Nano, Mariana, Yvonne, Jan, Bruno, Daiane e Enrico(ão). You were always there for me and I cannot wait to see everybody together again at the beach. Mom and dad, I hope to spend more time with you and thank you for supporting my decision to travel to Canada for my PhD.

To my former advisor, Dr. Aparecida Maria Catai for the valuable advices and opportunities throughout my academic career. Thank you so much Catai!

To my friends Cleyton, Lucas, Carolina and Ico for all the good times in Waterloo. To my great friends from my hometown, Bruninho, Ney and Elton. To my BJJ friends, Doc, Connor, Wes, Tony, Tom, Brad, Tico, Mahir, Mo and Cam. To my UW co-workers and friends, Travis, Chris, Kathryn, Robert, Rodrigo, Jon, Dan, Keyma, Danielle, Jing, Dianne, Jason, Katelyn, Andrew, Erik, Rose, Paola, Cristina and Frenk.

In memory of my grandmother Ignes Loli Beltrame, my grandfather Hendrikus Jacobus Wilhelmus Schreurs and my great friend Ralpho Wolpereis.

Table of Contents

List of Figures

List of Tables

List of Equations

List of Abbreviations

a	Amplitude (exponential)
a_0	Baseline amplitude
a_1	Cardio-dynamic amplitude
a_2	Fundamental phase amplitude
ACC	Accelerometer
ACC_{HIP}	Hip acceleration
ADL	Activities of daily living
ACSM	American College of Sports Medicine
Amp	Amplitude (FFT)
$\widehat{Amp}$	Normalized amplitude
ANN	Artificial neural network
ANOVA	Analysis of variance
ATP	Adenosine triphosphate
ATT	Adipose tissue thickness
$a-vO_2diff$	Arteriovenous O_2 difference
BF	Breathing frequency
CAD	Walking cadence
$\dot{C}apBF$	Capillary blood flow
CI_{95}	95% confidence interval
DC_{offset}	Average response
DFT	Discrete Fourier Transformation
ECG	Electrocardiogram
EE	Energy expenditure
FFT	Fast Fourier transformation
f_1	Fundamental frequency
RMR	Resting metabolic rate
SE	Absolute standard error
$sm\dot{V}O_2$	Simulated muscle oxygen uptake
TD	Time delay
tHb	Total hemoglobin
τ_{on}	On-transient time constant
$Tree_T$	Regression trees
τ_s	Time constant of simulated data
TSI	Tissue saturation index
τ	Time constant
τ_2	Fundamental phase time constant
$\%SE$	Relative standard error
$gAmp$	System gain
GET	Gas exchange threshold
h	Harmonic
H_{acc}	Hip acceleration
HHb	Deoxy-hemo/myoglobin
HR	Heart rate
ML	Machine learning
MNG	Mean normalized gain
$METS$	Metabolic equivalents
$MLPR_{ANN}$	Multi-layer perceptron regressor
MRT	Mean response time
$m\dot{V}O_2$	Muscle oxygen uptake
n	Sample size or number
NIRS	Near infrared spectroscopy
O_2	Oxygen
O_2Hb	Oxy-hemo/myoglobin
p	Statistical significance level
PA	Physical activity
PCr	phosphocreatine
PRBS	Pseudorandom binary sequence
PRTS	Pseudorandom ternary sequence
$p\dot{V}O_2$	Pulmonary oxygen uptake
$\dot{Q}$	Cardiac output
r	Pearson coefficient
r^2	Coefficient of determination
$uADL$	Unsupervised activities of daily living
$\dot{V}CO_2$	Carbon dioxide output
$\dot{V}E$	Ventilation minute
$\dot{V}O_2$	Oxygen uptake
$\widehat{\dot{V}O_2}$	Predicted oxygen uptake
$\dot{V}O_{2-peak}$	Oxygen uptake peak
$\dot{W}$	Work rate
wl	Window length
Σ	Module addition feedback
μM	Micromole
λ	Wavelength

Chapter 1: General Introductions

It is estimated that by the year 2020, 73% of all deaths will be related to chronic, non-communicable, degenerative diseases (Guilbert, 2003). Many of these diseases are commonly associated with a low physical activity (PA) profile related to modern lifestyle. A correlation between physical fitness and mortality has been reported (Sui et al., 2007) and a recent study has shown that lower PA levels may result in a mortality risk two times higher than elevated body mass index alone (Ekelund et al., 2015). Furthermore, many risk factors for non-communicable diseases are largely preventable and modifiable, which attracts great public health interest. Factors such as elevated cholesterol levels, high blood pressure, and excessive body mass, all linked to low PA levels (Kim & Jung, 2014; Mora, Lee, Buring, & Ridker, 2006), have been associated with 80% of heart disease and 40% of all cancer cases (Guilbert, 2003). Hence, efforts to optimize PA level assessment and engagement are relevant for improving health-related clinical outcomes (A. E. Bauman, 2004; Sui et al., 2007). However, methods of acquiring the correct measurement of PA level and physical fitness during a realistic scenario remain a challenge (Sallis & Saelens, 2000) and, therefore, new technologies and data processing approaches are necessary.

1.1 Evaluation of Physical Activity

Daily PA levels can be objectively estimated by calculating body energy expenditure (EE) that is proportional to the total body heat generated for a given energetic demand. Additionally, the total amount of heat generated is proportional to oxygen uptake ($\dot{V}O_2$) by the active muscle. Based on the association between $\dot{V}O_2$ and EE, steady state pulmonary $\dot{V}O_2$ ($p\dot{V}O_2$) measurements represent an indirect calorimetry method for the assessment of EE. However, activities of daily

living (ADL) are generally not steady state in nature increasing the complexity of daily PA assessment.

During work rate ($\dot{W}$) transitions, there is a momentary uncoupling between the delayed $p\dot{V}O_2$ response and the energy demand (Selinger & Donelan, 2014). However, it is during PA transitions that the physiological systems demonstrate their integrity for the interactions with the environment (i.e., period of higher homeostatic perturbation) which ultimately influence the individual's tolerance to ADL. It was previously reported that the $p\dot{V}O_2$ data analysis during PA transitions can provide valuable information about aerobic system power (Chilibeck, Paterson, Petrella, & Cunningham, 1995; Hagberg, Hickson, Ehsani, & Holloszy, 1980; Hughson, 2009; Powers, Dodd, & Beadle, 1985). Therefore, attempts to predict $p\dot{V}O_2$ during PA transitions may have more clinical relevance beyond EE estimation.

Methods that individually characterize the energetic demand for a given PA pattern may offer an effective and objective way to measure PA levels during ADL. However, the complexity of the energy requirements during ADL presents additional challenge. The lack of PA evaluation during transitions exclude the possibility to predict $p\dot{V}O_2$ within realistic ADL scenarios. It is common to have PA short enough to be entirely composed by $p\dot{V}O_2$ transitions, which complicates PA predictions by algorithms calibrated to steady state responses. In general, traditional predictive algorithms generated for EE estimation are not applicable for $p\dot{V}O_2$ estimation during high frequency changes in stimulus as expected during ADL (Orendurff, Schoen, Bernatz, Segal, & Klute, 2008). Therefore, new algorithms are required to accurately predict $p\dot{V}O_2$ during the high frequency transitions commonly experienced in ADL.

1.2 Oxygen uptake During Transition

At the beginning of an activity, there is a step increase in the energetic demand needed for the working skeletal muscle tissue (Barstow, Buchthal, Zanconato, & Cooper, 1994). However, during this transition, the aerobic supply of energy is delayed requiring the input of other energy systems to meet the demand (Figure 1). Interestingly, the velocity of the aerobic system adaptation during transitions seems to have clinical relevance.

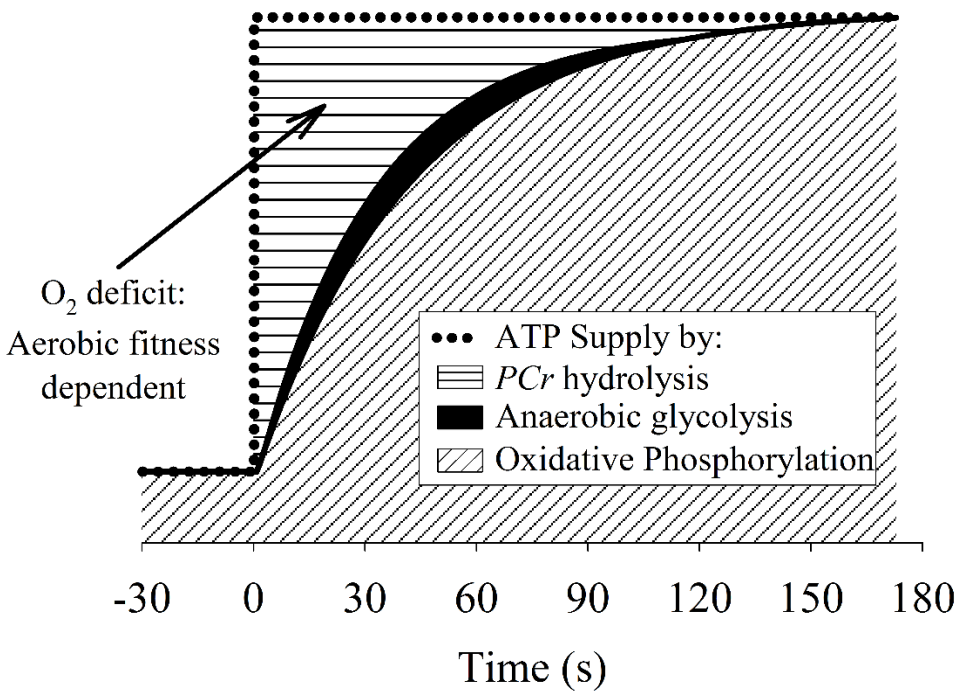

Figure 1.Energy supply systems
Illustration modified from Hughson *et. al*. (Hughson, Tschakovsky, & Houston, 2001). Interaction of the energetic supply systems during exercise transition. The adenosine triphosphate (ATP) required from new energetic demand is supplied by three major integrated systems: phosphocreatine (PCr), anaerobic glycolysis and oxidative phosphorylation. Initially, the PCr system supplies the most ATP demand, but this system becomes less prominent as the oxidative phosphorylation (and consequently the pulmonary oxygen consumption) increases following an exponential pattern. Between these two systems, the anaerobic glycolysis contribution depends on the O_2 provision-utilization balance.

Although $p\dot{V}O_2$ is the resultant of the O_2 exchange from the entire body during sustained dynamic exercise, $p\dot{V}O_2$ is mainly maintained by muscle aerobic metabolism (Barstow, Lamarra, & Whipp, 1990). Therefore, the majority of delayed $p\dot{V}O_2$ response to an increased energy demand seems to originate from the muscular $\dot{V}O_2$ ($m\dot{V}O_2$) that also increases following an exponential-like function (Grassi et al., 1996; Hughson et al., 1996). The gas exchanges occurring at muscle site must be somehow connected with the lungs, where the atmospheric gas exchanges occur. Since these two compartments, lung and peripheral tissue, are coupled by the cardiovascular system, the $m\dot{V}O_2$ behaviour is reflected at the pulmonary site ($p\dot{V}O_2$) after a given transit time (Casaburi, Weissman, Huntsman, Whipp, & Wasserman, 1979; Grassi et al., 1996). Therefore, distortions that might occur in the cardiovascular system will influence the degree of similarities between $p\dot{V}O_2$ and $m\dot{V}O_2$ dynamics (Hoffmann, Drescher, Benson, Rossiter, & Essfeld, 2013).

During exercise transition, the moment when the $p\dot{V}O_2$ seems to reflect $m\dot{V}O_2$ time course (Grassi et al., 1996) is known as the fundamental phase. However, during the first 15-20 seconds of dynamic exercise, the $p\dot{V}O_2$ presents a faster component as a consequence of an abrupt elevation of pulmonary blood flow (Whipp & Ward, 1982). Such initial excess of pulmonary circulation is caused mainly by the muscle pump at the onset of exercise which increases venous return (Tschakovsky, Saunders, Webb, & O'donnell, 2006) and consequently the cardiac output ($\dot{Q}$) (Yoshida, Yamamoto, & Udo, 1993). Since blood flow at the alveolar capillaries is elevated, more blood with low O_2 content reaches the lungs causing a higher atmospheric O_2 extraction. This phenomenon results in higher $p\dot{V}O_2$ and is referred to as the cardio-dynamic phase (Barstow et al., 1990; Whipp, Ward, Lamarra, Davis, & Wasserman, 1982).

The $p\dot{V}O_2$ is a product of systemic O_2 delivery estimated by $\dot{Q}$ and total O_2 extraction estimated by total arteriovenous O_2 difference ($a - vO_2diff$). This principle was originally

described by Adolf Eugen Fick (1870) as a method for $\dot{Q}$ estimation and it is still widely used for a variety of physiological discussions regarding $p\dot{V}O_2$ dynamics (Jones & Poole, 2005). Not just the steady state $p\dot{V}O_2$, but the $p\dot{V}O_2$ dynamics during transitions are also governed by the Fick principle (Hughson, 2009). During transitions, if the systemic oxygen delivery ($\dot{Q}$) is slower, the $a-vO_2diff$ will be proportionally faster. This behaviour is evident during exercise performed by patients with impaired O_2 delivery (Chiappa et al., 2008). On the other hand, an optimized systemic O_2 delivery (i.e., faster $\dot{Q}$) should cause slower $a-vO_2diff$ dynamics during transitions.

With an increase in exercise intensity, the new energy demand disturbs the cellular homeostasis promoting an elevation in metabolic rate by the activation of ATP_{ase} enzymes whose catalytic function increases the concentration of intracellular ADP and P_i. These products are the main mitochondrial ATP turnover rate regulators (Tschakovsky & Hughson, 1999). The O_2 molecule is coupled with this process since it acts as the final electron acceptor on the electron transport chain in the mitochondrial matrix. Therefore, changes in the intracellular O_2 pressure will, by definition, alter the metabolic pathway chain (Tschakovsky & Hughson, 1999). However, ongoing research describes possible explanations regarding the origin for the $p\dot{V}O_2$ rate-limiting factor(s) (Brittain, Rossiter, Kowalchuk, & Whipp, 2001; Hughson, 2009; Hughson & Morrissey, 1983; Murias, Spencer, & Paterson, 2014; Robergs, 2014). The discussion surrounding this topic often involves the Fick principle, and it is still unclear if delayed $p\dot{V}O_2$ response is caused by limitations on O_2 delivery and/or on O_2 utilization (Murias et al., 2014; Tschakovsky, 2014).

The delay in the aerobic ATP supply system is particularly important during ADL where there is great variability in the duration of each ADL. For a given $p\dot{V}O_2$ dynamic response and activity O_2 cost (i.e., energetic demand), the ADL duration will determine the $p\dot{V}O_2$ value. As

depicted in Figure 2, $p\dot{V}O_2$ during ADL is related to the duration of ADL, O_2 demand, and aerobic fitness of the individual. As an example, for a short ADL with a high O_2 demand an aerobically fit individual may rapidly increase $p\dot{V}O_2$ to meet the O_2 demand within the course of the ADL whereas an individual with poor aerobic fitness may not meet the O_2 demand during the ADL time frame. Also of note, short ADL with low O_2 cost may not increase the $p\dot{V}O_2$ enough to be differentiated from resting $p\dot{V}O_2$ oscillation (even for a fast $p\dot{V}O_2$ dynamic).

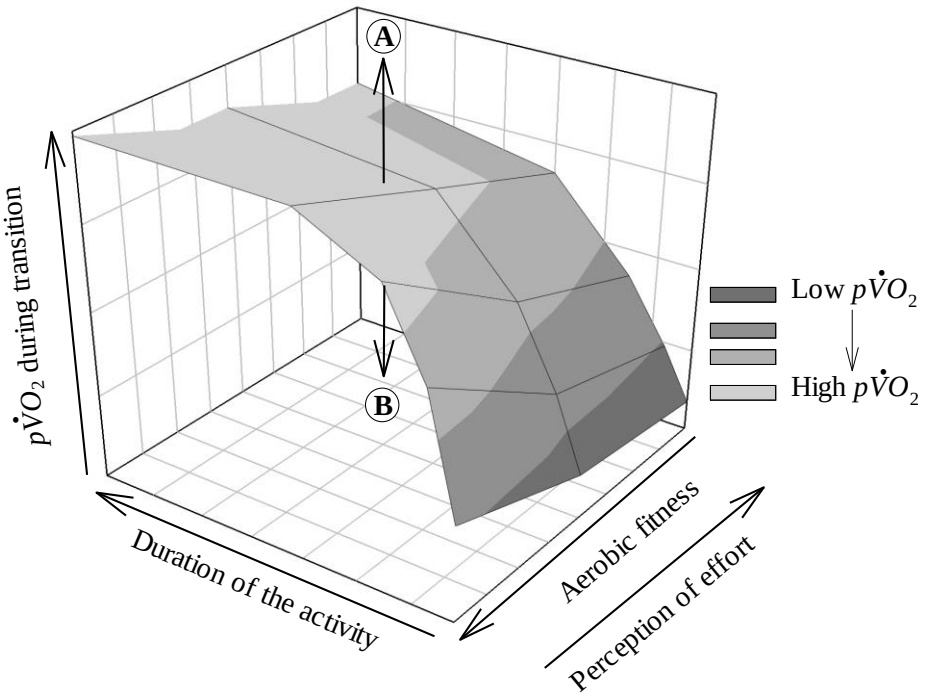

Figure 2. Pulmonary oxygen uptake as a function of aerobic fitness
Projection of the pulmonary oxygen uptake ($p\dot{V}O_2$) during exercise transition as a function of changes in aerobic fitness (or the perception of effort) and the physical activity duration. At a given physical activity duration, a faster $p\dot{V}O_2$ dynamic (well-fit person, for example) will present a higher $p\dot{V}O_2$ value in comparison with an impaired aerobic fitness person. Individuals with lower aerobic fitness will take more time to achieve the same $p\dot{V}O_2$ of a highly fit individual. After the transition phase, the $p\dot{V}O_2$ steady state may be similar between individuals with different aerobic fitness if the O_2 cost is equal. The activity type could shift this plane up (A) or down (B) according to a higher or a lower O_2 cost, respectively.

The differences in $p\dot{V}O_2$ dynamics between subjects during ADL depend on the interaction between the cardiovascular and muscular systems to supply and utilize O_2, respectively (Hughson, 2009). This interaction modulates how fast (i.e., the temporal dynamics) the $p\dot{V}O_2$ increases after the beginning of ADL which suggests association with aerobic fitness (Norris & Petersen, 1998; Powers et al., 1985), severity of some diseases (Borghi-Silva et al., 2012; Pessoa et al., 2013; Regensteiner et al., 1998) and functional mobility (Alexander, Dengel, Olson, & Krajewski, 2003). In order to characterize the aerobic system dynamics between different conditions or populations, mathematical methods were developed to extract information regarding the aerobic system dynamics based on $p\dot{V}O_2$ data (Hughson, Winter, Patla, Swanson, & Cuervo, 1990; Whipp et al., 1982).

1.2.1 Oxygen Uptake Kinetics Analysis

The assessment of aerobic system temporal dynamics during laboratory-based exercise protocols is commonly performed based on time domain $p\dot{V}O_2$ data analysis (Whipp et al., 1982). Initially, when the exponential nature of $p\dot{V}O_2$ response was just a speculation (Hill & Long, 1925), several authors (Henry, 1951; Margaria, Manglli, Cuttica, & Cerretelli, 1965) investigated many different equations to describe, in physiological terms, the $p\dot{V}O_2$ response during exercise transitions. Currently, there is a consensus on the exponential nature of the $p\dot{V}O_2$ response to changes in exercise intensity (Hughson, 2009) and the fundamental fitting equation for moderate exercise has been established as:

Equation 1 $$p\dot{V}O_2(t) = a_0 + a_1\left(1 - e^{-\left(t-TD_1/\tau_1\right)}\right) + a_2\left(1 - e^{-\left(t-TD_2/\tau_2\right)}\right);$$

where "t" is time, "a_0" is the baseline during resting, "a_1" and "a_2" are the steady state amplitudes for each phase (cardio-dynamic and fundamental, respectively), "τ_1" and "τ_2" are time constants (related to system temporal dynamics) for each phase, and "TD_1" and "TD_2" are time delays for each phase. To illustrate the $p\dot{V}O_2$ dynamic and the time-domain data modeling parameters during moderate exercise transition, a computer simulation was performed with results depicted in Figure 3. This response was generated with a random noise of 3% and fitted by the same equation 1. The physiological meaning and how these parameters can be influenced are described in Table 1.

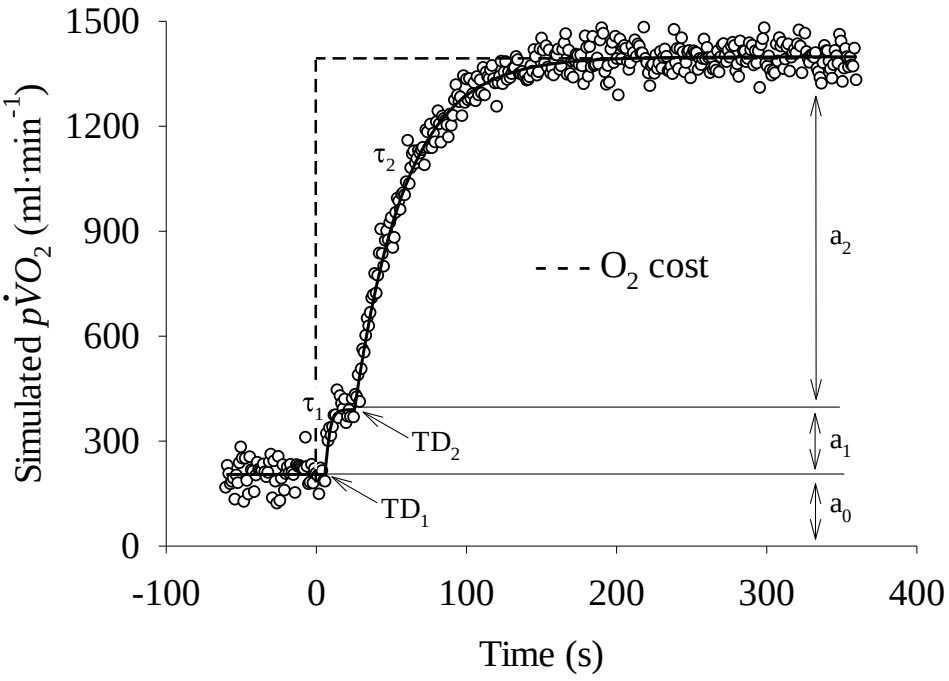

Figure 3. Simulated pulmonary oxygen uptake
Simulation of pulmonary oxygen uptake ($p\dot{V}O_2$) dynamic during moderate exercise transition. The cardio-dynamic phase (first response component) is originated from the elevation of pulmonary blood flow due to muscle pump activation at the onset of exercise. After ~20 s, the $p\dot{V}O_2$ dynamic apparently reflects the muscle oxygen uptake. A bi-exponential model was used to simulate these data with 3% of random error. The same equation used to generate the data was used to fit the data (—). See text for further details about the equation and fitting parameters.

Table 1. Description of equation parameters used to fit the pulmonary oxygen uptake ($p\dot{V}O_2$) data in time domain during exercise transitions.

Parameter	Meaning	Origin	Physiological importance level	Could be changed by
$\boldsymbol{a_0}$	Baseline metabolic rate amplitude	Resting metabolic rate	Medium	Warm-up intensity and resting metabolic rate
$\boldsymbol{a_1}$	Cardio-dynamic phase steady state amplitude	Muscle pump	Medium	Muscle recruitment and warm-up
$\boldsymbol{a_2}$	Fundamental phase steady state amplitude	O_2 cost	High	Work rate intensity and muscle fiber types
$\boldsymbol{\tau_1}$	Temporal dynamics of cardio-dynamic phase adaptation	Muscle and cardiovascular	Low	N/A
$\boldsymbol{\tau_2}$	Temporal dynamics of fundamental phase adaptation related to muscle metabolism	Muscle and cardiovascular	High	Aerobic fitness or disease
$\boldsymbol{TD_1}$	Short delay of the cardio-dynamic phase onset due muscle pump	Muscle pump	Low	Distance between active muscle and lungs
$\boldsymbol{TD_2}$	Delay of the fundamental phase onset due to muscle-to-lungs low O_2 content time delay	Muscle and cardiovascular	Medium	Distance between active muscle and lungs

The utilization of multi-parameter equations for $p\dot{V}O_2$ time domain analysis can be used to characterize the aerobic system dynamics (Whipp & Ward, 1990). However, equations with too many parameters have issues related to high degrees of freedom and lack of physiological meanings (Table 1). The best data fitting approach is a combination of balanced fitting quality and

meaningful physiological model (Hughson, 2009; Hughson & Morrissey, 1983; Hughson, Sherrill, & Swanson, 1988; Swanson, 1990). Unfortunately, the usual duration of ADL is not sufficient to allow the aerobic system analysis by time domain modelling. Therefore, $p\dot{V}O_2$ analysis in the frequency domain seems to be more capable of assessing aerobic system dynamics with ADL.

Characterization of $p\dot{V}O_2$ dynamics in the frequency domain uses fast Fourier transformations (FFT) to convert the $p\dot{V}O_2$ time series response into frequency space. The FFT has a comprehensive applicability in a wide spectrum of study disciplines (Kerlin, 1974). In exercise physiology, FFT is commonly used to compute amplitudes of the exercise stimulus (input) along with the physiological responses (outputs) for a selected range of frequencies or harmonics (h) (Casaburi, Whipp, Wasserman, Beaver, & Koyal, 1977; Eßfeld, Hoffmann, & Stegemann, 1987; Hughson et al., 1990). To obtain the total amplitude (Amp) for each h, FFT estimates the sinusoidal function by calculating sine and cosine curves per the fundamental equation:

Equation 2 $$p\dot{V}O_2(t) = a_0 + 2 * \sum_{h=1}^{h}(A_h * cos(2\pi * h * f_1 * t) + B_h * sin(2\pi * h * f_1 * t));$$

where "a_0"is the $p\dot{V}O_2$ baseline value, "h" is the harmonic number, defined as the integer numbers that multiply "f_1", the fundamental frequency calculated as the inverse of the protocol length. As depicted in Figure 4, the f_1 can be defined as the lowest frequency evaluated and the subsequent frequencies were defined by the product between f_1 and the harmonics (h). Harmonics are integer numbers that define in how many complete sinusoidal cycles the time series signal was decomposed. The "A_h" and "B_h" are the cosine and sine amplitudes, respectively. From "A_h" and "B_h", Amp values can be obtained for each h by:

Equation 3 $$Amp_h = \sqrt{A_h^2 + B_h^2}.$$

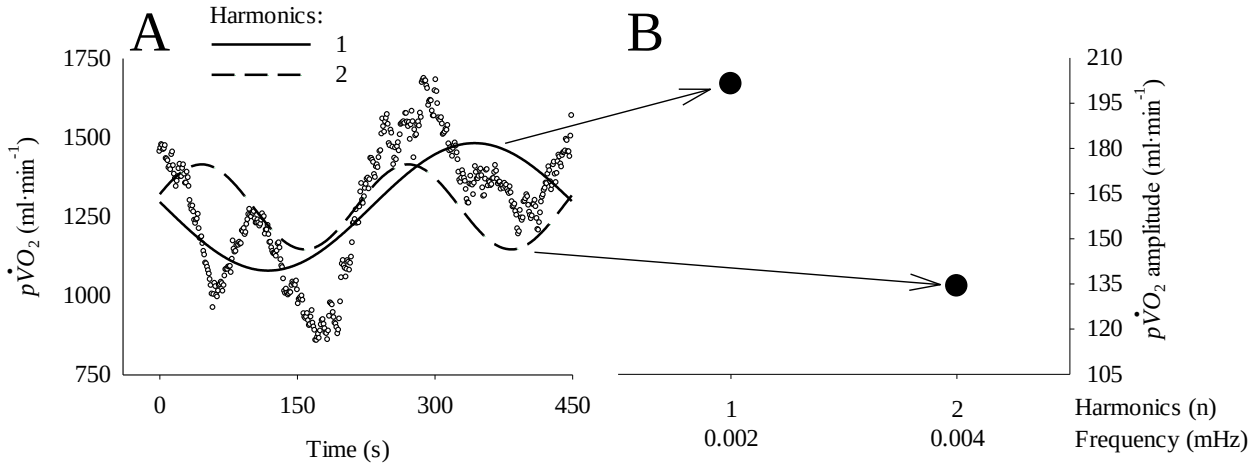

Figure 4. Fast Fourier transformation
A: Illustration of how pulmonary oxygen uptake ($p\dot{V}O_2$) response in time-domain (A) can be transformed into the frequency-domain (B) for an exercise protocol involving pseudorandom variations in work rate (see Figure 17 for pattern of work rate variation). Fourier transformations (please see text) decomposed the $p\dot{V}O_2$ time series response (A) into amplitudes of sinusoidal functions at specific frequencies. In this example, only the first two harmonics are shown for clarity in A; further analysis incorporated up to 4 harmonics to yield an amplitude spectrum as shown in Figure 17.

As opposed to constant workload protocols used for time domain analysis, the $p\dot{V}O_2$ dynamics characterized in frequency domain requires a more dynamic exercise protocol. Pseudorandom sequence protocols offer optimized stimulus to study the physiological responses in frequency domain for a wide frequency range simultaneously (Hoffmann, Eßfeld, Wunderlich, & Stegemann, 1992).

The aerobic system dynamics evaluated by the $p\dot{V}O_2$ responses in frequency-domain (amplitudes in Figure 4B) can be influenced by differences in the relationship between metabolic demand and $p\dot{V}O_2$ steady-state (investigated in time-domain by a in equation 1) or by variations in the speed of $p\dot{V}O_2$ adaptation during transition (investigated in time-domain by τ in equation 1). Since the speed of the $p\dot{V}O_2$ dynamics was previously associated with aerobic fitness (Powers

et al., 1985), further methods need to isolate the speed component of the $p\dot{V}O_2$ response in frequency domain from the inter-subjects' $p\dot{V}O_2$ steady-state variability. Chapter 2 describes the development of a novel method to extract the speed of the aerobic response based on frequency-domain responses as a new parameter designated mean normalized gain (MNG).

1.3 Pseudorandom Sequence Protocols

For a complete random protocol, the occurrence of low energy stimulus may increase extremely fast during higher frequencies; therefore, the observed $p\dot{V}O_2$ response cannot be differentiated from non-exercise related $p\dot{V}O_2$ oscillation caused mainly by interbreath noise (Lamarra, Whipp, Ward, & Wasserman, 1987). Therefore, the optimized protocols for frequency domain analysis are composed of pseudorandom sequence protocols that switch the exercise intensity between two levels, also known as pseudorandom binary sequence (PRBS), or between three levels, known as pseudorandom ternary sequence (PRTS).

The PRBS and PRTS protocols are generated by n-stage digital shift register as previously reported (Hughson et al., 1990; Peterka, 2002). The PRBS protocol will be further explained in Chapter 2, 3 and 5 and the PRTS protocol will be further described in Chapter 5. These protocols are composed by n units of different work rate levels, each of 30s of duration. For PRBS and PRTS, an extra sequence was added at the onset of the protocol as warm-up

Examples of a PRBS and PRTS are depicted in Figure 5 for both the time and frequency domain. In general, these protocols are useful for studying $p\dot{V}O_2$ dynamics at multiple frequencies of stimulus simultaneously (Hoffmann et al., 1992). In addition, these protocols also vary the stimulus applied to aerobic system stimulus following a pattern that might better reflect what

occurs during ADL. Figure 6 illustrates how the parameters of the equation 1 can hypothetically influence the $p\dot{V}O_2$ dynamics during the PRBS protocol.

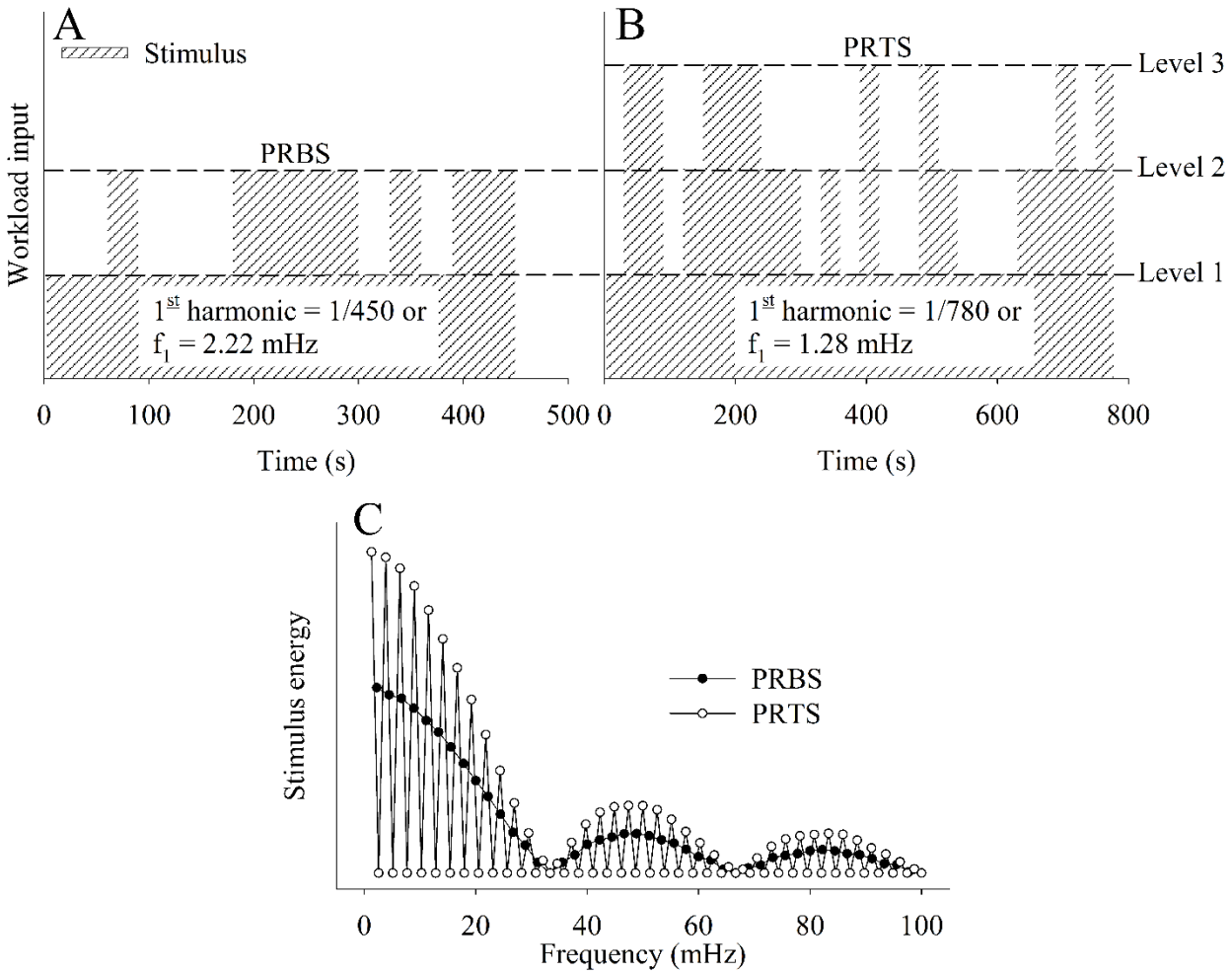

***Figure 5*. Pseudorandom binary and ternary sequence protocols**
Example of 30s unit pseudorandom binary sequence (PRBS, A) and pseudorandom ternary sequence (PRTS, B) protocols in time domain. Fourier transformations were used to compute the stimulus energy amplitudes (C) for these protocols for frequencies from 0 to 0.1 Hz. In frequency domain, both protocols present similar behaviour throughout the frequencies, however, the PRTS decreases the energy close to zero during even harmonics (Kerlin, 1974). The frequency correspondent to the first harmonic (fundamental frequency or f_1) is calculated from dividing 1 by the protocol duration.

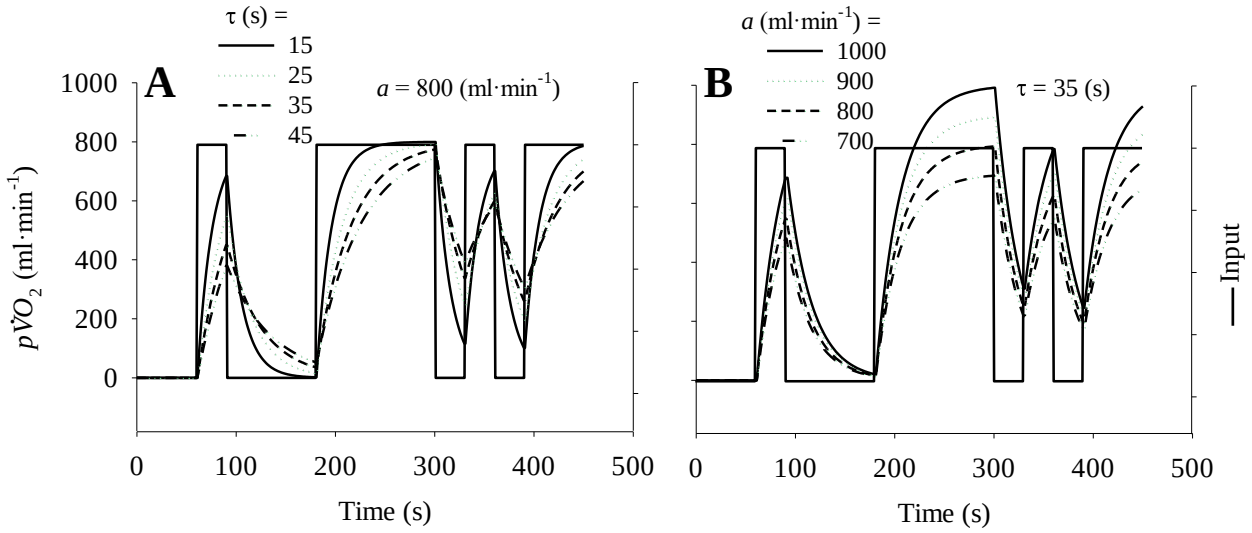

Figure 6. Simulations of the pulmonary oxygen uptake
Simulations of the pulmonary oxygen uptake ($\dot{V}O_2$) dynamics during a pseudorandom binary sequence protocol. A: different adaptation speeds (varying time constant τ_2 values) for a given constant O_2 cost of 800 ml·min^{-1} (constant a_2). Notice that faster kinetic responses are observed at lower τ values. B: constant adaptation speed of 25 s (constant τ_2 value) for different O_2 cost (varying a_2 values). See text for details about the parameters.

The assessment of the rate at which $\dot{V}O_2$ adapts to randomly varying exercise intensities, as in PRBS and PRTS protocols, might be indicative of aerobic fitness (Eßfeld et al., 1987).

Thus, the $p\dot{V}O_2$ prediction during random exercise stimulus with an adequate time resolution may provide an opportunity to evaluate the aerobic system in addition to EE. However, the correct $p\dot{V}O_2$ prediction during randomly varying realistic stimulus is a challenge (Sallis & Saelens, 2000) and new data analysis and wearable technologies are necessary.

1.4 Wearable Sensors and Machine Learning

Estimating energy expenditure from measurement of physical activity levels during realistic scenarios remains a challenge (Sallis & Saelens, 2000) requiring introduction of new wearable technologies and new approaches to data processing. The associations between $p\dot{V}O_2$, heart rate

(HR), and data from wearable sensors such as accelerometers during different PA have a solid theoretical foundation (MacKey et al., 2011; Schmitz et al., 2005). However, studying these associations in practice is still very limited due to the complexity in varying levels of ADL as well as the health status of participants (Chen, Acra, Donahue, Sun, & Buchowski, 2004; Jacobi et al., 2007; Schrack et al., 2014; Tan, Batterham, & Tapsell, 2011). For example, there was a high linear correlation between the activity counts calculated from the summation of all acceleration signals during walking activities and the $p\dot{V}O_2$ steady-state response (Whitcher & Papadopoulos, 2014). However, this same linear model could not be applied for $p\dot{V}O_2$ data prediction during the beginning of walking due to the uncoupling between the energetic demand and $p\dot{V}O_2$ during transition (Selinger & Donelan, 2014).

In controlled conditions, some anthropometric characteristics and accelerometer output signals are applied to estimate EE based on $p\dot{V}O_2$ measurements (Puyau, Adolph, Vohra, Zakeri, & Butte, 2004). However, this approach may not always work for $p\dot{V}O_2$ estimation in unsupervised scenarios. To contextualize, consider two individuals with the same weight, height and age who perform a light self-paced walking exercise (a common ADL). The first individual is healthy, whereas the second is a cigarette smoker with very mild, but un-diagnosed chronic pulmonary obstruction. The $p\dot{V}O_2$ steady state value and consequently the EE for this specific PA is likely similar between these two individuals, because both individuals have the same weight, height, age and movement patterns (Nery et al., 1982). However, the way in which the cardiorespiratory system responds to the walking stimulus is vastly different between these individuals due to differences in aerobic fitness (Borghi-Silva et al., 2012).

For a precise prediction of $p\dot{V}O_2$ during transitions and consequently ADL, it is necessary to have at least one variable that is physiologically linked to the $p\dot{V}O_2$ response. Often times, HR

is the variable of choice (Altini, Penders, & Amft, 2016; Keytel et al., 2005). In addition to HR, the ideal way to estimate $p\dot{V}O_2$ in a realistic scenario is to employ devices that do not cause discomfort to the subject, and at the same time, record all body movements and physiological variables with optimal sample rate and consistency. To estimate EE, accelerometers are one of the most common devices used due to their low cost, small size, energy efficiency, and good data quality and resolution (Bouten, Koekkoek, Verduin, Kodde, & Janssen, 1997). In addition, accelerometers are now present in smartphones, wearable devices and may become implantable in the near future (Theodor et al., 2014).

Accelerometers are compact and they can capture almost all expected ADL movements (Bouten et al., 1997). In addition, accelerometers can provide valuable information about the energy required from the aerobic system (i.e., O_2 cost) that is useful for $p\dot{V}O_2$ predictions (Altini et al., 2016; Puyau et al., 2004). However, accelerometers do not provide information about $p\dot{V}O_2$ during transitions since they are only related to the external work applied to the aerobic response. Recently, more wearable sensors were combined into integrated system to obtain variables with more physiological significance. The Hexoskin® smart vest (Montréal, Canada) integrates the monitoring of heart electric activity, respiration and hip acceleration. This device was previously validated (Villar, Beltrame, & Hughson, 2015) for the acquisition of HR, ventilation minute ($\dot{V}E$), breathing frequency (BF) and total hip acceleration (ACC_{HIP}). The data are recorded in a local data logger or smartphone that can be remotely accessed by the user, physician or trainer, which provides a promising way to deal with sensor fusion data during unsupervised ADL. The data collected by Hexoskin® sensors (Figure 7) integrates ACC_{HIP} data with physiological variables such as HR, $\dot{V}E$ and BF with the potential to be incorporated into predictors of $p\dot{V}O_2$ data during ADL.

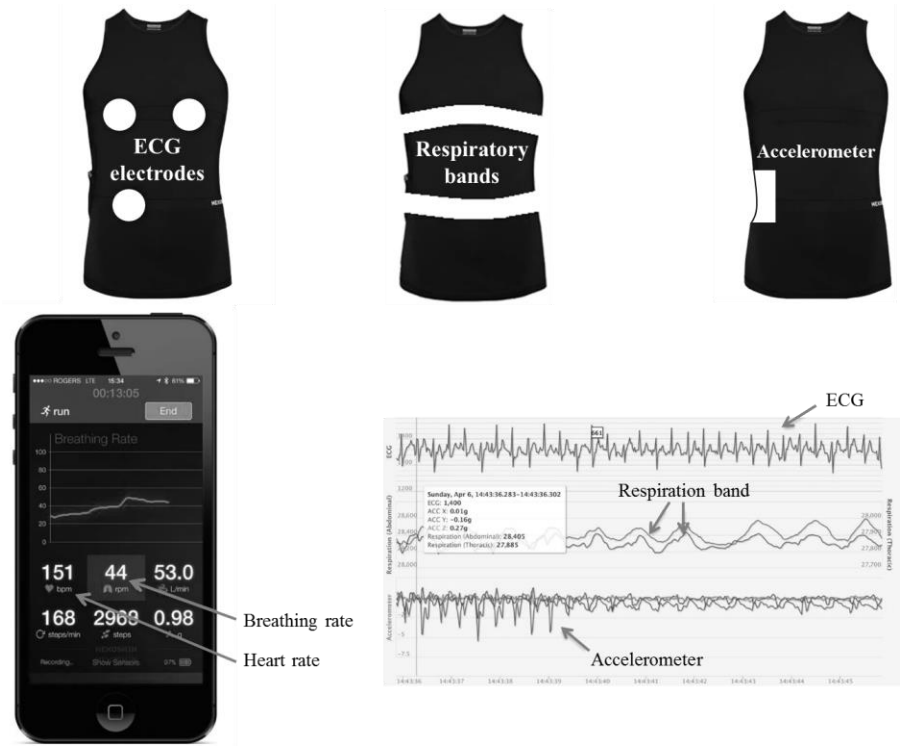

Figure 7. Illustration of the Hexoskin® device
Top images, the locations of the sensors are shown in blue. In the bottom, cellphone application provides real time data visualization. User can access raw or processed physiological data. Figure adapted from www.hexoskin.com.

Based on data from wearable sensors, the EE estimated during ADL is usually obtained from measuring movement patterns, number of steps and/or body acceleration. However, more important than quantifying the mechanical input to the physiological systems is understanding how the aerobic system is handling this stimulus during transitions. This form of analysis may be more valuable when characterizing the actual impact of PA levels on health status.

The $p\dot{V}O_2$ and EE prediction by wearable sensors is generally based on relatively small quantities of simulated laboratory activities (Ali, Messina, & Bisiani, 2013; Altini et al., 2016; Pober, Staudenmayer, Raphael, & Freedson, 2006), which decreases the applicability of the findings in realistic scenarios. Studies that have used multiple linear regressions introduced an elevated number of models specific for each PA type, thereby complicating the comparison

between studies and the definition of a ultimate prediction algorithm (Hendelman, Miller, Baggett, Debold, & Freedson, 2000; Swartz et al., 2000). Additionally, linear methods ignore the intrinsic complexity of the input-output relationships, possibly explaining the growth of the use of machine learning (ML) approaches that can generate more complex algorithms based on practical examples.

In parallel with the advances in wearable device hardware making them smaller, more accessible, and more accurate, ML techniques are becoming more frequently used to handle the elevated amount of data generated by these sensors. Some classical data analysis approaches for pattern discovery have become inadequate due to the incredible amount of data collected and shared by new devices with higher sampling rates. At the same time of hardware improvements, the increased data processing capacity of today's personal computers allow more complex calculations to be performed in a shorter period of time, thereby improving pattern recognition in big datasets through ML algorithms that are widely accessible(Witten & Frank, 2005).

In order to mine a huge amount of data, ML algorithms provide the technical basis to better identify non-trivial patterns due to their ability to learn even with relatively small numbers of examples (Witten & Frank, 2005). The learning process of ML is often based on labelled training data that explicitly maps the relationship between known inputs and outputs (supervised approach). The algorithm builds a prediction process by searching for general structures in the input-output relationship in the training data. Once the machine is "smart" enough, the output can be removed and then predicted by the input. The use of ML to estimate $p\dot{V}O_2$ is a groundbreaking approach to build a $p\dot{V}O_2$ predictor that can compose integrated wearable systems in the future.

1.5 General Objective, Hypothesis, and Impact

The main objective of this thesis was to develop novel tools for data prediction and analysis for the evaluation of the aerobic response during ADL by wearable sensors. We hypothesized that it is possible to extract information regarding the aerobic system dynamics based on wearable sensors during unsupervised activities of daily living. To accomplish this, seven studies were conducted. Initially, studies were developed based on controlled laboratory conditions on a cycle ergometer followed by exercise protocols performed using a treadmill, over-ground walking, and simulated activities of daily living. Finally, the last study evaluated data during unsupervised activities of daily living. The results presented in this thesis demonstrate that it is possible to obtain information with more relevance regarding the aerobic system dynamics during activities of daily living.

As discussed before and further tested in this thesis, the aerobic system response is a consequence of stimulus patterns and different physiological events related to the O_2 delivery and utilization. In addition, the aerobic system dynamics can be characterized by the examination of $p\dot{V}O_2$ data. Therefore, methods that can predict $p\dot{V}O_2$ data can be used to study the aerobic system dynamics without the need to measure $p\dot{V}O_2$. From a practical point of view, the $p\dot{V}O_2$ prediction by wearable sensors has even more applicability due to the possibility to obtain $p\dot{V}O_2$ data beyond the laboratory confinements. The impacts of this thesis are:

1. Develop cutting edge technologies to assess data streamed from wearable sensors for the prediction of health-related outcomes.
2. Understanding of aerobic system dynamics during stimulus similar to activities of daily living.
3. Development of methods for a daily basis characterization of fitness status.

4. Precise prediction of oxygen uptake and energy expenditure through wearable sensors during activities of daily living.
5. Create a technology for the ambulatory identification of periods that might precede unhealthy state.

1.6 Chapter Overview

The studies were based on multi-level investigations (Seals, 2013), progressing from controlled laboratory investigation to real life assessments. Chapter 2, **"Linear and Nonlinear Contributions to Oxygen Transport and Utilization During Moderate Random Exercise in Humans",** investigates the linearity of the aerobic system and how the O_2 delivery-utilization balance behaves during random exercise in humans. In addition, this Chapter introduces some of the methodological basis for further studies and describes the algorithm used to generate computer simulations. The study of aerobic system dynamics during controlled environments was essential to test some physiological assumptions used for the subsequent studies. Based on these concepts, Chapter 3, "**Mean Normalized Gain: A New Method for the Assessment of the Aerobic System Temporal Dynamics During Randomly Varying Exercise in Humans**", proposes and tests a new method able to extract the temporal dynamics of the aerobic system during pseudorandom protocols.

Cycling experiments, used in Chapters 2 and 3, allow precise control over the aerobic system stimulus beneficial for testing precise physiological hypotheses regarding $p\dot{V}O_2$ dynamics. However, cycling is not a common ADL and it is not widely used between different populations and cultures. Walking is a unique physical activity that is performed by the general population almost in all ages and conditions. In addition to its high prevalence, walking is considered an ADL

that requires a higher O_2 cost (and therefore, greatest increase in $p\dot{V}O_2$) due to the large degree of muscle activation that enables the differentiation of the $p\dot{V}O_2$ response from the resting metabolic rate. Therefore, $p\dot{V}O_2$ dynamics were studied during treadmill walking activities in Chapter 4, "**Estimating Oxygen Uptake and Energy Expenditure During Treadmill Walking by Neural Network Analysis of Easy-to-obtain Inputs**". This chapter introduces the use of ML techniques to estimate $p\dot{V}O_2$ during treadmill walking activities.

Although treadmill walking is a sufficient method to study and predict the aerobic system dynamics during walking at a precisely controlled speed and grade, it is not a completely realistic scenario. Chapter 5, "**Aerobic System Analysis Based on Oxygen Uptake and Hip Acceleration During Random Over-ground Walking Activities**" outlines the development of a new over-ground walking protocol that could be used to evaluate the aerobic system dynamics during pseudorandom stimulus that mimics what occurs during ADL. This protocol is then applied in Chapter 6, "**Prediction of Oxygen Uptake Dynamics by Machine Learning Analysis of Wearable Sensors During Activities of Daily Living**", where ML methods are used to predict the $p\dot{V}O_2$ during the over-ground walking and during simulated ADL. Finally, Chapter 7, **"Longitudinal Aerobic System Analysis During Unsupervised Activities of Daily Living Based on Wearable Sensors"** uses the algorithm generated in Chapter 6 to investigate the longitudinal $p\dot{V}O_2$ response during four days of unsupervised ADL.

In addition, we found that the $p\dot{V}O_2$ dynamics during treadmill walking differed between women and men. Therefore, in Appendix A, the study titled **"Sex Differences in the Oxygen Delivery, Extraction and Uptake During Moderate Walking Exercise Transition"** will address the sex influences on the integrated aerobic responses (peripheral vs. central) during

walking activity on treadmill. This study will focus on time domain kinetics analysis of peripheral and central physiological variables and how they seemed to be different between women and men.

In addition to study details within each Chapter, further information related to the population studied, physical examination and the questionnaires applied are in Appendix B.

Chapter 2: Linear and Nonlinear Contributions to Oxygen Transport and Utilization During Moderate Random Exercise in Humans

This chapter was submitted as:

Beltrame T., Hughson R. L. Linear and nonlinear contributions to oxygen transport and utilization during moderate random exercise in humans. Submitted to Exp Physiol on October 28, 2016 .

2.1 Overview

The assumption of the aerobic system linearity implies that the pulmonary oxygen uptake ($p\dot{V}O_2$) dynamic during exercise transitions present a first-order characteristic. The main objective of this study was test the linearity of the oxygen delivery-utilization balance during random moderate exercise. In addition, the aerobic system linearity was tested by comparing experimentally-obtained $p\dot{V}O_2$ response to *in silico* oxygen uptake data ($sm\dot{V}O_2$). The cardiac output ($\dot{Q}$) and deoxygenated hemoglobin (HHb) were measured to infer about the central and local O_2 availability, respectively. Thirteen healthy men enrolled in this study. Participants performed two consecutive pseudorandom binary sequence cycling exercises followed by a incremental protocol. The system input and the outputs $p\dot{V}O_2$, $sm\dot{V}O_2$, HHb and $\dot{Q}$ were submitted to frequency domain analysis that decomposed the signals into target frequency gains of each variable. The linearity of the responses was tested by computing the ability of the normalized system gain at a specific frequency to predict the normalized system gain at another frequency. The predictability levels were assessed by coefficient of determination. In a first-order system, a participant who presents faster dynamics at a specific frequency should also present faster dynamics at any other frequency. All experimentally-obtained variables ($p\dot{V}O_2$, HHb and $\dot{Q}$) presented a certainly degree of non-linearity. In conclusion, the oxygen delivery-utilization balance behaved as a nonlinear phenomenon. Therefore, the elevated complexity of the pulmonary oxygen uptake dynamics is governed by a complex multiple-order interaction between the oxygen delivery and utilization systems.

2.2 New Findings

What is the central question of this study?

The pulmonary oxygen uptake ($p\dot{V}O_2$) data used to study the muscle aerobic system dynamics during moderate exercise transitions is classically described as a mono-exponential function controlled by a complex interaction of the oxygen delivery-utilization balance. This elevated complexity complicates to obtain relevant information regarding aerobic system dynamics based on $p\dot{V}O_2$ data during complex exercise stimulus.

What is the main finding and its importance?

The elevated complexity of pulmonary oxygen uptake ($p\dot{V}O_2$) dynamics is a consequence of a multiple-order interaction between muscle oxygen uptake and circulatory distortion. Our findings challenge the use of first-order function to study the influences of the oxygen delivery-utilization balance over the $p\dot{V}O_2$ dynamics.

2.3 Introduction

The linear first-order relationship between steady-state pulmonary oxygen uptake ($p\dot{V}O_2$) and work rate ($\dot{W}$) amplitude during moderate exercise is one of the constants of exercise physiology that enable the system output (i.e., steady-state $p\dot{V}O_2$) to be predicted from the input (i.e., $\dot{W}$) yielding an estimate of energy expenditure (Åstrand, 2003; Pescatello, 2014). The linear characteristic follows the superposition law such that any further input increment should lead to a proportional first-order output response (linear static gain) (Hughson et al., 1990; Whipp & Wasserman, 1972). In addition, in a purely linear system the rate at which the $p\dot{V}O_2$ increases during moderate exercise transitions (usually characterized by the time constant "τ") is

independent of the $\dot{W}$ amplitude, denoted as linear dynamic gain (Hansen, Casaburi, Cooper, & Wasserman, 1988; Hughson, 2009; Ozyener, Rossiter, Ward, & Whipp, 2001). However, previous studies (Brittain et al., 2001; Faisal, Beavers, & Hughson, 2010; Hughson & Morrissey, 1982; Wilcox, Broxterman, & Barstow, 2016) have challenged the dynamic gain linearity, even in the moderate intensity domain, by varying the baseline $\dot{W}$ that precedes exercise transitions. Previous studies (Hughson & Morrissey, 1983; Keir, Robertson, Benson, Rossiter, & Kowalchuk, 2016; Wilcox et al., 2016) have shown that the apparent first-order $p\dot{V}O_2$ dynamics to a $\dot{W}$ increase can be the resultant of the complex interaction between the static and dynamic aerobic system gains that are directly influenced by the O_2 delivery-utilization balance

The analysis of $p\dot{V}O_2$ kinetics in the frequency domain using a pseudo random binary sequence (PRBS) protocol (Eßfeld, Hoffmann, & Stegemann, 1991; Hoffmann et al., 2013; Hughson et al., 1988, 1990) might provide an alternative way to assess $p\dot{V}O_2$ dynamic distortions. The PRBS protocol switches the system input between two moderate levels following a very specific order and, as opposed to constant $\dot{W}$ protocols (Bowen et al., 2011; Brittain et al., 2001; DiMenna, Bailey, Vanhatalo, Chidnok, & Jones, 2010), offers a unique possibility to simultaneously test $p\dot{V}O_2$ dynamics distortions across a wide range of stimulus frequencies and metabolic rates (Hughson, 1990). For the sake of comparison between time- and frequency-domain responses, the study of the $p\dot{V}O_2$ gain at a specific $\dot{W}$ frequency can be interpreted as the investigation of the aerobic system kinetics at a specific portion of the transient response in the time domain (Hoffmann, Eßfeld, Leyk, Wunderlich, & Stegemann, 1994). Higher frequencies refer to the beginning of the transient phase response whereas lower frequencies refer to the responses closer to steady state (Hoffmann et al., 1994). A linear aerobic system with constant static and dynamic system gains should follow a single-order function where the system output at

any $\dot{W}$ frequency is fully predictable by the system analysis at any other frequency (Hoffmann et al., 1994).

To further explore the aerobic system linearity and how the O_2 delivery-utilization balance behaves in random exercise, the present study aimed to compare experimental and *in silico* $\dot{V}O_2$ data obtained during the PRBS protocol along with cardiac output ($\dot{Q}$) and deoxygenated hemoglobin (HHb) measures as indications of central and local O_2 availability respectively. It was hypothesized that the apparent high complexity of the $p\dot{V}O_2$ rate of increase to a $\dot{W}$ stimulus is a consequence of the complex interaction between the O_2 delivery and utilization systems. In addition, a new method, based on the mean normalized gain amplitude (MNG) in the frequency domain, will be introduced for the characterization of the $p\dot{V}O_2$ response and its contributing components during random exercise stimulus.

2.4 Methods

2.4.1 Study Design

Thirteen active, not athletically trained, healthy male adults (27 ± 7 years old, 174 ± 7 cm and 78 ± 14 kg) enrolled in this study. The Office of Research Ethics at the University of Waterloo reviewed and approved the research procedures that were consistent with the Declaration of Helsinki. Written, informed consent was obtained from all participants. The PRBS exercise protocol was repeated two times in a row followed by a symptom-limited incremental protocol (25 watts·min^{-1} ramp) for the determination of the gas exchange threshold (Beaver, Wasserman, & Whipp, 1986) and peak $p\dot{V}O_2$. All participants had previous experience with cycle ergometer exercise and performed an additional familiarization protocol (1-minute at 25 and 100 watts) before each test. The exercise testing was performed on an electrically braked cycle ergometer

controlled by an external, pre-programmed module (Lode Excalibur Sport, Lode B.V., Groningen, Netherlands) that reaches the desired $\dot{W}$ to be achieved in less than 1.5 s.

A digital shift register with an adder module feedback (Figure 8A) was used to generate the PRBS protocol (Figure 8B) (Bennett, Reischl, Grodins, Yamashiro, & Fordyce, 1981; Hughson et al., 1990; Kerlin, 1974). Each of the two consecutive PRBS protocols comprised 45 units (25 or 100 watts) of 30 s duration (15 min total). The target cadence was controlled by visual feedback and maintained between 60-65 rpm. In addition, 200s of extra PRBS segment was added at the beginning of the protocol (denoted as "warm-up" in Figure 8B) in order to minimize the influences of the rest-to-exercise transition (Eßfeld et al., 1987; Hughson et al., 1990). The selected higher $\dot{W}$ (100 watts) provided a reasonable stimulus that excludes, in this population, the influences of the slow component on the overall $p\dot{V}O_2$ gain but still delivers sufficient input signal energy to identify $p\dot{V}O_2$ responses for a good range of frequencies (Eßfeld et al., 1987; Hoffmann et al., 2013).

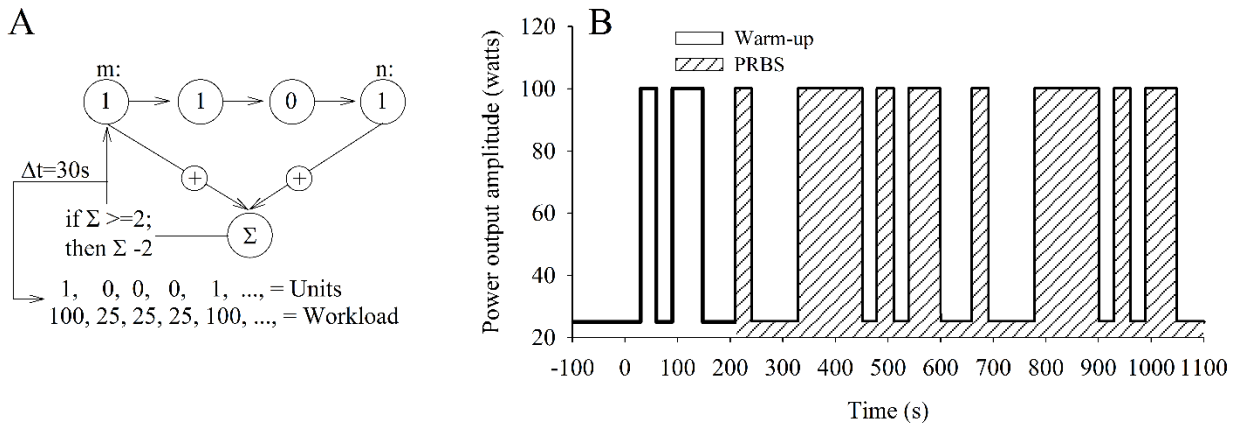

Figure 8. Pseudorandom binary sequence protocol generation.
A: structure of the 4-stage shift register used to generate the pseudorandom binary sequence protocol. The module addition feedback (Σ) sum the first and fourth stage values and test the "if" statement. This new bit is inserted into the first stage and the entire system shifts to the right. Each unit value is repeated "Δt" times to create the PRBS protocol in the time domain (B). An extra of 200s of PRBS segment was added at the beginning of the protocol as a warm-up to minimize the rest-to-exercise influences.

2.4.2 Data Acquisition

The $p\dot{V}O_2$ and the carbon dioxide output were measured breath-by-breath by a portable metabolic system ($K4b^2$, COSMED, Italy). Before each visit, the gas concentrations and air volume/flow were calibrated following manufacturer's specifications.

A multi-distance continuous-wave near infrared spectroscopy device (PortaMon, Artinis, The Netherlands) was used to evaluate the dynamic changes in *vastus lateralis* deoxy-hemoglobin concentration ($[HHb]$ in μM) (Boushel et al., 2001). The light emitting probe was composed of three light-emitting diodes operating at two wavelengths (λ_1=845 and λ_2=759 nm) resulting in six different light sources with different light in/out distances (≈ 35 mm). All cautions regarding the differential path length factor (set at 5.8) were taken based on previous literature (Kowalchuk, Rossiter, Ward, & Whipp, 2002). The probe was placed in the target area and the device was warmed-up for at least 30 min before the data collection. In order to avoid any motion artifact and

ambient light influences, the probe was fixed by tape and then a dark cloth was gently wrapped around the thigh. The sample rate was 10 Hz. To ensure that the near infrared light was penetrating into the muscle layer, a caliper was used to measure the skinfold thickness under the probe. The average thickness was 5.6 ± 3.4 mm, ≈ 32% lower than the half of the light in/out distance, which indicates a good light penetration and a good muscle-to-skin blood flow signal proportion. The $[HHb]$ data were normalized by the steady-state signal obtained during a 3-min free-wheel cycling prior to the PRBS protocol; therefore, the $[HHb]$ unit was expressed as $\Delta\mu M$.

The $\dot{Q}$ was estimated beat-by-beat (Finometer, Finapres Medical System, Arnhem, The Netherlands) by the analysis of the third finger pulse-wave pressure (Wesseling, Jansen, Settels, & Schreuder, 1993). Linearity between this estimate and rebreathing $\dot{Q}$ has previously been demonstrated in exercise (Faisal, Beavers, Robertson, & Hughson, 2009).

2.4.3 Time-domain Analysis

In addition to the frequency-domain analysis described below, time domain analysis of the $p\dot{V}O_2$ data was performed on a data segment of the PRBS protocol. Data from the two consecutive PRBS were filtered by 5-breath moving average, time aligned and ensemble-averaged (Keir, Murias, Paterson, & Kowalchuk, 2014) to obtain a single response per participant. The total data window length for this analysis was 130s which included 10s of baseline (25 watts) followed by 120s at 100 watts. The 120th second of the PRBS protocol was set as the time zero. This specific data window corresponding to the longest period without $\dot{W}$ variation was the best PRBS protocol window for time-domain analysis. The following equation was used to fit the $p\dot{V}O_2$ data (Hughson & Morrissey, 1982; Whipp et al., 1982): $p\dot{V}O_{2(t)} = a_0 + a\left(1 - e^{-(t-TD/\tau)}\right)$; where t is time; a_0 is the baseline at 25 watts; a is the steady state increment at 100 W; τ is time constant and TD is

the time delay of the exponential function. The initial data associated to the cardio-dynamic component (≈ 22 s) were excluded by detection of the change in total arteriovenous O_2 difference ($a - vO_2diff$) obtained by the ratio $p\dot{V}O_2/\dot{Q}$ (Barstow et al., 1990). According to previous literature (Macdonald, Pedersen, & Hughson, 1997), the mean response time (MRT) was calculated by adding τ and TD. The quality of the fitting was assured by the analysis of residuals, degree of linear correlation between experimental data and fitted function (r), 95% confidence interval band (CI_{95}) (Fawkner, Armstrong, Potter, & Welsman, 2002; Keir et al., 2016), absolute and relative standard error (SE and $\%SE$, respectively) and the statistical significance level (p) of the estimated parameters.

2.4.4 In Silico Aerobic Response

To test the aerobic system linearity, *in silico* simulations were conducted to create a purely linear aerobic response for comparison with the experimentally-obtained variables. This comparison allowed us to investigate the aerobic system complexity during random stimuli. The simulated linear muscular aerobic system signal ($sm\dot{V}O_2$) (Hoffmann et al., 2013; Ozyener et al., 2001) was based on each participant's own time-domain $p\dot{V}O_2$ kinetics parameters (a_0, a and MRT). These simulations (thirteen in total) considered the first-order delayed exponential nature of the on and off muscular $\dot{V}O_2$ kinetics (Henry, 1951; Hughson, 2009). The single time constant was obtained by incorporating TD into the MRT as performed for PRBS by Hoffmann et al. (Hoffmann et al., 2013). Simulations were based on a constant muscle compartment(s) activation/deactivation (Barstow et al., 1990; Keir et al., 2016) between the monotonic exercise transitions (25↔100 watts), with identical system dynamics between on- and off-transitions (Hoffmann et al., 2013); thus: $\left((a_0 + a) * tf\right) - (\sum_{t=0}^{tf} a_0 + a * (1 - e^{-t/MRT})) = \left(p\dot{V}O_{2(tf)}\right) - \left(p\dot{V}O_{2(tf)} - a_0\right) * (1 -$

$e^{-t/MRT}$); where tf is the length of the PRBS unit. Therefore, based on these physiological assumptions and individual time-domain parameters, the following algorithm was programmed to generate the $sm\dot{V}O_2$ time-series signal in response to PRBS input:

$$sm\dot{V}O_{2_{(t,MRT,a_0,a_1)}} = \begin{cases} y_1 + a_0 \\ y_2 + a_0 \\ \quad . \\ \quad . \\ \quad . \\ y_n + a_0 \end{cases};$$

$$if = \begin{cases} 0 \le t < 30;\ sm\dot{V}O_{2_{(t,MRT,a_0,a_1)}} = y_1 \\ 30 \le t < 90;\ sm\dot{V}O_{2_{(t,MRT,a_0,a_2)}} = y_2 \\ \qquad\qquad . \\ \qquad\qquad . \\ \qquad\qquad . \\ u_b \le t < u_e;\ sm\dot{V}O_{2_{(t,MRT,a_0,a_n)}} = y_n \end{cases} ; where$$

$$= \begin{cases} y_1 = a_1\left(1 - \mathrm{e}^{-\frac{\mathrm{t}}{\mathrm{MRT}}}\right) \\ y_2 = a_2 - a_2\left(1 - \mathrm{e}^{-\frac{(\mathrm{t}-30)}{\mathrm{MRT}}}\right);\ a_2 = sm\dot{\mathrm{V}}\mathrm{O}_{2_{(\mathrm{t,MRT,a_2})}} \\ \qquad\qquad . \\ \qquad\qquad . \\ \qquad\qquad . \\ y_\mathrm{n} = a_\mathrm{n} - a_\mathrm{n}\left(1 - \mathrm{e}^{-\frac{(\mathrm{t}-u_\mathrm{b})}{\mathrm{MRT}}}\right);\ a_\mathrm{n} = sm\dot{\mathrm{V}}\mathrm{O}_{2_{(\mathrm{t,MRT,a_n})}} \end{cases}$$

where y is the $sm\dot{V}O_2$ value at a given PRBS time n, and u is the PRBS time at the beginning b and at the end e of the protocol unit.

2.4.5 Frequency-domain Analysis

The raw data from the input ($\dot{W}$) and outputs ($sm\dot{V}O_2$, $p\dot{V}O_2$, $\dot{Q}$ and [HHb]) were submitted to frequency-domain analysis. The target frequencies from 0.002 to 0.013 Hz (i.e., from the fundamental to the 6th harmonic) were selected according to previous literature (Hoffmann et al., 2013, 1992; Hughson et al., 1990). The following trigonometric form of the Fourier series was

solved for each harmonic h: $y_{(t)} = a_{DC} + 2 * \sum_{n=1}^{6}(A_h * \cos(2\pi * h * f_1 * t) + B_h * \sin(2\pi * h * f_1 * t))$; where y is the signal to be fitted, t is the time, a_{DC} is average response (system DC_{offset}), f_1 is the fundamental frequency (1/450 s or 0.002 Hz in this case), A_h and B_h are the cosine and sine amplitudes for a given harmonic h, respectively. From A_h and B_h, the total amplitude can be calculated for each harmonic h by: $Amp_h = \sqrt{A_h^2 + B_h^2}$. Secondary variables were obtained from these parameters. As a proxy of local O_2 delivery, the Amp_h of the capillary blood flow ($\dot{C}apBF$) was obtained by the ratio $p\dot{V}O_2$-Amp_h/$[HHb]$-Amp_h at each h (Buchheit, Laursen, & Ahmaidi, 2009; Ferreira, Townsend, Lutjemeier, & Barstow, 2005). Similarly, the Amp_h of the $a - vO_2diff$ was obtained by the ratio $p\dot{V}O_2$-Amp_h/$\dot{Q}$-Amp_h at each h (Barstow et al., 1990).

2.4.6 Normalized Frequency-domain Responses

To allow the comparison between variables and to eliminate the influence of the static gain intra-subject variability (Hoffmann et al., 1994, 1992), the system normalized gain ($\hat{A}mp_h$) was obtained from dividing the output by the input Amp_h (system gain) for each harmonic h and then normalizing as a percentage of the Amp gain at the fundamental frequency (i.e, Amp_1 gain). A new index to characterize system dynamics in the frequency domain, the mean normalized gain amplitude (MNG in %), was calculated based on the average of the normalized gain from $\hat{A}mp_2$ to $\hat{A}mp_6$. In a purely linear system (like the *in silico* response), the MNG can be used as an overall kinetics description, hypothetically similar to the MRT obtained from time domain-analysis. In this case, MNG isolates speed components of the dynamics from variable system static gain and DC_{offset} (Shmilovitz, 2005). Therefore, in a purely linear first-order exponential response, higher

MNG means, by definition, faster system adjustment. However, MNG can also be used to assess system complexity (i.e., order) by identifying distortions over the dynamic gain across the frequencies. Accordingly, in a multiple-order system, higher MNG values could mean either higher system complexity or faster system adjustment. Therefore, the possibility to use MNG as an index to exclusively asses the aerobic system temporal dynamics depends on the linearity (i.e., order) of the signal. Both kinetics analyses and data simulations were performed by a certified (#100-314-4110) LabVIEW associated developer (National Instruments, Austin, TX, US).

2.4.7 Statistical Analysis and System Linearity Assessment

The one way repeated measures analysis of variance (ANOVA) was chosen for statistical analysis. The $\hat{A}mp_h$ obtained from the *in silico* data ($sm\dot{V}O_2$) and from the primary variables ($p\dot{V}O_2$, $\dot{Q}$ and $[HHb]$) was compared between variables within the same harmonic h (i.e., each tested frequency). Similarly, secondary variables derived from the primary variables $\hat{A}mp_h$ (i.e., $a-vO_2diff$- and $\dot{C}apBF$-$\hat{A}mp_h$) were compared between them and also with $sm\dot{V}O_2$-$\hat{A}mp_h$. These comparisons assessed the dynamic responses between variables at specific input frequencies. Higher $\hat{A}mp_h$ values indicate a faster rate of increase at a given h or frequency. The MNG was compared following the same variables split (primary and secondary) where higher MNG values indicate a faster dynamics of the overall response (the entire pool of frequencies). Student-Newman-Keuls method was used as post hoc test when significant differences were found. Significance level was set at $p < 0.05$. The agreement level between MRT and MNG was verified by Pearson product-moment correlation coefficient (r) and the significance level (p value).

In a linear first-order system, the temporal dynamics between frequencies (i.e., the $\hat{A}mp_h$ for the different h's) have to be commutable, allowing the prediction of the output dynamics at

any frequency by analyzing the output dynamics at any other frequency. In contrast, multiple-order systems do not present a predictable linear pattern between the different $\hat{A}mp_h$. For example, in a first-order system, a participant who presents faster dynamics at $\hat{A}mp_2$ should also present faster dynamics at $\hat{A}mp_6$ thus $\hat{A}mp_2$ is, at a certain degree, predictable by $\hat{A}mp_6$, and vice-versa. Therefore, the linearity was tested for each variable for all possible combinations of $\hat{A}mp$ between the different h's (ten in total for each variable). The coefficients of determination (r^2) and the p values were used to measure the linearity level of the $\hat{A}mp$ between h's. When the p values were higher than 0.05, the null hypothesis of linearity was rejected indicating the presence of non-linearities. In addition, the ability of a given $\hat{A}mp_h$ to predict the overall response (i.e., MNG) was also assessed. For these assessments, MNG was calculated excluding the $\hat{A}mp_h$ being tested.

2.5 Results

2.5.1 Time-domain Fitting

Figure 9 displays the mean $p\dot{V}O_2$ response in time domain fitted by a mono-exponential function as well as the fitting residuals. These data were used to derive the fitting parameters used for the $sm\dot{V}O_2$ *in silico* data in response to the PRBS input. Also, the calculated MRT for each individual will be compared to a kinetics estimate from the frequency-domain analysis (i.e., MNG).

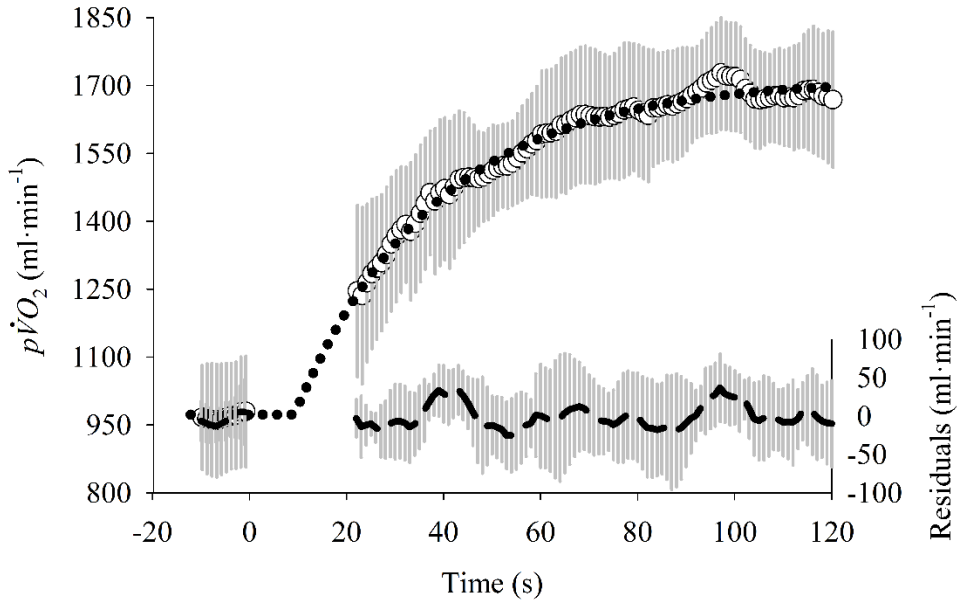

Figure 9. Fitted experimental pulmonary oxygen uptake data and the residuals
Mean ± SD (vertical gray bars) of the 13 subjects for pulmonary oxygen uptake (○, $p\dot{V}O_2$) and the residuals (---) between the individual fitted function and experimental data. For the sake of data modeling representation, the mean $p\dot{V}O_2$response was fitted by a mono-exponential function (•••).

The p values for the exponential parameters and the data fitting quality indexes were lower than 0.001 for all estimated parameters (Table 2). The CI_{95} band was equivalent to 2.3, 5.59, 21.62 and 17.6 % of the average a_0, a, τ and TD, respectively. The CI_{95} band in association with a high r and r^2 and the evenly distributed residuals across the transition indicate that the time-domain data fitting procedure can be considered reliable. The chosen $\dot{W}$ (100 watts) did not elevate the $p\dot{V}O_2$ total gain (a_0+a_1) beyond each participant's gas exchange threshold.

Table 2. Parameters obtained during time-domain pulmonary oxygen uptake kinetics analysis and the quality of the data fitting

	Value	SE	%SE	$+CI_{95}$	$-CI_{95}$	p value
a_0	973±114	11±4	1.23±0.47	996±114	949±114	<0.0001±0.00
a	751±149	21±12	2.76±1.46	793±164	709±137	<0.0001±0.00
τ	25.53±13.43	2.78±2.32	10.14±3.67	31.05±17.71	20.01±9.45	<0.0001±0.00
TD	17.01±9.08	1.47±0.71	13.79±14.17	19.93±9.01	14.08±9.36	<0.0001±0.00
MRT	42.54±11.07	N/A				
r	0.98±0.01					

Abbreviation: a_0 is the baseline from the final 30s at 25 watts; a is the steady state amplitude at 100 watts; τ is time constant and TD is the time delay of the exponential function onset; MRT is the mean response time, r is the Pearson product moment coefficient; SE: absolute standard error; $\%SE$: relative standard error, CI_{95}: confidence interval and p: significance level.

Figure 10 displays the mean time-domain response averaged across all participants (n=13) for the variables measured during the PRBS protocol.

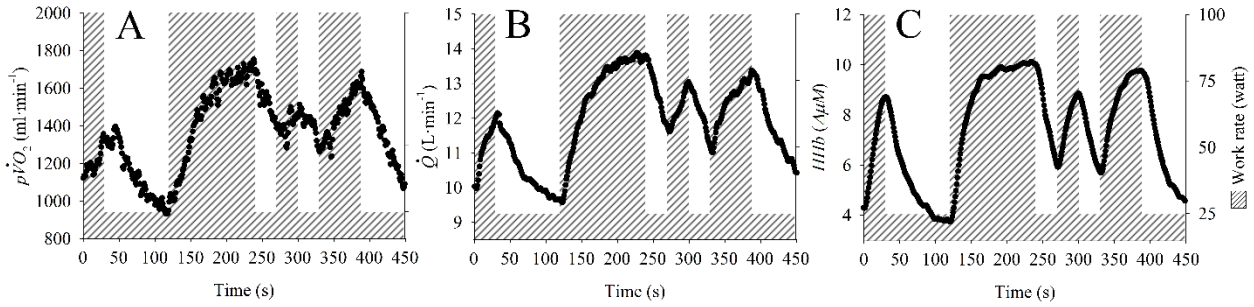

Figure 10. Time domain response during pseudorandom binary sequence exercise.
Group mean time domain responses of the pulmonary oxygen uptake (A, $p\dot{V}O_2$), cardiac output (B,$\dot{Q}$) and deoxy-hemoglobin (C, [HHb]) The power output (▨) of the pseudorandom binary sequence protocol is displayed in each graph.

2.5.2 Speed of the System Output Responses

The data related to the variables displayed in Figure 10 were submitted to frequency-domain analysis and the results were used to estimate the Amp_n of secondary variables. Figure 11 shows the system normalized gain ($\hat{A}mp_h$) for the primary variables at each tested frequency (or harmonic h) expressed as a percentage of the gain at 0.002 Hz (Amp_1). The purpose of these comparisons was to verify the differences of the adaptation speed between variables at different frequencies, or h. Higher $\hat{A}mp_h$ values indicate faster temporal dynamics of the response.

The $\dot{Q}$-$\hat{A}mp$, as a proxy of central O_2 provision dynamics, presented the same speed of adaptation in comparison to the $in\ silico$ data with no statistical differences found in comparison to $sm\dot{V}O_2$-$\hat{A}mp$ at any frequency (Figure 11). Likewise, the $p\dot{V}O_2$-$\hat{A}mp$ was not statistically ($p >$ 0.05) different to $sm\dot{V}O_2$-$\hat{A}mp$ at any tested frequency, indicating a similar speed of adaptation at all tested frequencies.

As a proxy of the O_2 extraction at the muscle site, the $[HHb]$ dynamics for frequencies all tested frequencies were faster than the central O_2 provision dynamics ($\dot{Q}$-$\hat{A}mp$) and the $p\dot{V}O_2$ (Figure 11). In comparison to the *in silico* response, the $[HHb]$-$\hat{A}mp$ was also statistically ($p <$ 0.05) elevated at all frequencies.

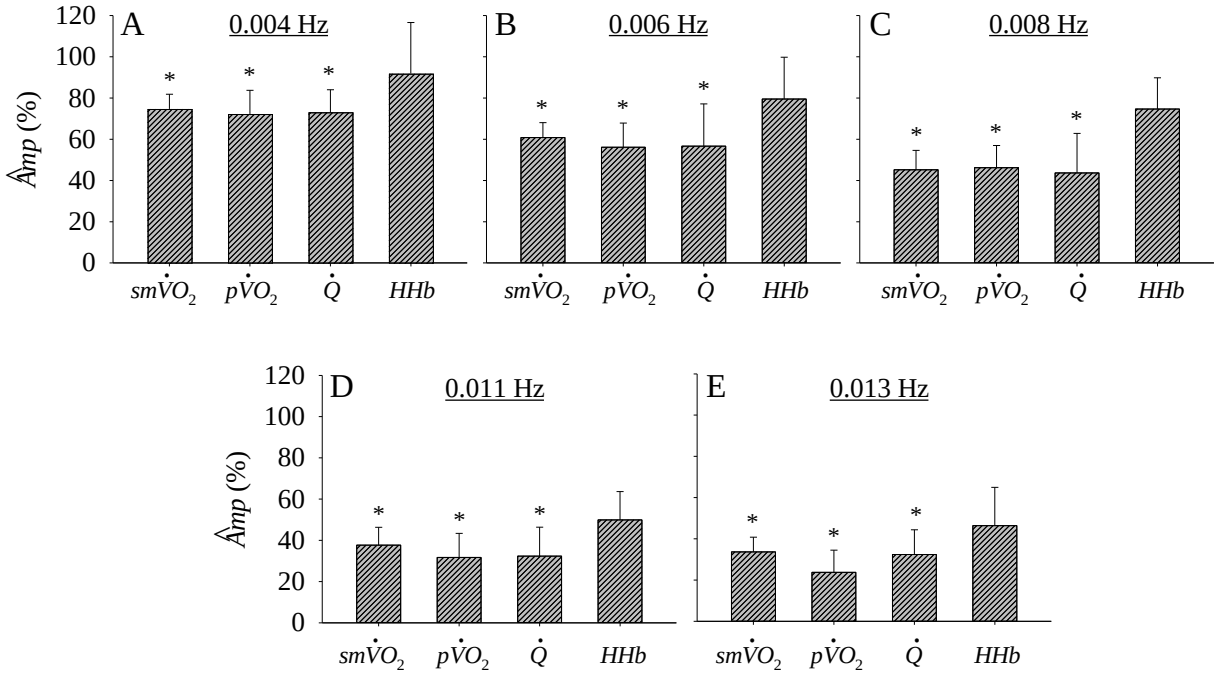

Figure 11. Normalized system amplitude gain of primary variables
Mean ± SD of the normalized system amplitude gain ($\hat{A}mp$) of simulated muscular oxygen uptake ($sm\dot{V}O_2$), pulmonary oxygen uptake ($p\dot{V}O_2$), cardiac output ($\dot{Q}$), and deoxy-hemoglobin concentration ($[HHb]$) at the frequencies 0.004 (A), 0.006 (B), 0.008 (C), 0.011 (D) and 0.013 (E) Hz. * mean statistically ($p < 0.05$) lower than $[HHb]$.

The dynamics of the O_2 extraction across the lung ($a - vO_2diff$-$\hat{A}mp_h$) and the local O_2 delivery ($\dot{C}apBF$-$\hat{A}mp_h$) were compared between variables and to $sm\dot{V}O_2$-$\hat{A}mp_h$ at each h. The $\dot{C}apBF$ was statistically ($p < 0.05$) slower (i.e., lower $\hat{A}mp$) than $a - vO_2diff$ at the first three harmonics (0.004, 0.006 and .008 Hz, Figure 12). The *in silico* system ($sm\dot{V}O_2$) was statistically ($p < 0.05$) slower (i.e., lower $\hat{A}mp$) than $a - vO_2diff$ in all tested frequencies and also slower than $\dot{C}apBF$ at 0.011 and 0.013 Hz.

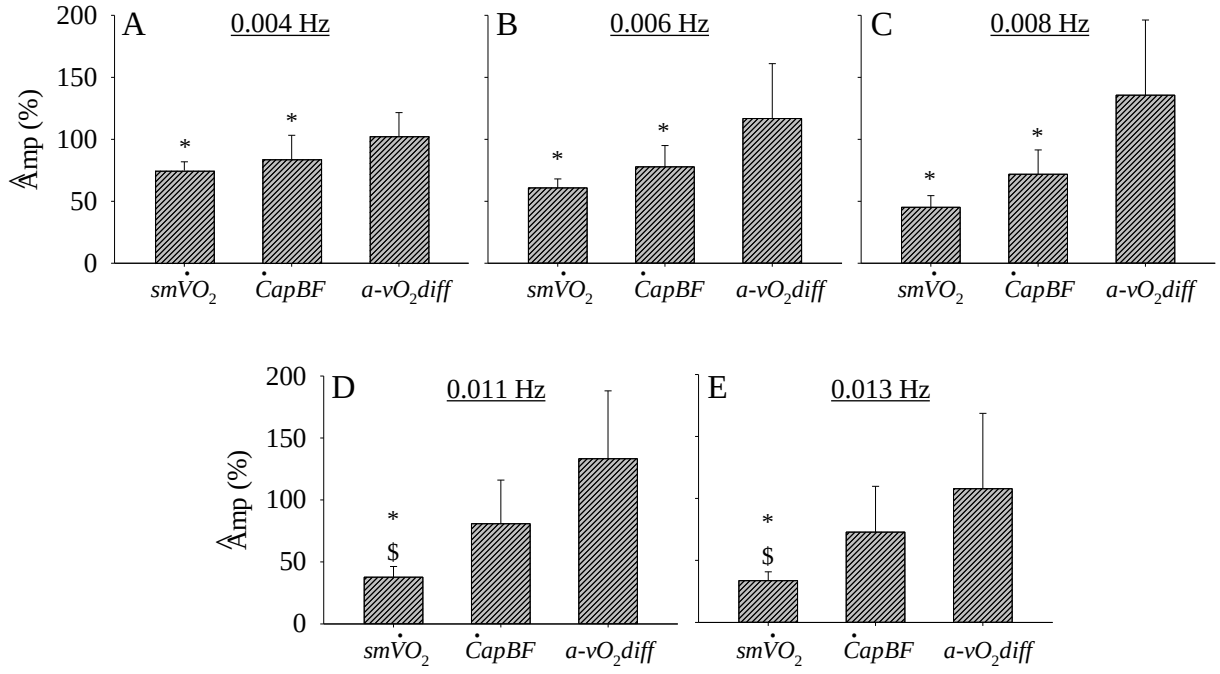

Figure 12. Normalized system amplitude gain of secondary variables
Mean ± SD of the normalized system amplitude gain ($\hat{A}mp$) of capillary blood flow ($\dot{C}apBF$) and total arteriovenous O_2 difference ($a - vO_2diff$) at the frequencies 0.004 (A), 0.006 (B), 0.008 (C), 0.011 (D) and 0.013 (E) Hz. Abbreviations: *, statistically ($p < 0.05$) lower than $a - vO_2diff$ and $, statistically ($p < 0.05$) lower than $\dot{C}apBF$.

Like MRT obtained by time-domain analysis, the MNG can be used in the frequency-domain to describe the overall characteristics of the dynamics response. The local O_2 extraction dynamics investigated by the $[HHb]$-MNG was faster (i.e., higher MNG) than the $sm\dot{V}O_2$, $p\dot{V}O_2$ and $\dot{Q}$ (Figure 13A). As described in Figure 7B, the $a - vO_2diff$-MNG was statistically ($p < 0.05$) faster (i.e., higher) than the $sm\dot{V}O_2$ and $\dot{C}apBF$-MNG. In addition, the $\dot{C}apBF$-MNG was statistically ($p < 0.05$) faster than the $in\ silico$ response ($sm\dot{V}O_2$).

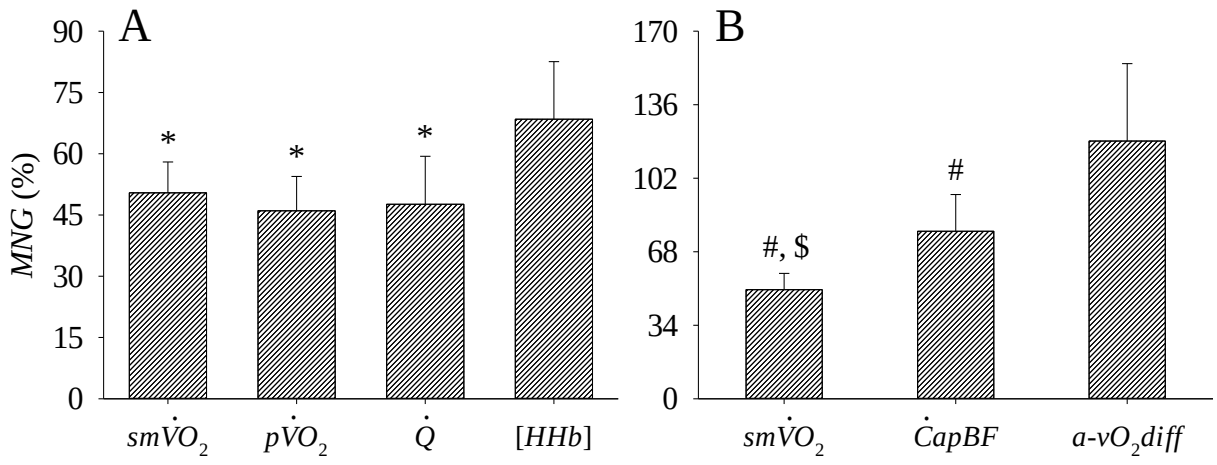

Figure 13. Mean normalized gain obtained by frequency-domain analysis.
A: mean ± SD of the mean normalized gain (MNG) obtained by frequency-domain analysis and used as an index of the overall dynamics behaviour of the simulated muscular oxygen uptake ($sm\dot{V}O_2$), pulmonary oxygen uptake ($p\dot{V}O_2$), cardiac output ($\dot{Q}$) and deoxy-hemoglobin concentration ([HHb]). B: mean ± SD of the MNG of the $sm\dot{V}O_2$, capillary blood flow ($\dot{C}apBF$) and arteriovenous O_2 difference ($a - vO_2diff$). Abbreviations: *, statistically (p < 0.05) lower than [HHb]; #, statistically (p < 0.05) lower than $a - vO_2diff$ and $, statistically ($p$ < 0.05) lower than $\dot{C}apBF$.

The agreement level between the $p\dot{V}O_2$-MRT and $p\dot{V}O_2$-MNG was also verified. As demonstrated by a strong negative linear correlation (r = -0.84) in Figure 14, subjects with a faster overall system dynamic (indicated by lower $p\dot{V}O_2$-MRT values in time-domain analysis) maintained an elevated gain across the frequency spectra (assessed by the $p\dot{V}O_2$-MNG in frequency-domain analysis).

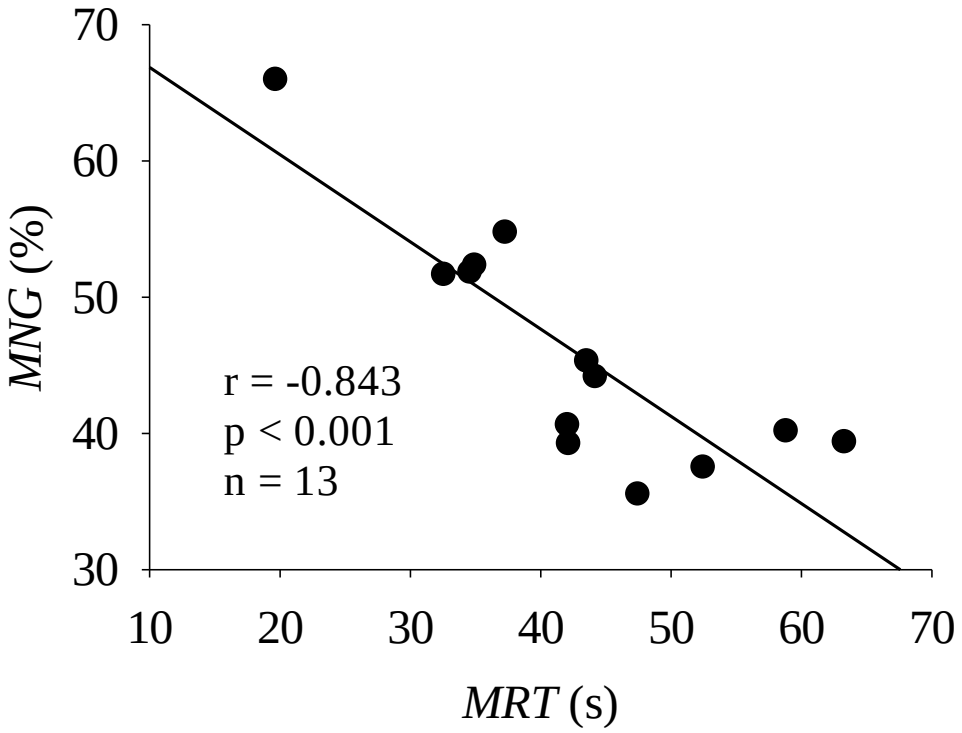

Figure 14. Mean response time and mean normalized gain
Correlation between the mean response time (MRT) obtained by time-domain and the mean normalized gain (MNG) obtained by frequency-domain analysis of the pulmonary oxygen uptake response of each individual subject (n = 13).

2.5.3 Linearity of the System Output Responses

Figure 15 displays the ability to predict another $\hat{A}mp_h$ based on a given value of $\hat{A}mp_h$ obtained at a different h (frequency) assessed by the r^2 and p values. For a better visualization, the r^2 values were transformed into a black color spectrum where lower values are lighter and higher values darker. White cells mean that the agreement level did not reach statistical significance (p > 0.05). As expected from the algorithm used to generate the *in silico* data, the $sm\dot{V}O_2$-$\hat{A}mp$ response at a given frequency can be obtained from the analysis of the $sm\dot{V}O_2$-$\hat{A}mp$ response at any other frequency. On the other hand, all variables (primary and secondary) seemed to behave as a multiple-order system with possible multiple controllers that define the overall dynamic of the system in response to a stimulus with different levels of r^2 across the harmonics (Figure 15). The

$\dot{C}apBF$ response presented the most irregular behaviour and from ten possible combinations, the $\hat{A}mp_h$ did not predict the $\hat{A}mp_h$ at another frequency eight times. The $p\dot{V}O_2$ and $a-vO_2diff$ dynamics were irregular (i.e., not predictable by another frequency) in six comparisons. The $\dot{Q}$ and HHb showed elevated complexity at five and four comparisons, respectively.

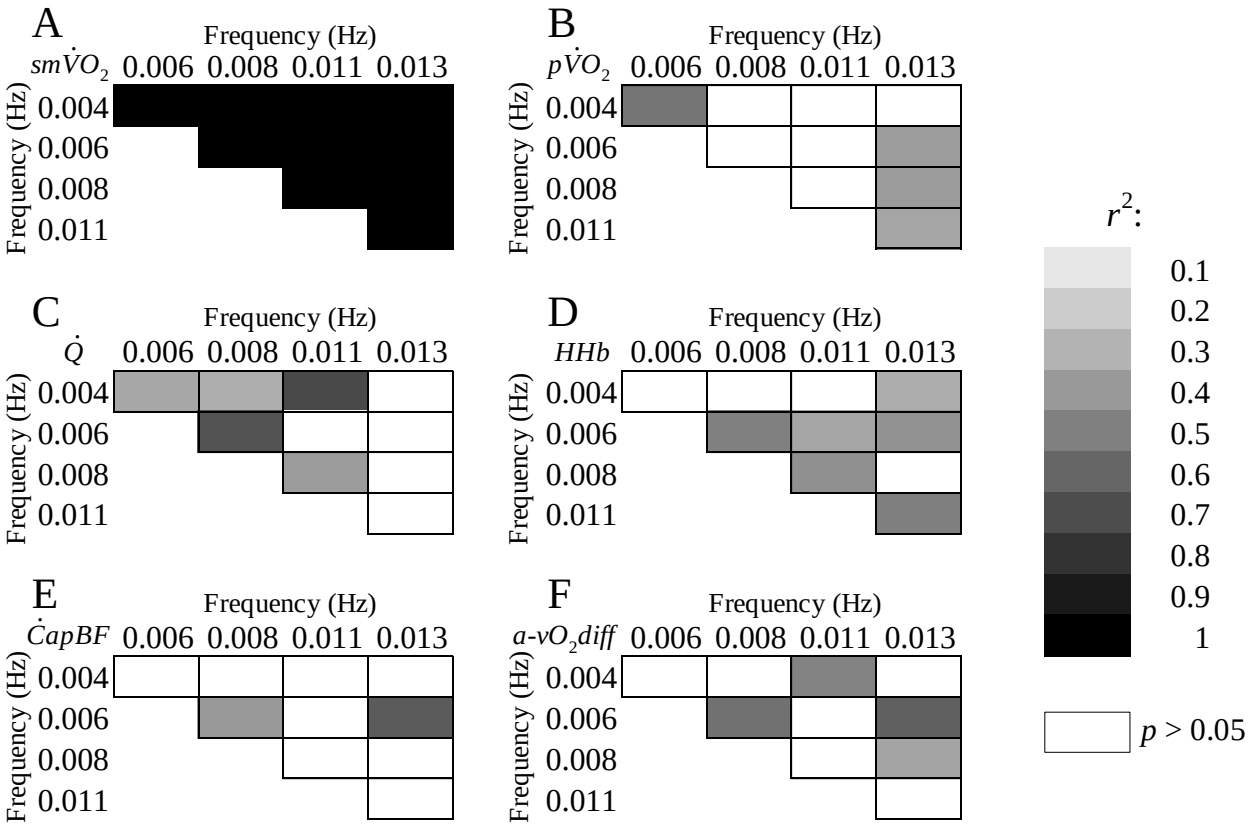

Figure 15. Linearity assessment by coefficient of determination.
Graphs of the coefficient of determination (r^2) between the normalized system gain obtained at different frequencies (0.004, 0.006, 0.008, 0.011 and 0.013 Hz). The r^2 and the p-values indicate the ability of a given normalized system gain to predict another normalized system gain at a different frequency. These comparisons were performed to evaluate the linearity of the dynamics of the simulated muscular oxygen uptake (A, $sm\dot{V}O_2$), pulmonary oxygen uptake (B, $p\dot{V}O_2$), cardiac output (C, $\dot{Q}$) and deoxy-hemoglobin concentration (D, $[HHb]$), capillary blood flow (E, $\dot{C}apBF$) and total arteriovenous O_2 difference (F, $a-vO_2diff$). In a first-order linear system, participants who present faster dynamics at a specific frequency should also present faster dynamics at any other frequency. For a better visualization, the r^2 values were transformed into a black color spectrum where lower values are lighter and higher values darker. White cells mean that the agreement level did not reach statistical significance ($p > 0.05$).

Figure 16 displays the ability of a given $\hat{A}mp_h$ to predict the overall response (i.e., MNG calculated excluding the $\hat{A}mp_h$ being tested). Like Figure 15, the predictability levels were assessed by the r^2 and p values. As expected, the $sm\dot{V}O_2$-$\hat{A}mp$ response at any frequency can predict the dynamics of the rest of the response (characterized by the MNG). The $p\dot{V}O_2$-$\hat{A}mp_h$ at frequency 0.011 Hz was not able to predict the MNG estimated from the others frequencies. The $\dot{Q}$- and HHb-$\hat{A}mp_h$ were not able to predict the MNG at the last and first frequency tested, respectively. The $\dot{C}apBF$ presented the most irregular behaviour. Only the $\dot{C}apBF$ - $\hat{A}mp_h$ obtained at 0.006 and 0.013 Hz were able to predict the dynamics of the rest of the response (i.e., MNG). The $a - vO_2diff$-$\hat{A}mp_h$ at frequency 0.011 Hz was not able to predict the MNG.

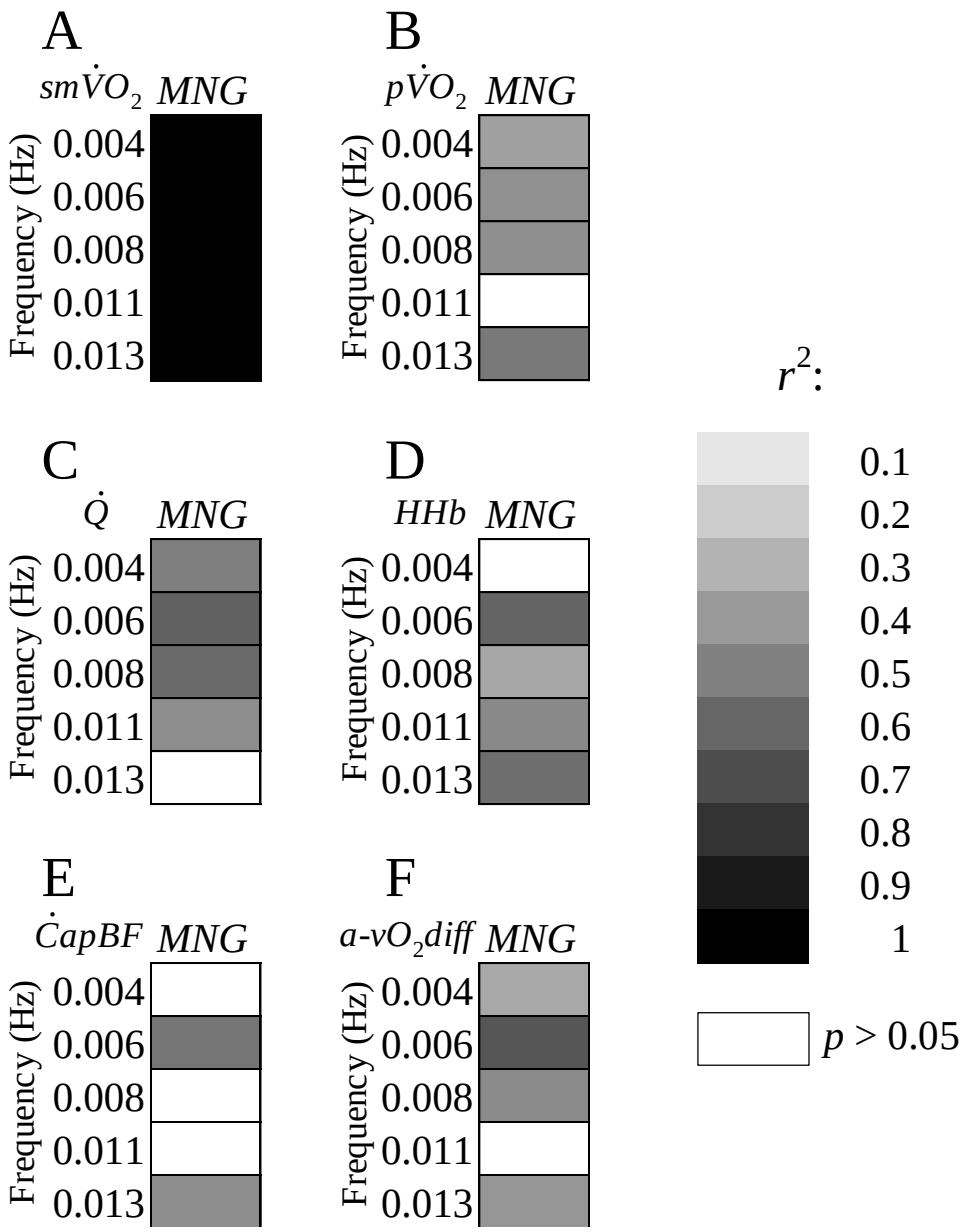

Figure 16. Linearity and mean normalized gain.
Graphs of the coefficient of determination (r^2) between the normalized system gain obtained at different frequencies (0.004, 0.006, 0.008, 0.011 and 0.013 Hz) and the mean normalized gain (MNG) calculated as the mean of the normalized system gain of all frequencies except the frequency to be tested. The r^2 was used to assess the ability of a given normalized system gain at a specific frequency to predict the MNG. These comparisons were performed to evaluate the dynamics of the simulated muscular oxygen uptake (A, $sm\dot{V}O_2$), pulmonary oxygen uptake (B, $p\dot{V}O_2$), cardiac output (C, $\dot{Q}$) and deoxy-hemoglobin concentration (D, $[HHb]$), capillary blood flow (E, $\dot{C}apBF$) and total arteriovenous O_2 difference (F, $a-vO_2diff$). In a first-order linear system, participants who present faster dynamics at a specific frequency should also present faster dynamics of the rest of the response (characterized by the MNG). For a better visualization, the r^2 values were transformed into a black color spectrum where lower values are lighter and higher values darker. White cells mean that the agreement level did not reach statistical significance ($p > 0.05$).

2.6 Discussion

In agreement with our primary hypothesis, the O_2 delivery-utilization balance in response to a dynamic exercise stimulus was not linear across the tested frequencies. As the MNG is composed by multiple-order responses, we experimentally demonstrated that the time constant estimated from time domain analysis (such as MRT) is in fact a simple abstraction of responses with variable temporal dynamics. The peripheral and central O_2 extraction dynamics (HHb and $a - vO_2diff$, respectively) were systematically faster than the peripheral and central O_2 delivery ($\dot{C}apBF$ and $\dot{Q}$, respectively).

The current study employed novel analyses in the frequency domain referenced to *in silico* data ($sm\dot{V}O_2$) to reinforce the elevated complexity of the aerobic system response to exercise. We demonstrated that the overall $p\dot{V}O_2$ kinetics, can be decomposed to multiple-order kinetics (Figure 9 and 10). The frequency range (0.002 to 0.013 Hz) used in this study represented a realistic exercise stimulus which corresponded to a sinusoidal function with a period range of 77 to 450s.

2.6.1 Speed of the System Output Responses

The speed of the output responses for a given stimulus at a given frequency was investigated by comparing the $\hat{A}mp_h$ between variables. As a normalized index, the $\hat{A}mp_h$ separates the temporal dynamics of the system from the static system gain (Hoffmann et al., 1992). Therefore, faster responses will present higher $\hat{A}mp_h$ values independently of the static system gain.

The O_2 extraction dynamics at both, peripheral (HHb) and central ($a - vO_2diff$) compartments, were faster than the *in silico* data across all tested frequencies (Figures 11 and 12). The speed of the aerobic system dynamics was not statistically different ($p > 0.05$) from the central O_2 delivery at all tested frequencies (Figure 11). The $\dot{Q}$ responses, that represent the central O_2

delivery, were slower than the peripheral O_2 extraction, evaluated by the $[HHb]$ dynamics, at all tested frequencies. In addition, the $\dot{C}apBF$ responses, that represent the peripheral O_2 delivery, were slower than the alveolar O_2 extraction, represented by the $a - vO_2diff$ dynamics, at lower frequencies. These data together suggest that O_2 extraction kinetics were in general faster than the aerobic adjustment, suggesting a lack of O_2 provision which would be consistent with observations in the time domain (DeLorey, Kowalchuk, & Paterson, 2003). In agreement with our findings within each frequency, the overall temporal dynamics evaluated by the MNG (Figure 13) showed systematically faster kinetics for the O_2 extraction in comparison to the O_2 delivery and uptake. In addition, like the MRT obtained in time-domain analysis, the use of the MNG to characterize the temporal dynamics of the aerobic response based on $p\dot{V}O_2$ signal can be used to describe the overall system temporal dynamics analysis (Figure 9).

2.6.2 Linearity of the System Output Responses

The linearity of the output responses was tested by estimating the ability of a given $\hat{A}mp_h$ to predict another $\hat{A}mp_h$ at different frequencies as a method to assess the commutability of the dynamics measure at different frequencies. In addition, we tested the ability of a given $\hat{A}mp_h$ to predict the MNG. The r^2 and p value of a linear regression model were used for this evaluation.

In agreement with Koga et al. (Koga, Rossiter, Heinonen, Musch, & Poole, 2014), the local O_2 delivery presented the lowest degree of linearity (Figures 15 and 16). This might indicate that attempts to fit the $\dot{C}apBF$ response into first-order models (Ferreira et al., 2005; Harper, Ferreira, Lutjemeier, Townsend, & Barstow, 2006), that refer to the "fundamental phase" of the $p\dot{V}O_2$ response, may fail to characterize "physiological" events but rather represent an aggregate of multiple-order responses that are treated as the local O_2 delivery dynamics. This observation

indicates some advantages of the frequency-domain approach in the sense of offering a more detailed description of the system dynamics resulting from the provision of optimal energy to study multiple-frequencies simultaneously with the PRBS protocol.

Non-linearities were also identified in all other variables (Figure 15). As indicated in Figure 16, in at least one frequency the output temporal dynamics, characterized by the $\hat{A}mp_h$, failed to predict the dynamic of the rest of the response (MNG). However, the presence of non-linearities in a physiological response does not mean that the overall system temporal dynamics (aggregated of multiple-order responses) cannot be used to investigate health-related outcomes. For example, it is well described in literature (Chilibeck et al., 1995; Eßfeld et al., 1987; Powers et al., 1985; Yoshida, Abe, Fukuoka, & Hughson, 2008) that the overall dynamics of the $p\dot{V}O_2$ response varies according to fitness status and it was previously associated with clinical outcomes (Borghi-Silva et al., 2012) and functional mobility performance (Alexander et al., 2003).

The presence of non-linearities points to the question of whether there is a single controller that limits the aerobic adjustment during different stimulus frequencies or within the same exercise transitions (Hughson, 2009). Classically, the discussion of the mechanisms that limit the aerobic adjustment are based on the "O_2 delivery *vs.* O_2 utilization" issue (Tschakovsky & Hughson, 1999) with part of the literature supporting one or another factor. However, it is becoming clearer (Hughson, 2009; Keir et al., 2016) that models that consider the complex interaction between O_2 delivery and utilization are more appropriate to study aerobic system dynamics. In fact, we showed that the overall $p\dot{V}O_2$ dynamic is composed of a complex interaction between multiple-order systems and it seems illusory to believe that there is a single controller that defines the rate at which the aerobic system will supply the energetic demand.

Despite different HHb data modeling approaches, our findings are in agreement with previous studies (Bowen et al., 2013; Dumanoir, Delorey, Kowalchuk, & Paterson, 2010; Harper et al., 2006) that reported a HHb overshooting during exercise transition, highlighting an increased data complexity. To solve this, some methods were developed to select the best [HHb] data window related to the muscular $\dot{V}O_2$, where the data apparently fit a first-order exponential-like function within the transition phase (Murias, Spencer, Kowalchuk, & Paterson, 2011b). However, instead of taking the same approach of searching for the best data window for all non-linear variables, the system analysis in the frequency domain in association with the PRBS protocol of the current study provides an alternative to achieve greater information. If a detailed response is needed, the $\hat{A}mp_h$ at each individual frequency can be analyzed, otherwise, the overall system temporal dynamics can be obtained from the MNG calculation.

An important advantage of the frequency-domain analysis is that no model assumptions are taken before data fitting. This approach allows the data to express the inherent degree of complexity across the different frequency gain amplitudes. In contrast, the time-domain approach has to assume the system transfer function characteristics and order beforehand (Motulsky & Ransnas, 1987). Theoretically, time-domain forcing functions can incorporate multiple components to increase model complexity (Bell, Paterson, Kowalchuk, Padilla, & Cunningham, 2001). However, the elevated model degree of freedom associated to a limited signal-to-noise ratio usually precludes this approach.

Data simulations have been used to test hypotheses regarding $p\dot{V}O_2$ control (Barstow et al., 1990; Bowen et al., 2011; Cochrane & Hughson, 1992; Eßfeld et al., 1991; Hoffmann et al., 2013). The current study utilized the $p\dot{V}O_2$ response to a low frequency square input (longest step inside the PRBS) of each participant to generate, for him, purely linear responses to the PRBS

exercise. The *in silico* output dynamics of $sm\dot{V}O_2$ are predictable at any frequency by the input through a single exponential transfer function with single temporal system dynamics (Figures 15A and 16A). In contrast to this "predictable" system, all variables presented a certain degree of non-linearity, especially the $\dot{C}apBF$. As hypothesized by Hughson (Hughson, 2009), these observations imply that the time course at a specific portion of the response is not similar and possibly not controlled by the same underlying regulatory factor(s) that establish the time course at another phase of the adaptive response.

2.7 Limitations

As a characteristic of PRBS protocol that evaluates multiple frequencies simultaneously, the system input ($\dot{W}$) also occurs at elevated metabolic rates (as depicted in Figure 10A). As previously reported (Brittain et al., 2001; Hughson & Morrissey, 1982; Keir et al., 2016), the $p\dot{V}O_2$ kinetics are delayed by a higher initial metabolic rate. However, the $p\dot{V}O_2$ temporal dynamics were similar to the *in silico* data that were dynamically invariant across the $\dot{W}$ transitions. In addition, a previous study (Hoffmann et al., 1992) demonstrated that the multi-frequency PRBS protocol was virtually similar to a sinusoidal exercise protocol initiated from a constant metabolic rate. In addition, evident nonlinearities caused by an elevated metabolic rate might be present at higher frequencies not considered in the current study (i.e., periods shorter than 77s).

The Modelflow algorithm, used to estimate the $\dot{Q}$ (and consequently $a - vO_2diff$), might present bias in comparison to $\dot{Q}$ estimated from other methods (Dyson, Shoemaker, Arbeille, & Hughson, 2010) when changes in the total peripheral resistance is expected as during exercise. However, previous studies validated the use of Modelflow $\dot{Q}$ during dynamic exercise (Faisal et al., 2009; Sugawara et al., 2003). In addition, the current study used relative $\dot{Q}$ values (normalized

response in frequency domain) thus linear bias should not influence the temporal dynamic of the $\dot{Q}$ response.

The HHb response has been extensively used to investigate the local O_2 extraction dynamics (Dumanoir et al., 2010; Keir et al., 2016; Murias et al., 2011b) and when evaluated together with $p\dot{V}O_2$ data, can be used to infer the local $\dot{C}apBF$ (Buchheit et al., 2009; Ferreira et al., 2005). As a characteristic of the NIRS device used in this study, the interpretation of the HHb was constrained to its relative changes from a given baseline. However, as with $\dot{Q}$, the HHb data were normalized when submitted to the proposed frequency-domain analysis. Therefore, since the focus of this study was the dynamic response of the variables, the temporal dynamics of the NIRS signals were reliable.

2.8 Conclusion

In agreement with our hypothesis, the aerobic response behaved as a nonlinear phenomenon possibly governed the complex multiple-order interactions between the O_2 delivery and utilization systems. To the best of our knowledge, this is the first study that evaluated $\dot{Q}$ and $[HHb]$ responses during random exercise stimulus in humans, thereby incorporating measurements of central and peripheral cardiovascular responses into an investigation of the $p\dot{V}O_2$ linearity. This study demonstrated the potential of the MNG to characterize the overall temporal dynamics of the aerobic system based on random $p\dot{V}O_2$ data which have clinical relevance. However, indexes such as MNG and MRT ignore the system nonlinearity since the $p\dot{V}O_2$ dynamics during exercise transitions are composed of amalgamated responses of multiple-order systems related to the O_2 delivery and utilization systems acting simultaneously to supply the energy demand that often cannot be isolated when applying pre-conceived models (Hughson, 2009). In the current study,

characterization of system dynamics across the frequency spectrum by investigating the relationships between the $\hat{A}mp_h$ revealed these nonlinearities. Therefore, indices such as τ, MRT and MNG cannot be used as a detailed system dynamics index but as an overall description of the system temporal dynamics.

Chapter 3: Mean Normalized Gain: A New Method for the Assessment of the Aerobic System Temporal Dynamics During Randomly Varying Exercise in Humans

This chapter was under review as:

Beltrame T, Hughson RL. Mean normalized gain: a new method for the assessment of the aerobic system temporal dynamics during randomly varying exercise in humans. Under review at J Appl Physiol since September 6, 2016

3.1 Overview

The temporal dynamics of the oxygen uptake ($\dot{V}O_2$) during moderate exercise has classically been related to physical fitness and a slower $\dot{V}O_2$ dynamics was associated with deterioration of physical health. However, methods that better characterize the aerobic system temporal dynamics data remain challenging. The purpose of this study was to develop a new method to systematically characterize the $\dot{V}O_2$ temporal dynamics. Nine healthy, young adults (23 ± 2 years old, 171 ± 5 cm and 75 ± 14 kg) participated in this study. They performed multiple pseudorandom binary sequence cycling protocols on different days and time of the day. This new index (named mean normalized gain amplitude, MNG) was based on the normalized amplitude of the $\dot{V}O_2$ signal in frequency-domain. The MNG was validated considering the time constant τ obtained from time-domain analysis as reference. The intra-subject consistency of the MNG was checked by testing the same participant on different days and times of the day. The MNG and τ were strongly negative correlated (r=-0.75 and p=0.019). The MNG measured on different days and periods of the day were similar between conditions. Calculations for the MNG have inherent filtering characteristics enhancing reliability for the evaluation of the aerobic system temporal dynamics. In conclusion, the present study successfully validated the use of the MNG for a precise aerobic system analysis and as a potential tool to assess changes in physical fitness.

3.2 New & Noteworthy

The temporal characteristics of the oxygen uptake ($\dot{V}O_2$) dynamic during moderate exercise have previously been related to maximal aerobic power and a faster $\dot{V}O_2$ response was associated with a better aerobic fitness, functional mobility and disease prognosis. This study introduced and

validated a new method to assess $\dot{V}O_2$ dynamics in random exercises more typical of daily life with potential importance to rehabilitation programs, exercise prescription and fitness evaluation.

3.3 Introduction

The study of the oxygen uptake ($\dot{V}O_2$) kinetics deals with the ability of data modeling to describe, in mathematical terms, the temporal characteristics of the aerobic response to the challenge of a step increase in work rate ($\dot{W}$) (Hughson, 2009). Time-domain kinetic analysis has several limitations including the need for explicit complex modeling techniques (Bell et al., 2001; Markovitz, Sayre, Storer, & Cooper, 2004). Moreover, the white Gaussian noise associated with breath-by-breath fluctuation (Lamarra et al., 1987) adds uncertainty to time-domain index predictions estimated from a single test dataset. To increase signal-to-noise ratio, studies commonly repeat similar tests multiple times within the same session (Christensen et al., 2016; Ozyener et al., 2001) or on different days (Keir, Nederveen, Paterson, & Kowalchuk, 2014; Whipp et al., 1982) and average repetition-like transitions before time-domain data modeling.

An attractive alternative for evaluating the kinetic behavior of the aerobic energy supply system is the pseudo-random binary sequence (PRBS) in which $\dot{W}$ varies between two levels which are normally constrained to the light to moderate intensity exercise domains (Eßfeld et al., 1987; Hughson et al., 1990). The $\dot{V}O_2$ response to PRBS protocols is evaluated in the frequency-domain filtering out non-periodic signals associated with noise, improving the extraction of parameters related to the aerobic system dynamics. The attractiveness of the PRBS approach results from the potential to gain a quantitative index of kinetics from fewer exercise testing sessions in comparison to time-domain approaches (Edwards, Challis, Chapman, Claxton, & Fysh, 2001; Hughson, Xing, Borkhoff, & Butler, 1991; Yoshida et al., 2008).

To date, there are few studies of the variability of the methodology and the requirements for precision in estimation from PRBS testing (Edwards et al., 2001; Edwards, Claxton, & Fysh, 2003). The purpose of this study was to systematically characterize the $\dot{V}O_2$ kinetics by a new index (named mean normalized gain amplitude, MNG) obtained from frequency domain analysis. The MNG will be validated against the time-domain approach, and checked for intra-subject consistency by applying multiple PRBS protocols on different days and times of the day. In addition, the MNG was also evaluated considering different number of repeated tests averaged together before data modeling and different filtering levels.

The hypothesis of this study was that the $\dot{V}O_2$ dynamics characterized by MNG during random exercise would be similar to the dynamics indices obtained by time-domain analysis, even with fewer exercise repetitions. In addition, we hypothesized that MNG was independent of the testing day and the time of the day, demonstrating therefore that it can be used to evaluate the individual aerobic response during random exercise in humans. These results could set the stage for advancing frequency domain analyses outside the confines of the research laboratory to assess kinetics, and therefore an index of physical fitness, in activities common to daily living or athletic training.

3.4 Methods

3.4.1 Study Design

Nine healthy, young adults (23 ± 2 years old, 171 ± 5 cm and 75 ± 14 kg), who were not athletically trained, participated in this study. All participants visited the laboratory four separate times to complete submaximal exercise protocols. The study was approved by the Office of Human Research of the University of Waterloo and was in agreement with Declaration of Helsinki.

On each visit, three successive PRBS sequences were completed in a single, continuous session. The signal related to the first PRBS in each visit was excluded *a priori* as a warm-up (Hughson et al., 1990) and the remaining PRBS (1 to 8) were considered under separate conditions defined by their time of day (morning and afternoon, separated by six hours) and by their different days (1 and 2, separated by one week). The tests were subsequently analyzed by condition and by the method of pre-processing including moving average and multiple tests averaging (see Table 3).

Table 3. Description of the pseudorandom binary sequence (PRBS) protocols used to test the influence of some conditions and data pre-processing.

			PRBS evaluated	Repetitions
Condition	**Time of the day**	**Morning**	Average of 1+2+5+6	4
		Afternoon	Average of 3+4+7+8	4
	Day	**1**	Average of 1+2+3+4	4
		2	Average of 5+6+7+8	4
Pre-processing	**Moving average**	**3**	1	1
		5	1	1
		7	1	1
	Repetitions	**1**	1	1
		2	Average of 1+2	2
		3	Average of 1+2+3	3
		4	Average of 1+2+3+4	4
		5	Average of 1+2+3+4+5	5
		6	Average of 1+2+3+4+5+6	6
		7	Average of 1+2+3+4+5+6+7	7
		8	Average of 1+2+3+4+5+6+7+8	8

3.4.2 Pseudorandom Binary Sequence Exercise Test (PRBS)

All exercise tests were performed on an electrically braked cycle ergometer controlled by an external, pre-programmed module (Lode Excalibur Sport, Lode B.V., Groningen, Netherlands). The PRBS protocol (Figure 17B) was generated by a digital shift register with an adder module feedback (Bennett et al., 1981) (Figure 17A). The target $\dot{W}$ (reached after <1.5 s of transition

following a modification of the ergometer controller) was 25 or 100 W, and the cadence was maintained at ~1 Hz. As described in Figure 17, the PRBS protocol comprised 15 units (25 or 100 W) for 30 s (total of 450 s for each PRBS).

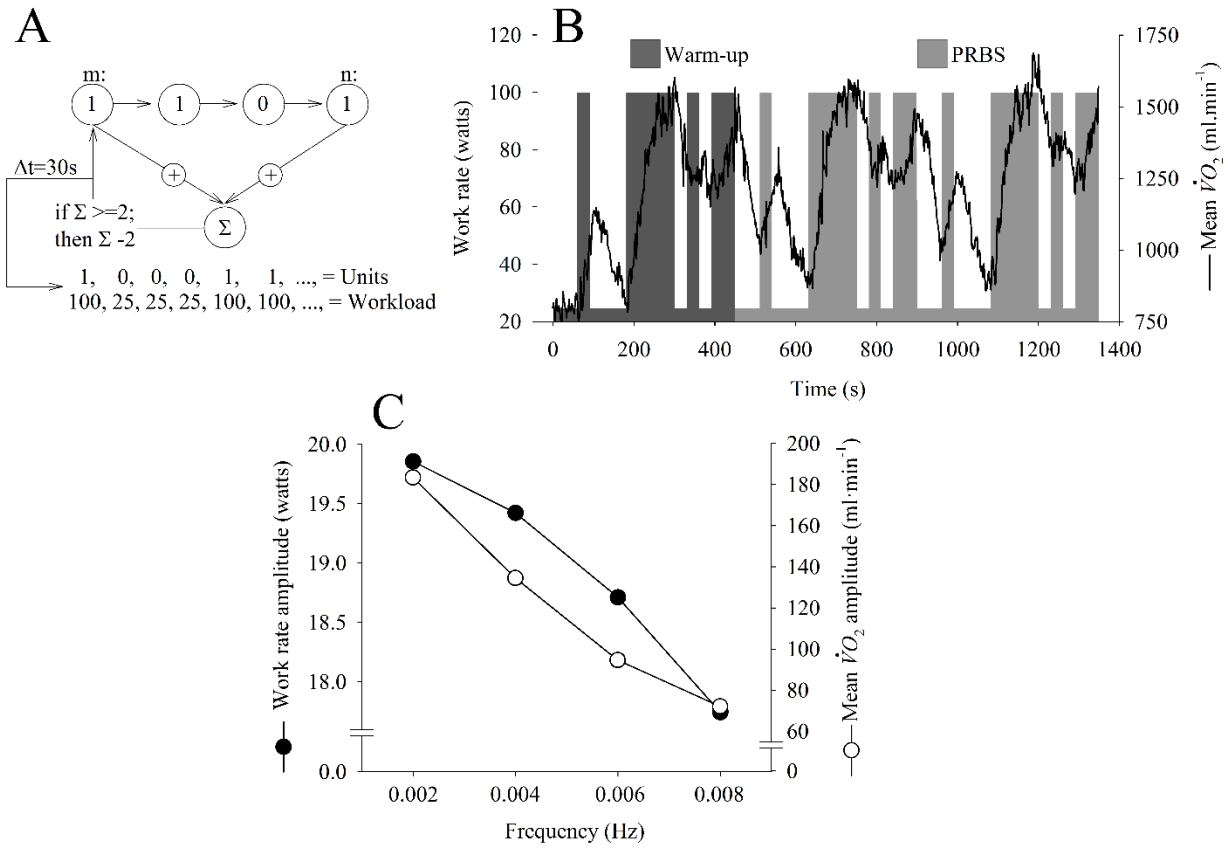

Figure 17. Pseudorandom binary sequence protocol.
A: illustration of the 4-stage shift register used to generate the pseudorandom binary sequence protocol (PRBS). The module addition feedback (Σ) sums the first and fourth stage values and tests the "if" statement. The value is then inserted into the first stage and the entire system shifts to the right, and the sequence repeats after 15 values. Each unit is maintained for 30s to create the PRBS protocol in the time domain (B). The system input stimulates the oxygen uptake ($\dot{V}O_2$) response (—), here represented by the mean signal of all participants (n=9) during the first visit. C: Fourier transformations were used to convert the time-domain responses (B) into amplitudes at specific range of frequencies.

3.4.3 Data Acquisition and Analysis

The $\dot{V}O_2$ data were measured breath-by-breath by the V_{max} system (CareFusion, San Diego, CA, US) that estimates the air volume through a low resistance mass flow sensor (accuracy of > 97%), the O_2 pressure by an electro-chemical cell (accuracy of > 99%), and the CO_2 pressure by an infrared light with a thermopile (accuracy of > 99%). For one participant, the breath-by-breath $\dot{V}O_2$ data were measured by a portable metabolic system (K4b^2, COSMED, Italy). The COSMED system gas analysis is based on a chemical galvanic O_2 sensors (accuracy of > 99%) and an infrared absorption CO_2 sensor (accuracy of > 99%). Air volumes was also measured by a low resistance turbine (accuracy of > 98%). The gas concentrations and air volume/flow were calibrated following manufacturer's specifications before each test.

3.4.4 Frequency Domain Analysis

The MNG was calculated based on the frequency-domain data transformation. Firstly, data from the input ($\dot{W}$) and output ($\dot{V}O_2$) were inputted to frequency-domain analysis using a Discrete Fourier Transformation algorithm. The following sinusoidal function was solved for each harmonic n (integer number):

Equation 4 $$\dot{V}O_{2(t)} = a_{DC} + 2 * \sum_{h=1}^{4}(A_h * cos(2\pi * h * f_1 * t) + B_h * sin(2\pi * h * f_1 * t));$$

where t is the time, a_{DC} is the system DC offset amplitude (i.e., average response), f_1 is the fundamental frequency (1/450 or 0.002 Hz in this case), A_h and B_h are the cosine and sine amplitudes for a given harmonic h, respectively. From A_h and B_h, the total amplitude (Amp) was computed for each h by:

Equation 5 $$Amp_n = \sqrt{A_h^2 + B_h^2}.$$

The system gains for each n ($gAmp_h$) were obtained by the ratio:

Equation 6 $$\dot{V}O_2Amp_h/\dot{W}Amp_h.$$

3.4.5 Isolating Temporal Dynamics From the Frequency Domain Responses

The system gains were normalized as a percentage of the Amp gain at the fundamental frequency (i.e, $gAmp_1$) (Hoffmann et al., 1994, 1992). Normalization isolates the temporal dynamics of the system by removing the influences of the total gain (i.e., steady-state gain) across the harmonic amplitudes. Therefore, based on the concept of the total harmonic distortion (Shmilovitz, 2005), the new index of system dynamics called mean normalized system gain (MNG, expressed in %) was obtained by:

Equation 7 $$MNG = (\sum_2^4 gAmp_h/3 * 100)/gAmp_1;$$

where the mean of the system gain amplitudes ($gAmp_h$) of the harmonics 2, 3 and 4 (h=2, 3 and 4) is normalized by the system gain of the fundamental harmonic ($gAmp_1$).

3.4.6 Time Domain Analysis

The time domain analysis of the $\dot{V}O_2$ data was conducted on a segment of the PRBS for comparison to the MNG obtained by frequency domain analysis. To reduce the uncorrelated

interbreath noise (Keir, Murias, et al., 2014; Lamarra et al., 1987), the $\dot{V}O_2$ signals were time aligned and ensemble-averaged to obtain a single response per participant from the eight PRBS (last condition described in Table 1). The data window length for time domain analysis included the final 10s of a 90s period of 25 W followed by 120s at 100 W (starting at the 120th second of the PRBS protocol). This exercise window corresponded to the longest period without input variation, thus the best window for time domain analysis within the PRBS protocol. The following equation was used to fit the $\dot{V}O_2$ data (Hughson & Morrissey, 1982; Whipp et al., 1982):

Equation 8

$$\dot{V}O_{2(t)} = a_0 + a\left(1 - e^{-(t-TD/\tau)}\right);$$

where t is time; a_0 is the baseline at 25 W; a is the steady state amplitude at 100 W; τ is time constant (i.e., the "speed" of the system) and TD is the time delay of the exponential function onset. The initial data associated to the cardio-dynamic component were excluded prior to data fitting. The mean response time (MRT) was calculated by adding τ and TD (Macdonald et al., 1997). The quality of the fitting was assured by the analysis of squared error, coefficient of determination (r^2), 95% confidence interval band (CI_{95}) (Fawkner et al., 2002; Keir et al., 2016) and the significance level (p value) of the estimated parameters.

3.4.7 MNG vs. Time Constant

Simulations of the $\dot{V}O_2$ response stimulated by PRBS input were performed in order to determine the relationship between the time constant (for the simulations denoted τ_s) and MNG, derived from time- and frequency-domain analysis, respectively. Similarly to τ_s, MNG should extract information regarding the $\dot{V}O_2$ system adaptation speed from random exercise stimulus which

ultimately is associated with aerobic fitness (Chilibeck et al., 1995; Hagberg et al., 1980; Hughson, 2009; Powers et al., 1985).

As previously described elsewhere (Hoffmann et al., 2013), an algorithm was created to simulate the $\dot{V}O_2$ response to PRBS considering the function described above in the ***Time domain analysis*** section. This algorithm assumed a linear static and dynamic $\dot{V}O_2$ gain (Eßfeld et al., 1991; Hoffmann et al., 1992) with no time delay, as expected in muscular $\dot{V}O_2$ response (Hoffmann et al., 2013). Firstly, ten simulations were generated by arbitrarily selecting different combinations between a_0 ($250<a_0<650$ ml·min^{-1}), a_1 ($125<a_1<400$ ml·min^{-1}) and τ_s ($15<\tau_s<52$ s) as described in Table 4. The average Amp gain between the analysed frequencies and the MNG are also described in Table 4. For further discussion, the physiological range of τ and τ_s was defined as $10<\tau$ and $\tau_s<100$ s.

Table 4. Description of the parameter used for the computer simulations and the parameters obtained by frequency-domain analysis.

Simulation	**1**	**2**	**3**	**4**	**5**	**6**	**7**	**8**	**9**	**10**
a_0 **(ml·min^{-1})**	300	400	350	250	200	150	125	350	250	330
a_1 **(ml·min^{-1})**	700	800	750	900	750	600	800	600	750	650
τ_s **(s)**	15	45	25	21	39	52	42	35	48	19
Average $gAmp$ **(ml.min^{-1}·$\dot{W}^{-1}$)**	7.9	5.2	7.0	9.0	5.4	3.5	5.5	4.6	4.6	6.8
MNG **(%)**	86	58	74	79	61	54	59	64	56	81

Abbreviations: a_0: baseline; a_1: steady state amplitude, τ_s: exponential time constant of the simulations, $gAmp$: gain amplitude and MNG: mean normalized gain amplitude.

The apparent system gains (Figure 18A) are dependent in the simulations on the values of a_0 and a_1 as well as τ_s. Thus, as shown in Figure 18B, the simple average of the absolute gains across the tested frequencies was not able to perfectly predict τ_s; however, the normalization method used to obtain the MNG was able to better isolate τ_s from the different system gains and baselines (Figure 18C). In addition to the simulations that used a physiological range of the parameters, more simulations were performed to further investigate the expected behaviour of the relationship between MNG and τ_s. These simulations (n=10) used a constant a_0 and a_1 but varied τ_s to extreme values (0.001, 0.1, 1, 5, 15, 35, 80, 200, 500 and 1500 s). Different combinations of harmonics (i.e., h's) to calculate MNG (derived from equation 7) were also tested. Specifically, the following combinations between n were tested for the MNG calculation: $2 \leq h \leq 3$, $2 \leq h \leq 4$, $2 \leq h \leq 5$ and $2 \leq h \leq 10$. The relationship between MNG and τ_s (Figure 18C and Figure 19) was described by a sigmoid function. The x-axis scale in figure 19 was converted to log_{10} for a better visualization of this relationship.

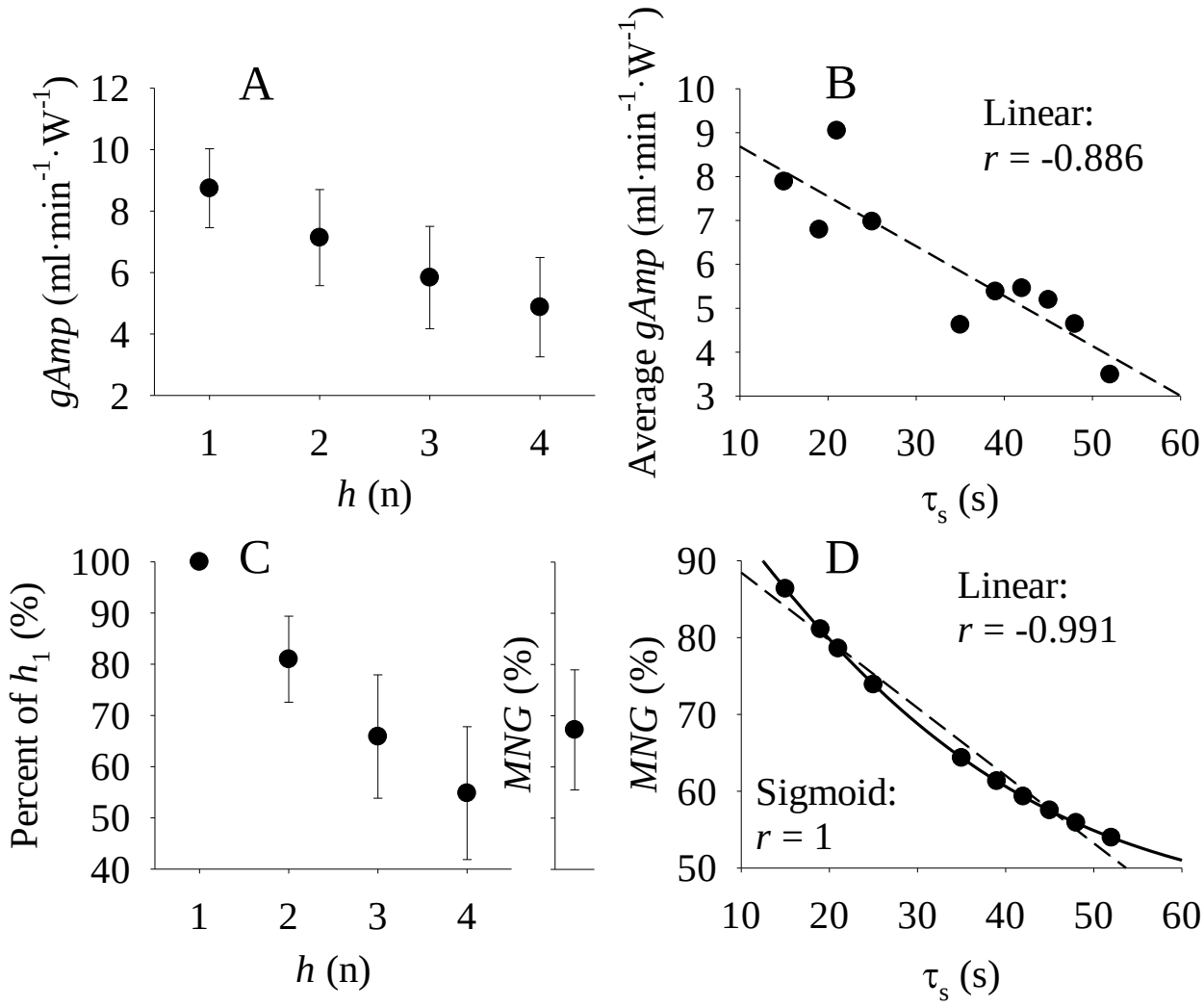

Figure 18. Simulated response in frequency domain.
A: mean ± SD of ten simulations of the system gain ($gAmp$) calculated in the frequency domain from data generated using different values of system time constants (τ_s), amplitudes and baselines (see Table 4). B: linear (— —) relationship between τ_s and the average absolute oxygen uptake gain between all tested harmonics (h) for each of the ten simulations. C: mean ± SD of data displayed in A normalized by the $gAmp$ at h_1. The mean normalized gain (MNG) was calculated as the mean of the $gAmp$ between h_2, $h_3$and h_4 (please see text and equation 7). D: relationship between τ_s and MNG. This relationship was fitted by a linear (— —) and sigmoid (——) function. Notice in D that the normalization procedure isolated the relationship between amplitude and τ_s from other sources of system distortion such as system gain and baseline. The correlation coefficient "r" was used to indicate the degree of correlation between τ_s and MNG. Please see text for further details regarding the sigmoid function.

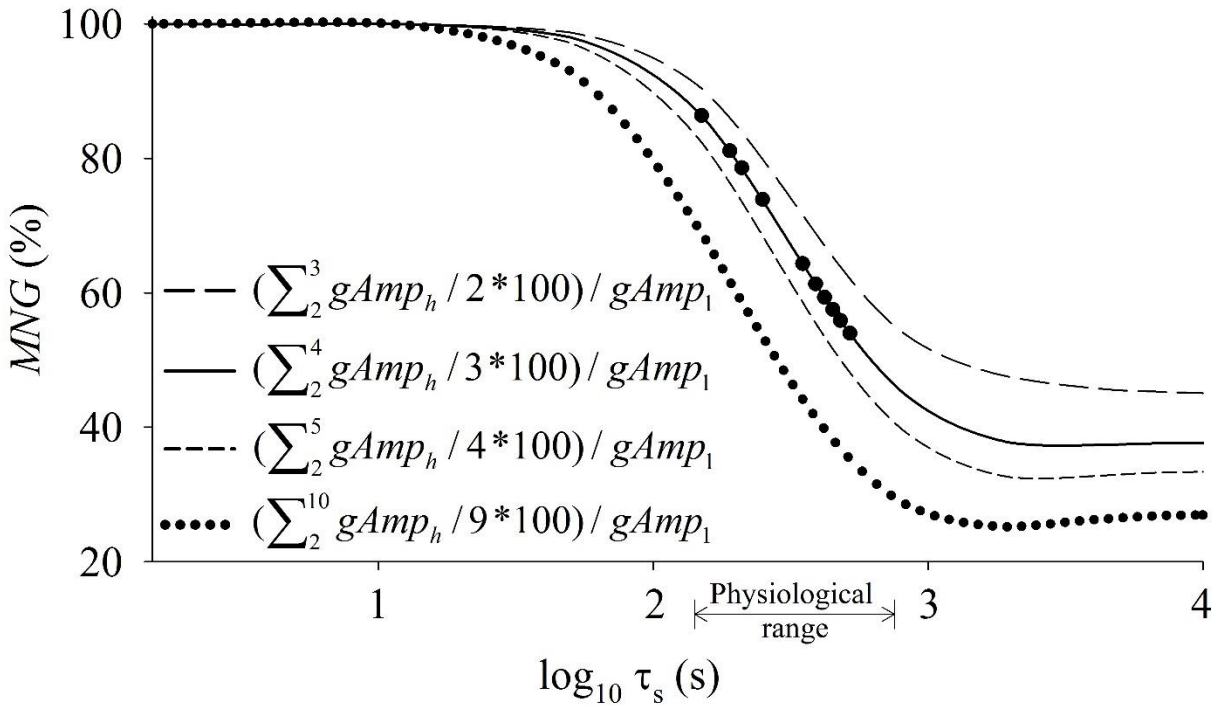

Figure 19. Computer simulations were performed to generate different oxygen uptake responses. Simulations considered different values of time constant (τ_s) that defines the speed of the oxygen uptake ($\dot{V}O_2$) adjustment to random exercise. The $\dot{V}O_2$ data were transformed to frequency domain and the mean normalized gain amplitude (MNG) was obtained considering the normalized system gain obtained from different frequency ranges. The equations describe how the MNG was obtained from the $\dot{V}O_2$ data. The x-axis scale was converted to log_{10} for a better visualization of the sigmoidal characteristics of the relationship between MNG and τ_s. The symbols "●" represent the simulated data from Figure 18C. Please see equation 8 and text for further details regarding the equation parameters and procedures. Notice that the linear portion of the sigmoid function is always located at the physiological portion of tau values (i.e., from 10 to 100 s).

If more normalized gains from the simulated linear systems are considered into MNG calculation (equations in Figure 19), the sigmoid is shifted to left and the plateau for longer τ_s became smaller. However, the physiological range (arrow in Figure 19) of τ_s was always located at the approximately-linear portion of the sigmoid, independently of the number of harmonics used to calculate MNG. The improvements (measured by the r value) from the sigmoidal to the linear fitting was minimal (or 0.9 % as displayed in Figure 18C). Therefore, considering the model degree of freedom, the physiological range in τ, and the error associated to the τ estimation from real data,

the relationship between MNG and τ was simplified to a linear relationship (— —, in Figure 18B and C). The system analysis of the current study was limited to the fourth harmonic (Figure 18A, h=4 or 0.008 Hz) because the $\dot{V}O_2$ data, and presumably the aerobic system response, can be analyzed as a first order linear system (Hoffmann et al., 1992). Kinetics analyses and data simulations were performed by a certified (#100-314-4110) LabVIEW associated developer (National Instruments, Austin, TX, US).

3.4.8 Statistical Analysis

According to Shapiro-Wilk test, most of the data were normally distributed. The MNG was compared between the different conditions (time of day, or different days) by paired t-test. One-way repeated measures analysis of variance (ANOVA) was used to compare the MNG obtained from different multiple test averaging repetitions and between different filtering levels. Student-Newman-Keuls method was selected for *post hoc* analysis. Paired t-test was used to compared the the individual CI_{95} and the squared error between different linear regrssions.

To compare the MNG obtained from different quantities of similar PRBS averaged together before data analysis, the eight-repetition signal was used as the "gold standard" since it was the dataset with the highest signal-to-noise ratio. The impact of the moving average filtering (Table 4) was assessed by comparing the different filtering levels applied over the first PRBS protocol signal with the raw signal from this same protocol. When appropriate, sample size was calculated using Student t-test or paired t-test as the test reference and considering the SD of the MNG with the power set at 0.8. The linear correlation was measured by Pearson product-moment correlation coefficient (r) and the agreement level was assessed by Bland-Altman plot and the CI_{95} (Altman & Bland, 1983). For all statistical tests, the null hypothesis was rejected at $p \leq 0.05$.

Statistical analysis was conducted in SigmaPlot 12.5 software (Systat Software, San Jose, CA, US).

3.5 Results

3.5.1 MNG vs. τ

The values and the representation of the parameters obtained by the time-domain kinetics analysis are displayed in Figure 20. As a reference, the mean $\dot{V}O_2$ response (n=9) in Figure 20 was fitted by an exponential function in the time-domain. The function TD was 16.66 ± 4.45 s.

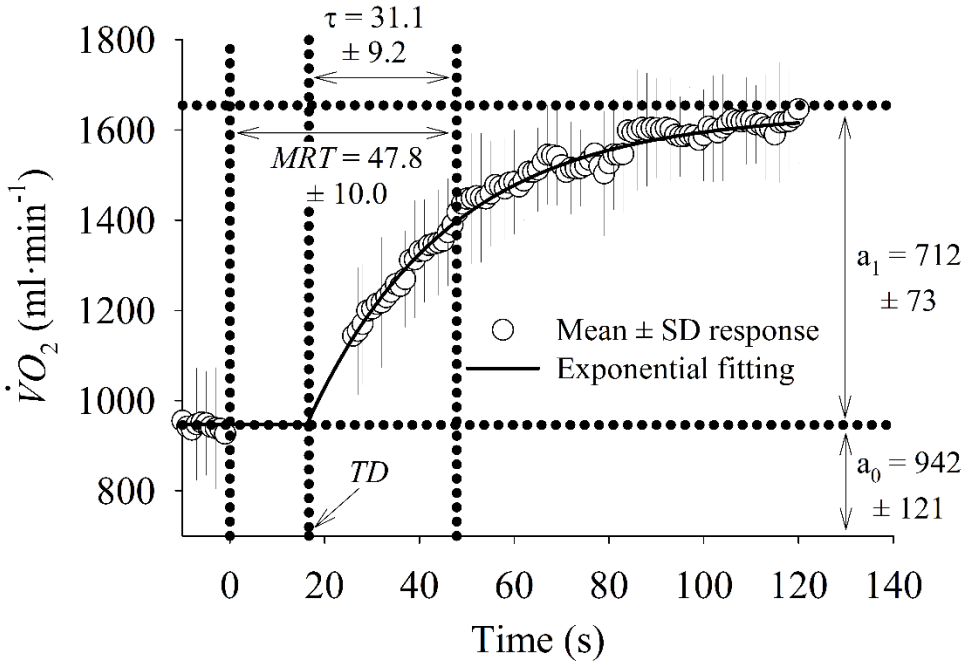

Figure 20. Oxygen uptake during transition.
Mean ± SD (vertical gray bars) of the oxygen uptake ($\dot{V}O_2$) response between all participants (n=9). In addition to the reference lines (•••), the mean response was fitted by a mono-exponential function (—) to demonstrate the parameters baseline (a_0), steady state response (a_1), time to reach 63% of the steady state (τ) after a given time delay (TD) and the mean response time (MRT or $TD + \tau$).

Figure 21 shows the correlation between τ and MNG obtained by time- and frequency-domain analysis, respectively. Both parameters were obtained based on eight-repetition dataset. For visual comparison, the simulated data displayed in Figure 18C are also plotted in Figure 21. The MNG of the experimental data were consistently less for all participants than the values obtained with the simulated data for any value of τ.

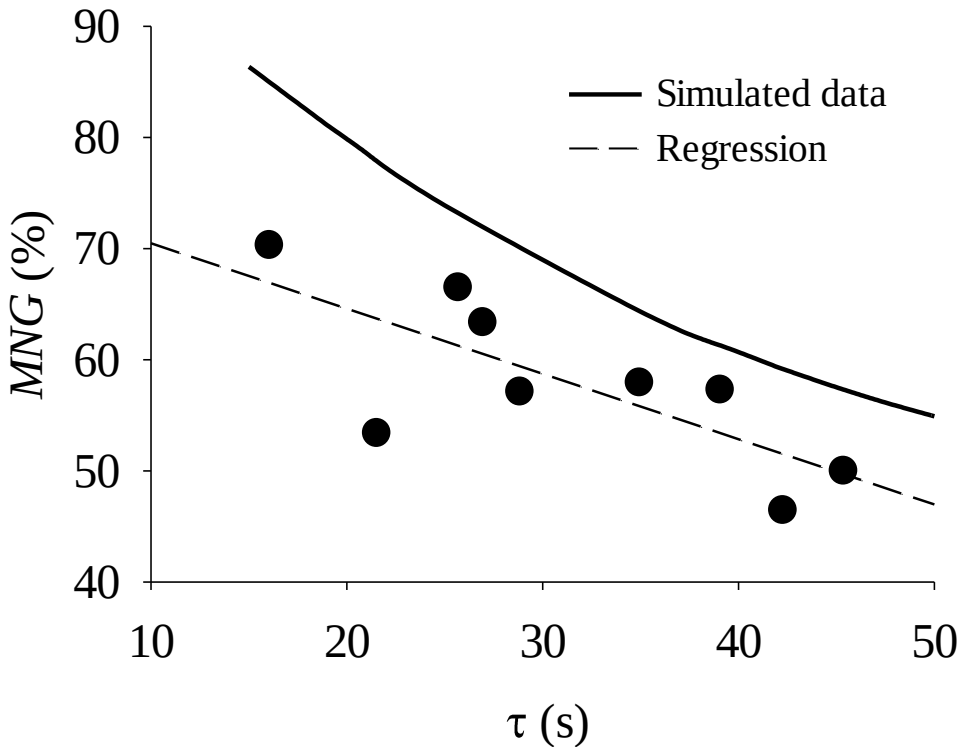

Figure 21. Time constant and mean normalized gain.
Relationship between time constant (τ) and mean normalized gain (MNG). The MNG and τ were obtained from eight repetitions of the pseudorandom binary sequence test is shown in comparison to the simulated data (solid line for MNG vs. τ_s as in Figure 18C). Correlation coefficient (r) = -0.754, p = 0.019 (n=9).

3.5.2 Influence of Time of Day and Between Days

The MNG was statistically similar between time of day (p=0.117) and between days (p=0.104). Figure 22 shows the relationship and the agreement level of the MNG obtained during the morning and afternoon (Figure 22A and C) and in different days (Figure 22B and D). The MNG was

strongly correlated between the time of day (morning *vs.* afternoon) and between days (day 1 *vs.* day 2). The bias of the MNG calculation represented 5.43 and 6.26 % of the total MNG variation during the different time of the day and between days, respectively. The CI_{95} were equivalent to 16.43 and 19.85 % of the total MNG variation of the sample for the different time of the day and between days, respectively.

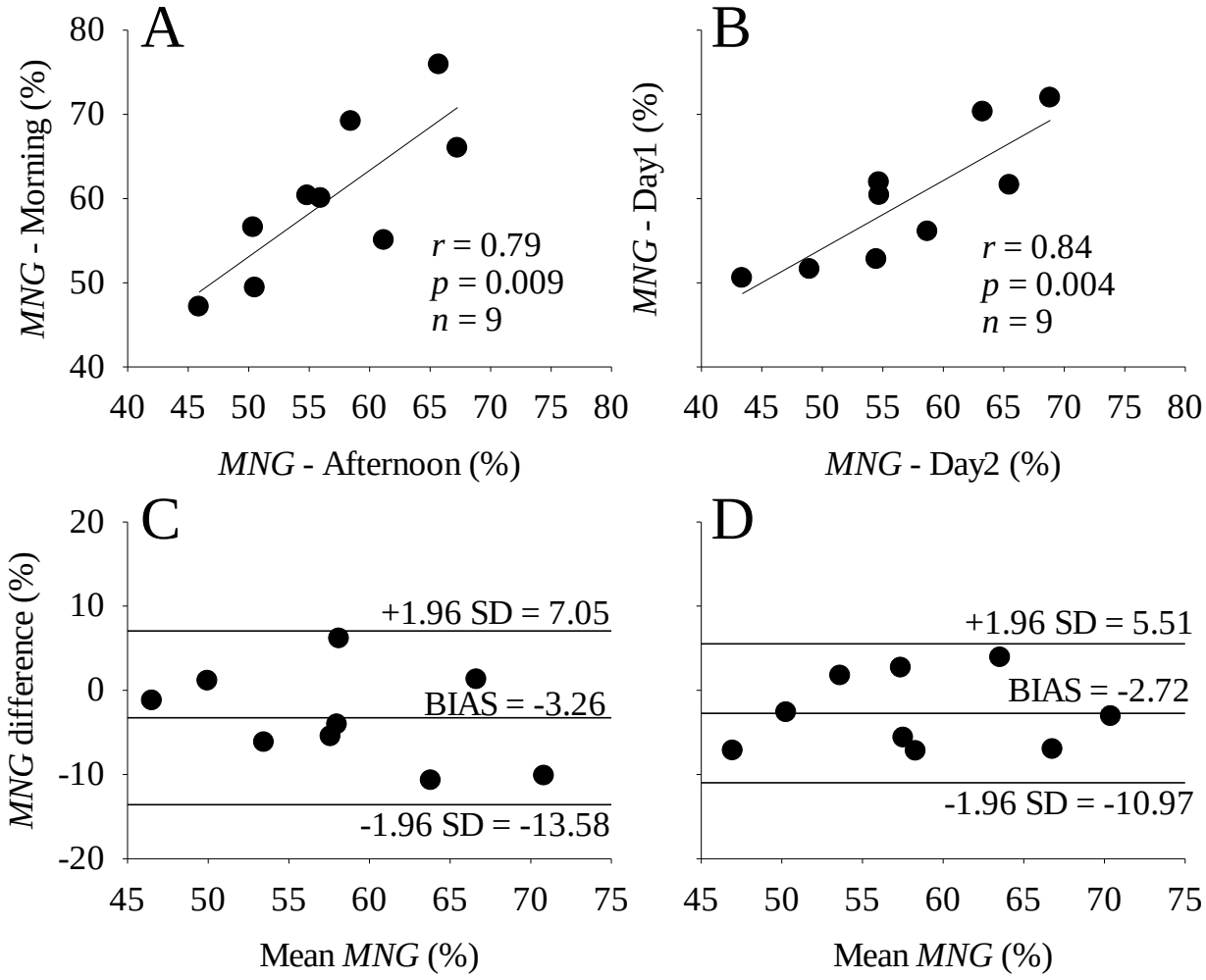

Figure 22. Mean normalized gain amplitude consistency.
Correlation between the mean normalized gain amplitude (MNG) estimated under the influence of different time of the day (A, Morning vs. Afternoon) and different day of testing (B, Day 1 vs. Day 2). The agreement level between the factors plotted in A and B are displayed in C and D, respectively. Abbreviation: r: Pearson's correlation level, p: statistical significance level and n: sample size.

3.5.3 Influence of the Averaging Level and Number of Repetitions

The different moving average filtering levels (3, 5 or 7) have not impacted the MNG estimation during the first PRBS protocol. The correlation coefficient r was 0.99 for all levels in comparison to the raw signal without filtering. In addition, the bias and the CI_{95} between all filtering levels and the raw signal was minimal (< ~1 %).

Figure 23A displays the correlation level between the MNG calculated based on the $\dot{V}O_2$ signal obtained from different number of exercise repetitions with the eight repetitions as reference. The correlation coefficient r stabilized at ~ 0.95 after three exercise repetitions. The average of more than two datasets seemed to be enough to reach statistical significance (Figure 22B) in comparison to eight repetitions. The bias (Figure 23C) of using a single dataset in comparison to eight repetitions was -3.7 % and became steady at ~ 0.9 % when more than two repetitions are considered. The CI_{95} (grey area in Figure 23C) progressively decreased as the number of repetitions increased but it stabilized after three repetitions.

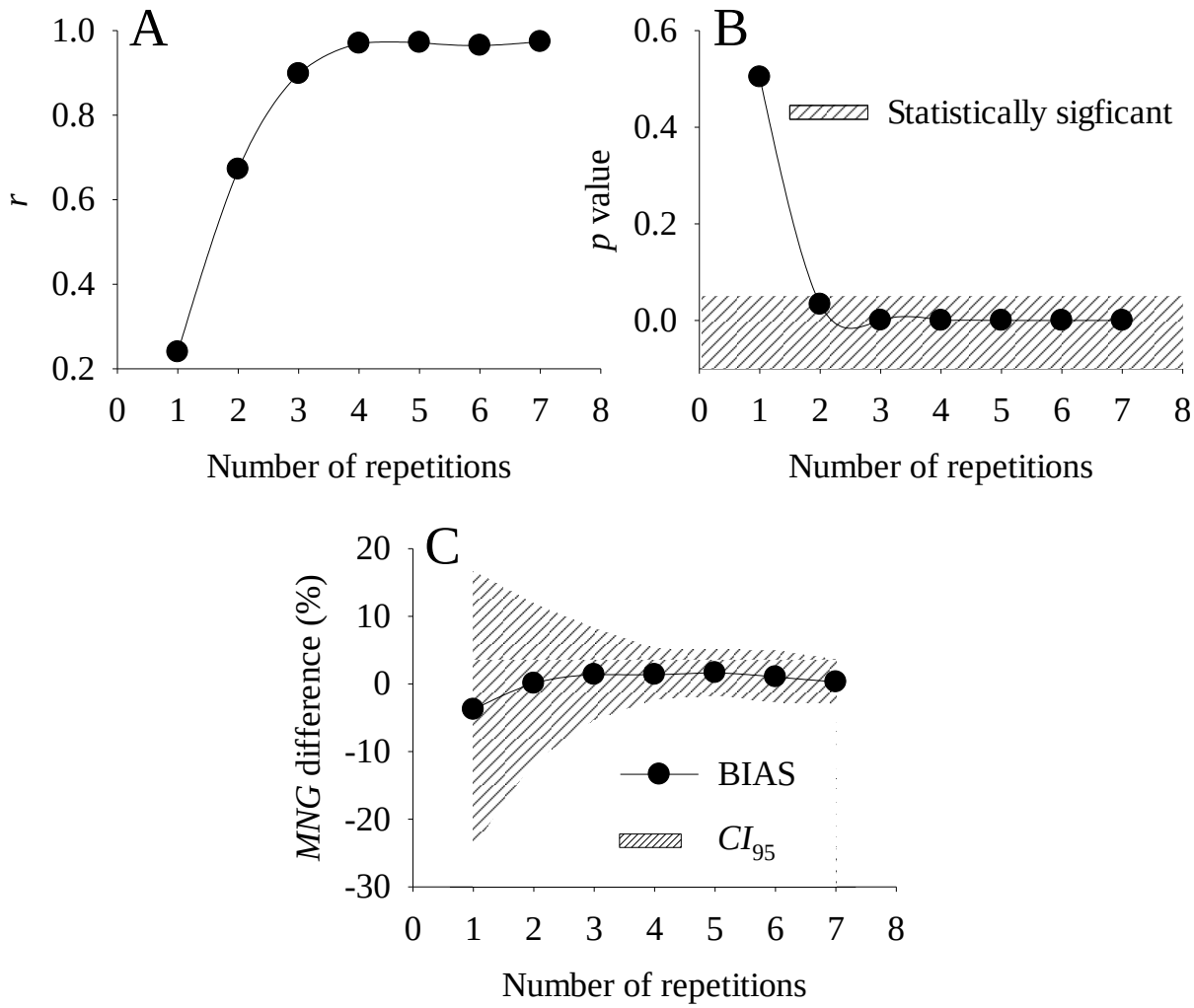

Figure 23. Mean normalized gain and exercise repetition.
Correlation coefficient (r) level (A), p value (B), bias and the limits of agreement (CI_{95}, C) of the mean normalized gain amplitude (MNG) estimated from different combination of exercise repetitions (1 to 7) with eight ensemble-averaged repetitions.

Figure 24 illustrates the sample size needed to find statistical significance for a given effect size (changes in MNG) by Student t-test (Figure 24A) or Paired t-test (Figure 24B) considering different number of repetitions averaged together before data analysis. The relationship between sample size and the effect size suggested an exponential-decay-like function.

The sample size was independent from the number of repetitions, except for the single repetition that apparently needs a higher effect size to be detected by statistical analysis. In addition, the sample size seemed to stabilize at ~10 participants after an effect size higher than ~8 %, independently of the number of repetitions.

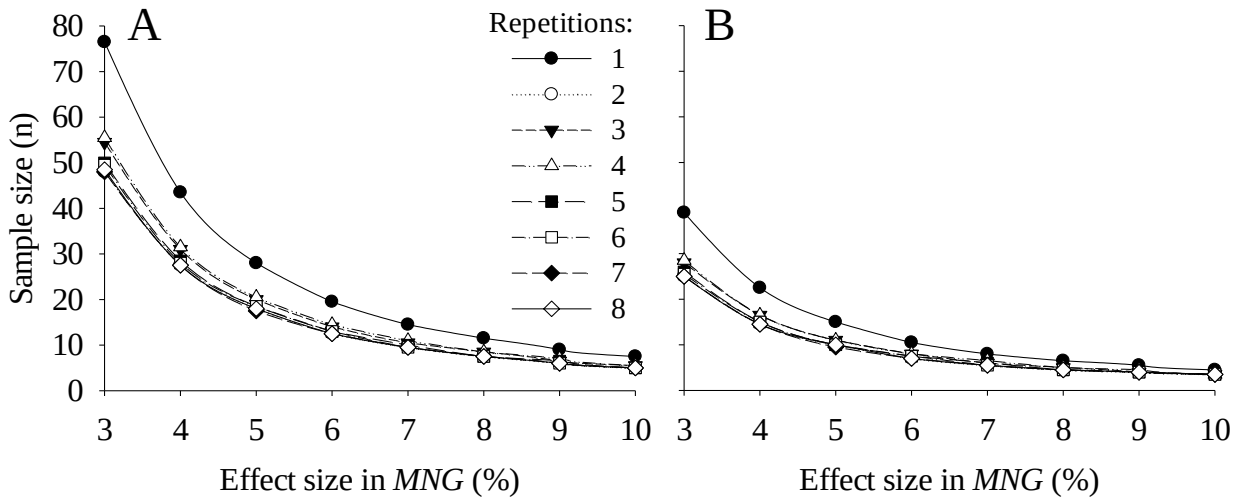

Figure 24. Effect size and mean normalized gain.
Relationship between the expected differences (effect size) in the mean normalized gain amplitude (MNG) and the sample size needed to find statistical significance by A: student t-test or B: paired t-test considering different number of exercise repetitions (symbols). The desired power and the significance level considered for the sample size calculations were 0.8 and 0.05, respectively.

3.6 Discussion

In agreement with our initial hypothesis, the calculation of mean normalized gain (MNG) was able to characterize the temporal dynamics of $\dot{V}O_2$ to random exercise input being strongly correlated with the time domain indicator, τ, obtained in the same persons. The MNG eliminates the expected differences in static gain between individuals by expressing the dynamic response as a percentage of the fundamental harmonic value. The comparison of MNG against the time-domain $\dot{V}O_2$ kinetics analysis was shown to be independent of the period of the day, the day of the test and the filtering

technique used. The detection of differences in MNG was independent of the number of exercise repetitions for differences higher than ≈ 8 % which correspond to a τ variation of ≈ 15 s. Further, these data are important for the experimental design of further studies by informing the number of repetitions necessary according to an expected effect size (Figure 24).

The breath-by-breath fluctuation (Lamarra et al., 1987) during exercise transitions adds uncertainty to time-domain parameters prediction, mainly from a single test dataset. The confidence interval of the estimated τ, and therefore the "sensitivity" to identify aerobic fitness differences, depends on the $\dot{V}O_2$ signal-to-noise ratio (Keir, Murias, et al., 2014; Lamarra et al., 1987), the model complexity (i.e, the degree of freedom) (Motulsky & Ransnas, 1987) and the selected data window (Bell et al., 2001; Murias, Spencer, Kowalchuk, & Paterson, 2011a). To increase signal-to-noise ratio, studies commonly repeat similar tests multiple times within the same session (Christensen et al., 2016; Ozyener et al., 2001) or on different days (Keir, Nederveen, et al., 2014; Whipp et al., 1982) and average repetition-like transitions before time-domain data modeling.

The frequency-domain analysis has some advantages over the time domain approach. Firstly, no explicit data modeling with a degree of arbitrariness is necessary (Eßfeld et al., 1987) since the $\dot{V}O_2$ time series can be decomposed, and therefore rebuilt from the infinite sum of its harmonic components (Hughson et al., 1990). Second, the random noise associated with $\dot{V}O_2$ measured at the mouth (Lamarra et al., 1987) is filtered when transferred into frequency space, diminishing the impact of the inter-breath oscillations over the $\dot{V}O_2$ dynamics characterization.

The early studies from Eβfeld et.al (Eßfeld et al., 1991) and Hoffmann et. al. (Hoffmann et al., 1992) were the first to normalize the system gain amplitudes by the amplitude at the fundamental harmonic (i.e., $gAmp_1$ in equation 7). They successfully showed that a faster $\dot{V}O_2$

kinetics maintained a higher normalized gain across the frequency spectrum. However, since the focus of their experiments was to investigate possible aerobic system controllers, no further comparisons were carried out to explore the applicability of this normalization for the $\dot{V}O_2$ temporal dynamics assessment. Other studies used the absolute system gain to infer about $\dot{V}O_2$ dynamics (Eßfeld et al., 1987; Hughson et al., 1990, 1991). In fact, the use of absolute gains may be sufficient for intra-subject comparisons since the system static gain seems to remain constant as the aerobic system "speeds up" after training (Christensen et al., 2016). However, for the comparison between subjects by an absolute index such as τ, the gain has to be normalized.

We demonstrated by computer simulations (Table 2, Figure 18) that MNG was able to characterize the temporal characteristics of the aerobic system by comparing MNG with τ_s. The MNG refined the ability of the Fourier transformation to separate the system dynamic gain from the static gain, isolating therefore the rate at which the aerobic system supplies the energy demand (i.e., power) from the capacity of the aerobic system to supply the demand at steady state. The latter is susceptible to inter-individual variability which confounds the interpretation of the temporal dynamics based on the system absolute gains (as demonstrated in Figure 18B).

In the experimental data (Figure 21), we demonstrated that the MNG was significantly correlated to τ (used as reference). The τ calculated from eight repetitions has an intrinsic non-physiological variability that could be associated with the low signal-to-noise ratio as a consequence of noise, short data window and/or elevated modeling degrees of freedom. The CI_{95} of the τ estimation between all participants (n=9) was 6.76 ± 3.89s which represented ~20 % of the average τ value. In contrast, the MNG presented a lower variability in comparison to τ due to the inherent noise reduction and the lower degrees of freedom of the proposed method.

As demonstrated in Figure 21, the relationship between τ and MNG was systematically below the simulated data (MNG *vs.* τ_s, Figure 21 and 18C). There are two possible explanations for this. Firstly, following Hoffmann et. al. (Hoffmann et al., 2013) and as expected to occur in the muscle, the simulations were generated based on a non-delayed exponential response (single time constant τ_s, no TD). However, the $\dot{V}O_2$ response at the mouth is classically described as a delayed exponential response (single time constant τ with a TD). The addition of the TD term to the fitting model is a mathematical way to account for the "latency" period when the muscle responses have not started to be expressed at the mouth level due to circulatory transient time. Like the phase shift obtained from frequency-domain analysis (Eßfeld et al., 1987), the parameter TD has an elevated variability between subjects without main physiological relevance. Therefore, comparing the exponential characteristics (i.e., τ) of the $\dot{V}O_2$ response at the mouth to the simulated data τ_s appears to show an incorrect gain amplitude generated at the muscle in higher frequencies effectively "slowing down" the response in frequency domain (i.e., lower MNG values). A possible way to account for this issue is to consider the sum of τ and TD, or the mean response time (MRT), as the "effective" muscular $\dot{V}O_2$ time constant measured at the mouth level (Linnarsson, 1974; Whipp & Ward, 1990). In comparison to Figure 21 and as depicted in Figure 25, the addition of TD term brings the relationship between MRT and MNG in line with the simulated data. Despite the apparent differences in r and p values for the MNG vs. MRT compared to the MNG vs. τ (r = -0.682, p = 0.043 and r = -0.754, p = 0.019 respectively for 8 repetitions), the CI_{95} and the squared error were statistically similar (p > 0.05 by paired t-test) considering the individual responses. Therefore, the inclusion of the TD did not alter the relationship between MNG and the time-domain dynamics indicators (τ or MRT).

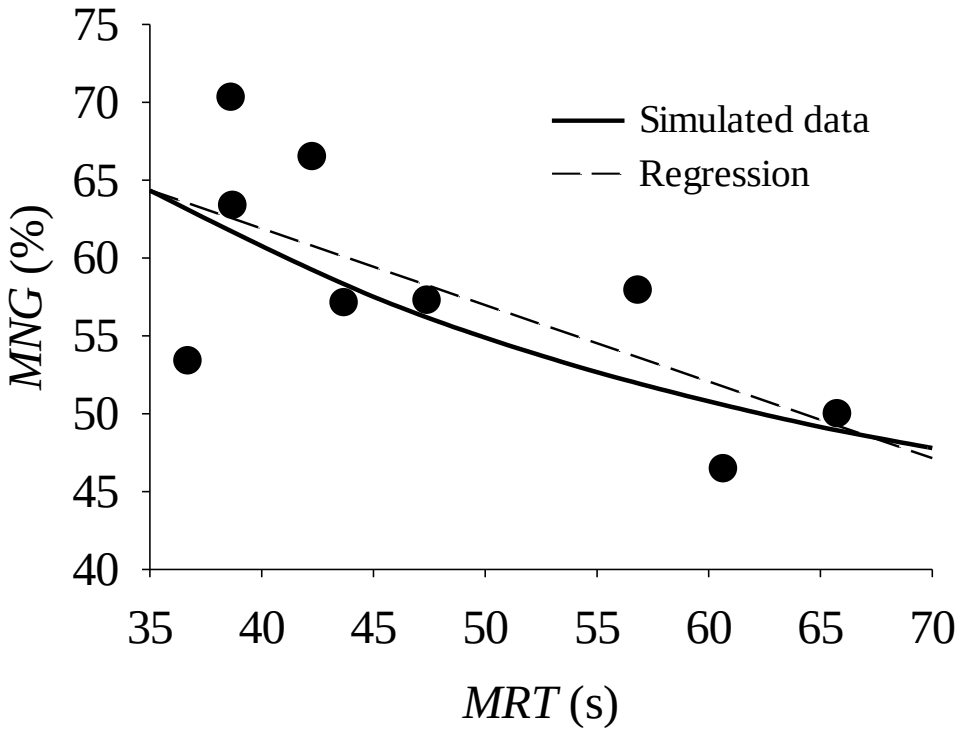

Figure 25. Mean response time and mean normalized gain.
Relationship between mean response time (MRT) and mean normalized gain (MNG), each obtained from 8 repetitions of the pseudorandom binary sequence test is shown in comparison to the simulated data (solid line for MNG vs. τ_s as in Figures 18C). Correlation coefficient (r) = -0.682, p = 0.043 (n=9).

An alternative explanation of why the MNG based on the experimental data is below the simulated data (Figure 21) is based on the $\dot{V}O_2$ system linearity. The $\dot{V}O_2$ measured at the mouth presented a certain degree of energy dispersion across the spectrum due to circulatory distortions and/or all the assumptions that are necessary to obtain an estimate of $\dot{V}O_2$ from ventilatory and gas concentration signals. In contrast, the data simulation was based on a purely linear system that did not present any source of distortion beyond the one related to the exercise stimulus. In the simulations, all energy applied to the system was perfectly converted into the same-order output response by the superposition law, maintaining a higher gain across the frequencies. The possibility exists that even in the range of input stimulation frequencies assumed to result in linear output

($\dot{V}O_2$) (Hoffmann et al., 1992) that nonlinearities exist effectively lowering the system response at the higher frequencies.

3.7 Limitations

The intrinsic degree of uncertainly associated with τ estimated from the exponential modeling precludes the use of τ as a "gold standard" method to validate the use of MNG to assess the system temporal dynamics. The CI_{95} of the relationship between τ (and MRT) with MNG might be influenced by the elevated CI_{95} of τ estimation (and TD for MRT). Therefore, there is an expected source of error also in the reference method (time domain) which complicates the validation method. Our data showed that a faster $\dot{V}O_2$ response will be translated to a higher MNG or a lower τ and MRT; however, the ability of the MNG to extract this information from $\dot{V}O_2$ data seemed optimized and more sensitive to detect differences in the system temporal dynamics due to its inherent filtering characteristics and the lower degrees of freedom.

As a Fourier transformation criterion, the proposed method assumes a symmetrical $\dot{V}O_2$ dynamic between the exercise onset and recovery transitions. However, the $\dot{V}O_2$ signal may be composed of asymmetries between these two phases during exercise intensities higher than moderate (Markovitz et al., 2004; Ozyener et al., 2001). The highest intensity used in the current study (100 watts) was restricted to moderate intensity (Bennett et al., 1981; Eßfeld et al., 1987; Hughson et al., 1988); therefore, the MNG can be compared to the τ obtained from the $\dot{V}O_2$ response during the onset exercise transition.

Although the frequency range selected in the current study limits the $\dot{V}O_2$ response to a range where the system linearity is reportedly preserved (Hoffmann et al., 1992) the MNG might still be susceptible to system non-linearities originating from circulatory distortions or some sort

of periodic noise can be present at higher frequencies. Further studies might explore the application of specific filtering techniques (Eßfeld et al., 1987; Hoffmann et al., 1992) to remove noises/responses uncorrelated to exercise in order to increase even more the precision of the proposed index to characterize the temporal dynamics of the $\dot{V}O_2$ response. However, consistent with the purpose of this index, we successfully showed that a faster aerobic response can be characterized by a higher MNG since that the majority of the evaluated harmonics were probably linear.

3.8 Conclusion

Characterization of physical fitness has classically been conducted by measurement of maximal $\dot{V}O_2$ (Astrand & Saltin, 1961; Drake, Jones, Brown, & Shephard, 1968). Varying levels of physical fitness and the effects of training programs are also associated with differing kinetics of adaptation of $\dot{V}O_2$, expressed by τ, to the challenge of a step increase in $\dot{W}$ (Phillips, Green, MacDonald, & Hughson, 1995).

The MNG has the potential to identify changes in the temporal aerobic system dynamics. The applicability of our findings may extend beyond controlled exercise protocols. Indeed, MNG has the potential to be used in the future for the evaluation of the temporal dynamics of the aerobic response during completely random activities, such as activities of daily living. The inherent filtering characteristics, the need for no model assumption and the low variability between days and time of the day seems to make MNG reliable for the evaluation of the aerobic system temporal dynamics. Additionally, because MNG is expressed as a % of the fundamental harmonic, it can be applied to comparisons of system dynamics across the variables contributing to the delivery and utilization of oxygen independent of their formal units. In conclusion, the present study

successfully validated the use of the MNG for a precise aerobic system analysis based on random exercise stimulus.

Chapter 4: Estimating Oxygen Uptake and Energy Expenditure During Treadmill Walking by Neural Network Analysis of Easy-to-Obtain Inputs

This chapter is published as:

Beltrame, T., Amelard, R., Villar, R., Shafiee, M. J., Wong, A., & Hughson, R. L. (2016). Estimating oxygen uptake and energy expenditure during treadmill walking by neural network analysis of easy-to-obtain inputs. *Journal of Applied Physiology*, *121*, 1226–1233.

4.1 Overview

The study of oxygen uptake ($\dot{V}O_2$) dynamics during walking exercise transitions adds valuable information regarding fitness. However, direct $\dot{V}O_2$ measurements are not practical for the general population under realistic settings. Devices to measure $\dot{V}O_2$ are associated with elevated cost, uncomfortable use of a mask, need of trained technicians and impossibility of long-term data collection. The objective of this study was to predict the $\dot{V}O_2$ dynamics from heart rate and inputs from the treadmill ergometer by a novel artificial neural network approach. To accomplish this, ten healthy young participants performed one incremental and three moderate constant work rate treadmill walking exercises. The speed and grade used for the moderate intensity protocol was related to 80 % of the $\dot{V}O_2$ response at the gas exchange threshold estimated during the incremental exercise. The measured $\dot{V}O_2$ was used to train an artificial neural network to create an algorithm able to predict the $\dot{V}O_2$ based on easy-to-obtain inputs. The dynamics of the $\dot{V}O_2$ response during exercise transition were evaluated by exponential modelling. Within each participant, the predicted $\dot{V}O_2$ was strongly correlated to the measured $\dot{V}O_2$ (r = 0.97 ± 0.0) and presented a low bias (~ 0.2 %), enabling the characterization of the $\dot{V}O_2$ dynamics during treadmill walking exercise. The proposed algorithm could be incorporated into smart devices and fitness equipment, making them suitable for tracking changes in aerobic fitness and physical health beyond the infrequent monitoring of patients during clinical interventions and rehabilitation programs.

4.2 New & Noteworthy

New technologies for the continuous assessment of aerobic fitness based on oxygen uptake data have the potential to be used for the early detection of deterioration of physical health. However,

direct oxygen uptake is costly, cumbersome and not applicable for the general population. An artificial neural network was trained to predict the oxygen uptake signal from easy-to-obtain inputs, possibly allowing future investigations of changes in aerobic fitness with higher applicability for general population.

4.3 Introduction

Walking is a common activity of daily living having strong association with good health and quality of life (Collins et al., 2011). During treadmill walking, speed, grade, and body mass are key variables affecting energy demand (Pescatello, 2014), and these variables are treated as physiological system inputs into models to predict output responses, such as, oxygen uptake ($\dot{V}O_2$). However, equations based on these variables are valid only in steady state and do not have applicability for walking transitions due to the delayed $\dot{V}O_2$ response. The $\dot{V}O_2$ dynamics during an exercise transition are related to the ability of the aerobic system to supply the energetic demand as fast as possible which is ultimately associated with aerobic fitness (Chilibeck et al., 1995; Powers et al., 1985). Nevertheless, direct measurements of $\dot{V}O_2$ are not feasible for the general population in realistic, natural settings. Devices to directly measure $\dot{V}O_2$ have a high cost, require an uncomfortable mask, need trained technicians and are not capable of long-term data collection. An alternative approach might be to consider inputs from simple physical and physiological responses that can be processed with machine learning algorithms (Staudenmayer, Pober, Crouter, Bassett, & Freedson, 2009) to obtain more generalizable system output of the $\dot{V}O_2$ with low bias and variance error to the point at which the prediction can be also applied to the dynamic phases of treadmill walking.

The study of $\dot{V}O_2$ dynamics during exercise transitions adds valuable information regarding aerobic fitness level (Buchheit et al., 2009; Carter et al., 2000; Hagberg et al., 1980; Hickson, Bomze, & Hollozy, 1978), severity of some diseases (Borghi-Silva et al., 2012; Pessoa et al., 2013), functional mobility (Alexander et al., 2003) and mortality rates (Brunner-La Rocca et al., 1999; Schalcher et al., 2003). The potential to predict $\dot{V}O_2$ based on easy-to-obtain inputs is of great interest for the development of tools for fitness and activity level evaluation on a daily basis. Such tools might be used to easily track changes in aerobic responses across the lifespan allowing monitoring of patients during clinical interventions and rehabilitation programs, and in natural settings.

The main objective of this study was to use input variables (treadmill speed and grade, participant body mass and sex, exercise/recovery time and heart rate (HR)) along with novel processing techniques to build a $\dot{V}O_2$ dynamics predictor. Precise predictions will allow not only the investigation of energy expenditure (EE) but the assessment of the $\dot{V}O_2$ dynamics during on-transitions that could have more relevance to activity patterns of daily living. It was hypothesized that $\dot{V}O_2$ and consequently EE could be predicted for an individual during the dynamic and steady-state phases of treadmill walking from system characteristics derived from a larger population. The predicted $\dot{V}O_2$ might be used in the future to assess the aerobic system dynamics from easy-to-obtain variables under conditions of normal daily living.

4.4 Materials and Methods

4.4.1 Participants

Five healthy young men (age 29.8 ± 7.6 years, height 178.4 ± 11.2 cm, body mass 75 ± 11.3 kg) and five healthy young women (age 22.8 ± 0.7 years, height 165.2 ± 7.5 cm, body mass 62.1 ± 5.8

kg) participated in this study. They were evaluated during walking activities on a previously calibrated treadmill (error lower than $1 \cdot 10^{-4}$% for speeds between 0.5 to 8 km.h^{-1}) (Bodyguard, St-Georges, QC, Canada). No volunteers reported any cardiovascular or orthopedic complications that impeded them from performing the tests. A University of Waterloo Research Ethics Committee reviewed and approved the research procedures, being in agreement with Declaration of Helsinki. Participants provided written informed consent after receiving complete written and detailed overview of the experimental procedures with potential risks involved and their right to withdraw from the study at any time without prejudice. Volunteers were instructed to refrain from consuming a large meal within 2 h of testing as well as alcohol, caffeinated beverages, and high intensity exercise for 24 h before testing.

4.4.2 Experimental Design

Prior to performing the experimental protocols, each participant's height and body mass were measured and 3-lead electrocardiogram (ECG) electrodes were applied over the skin. Each individual was familiarized with the protocols and trained to step on the treadmill in motion according to speed and grade requirements to achieve a step transition in work rate.

Data were collected in two separate visits; the first visit consisted of absolute walking speeds (1, 3 and 4.5 km·h^{-1}) with at least 20 min rest between each bout; an incremental test followed the final stage. The second visit consisted of three moderate intensity walking tests. With the exception of the incremental protocol, the constant work rate protocols were comprised of 1 min of baseline standing at the treadmill edge followed by 6 min walking at selected speeds and grades followed by a resting period of 6 min standing.

The incremental walking protocol consisted of 1 min baseline, 6 min warm-up at

4.5 km·h^{-1}, followed by a new increment in speed to individual maximum walking speed as previously determined by a treadmill walking test (~3.6 ± 0.3 km·h^{-1}) and then progressive increments in grade (1%·min^{-1}). The test was terminated when participants reached 80% of their predicted maximal heart rate. The incremental exercise protocol was performed to establish the gas exchange threshold (Beaver et al., 1986).

During the second visit, participants performed three moderate walking bouts at the speed (3.9 ± 0.1 km·h^{-1} for men and 3.4 ± 0.1 km·h^{-1} for women) and grade (5.9 ± 2 % for men and 7.6 ± 0.4 % for women) corresponding to 80% of their $\dot{V}O_2$ at the previously defined gas exchange threshold (Ozyener et al., 2001). The rest periods between all walking bouts lasted at least 20 min in the same day and 48 h between days of testing in order to minimize any carry over effect between protocols and/or day. To avoid anticipatory responses, the treadmill operated in the target speed and grade for at least 5 min prior to testing. A computer screen in front of the participant at eye level height displayed a message to indicate when they should start and stop walking on the treadmill.

4.4.3 Data Acquisition

The pulmonary $\dot{V}O_2$ and carbon dioxide output ($\dot{V}CO_2$) were measured breath-by-breath. The inhale/exhale air volumes and flows were measured by a low dead space bidirectional low resistance turbine (UVM-1725, Vacumed, Ventura, California, US) attached to an air cushion mask (Vacumed, Ventura, California, US). The total dead space of the system was 170 mL. The turbine was calibrated prior to each test using a 3 L syringe using different flow rates (0.5 to 2 L·s^{-1}). Air samples inside the mask were sent to a mass spectrometer (Amis 2000, Innovision, Odense, Denmark) by a short sample line (~1.5 m). Gas concentrations were calibrated using precise

medical gas tanks with known O_2, CO_2, N_2, and Ar concentrations (Praxair Canada Inc., Mississauga, ON, Canada). The signals from the turbine and mass spectrometer were synchronized and then used to estimate $\dot{V}O_2$ and $\dot{V}CO_2$ signals using the First Breath software (Waterloo, ON, Canada).

The beat-by-beat HR was derived from the electrocardiogram signal (Pilot 9200, Colin Medical Instruments, San Antonio, TX, US) by a specific routine on software LabChart 7.3.7 (ADInstruments, Colorado Springs, CO, US) that identifies the "R" peaks in the ECG signal.

4.4.4 Machine Learning and Data Analysis

4.4.4.1 Oxygen Uptake Predictor

Data containing inputs (treadmill speed and grade, participant body mass and sex, exercise/recovery time and HR) and the output ($\dot{V}O_2$) were time synced and 2 Hz re-sampled by linear interpolation, resulting in ~$1{\cdot}10^5$ samples for each variable. Data mining was performed in the KnowledgeFlow environment in WEKA (version 3.7, University of Waikato, Hamilton, New Zealand) (Hall et al., 2009).

To ensure generalizability, all tested algorithms were validated by 10-fold leave-one-out cross-validation (Witten & Frank, 2005). As illustrated in Figure 26, the predictor was created based on the training dataset from nine participants and the remaining participant data were used to test the algorithm accuracy (testing dataset). The mined input-output relationships from nine participants were used to generate the algorithm to translate the inputs from the remaining participant into $\dot{V}O_2$ signal (output). The accuracy of the predictor was computed and then, the order of the data folds changed nine more times (Figure 26). The training and testing datasets did

not contain any overlapping participants to avoid erroneously high accuracy of the predictor (Witten & Frank, 2005).

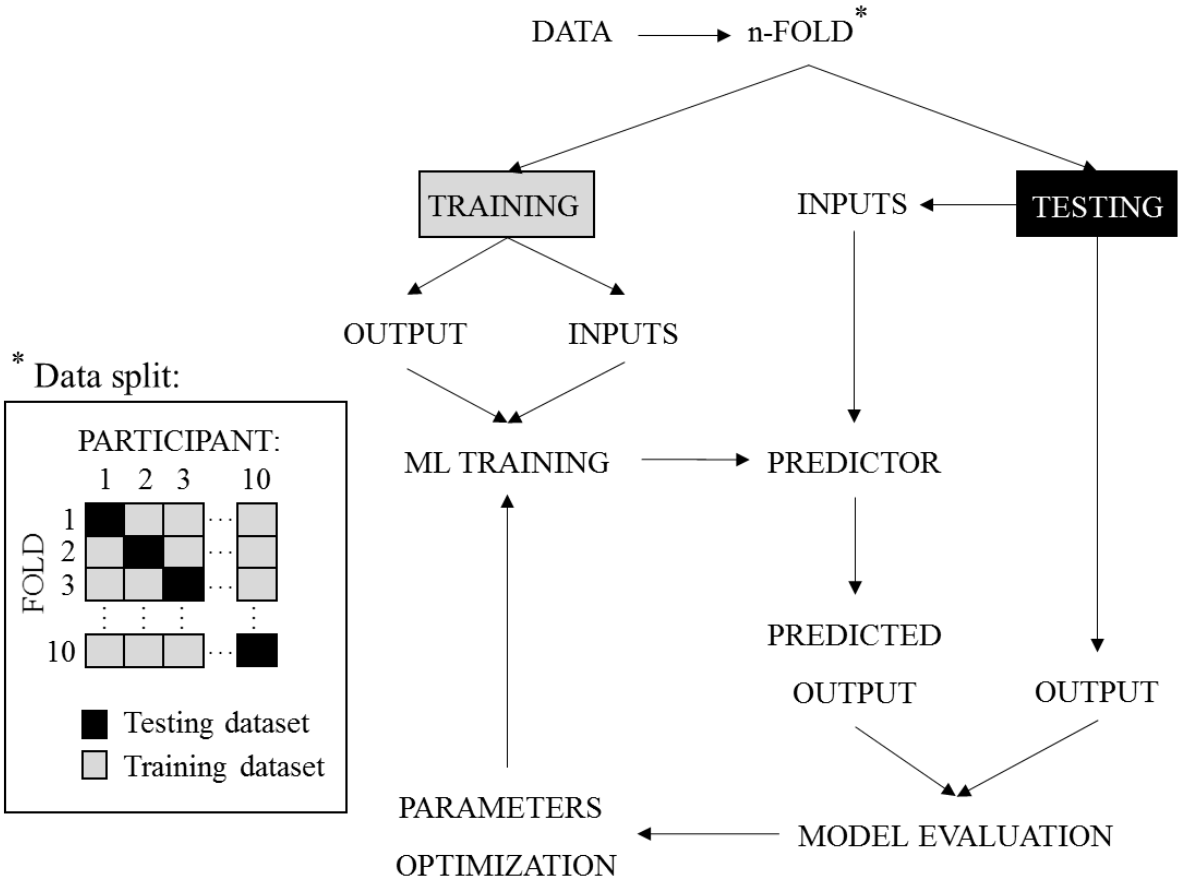

Figure 26. Flowchart of the machine learning algorithm validation.
Data were split according to the 10-fold leave-one-out cross-validation method where nine participants (training dataset) were used to create a predictor that was validated over the remaining participant (testing dataset). In total, 10 folds were generated. The input-output relationship in the training dataset was used to generate an algorithm that predicts the output based on input signals. Some machine learning (ML) parameters can be optimized in order to improve their predictions.

The overall algorithm performance was measured by the average of the Pearson's correlation coefficient (r) to verify the degree of linear correlation between predicted and measured signal (Mukaka, 2012) of all folds from the validation process.

Subsequently to the definition of the validation process, the machine learning algorithms for numerical attributes were tested one-by-one using WEKA's software optimized default parameters. The best predictions were generated by the artificial neural network (ANN) schemes. These algorithms are based on the propagation of the electrical impulses of biological neurons and how these cells interact and learn with the external environment. Like biological nervous tissues, ANN has to experience the cause/effect (examples) of a given problem before being able to predict it. The cause (i.e., inputs) should travel throughout the ANN to be compared with an effect (i.e., outputs). In this way, individual weights and thresholds are learned based on the importance of each artificial neuron in the final output prediction. Following a stimulus, the signal back-propagates through the neuron layers in order to tune the influence of each neuron on the signal prediction.

Between all tested ANN schemes, the multi-layer perceptron regressor ($MLPR_{ANN}$) presented the best results. $MLPR_{ANN}$ is a single-hidden-layer ANN which generates simpler algorithms (Carter et al., 2000) with more applicability for embedded systems. The signal propagation across each neuron inside $MLPR_{ANN}$ was optimized by a built-in function in the WEKA algorithm that minimizes the squared error additionally to a quadratic penalty using Broyden-Fletcher-Goldfarb-Shanno algorithm (Luenberger & Ye, 2015). Changing the $MLPR_{ANN}$ parameters arbitrarily (such as pool size, ridge, number of neurons and learning tolerance), the only factor that was consistently influencing the prediction quality was the number of artificial neurons. Therefore, the $MLPR_{ANN}$ optimization focused on the best number of neurons distributed across the single hidden layer. The optimization process started with a single neuron and then one neuron was cyclically added into the $MLPR_{ANN}$. The prediction precision based on the number of

neurons indicated that the $MLPR_{ANN}$ composed by eleven neurons presented the highest r (Figure 27).

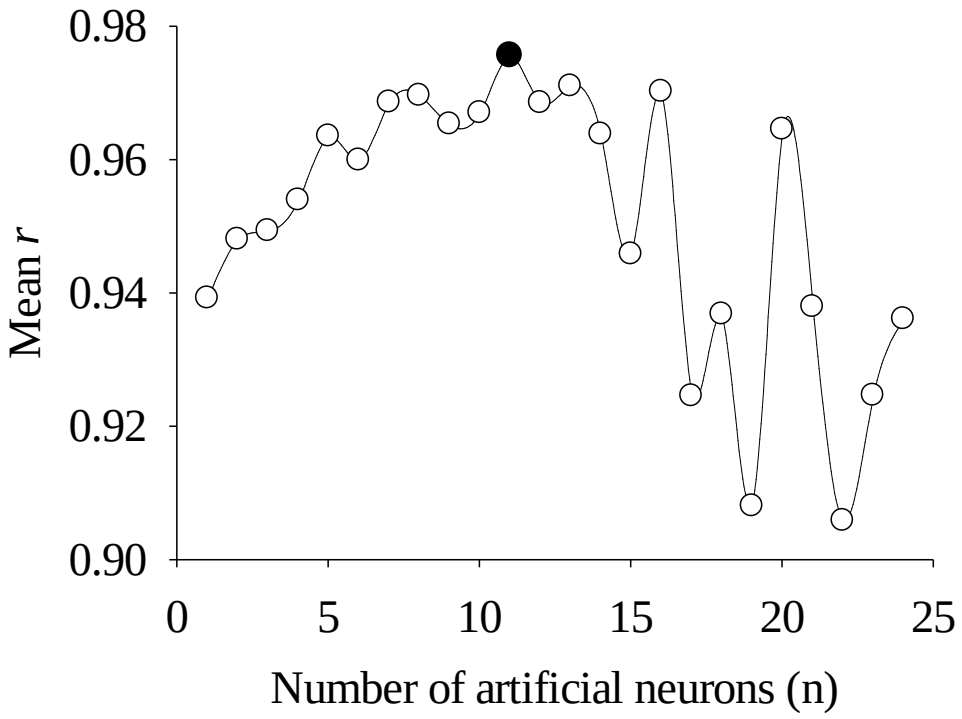

Figure 27. Number of artificial neurons and correlation coefficient.
Influence of the number of neurons on the pulmonary oxygen uptake ($\dot{V}O_2$) prediction by an artificial neural network generated by multi-layer perceptron regressor. The heteroscedasticity of the mean correlation level (r) between all tested datasets increases for networks with more than fourteen artificial neurons probably due to data overfitting. The network composed by eleven neurons (●) presented the highest r.

The selected $MLPR_{ANN}$ was comprised of seven inputs (sex, body mass, time of exercise (time on), time of recovery (time off), grade, speed and HR), eleven hidden neurons and a single output neuron for the prediction of the $\dot{V}O_2$ (Figure 28).

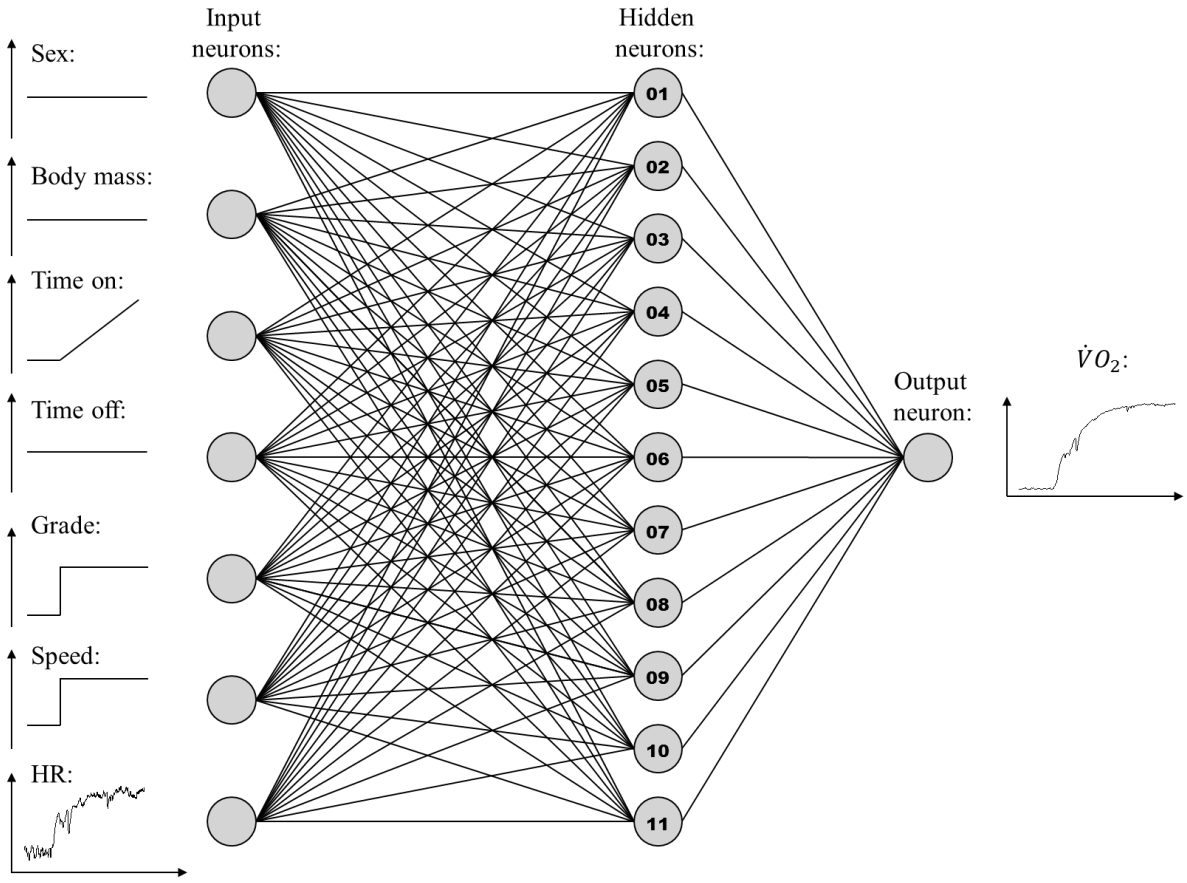

Figure 28. Artificial neural network for the prediction of oxygen uptake.
Selected artificial neural network (ANN) for the prediction of oxygen uptake ($\dot{V}O_2$) during treadmill walking exercise. The inputs were sex, body mass, time of exercise (time on), time of recovery (time off), grade, speed and heart rate (HR). This network is composed by seven input, eleven hidden and a single output neuron.

The influence of the sample size was also tested. Randomly removing participant's datasets from the data pool, the $MLPR_{ANN}$ precision followed a positive linear relationship with the sample size, but for sample sizes higher than eight participants, r was virtually steady representing an upper bound for $MLPR_{ANN}$ predictions. When a participant's own data were incorporated for training and testing the algorithm, the upper bound precision was r = 0.98, or 0.01% higher than findings without that participant's data included. Therefore, once our sample size is producing predictions close to the upper bound values, more participants should produce similar results.

4.4.4.2 Energy Expenditure Estimation

In order to compare the $MLPR_{ANN}$ EE estimation with the most common method proposed by the American College of Sports Medicine (ACSM) (Humphrey, 2006; Pescatello, 2014), another simpler $MLPR_{ANN}$ was trained using the same approach previously described. The validation and parameters optimization methods were also the same as previously described, but only grade, speed and body mass were considered as inputs, matching ACSM method, and the steady state $\dot{V}O_2$ as output. The output for the EE prediction was obtained from the average of the $\dot{V}O_2$ data during the last min of each absolute (day 1) and moderate (day 2) constant work rate protocol). A single-neuron $MLPR_{ANN}$ was found to be the most appropriate for EE estimation. The EE predictor was composed by the inputs weighting and a single nonlinear neuron transfer function defined by the $MLPR_{ANN}$ method. For the sake of comparison, the steady state $\dot{V}O_2$ was converted to EE (cal.min^{-1}) by dividing the final value by 200 according to ACSM (Pescatello, 2014).

4.4.4.3 Oxygen Uptake Dynamics Characterization

The $\dot{V}O_2$ kinetic analysis was used to characterize the aerobic system dynamics during moderate walking exercise transition. The $\dot{V}O_2$ signal experimentally obtained and the predicted values by the proposed algorithm were used in this investigation. Data from the average of the three repetitions of the transition for each participant were 5 s bin averaged, time aligned (time zero being the rest-to-exercise transition), and then submitted to kinetics analysis.

The first 20s of data were excluded in order to isolate the muscular component of the $\dot{V}O_2$ response during exercise transition (Bell et al., 2001; Hughson, 2009; Whipp & Ward, 1982). The remaining $\dot{V}O_2$ signal was modelled by a mono-exponential function. The fundamental equation used to fit the transitions signal was:

Equation 9 $$VO_2(t) = a_0 + a * \left(1 - exp^{-\left({}^{(t-TD)}/_{\tau_{on}}\right)}\right);$$

where: t *is time* (independent variable); a_0 is the mean $\dot{V}O_2$ during baseline; a is the amplitude of the $\dot{V}O_2$ steady-state; τ_{on} is the time constant (speed of the $\dot{V}O_2$ adaptation) and TD is the time delay before the exponential response. From the 30 individual on-transition datasets, the HR was drifting up for 2 transitions after ~200 s for one of the participants. Therefore, a single exercise transition (first) was considered for the kinetics analysis for this participant. In addition, another participant presented an atypical overshoot and multiple components in the HR response during all transitions. The data related to these transitions were excluded from τ_{on} validation. It is noteworthy that these transitions were still kept for the machine learning method since the steady-state and incremental responses (which compose ~50% of the total data) were comparable to the rest of the participants.

The peak $\dot{V}O_2$ ($\dot{V}O_{2-peak}$) was calculated by the average of the last 30 s of $\dot{V}O_2$ data before exercise interruption during the incremental protocol.

The kinetic analysis parameters were calculated by a computer program created in LabVIEW (National Instruments, Austin, TX, US). The fitting quality was assessed by the analysis of residuals, r and the 95% confidence interval band (CI_{95}) (Fawkner et al., 2002; Keir et al., 2016).

4.4.4.4 Statistical Analysis

Data were expressed as mean ± SD. In addition to r, Bland-Altman plot was used to assess the level of agreement between measured and predicted data. The Student t-test was used to compare the estimated and measured EE and τ_{on} and to compare the prediction bias with the equality line (i.e, bias=0). The sample size was calculated *a posteriori* using Student t-test as reference and considering the observed τ_{on} SD calculated based on the predicted $\dot{V}O_2$ data. The chosen power was 80% and the significance level (p) was set at 5%.

4.5 Results

4.5.1 Oxygen Uptake Predictor

The measured and predicted $\dot{V}O_2$ obtained for all participants during the experiments are depicted in Figure 29. Data related to the single incremental protocols are depicted in Figure 29A. Data related to all six constant work rate protocols are depicted in Figure 29B. The quality of the prediction was indicated by the significant strong positive r value within each participant in both exercise protocols.

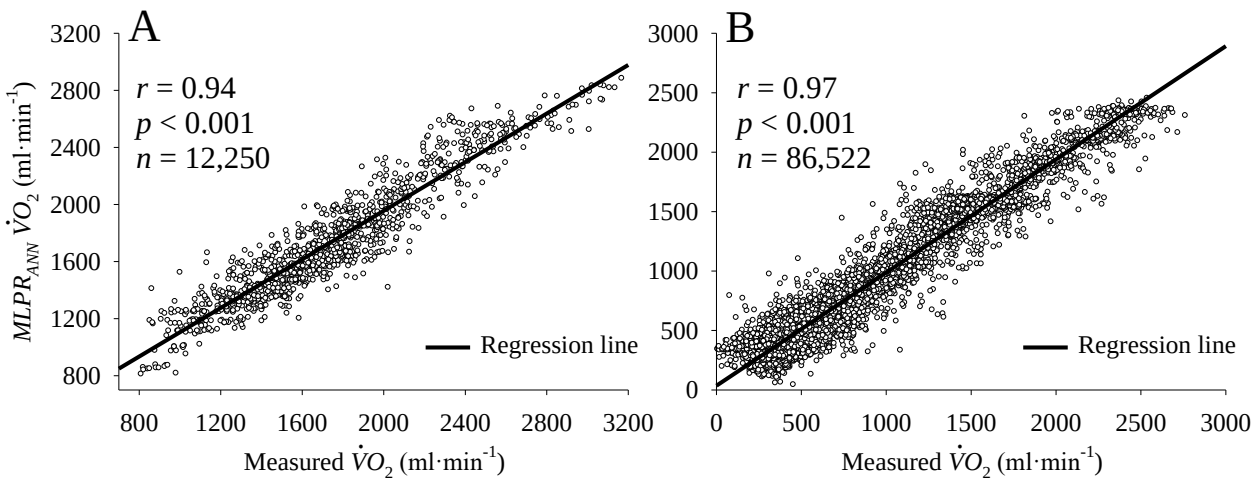

Figure 29. Measured and predicted oxygen uptake signal.
Linear correlation between measured and predicted oxygen uptake signal ($\dot{V}O_2$) during a single incremental (A) and six constant work rate (B) treadmill walking protocols. These data were acquired from ten subjects. The prediction was accomplished by an artificial neural network generated by the multi-layer perceptron regressor ($MLPR_{ANN}$) algorithm. Data were down-sampled to 0.2 Hz for a better visualization.

The Bland-Altman plot for the measured and predicted $\dot{V}O_2$ (Figure 30) indicated that there were small deviations of the differences from zero for both protocols, incremental (Figure 30A) and constant work rate (Figure 30B). The prediction bias was not statistically different ($p > 0.05$) from the equality line in any of the exercise protocols.

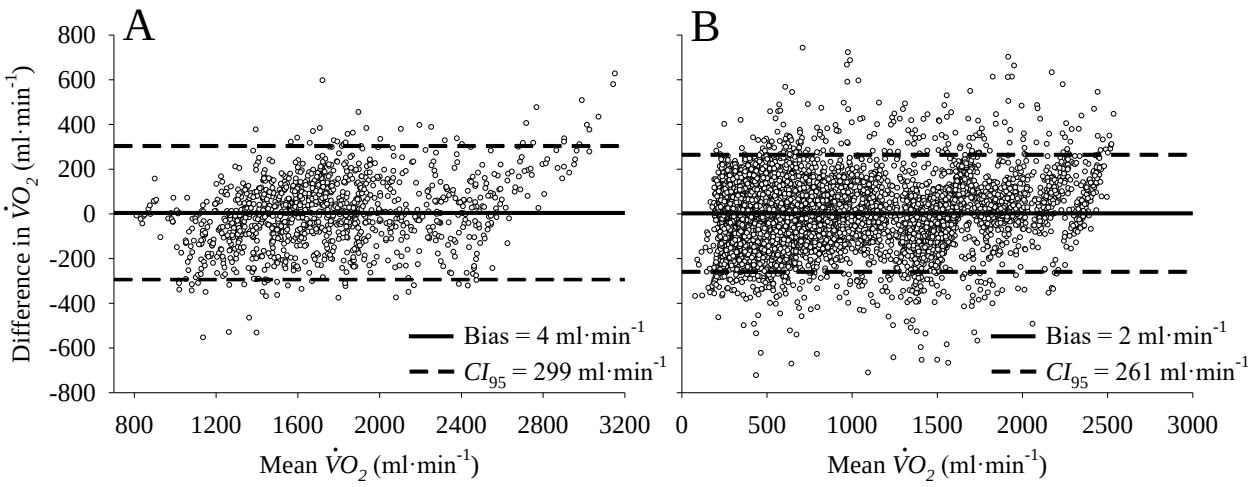

Figure 30. Bland-Altman plot of the measured and predicted oxygen uptake.
Bland-Altman plot of the measured and predicted oxygen uptake ($\dot{V}O_2$) during a single incremental (A) and six constant work rate (B) treadmill walking protocols. These data were acquired from ten subjects. The prediction was accomplished by an artificial neural network generated by multi-layer perceptron regressor ($MLPR_{ANN}$) algorithm. Solid horizontal black line shows the bias of the prediction and dotted black horizontal lines represent the limit of agreement. Data were down-sampled to 0.2 Hz for a better visualization.

4.5.2 Energy Expenditure Estimation

The measured EE during each of the three absolute work rate (day 1) and three relative moderate work rate (day 2) were compared to the predicted EE by the $MLPR_{ANN}$. As described in Figure 31, the bias (0.05±0.62 cal·min^{-1}) of the EE estimated by the $MLPR_{ANN}$ (single layer) was statistically (p = 0.002) lower compared to the EE bias of the ACSM estimation (0.83±0.70 cal·min^{-1}). In addition, the $MLPR_{ANN}$ bias was statistically similar (p > 0.05) and the ACSM bias was statistically (p < 0.001) higher in comparison to the equality line. The 95% limit of agreement was statistically similar between both predictions. The EE estimated by the $MLPR_{ANN}$ was strongly correlated (r = 0.99 ± 0.00) to the measured EE and statistically similar to ACSM (r = 0.99 ± 0.00).

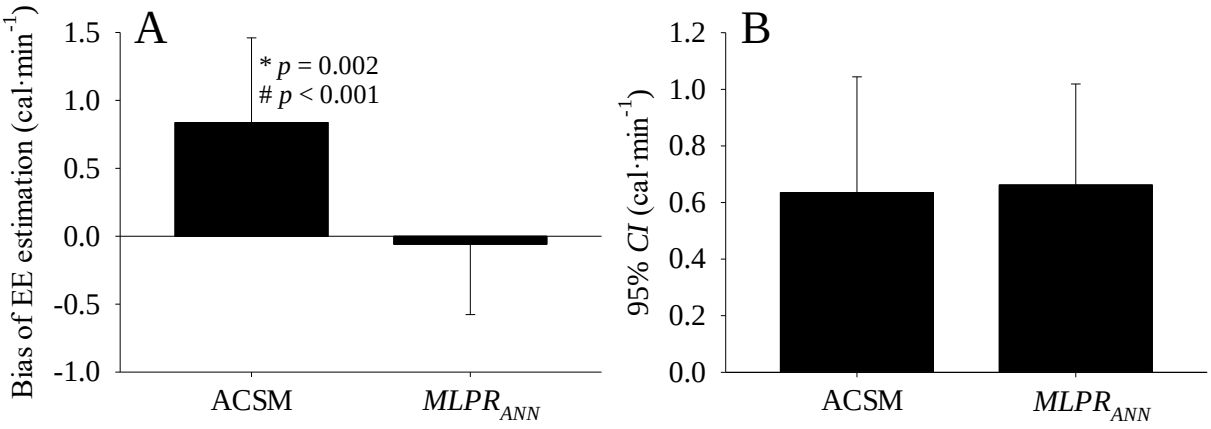

Figure 31. Comparison of different methods of energy expenditure estimation.
Comparison of different methods of energy expenditure (EE) estimation during treadmill walking. The EE was estimated according to the American College of Sport Medicine (ACSM) and by artificial neural network generated by multi-layer perceptron regressor ($MLPR_{ANN}$). Both algorithms used body mass, speed and grade as inputs. A: bias of the EE estimated by ACSM and $MLPR_{ANN}$ between all participants (n = 10). The bias of the EE predicted by the ACSM was statistically (*, p = 0.002) higher than the $MLPR_{ANN}$ bias and statistically (#, $p < 0.001$) higher than the equality line (i.e., bias=0). The 95% confidence interval (CI) of the EE estimation by ACSM and $MLPR_{ANN}$ is displayed in B. Abbreviation: p, significance level.

4.5.3 Oxygen Uptake Dynamics Characterization

The comparison of the mean τ_{on} value computed from the $\dot{V}O_2$ signal obtained from the predictor or from the metabolic cart is displayed in Table 5. The τ_{on} obtained from the predictor (predicted $\dot{V}O_2$ on-kinetics) was not significantly different ($p > 0.05$) from τ_{on} calculated from the measured $\dot{V}O_2$. The CI_{95} of the τ_{on} calculation was smaller considering the $\dot{V}O_2$ from the predictor (predicted $\dot{V}O_2$ on-kinetics) in comparison to the experimentally obtained $\dot{V}O_2$ ($p < 0.001$).

Table 5. Parameters obtained from a mono-exponential fitting of the measured and predicted oxygen uptake ($\dot{V}O_2$) during transitions of treadmill walking.

	τ_{on} (s)	τ_{on} CI_{95} (s)
Measured $\dot{V}O_2$	32.3 ±7.9	1.6 ±0.4*
Predicted $\dot{V}O_2$	37.4 ±6.0	0.5 ±0.1

Values are means ± SD. τ_{on}: time constant (speed of the response); CI_{95}: 95% confidence interval band and $\dot{V}O_2$: oxygen uptake. *: statistical difference between the parameter obtained from measured and predicted $\dot{V}O_2$ signal.

The linear correlation between τ_{on} obtained from the $\dot{V}O_2$ predictor (predicted $\dot{V}O_2$ on-kinetics) and from the measured $\dot{V}O_2$ is displayed in Figure 32. The τ_{on} based on the predicted $\dot{V}O_2$ was statistically correlated (r = 0.88, p = 0.001) to the τ_{on} obtained from the measured $\dot{V}O_2$ data fitting (Figure 32A). The bias of the estimated τ_{on} (-5.11 s) was statistically (p > 0.05) lower than the equality line. The 95% agreement level was ~7 s as indicated by the Bland-Altman plot analysis (Figure 32B).

The $\dot{V}O_{2-peak}$ obtained from the predicted $\dot{V}O_2$ data was strongly correlated (r = 0.91, p < 0.001) to the $\dot{V}O_{2-peak}$ obtained from measured $\dot{V}O_2$ data. In addition, the $\dot{V}O_{2-peak}$ bias (5 ml·min^{-1}) was not statistically (p = 0.937) different from the equality line.

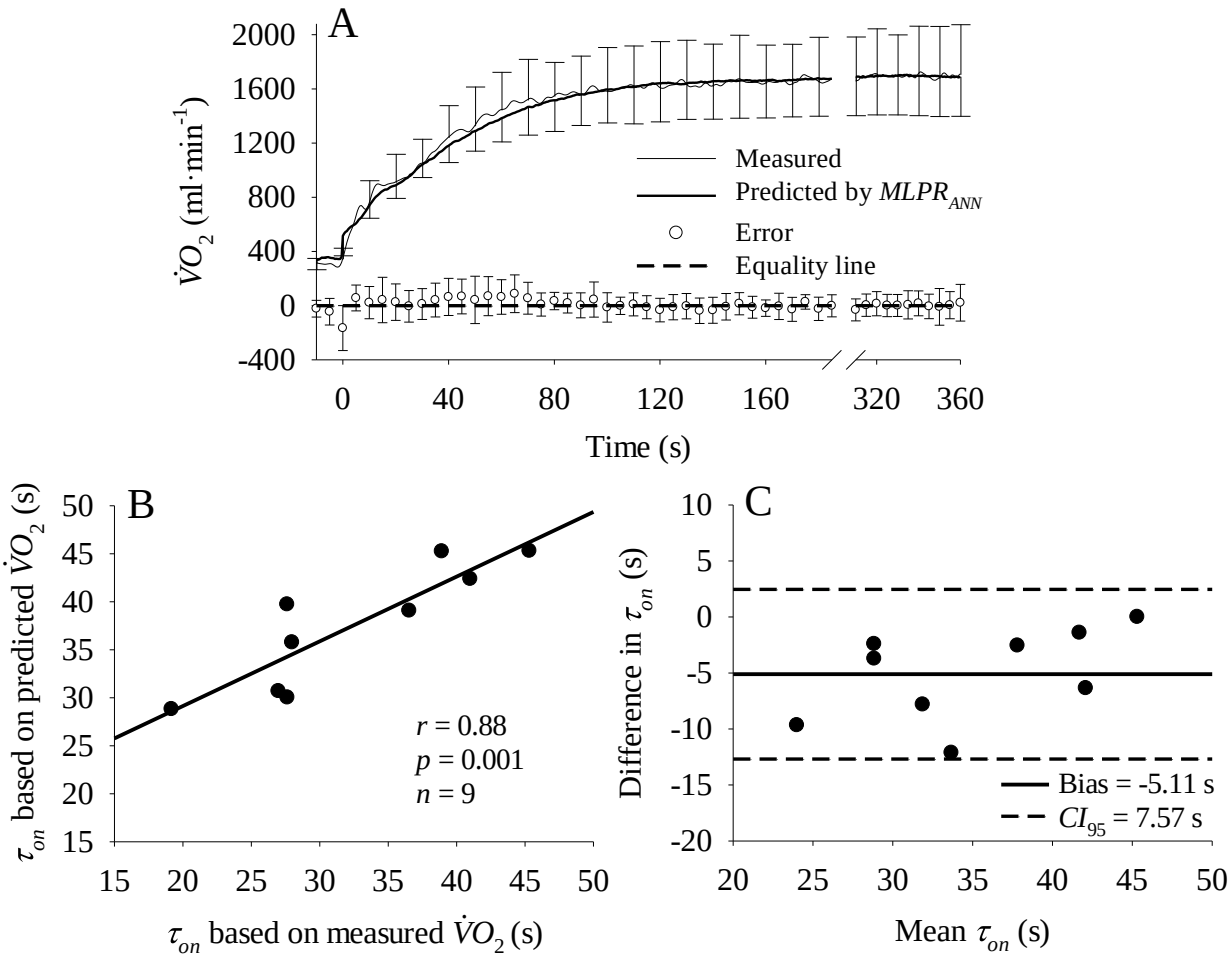

Figure 32. Measured and predicted oxygen uptake dynamics during treadmill walking.
A: group mean response of the measured and predicted oxygen uptake ($\dot{V}O_2$) data obtained during the exercise transition. The SD of the measured $\dot{V}O_2$ (upper vertical bars) and the predicted $\dot{V}O_2$ (lower vertical bars) were presented in 10s intervals. The error (measured minus predicted) and the equality line (error = 0) were also plotted. The SD of the error (vertical bars) were presented in 5s intervals. B: comparison between measured and predicted time constant (τ_{on}) based on measured and predicted ($\dot{V}O_2$) data. The Bland Altman plot of this relationship is displayed in C.

Figure 33 displays the relationship between an expected difference in the τ_{on} predicted by the $MLPR_{ANN}$ and the sample size needed to find statistical significance by Student t-test if there was a statistical difference. The τ_{on} SD considered into the sample size calculation was based on the predicted $\dot{V}O_2$ data. The grey area in the graph indicates the necessary combination of the expected effect size (i.e, differences in τ_{on} between groups) and the sample size to find statistical differences. In addition, the findings from Lambrick et al. (Lambrick, Faulkner, Westrupp, &

McNarry, 2013) and Barker et al. (Barker, Green, Green, & Walker, 2004) related to the sample size and the differences in τ_{on} between groups were added to exemplify the applicability of our algorithm.

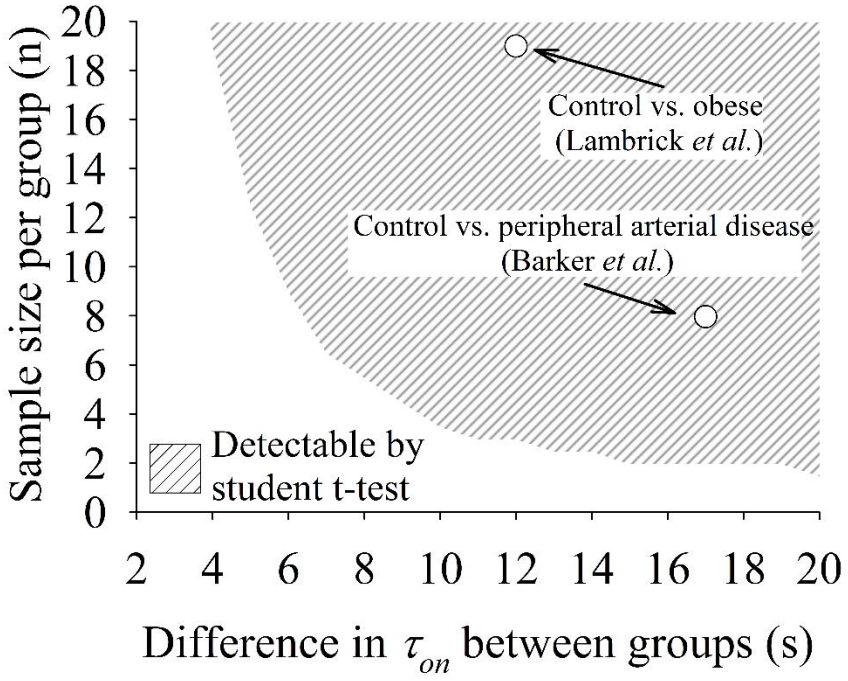

Figure 33. Detection sensitivity of changes in the time constant
Charts of the detection sensitivity of changes in the time constant (τ_{on}) calculated based on predicted oxygen uptake ($\dot{V}O_2$) data during exercise transition. The black area indicates the necessary combination of the expected effect size (i.e, differences in τ_{on} between groups) and the sample size to find statistical differences by t-test (if there is statistical difference). The findings reported by Lambrick et al. (Lambrick et al., 2013) and Barker et al. (Barker et al., 2004) related to the sample size and the differences in τ_{on} between groups were added to the figure to exemplify the applicability of our algorithm. These previous studies revealed the potential of the proposed algorithm to identify a significant difference for τ_{on} between groups from the predicted $\dot{V}O_2$.

4.6 Discussion

The main finding of this study, in support of the hypothesis, was that it is possible to predict the $\dot{V}O_2$ signal during steady-state and exercise transition based on easy-to-obtain inputs. Specifically,

the algorithm generated by the artificial neural network multilayer perceptron regressor predicted the $\dot{V}O_2$ signal during constant and incremental treadmill walking. The accuracy of the predictions was indicated by high linear correlation and low bias. In addition, a simpler artificial neural network was successfully created to estimate energy expenditure based on $\dot{V}O_2$ steady-state prediction by body mass and treadmill speed and grade. Consequently, the two algorithms might be incorporated into embedded treadmill systems as new approaches to monitor energy expenditure and changes in physical fitness.

With the advancements of wearable sensors built into devices like smart watches, garments (smart shirts) and phones, biological signals, such as HR, are becoming easier to obtain (Villar et al., 2015). These devices present new possibilities for ambulatory, unsupervised data collection. In association with hardware advancements, data processing has made considerable progress with the popularization of machine learning techniques that have offered smarter solutions for pattern recognition in large biological datasets. Combined, these technological trends open great possibilities to gather relevant information from the recorded data, having potential for practical applications in health science.

We found the $MLPR_{ANN}$ algorithm model to exhibit the best accuracy between ANN schemes. The comparison of the measured $\dot{V}O_2$ signal and the $\dot{V}O_2$ predicted by the proposed algorithm was associated with low bias and high r values (as shown in Figures 29 and 30), indicating accurate predictions. Our results are in line with previous findings (Montgomery et al., 2009; Smolander et al., 2008), although not every study reports the prediction bias.

The EE estimated by the simpler $MLPR_{ANN}$ algorithm based on speed, grade and body mass was similar to the measured EE based on the $\dot{V}O_2$ steady-state response. The lower bias and similarity to the equality line (Figure 31A) indicated that the $MLPR_{ANN}$ algorithm provided better

accuracy than the calculations proposed by the ACSM guidelines (Humphrey, 2006; Pescatello, 2014). As a simpler predictor, this EE algorithm has a greater potential to contribute to treadmill embedded systems in the future. The better ability of the proposed algorithm to predict EE based on simple-to-obtain inputs might be related to the non-linear model programmed inside the artificial neuron which contrasts with the linear algorithm of the ACSM model.

A unique aspect of the current study was to extend the prediction of $\dot{V}O_2$ beyond simple steady-state measurements to the assessment of $\dot{V}O_2$ dynamics during exercise transitions by application of the $MLPR_{ANN}$ to information obtained during transients. From these data, we investigated the validity of estimations of the τ_{on}. The correlation between predicted and measured τ_{on} was satisfactory (r = 0.88 and p = 0.001), the predicted τ_{on} bias was statistically similar to the equality line and the 95% limits of agreement between measured and predicted τ_{on} was ~7 s. These findings related to the ability of the current algorithm in evaluate $\dot{V}O_2$ dynamics based on τ_{on} values should be taken with precaution; however, the proposed algorithm was still able to identify τ_{on} variations (p = 0.001) within the sample used in this study. Further, the data permit extrapolation of our findings to a real scenario where the current study provided the basis for using our algorithm for future assessments of aerobic fitness in different populations or to evaluate the consequences of an intervention with guidance to sample size and effect size as displayed in Figure 33. In addition, even with a bias of ~5 s, the current algorithm might be more sensitive at identifying (by paired t-test) changes in τ_{on} as a consequence of an intervention since τ_{on} can be obtained from the same participant multiple times. As described in Figure 33, our algorithm would be able to identify differences in τ_{on} considering the sample size and effect size of previous longitudinal studies (Barker et al., 2004; Lambrick et al., 2013) revealing the potential to detect changes in aerobic fitness levels.

Another interesting finding was that the predicted $\dot{V}O_2$ had less variability in comparison with the measured data across the entire experiment. The average SD of the local 5-s mean was 9 and 28 ml.min^{-1} for the predicted and measured $\dot{V}O_2$ signal, respectively. It is well recognized that breath-by-breath measurement of $\dot{V}O_2$ has high variability, and that multiple repetitions of test protocols are required to enhance confidence in data fitting during dynamic transitions (Lamarra et al., 1987). In the Bland-Altman analysis of the current study, the relatively greater variability of the measured data might inflate the CI_{95} when comparing the predicted $\dot{V}O_2$ to the standard (Figure 30). That is, the elevated CI_{95} in this case might not be a consequence of predictions but rather, a higher "non-physiological" variability of the reference method. In addition, the CI_{95} of the τ_{on} calculated from the predicted data was statistically lower in comparison to that of τ_{on} estimated from the experimental $\dot{V}O_2$ signal (Table 1). This low variability might be occurring because the inputs used for the predictions were not susceptible to the inter-breath oscillations associated to metabolic carts (Hughson, 2009). When the expected non-exercise-related Gaussian-like noise (Lamarra et al., 1987) is randomly present in the $\dot{V}O_2$ training dataset, the $MLPR_{ANN}$ learning process did not "learn" these patterns, smoothing the output signal. This observation might suggest the future possibility to use machine learning techniques for system identification (Pillonetto, Dinuzzo, Chen, De Nicolao, & Ljung, 2014) and data filtering during exercise testing.

4.7 Study Limitations

Factors affecting walking economy, such as height (Ludlow & Weyand, 2016) or changes in mechanical efficiency (Zarrugh, 1981), can influence the prediction of EE. Future research should consider a wider range of participants to determine key factors that can further improve the predictions. However, these factors would not influence estimates of τ_{on}.

In addition, atypical HR responses to moderate exercise that do not follow the expected exponential response need to be further addressed. The initial vagal withdrawal followed by the progressive sympathetic activation throughout the exercise transition commonly produce exponential-like functions (Hughson & Morrissey, 1982). However, the autonomic control over the heart rate may vary and users that present atypical responses (as observed in two participants in our study) will not benefit from the proposed algorithm. Further refinements could be added to the proposed algorithm in the future (Rodríguez, Goñi, & Illarramendi, 2005) for the detection of abnormal HR responses.

4.8 Conclusions and Future Perspectives

To the best of our knowledge, this was the first time that the dynamic responses of $\dot{V}O_2$ (i.e., τ_{on} values) were derived by a machine learning algorithm from easy-to-obtain inputs during treadmill walking. This permitted the evaluation of the quality of the predictions during exercise transitions through exponential modeling of $\dot{V}O_2$ dynamics.

In conclusion, the proposed algorithm provided by the artificial neural network multilayer perceptron regressor presented good time resolution and high precision to predict the dynamics of the $\dot{V}O_2$ signals. This novel processing model allowed the building of a $\dot{V}O_2$ predictor using easy-to-obtain input variables permitting the investigation of $\dot{V}O_2$ signal during dynamic and steady-state phases. In the dynamic phase, extraction of the τ_{on} from simple inputs can provide insight concerning aerobic adaptations to the demands of transitions from rest to exercise, or variations in walking speed. In the steady-state, a modified, simpler algorithm provided estimates of EE that were statistically superior to the estimates from the standard ACSM algorithm. Further studies are necessary to test if the dynamic conditions algorithm can successfully assess aerobic fitness during

walking exercise transitions in populations with different aerobic fitness levels (such as athletes vs. sedentary, young vs. elderly), or if it can be used to follow changes in aerobic fitness (such as with physical training or detraining, and in healthy vs. disease state). Also, new studies are necessary to address the ability of the current algorithm to evaluate exercise capacity by maximum $\dot{V}O_2$ prediction.

Implementations of the algorithms developed in the current study could be utilized as physiological signal predictors incorporated into smart devices and fitness equipment, making them suitable for tracking changes in aerobic fitness and physical health beyond the infrequent monitoring of patients during clinical interventions and rehabilitation programs.

Chapter 5: Aerobic System Analysis Based on Oxygen Uptake and Hip Acceleration During Random Over-Ground Walking Activities

This chapter was accepted as:

Beltrame T., Hughson R. L. Aerobic system analysis based on oxygen uptake and hip acceleration during random over-ground walking activities. Accepted on *American Journal of Physiology - Regulatory, Integrative and Comparative Physiology* in November 16, 2016.

5.1 Overview

Deteriorated aerobic response to moderate exercise might precede the manifestation of clinical symptoms of non-communicable diseases. The purpose of the current study was to verify that the use of current wearable technologies for analysis of pulmonary oxygen uptake ($\dot{V}O_2$) dynamics during a pseudorandom ternary sequence (PRTS) over-ground walking protocol is a suitable procedure for the investigation of the aerobic response in more realistic settings. A wearable accelerometer located at the hip assessed the magnitude of the input changes delivered to the aerobic system. Eight adults (23.5 ± 3.7 years old, 174 ± 7 cm and 71.4 ± 7.4 kg) performed two identical PRTS over-ground walking protocols. In addition, they performed on the cycle ergometer two identical pseudo-random binary sequence (PRBS) protocols and one incremental protocol for maximal $\dot{V}O_2$ determination. In the frequency domain, mean normalized gain amplitude (MNG in %) quantified $\dot{V}O_2$ dynamics. The MNG during PRTS was correlated (r=-0.80, p=0.01) with the $\dot{V}O_2$ time constant τ obtain during cycling. The MNG estimated during PRBS was similar to the MNG estimated during PRTS (r=0.80, p=0.01). The maximal $\dot{V}O_2$ correlated with the MNG obtained during the PRBS (r=0.79, p=0.01) and PRTS (r=0.78, p=0.02) protocols. In conclusion, PRTS over-ground walking protocol can be used to evaluate the aerobic system dynamics by the simultaneous measurement of $\dot{V}O_2$ and hip acceleration. In addition, the aerobic response dynamics from PRBS and PRTS were correlated to maximal $\dot{V}O_2$. This study has shown that wearable technologies in combination with assessment of MNG, a novel indicator of system dynamics, open new possibilities to monitor cardiorespiratory health under conditions that better simulate activities of daily living than cardiopulmonary exercise testing performed in a medical environment.

5.2 Introduction

The evaluation of the aerobic response to exercise stimulus provides valuable information regarding the aerobic system integrity (Hughson, 2009; Whipp & Ward, 1992). Abnormal aerobic responses during exercise might occur before the clinical detection of non-communicable diseases (Guazzi et al., 2012), arousing interest in the development of tools for the aerobic system dynamics assessment in real life scenarios.

The mathematical characterization of the pulmonary oxygen uptake ($\dot{V}O_2$) in response to work rate changes can produce parameters in the time and frequency-domains related to aerobic system dynamics (Eßfeld et al., 1987; Hughson, 2009; Whipp et al., 1982). The time-domain analysis typically utilizes a single, or multiple repetitions of step work rate change protocol and the $\dot{V}O_2$ response is fitted with exponential functions. The time course of the $\dot{V}O_2$ response is reported by time constants. Time-domain approaches require specific laboratory conditions and classically deal with issues related to the reliability of the estimated parameters (Hughson, 2009) due to low signal-to-noise ratio associated with $\dot{V}O_2$ measured at the mouth (Lamarra et al., 1987) as well as high degree of freedom of the models chosen (Bell et al., 2001; Motulsky & Ransnas, 1987).

A faster aerobic system dynamics characterized by a faster $\dot{V}O_2$ adjustment is classically associated with a better aerobic fitness (Norris & Petersen, 1998; Phillips et al., 1995; Powers et al., 1985) and disease prognosis (Borghi-Silva et al., 2012; Pessoa et al., 2013; Regensteiner et al., 1998). On the other hand, slower aerobic responses are related to a higher lactate production (Koskolou, Calbet, Rådegran, & Roach, 1997) and seem to impact functional mobility (Alexander et al., 2003). As a marker for primary prevention of non-communicable diseases (Guazzi et al.,

2012), the early identification of the slowing of aerobic system adjustment has considerable potential in the future of health care.

The frequency-domain analysis of $\dot{V}O_2$ dynamics, while also constrained to date to laboratory conditions, has some advantages over the time domain approach in that there are no assumptions regarding the model used to fit data (Eßfeld et al., 1987). Instead of a single process that requires the signal to fit into a pre-defined complex model, the frequency-domain method fits the dataset into multiple sinusoidal functions. This process allows the investigation of the $\dot{V}O_2$ dynamics at different stimulus frequencies, thereby enabling a more detailed understanding of the aerobic system control during dynamic exercise transitions (Hoffmann et al., 1992; Hughson et al., 1990). In addition, the system dynamics parameters obtained through frequency-domain analysis are less susceptible to non-periodic signals, such as the intra-breath noise and can be used to fit signals obtained from random exercise stimuli. As opposed to constant work rate protocols used for time-domain analysis, the optimal $\dot{V}O_2$ dynamics investigation by frequency domain requires more variation in the exercise protocols (Hughson et al., 1990).

Cycle ergometer experiments allow the precise control of the work rate, and therefore a better control over the external stimulus (defined as system input). However, cycling is not a common activity of daily living and it is not widely used between different populations and cultures. On the other hand, walking is a universal physical activity that is performed in almost all age groups and health conditions thus the aerobic response investigation during walking is more applicable for the general population. Although treadmill walking can be a sufficient method to study the physiology of walking with precise control of speed and grade, it is not a completely realistic approach to represent over-ground walking.

The purpose of this study was to analyze the aerobic system dynamics during pseudorandom ternary sequence (PRTS) over-ground walking protocol to better simulate what occurs during activities of daily living than exercise testing performed in a medical environment. An accelerometer (ACC) located at the hip was used to assess the magnitude of the input changes delivered to the aerobic system. The aerobic system dynamics obtained during the proposed over-ground walking protocol were compared to a controlled cycling protocol and related to maximal $\dot{V}O_2$. The hypothesis of this study was that the aerobic system dynamics determined from frequency-domain analysis during a novel over-ground walking protocol would correlate with kinetics parameters from cycle ergometry testing. The results of this study based on $\dot{V}O_2$ response to changes in ACC could set the stage for future assessment of the $\dot{V}O_2$ dynamics based on random physical activities typically encountered in daily living.

5.3 Methods

5.3.1 Study Design

Eight healthy active non-athlete young men (23.5 ± 3.7 years old, 174 ± 7 cm and 71.4 ± 7.4 kg) participated in the study. This study was approved by the Office of Human Research of the University of Waterloo and was in agreement with Declaration of Helsinki.

For the first visit, exercise was performed on the cycle ergometer (Lode Excalibur Sport, Lode B.V., Groningen, Netherlands). After warm-up, participants completed two consecutive pseudorandom binary sequence (PRBS) protocols (Eßfeld et al., 1987; Hughson et al., 1990; Yoshida et al., 2008) followed by an incremental protocol (25 W·min^{-1}). From the incremental protocol responses, the individual maximal $\dot{V}O_2$ (40.7 ± 6.6 ml·min^{-1}·Kg^{-1}) and gas exchange threshold (GET, 28.2 ± 7.2 ml·min^{-1}·Kg^{-1}) were identified. The moving seven-breath average $\dot{V}O_2$

and carbon dioxide output signals were used to identify the maximal $\dot{V}O_2$ and the GET. The maximal $\dot{V}O_2$ was considered as the average of the last 15 s before recovery following the criteria: 1-) respiratory exchange ratio higher than 1.1 and 2-) identification of $\dot{V}O_2$ plateau with an increase in work rate (Howley, Bassett, & Welch, 1995). The GET was obtained for each participant by a standard method (Beaver et al., 1986). One participant was excluded from the GET analysis due to signal lost in the middle of the incremental test. The $\dot{V}O_2$ at GET corresponded to 70.7 ± 9.3 % of the maximal $\dot{V}O_2$.

After a minimum of one week, participants performed two PRTS over-ground walking protocols separated by a 30-min resting period. Before the first PRTS, participant's walking speed was determined from a timed 15m segment while they walked at three selected cadences: 75, 105 and 135 steps·min^{-1}. This procedure was repeated three to four times for a better reliability.

5.3.2 Pseudorandom Binary Sequence Protocol (PRBS)

A four-stage digital shift register was used to generate the PRBS protocol as previously reported (Hughson et al., 1990). The PRBS was composed by 15 units, each of 30s of duration, totaling 450s of protocol length. The work rate varied between 25 or 100 watts. The cycling cadence was maintained between 60-65 rpm. An extra 200s of the sequence was added at the onset of the PRBS protocol as warm-up and excluded *a priori*, then two identical sequences were completed.

5.3.3 Pseudorandom Ternary Sequence Protocol (PRTS)

The PRTS protocol included a variation of three walking cadences (75, 105 or 135 steps·min^{-1}). The choice to select a protocol with three levels of exercise was based on the frequent change in

speed of walking during real life scenarios. These walking cadences were chosen based on the variation of ±~30 % of the normal average cadence (Tudor-Locke & Rowe, 2012). The PRTS protocol generation was based on the approach proposed by Peterka (Peterka, 2002). The number of the shift register units was set at 3 in order to obtain a 13-min protocol (or 780s) with a unit length of 30s (Figure 34A), thereby allowing for two repetitions of the protocol in the same visit. An additional 300 s of PRTS was added to the beginning of the protocol as a warm-up and excluded *a priori*; therefore, each PRTS total length was 18 min (or 1080s). Due to the PRTS protocol length, a resting period of 20 min was performed between both PRTS protocols.

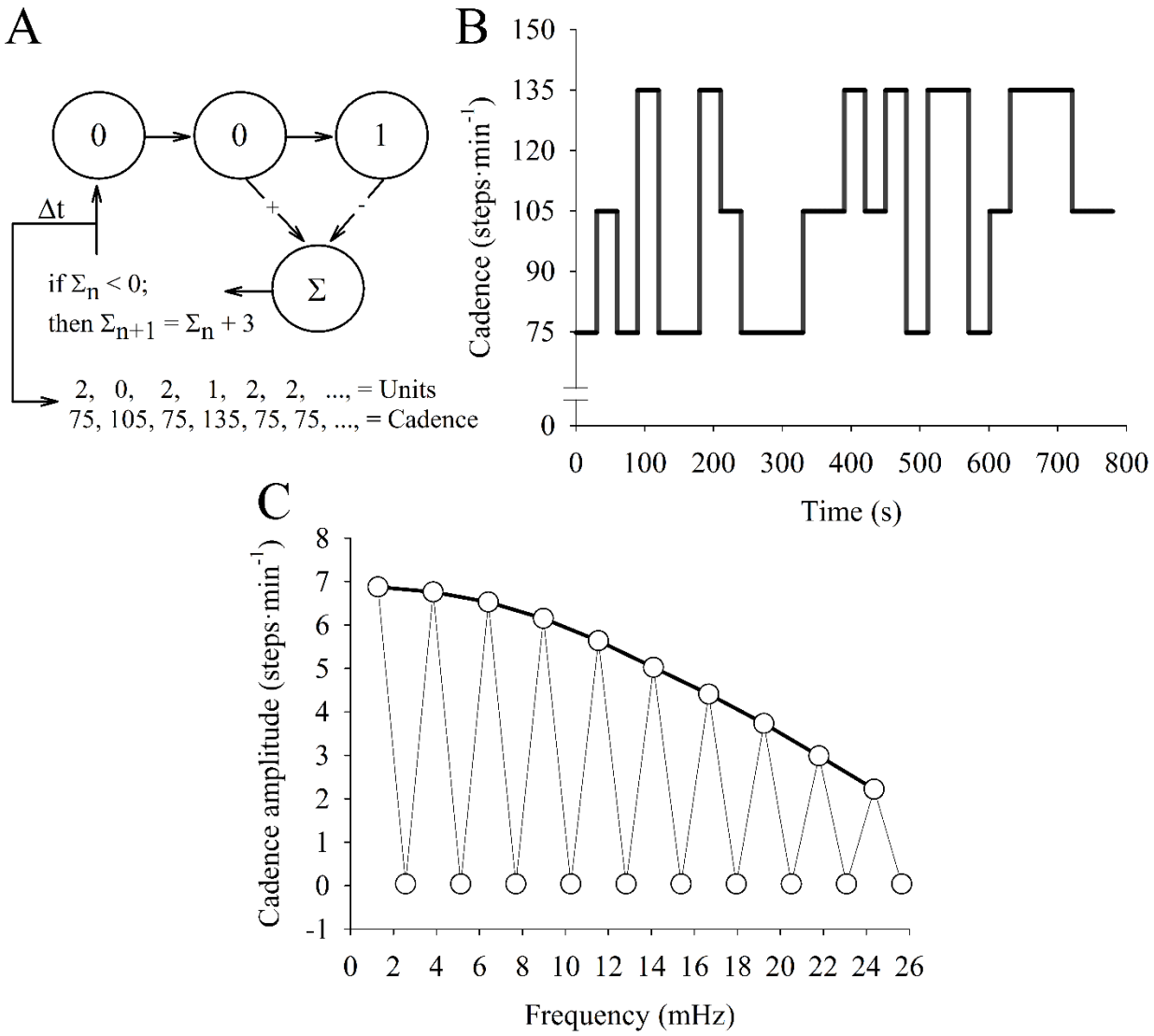

Figure 34. Pseudorandom ternary sequence over-ground walking protocol.
A: selected structure of the shift register used to generate the pseudorandom ternary sequence protocol. The module addition feedback (Σ) sums the negative value of the third stage with the second stage and tests the "if" statement. This new signal is inserted into the first stage and shifts the entire system to the right. The unit value is held for "Δt" s. The unit values (0, 1 or 2) were transformed in the selected walking cadences (0=105, 1=135 and 2=75). The six unit values shown in A correspond to the first six stages in B. The protocol in the time domain (**—** in B) was transformed into frequency domain by Fourier Transformation and the amplitudes for each corresponding sinusoidal function was computed across the frequencies (as displayed in C). Also in C, as a characteristic of PRTS protocols, the stimulus energy decreases to zero at even harmonics (Kerlin, 1974).

The shift register outputs (0, 1 or 2) were converted into target cadences (Figure 34A). A PRTS metronome audio file was created in Audacity 2.0.5 software (Carnegie Mellon University, Pittsburgh, PA, US) and listened to through ear buds to set the walking pace. The actual walking cadence performed by the participant was verified by a post hoc examination of walking cadence.

5.3.4 Data Acquisition

The $\dot{V}O_2$ was measured with a portable metabolic system (K4b^2, COSMED, Italy). The chemical galvanic O_2 sensor, infrared absorption CO_2 sensor and the low-resistance turbine rotor flowmeter were calibrated following manufacturer's specifications before every data collection.–When appropriate, the metabolic equivalents ($METS$) was calculated by: $\dot{V}O_2 . Kg^{-1} . 3.5^{-1}$.

The 3-axis hip ACC data were obtained from an previously validated (Villar et al., 2015) smart shirt (Hexoskin®, Carré Technologies Inc., Montréal, Canada). The ACC sample rate (64 Hz) and resolution (0.004g) were sufficient to capture all expected movements during the proposed walking protocol and activities of daily living (Bouten et al., 1997).

5.3.5 Data Analysis

The step cadence was converted into speed for each participant using the individual linear regression between the cadence and walking speed (Tanawongsuwan & Bobick, 2003). The ACC raw data were converted to the total vector magnitude (Cleland et al., 2013) by: $ACC = \sqrt{x^2 + y^2 + z^2}$; where x, y and z are the vertical, longitudinal and lateral ACC axis, respectively.

The system inputs (walking speed and ACC for PRTS and watts for PRBS) and output ($\dot{V}O_2$) collected during each two PRBS and two PRTS were linearly interpolated on a second-by-

second basis, time aligned and ensemble averaged to obtain a single response per participant for each protocol. The Discrete Fourier Transformation (DFT) was used to convert the finite time series response into frequency space. To adhere to the linearity principle (Hoffmann et al., 1992), the highest frequency analyzed was restricted at the maximum of 8.88 and 8.97 mHz for the PRBS and PRTS protocol, respectively. The DFT algorithm fitted the data into sinusoidal functions by calculating the sine and cosine coefficients by the following equation: $y_{(t)} = a_{DC} + 2 * \sum_{h=1}^{7}(A_h * \cos(2\pi * h * f_1 * t) + B_h * \sin(2\pi * h * f_1 * t))$; where y is the time-series signal to be fitted, t is the time, a_{DC} is average response (i.e., system DC_{offset} or zero-frequency component), f_1 is the fundamental frequency (2.22 and 1.28 mHz for PRBS and PRTS, respectively), A_h and B_h are the cosine and sine amplitude coefficients, respectively. The parameter h is the harmonic number (continuous and even integer numbers for PRBS and PRTS, respectively). From A_h and B_h, the total amplitude was calculated for each harmonic h by: $Amp_h = \sqrt{A_h^2 + B_h^2}$. Because f_1 was different between protocols the input and output Amp responses were linearly interpolated for each protocol at a common frequency range of 2.5 to 8.5 mHz, with a resolution of 0.5 mHz. This resulted in thirteen paired-between-protocol frequencies. To eliminate the influence of the intra-subject variability of the system static gain (Hoffmann et al., 1994, 1992), the system gain ($Amp_{output}.Amp_{input}{}^{-1}$) was normalized as a percentage of the Amp gain at the lowest common frequency (i.e., 2.5 mHz) (Hoffmann et al., 1992). Finally, the mean normalized gain (MNG) that describes the overall temporal system dynamics was obtained for both protocols by the average of the interpolated normalized gains between the same common frequencies (2.5 to 8.5 mHz).

To test the ability of the novel indicator MNG to extract the same dynamic characteristics of the $\dot{V}O_2$ response as observed in time domain analysis from the time constant, the $\dot{V}O_2$

ensemble-averaged data during the PRBS protocol were submitted to time domain analysis. The time scale was shifted to align time zero with the onset of the second 100-watts step at 120s of the PRBS protocol. The data window was composed of 15s of baseline (at 25 watts) followed by 120s of constant work rate at 100 watts. This dataset was the longest period without work rate variation within the PRBS protocol thus the best data window for time domain analysis. The first 20s of data related to the cardio-dynamic component (Barstow et al., 1990) were excluded from the analysis. For one participant, only 91 s after baseline was considered due to an unexpected $\dot{V}O_2$ overshoot. The remaining data were fitted by a mono-exponential model following a standard method (Hughson & Morrissey, 1982; Whipp et al., 1982) to obtain the time constant τ and the steady-state $\dot{V}O_2$. As displayed in Figure 35, the MNG was negatively correlated with τ considering ACC (r = -0.75, p = 0.03 and n = 8) or walking speed (r = -0.80, p = 0.01 and n = 8) as system input. Thus, higher MNG values are associated with faster $\dot{V}O_2$ dynamics (i.e., faster τ). Data analysis was performed by a certified (#100-314-4110) LabVIEW associated developer (National Instruments, Austin, TX, US).

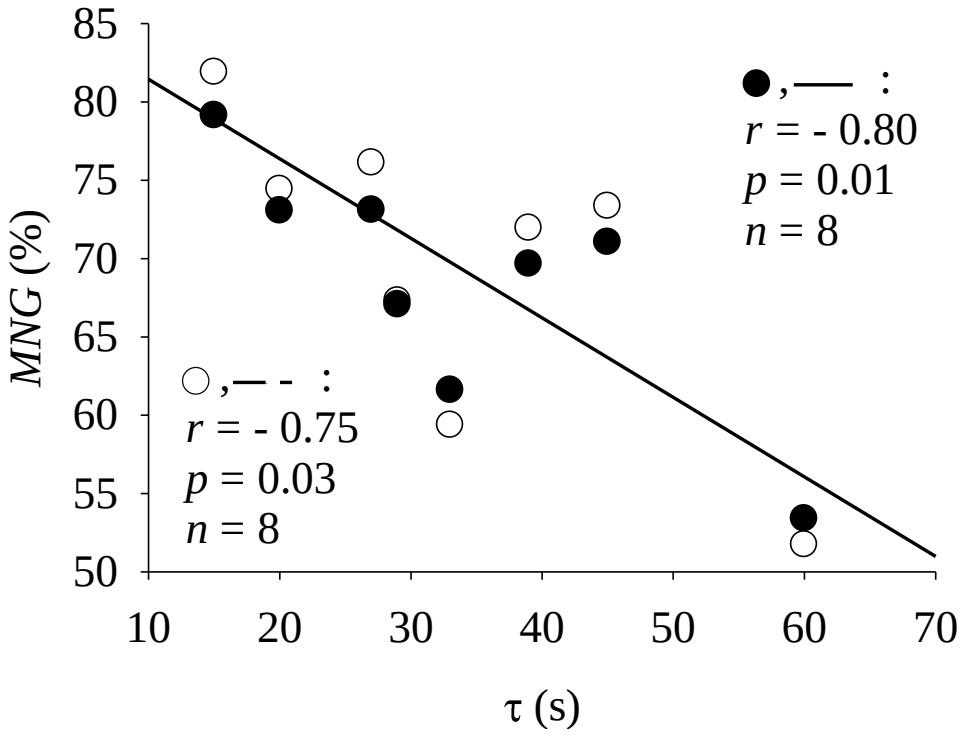

Figure 35. Time constant and mean normalized gain during pseudorandom sequences.
Relationship between the oxygen uptake time constant τ obtained during cycling and the mean normalized gain amplitude (MNG) obtained during pseudorandom ternary sequence (PRTS) over-ground exercise protocol. The MNG was estimated based on hip acceleration (○) or walking speed (●) as system inputs during PRTS. This relationship followed a linear pattern. r: Pearson's correlation coefficient, p: statistical significant level and n: sample size.

5.3.6 Statistical Analysis

Friedman repeated measures ANOVA was used to compare the interpolated normalized gain Amp between the different tested frequencies. Student-Newman-Keuls was used as post hoc test. The MNG obtained from PRBS and PRTS protocols were compared by Student t-test. Linear correlation was measured by Pearson product-moment correlation coefficient (r). Statistical significance was set at a level α=0.05. Statistical analysis was performed in SigmaPlot 12.5 software (Systat Software, San Jose, CA, US).

5.4 Results

Figure 36 illustrates the linear relationship between walking speed and hip acceleration during the PRTS protocol (780 samples per participant, 6240 in total). The hip acceleration presented a strong positive correlation (r = 0.94 and p < 0.001) with the walking speed. The ACC data can be used in place of directly measured walking speed.

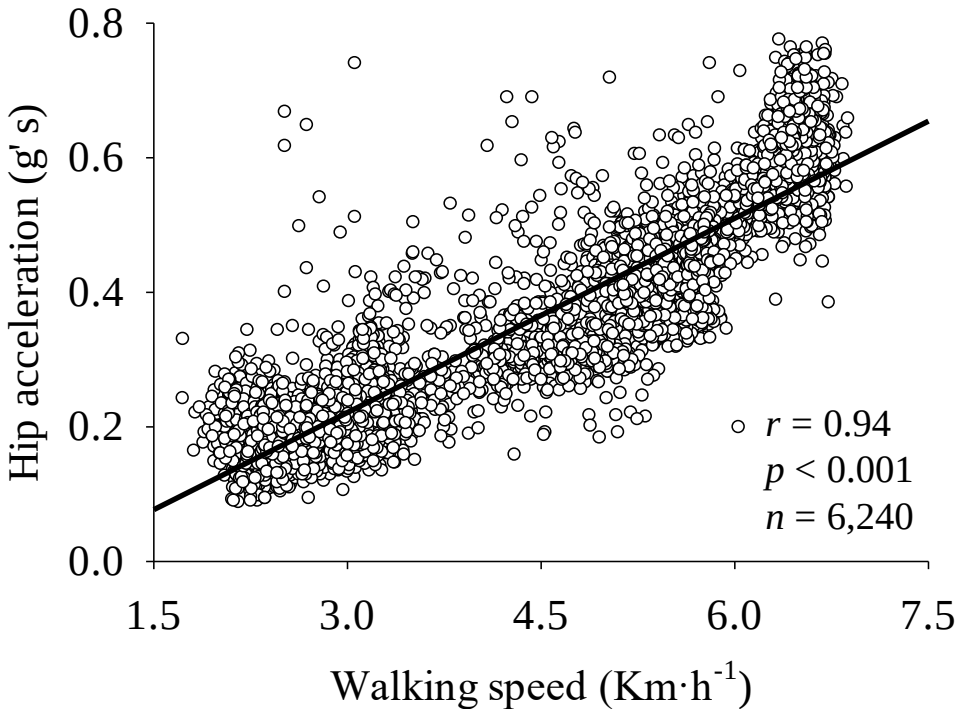

Figure 36. Accelerometer and walking speed.
Linear correlation between walking speed and hip acceleration.r: Pearson's correlation coefficient, p: statistical significant level and n: sample size taken as 13 minutes of data collection from each of 8 participants.

5.4.1 Time-series

The time-series mean $\dot{V}O_2$ response of all tested participants (n = 8) is displayed in Figure 37A and 37B for the PRBS and PRTS protocols, respectively. The work rate (watts) was used as the system input during cycling (PRBS) and the hip acceleration was displayed as a system input during over-ground walking (PRTS). As described in Figure 37C, the distribution of the metabolic equivalent varied between 3 and 8 $METS$ during both protocols and this range was similar to the metabolic demand of moderate activities of daily living (Hendelman et al., 2000). The higher relative incidence of $METS$ (≈ 30% of the samples) was ≈ 5.5 and ≈ 3.8 $METS$ for PRBS and PRTS, respectively. The $METS$ were consistently lower during PRTS in comparison to PRBS indicating that the metabolic demand during PRTS was also restricted to moderate intensity exercise. In addition, the average of the steady-state $\dot{V}O_2$ estimated from the mono-exponential data modeling during PRBS (23.9 ± 2.9 mL·kg^{-1}·min^{-1}, 85.6 ± 10.4 % of the $\dot{V}O_2$ at GET and 59.8 ± 8.4 % of the maximal $\dot{V}O_2$) indicated that the 100 watts work rate correspond to moderate intensity exercise. Therefore, considering similar dynamics between PRBS and PRTS (further demonstrated), PRTS protocol was also constrain to moderate exercise intensity.

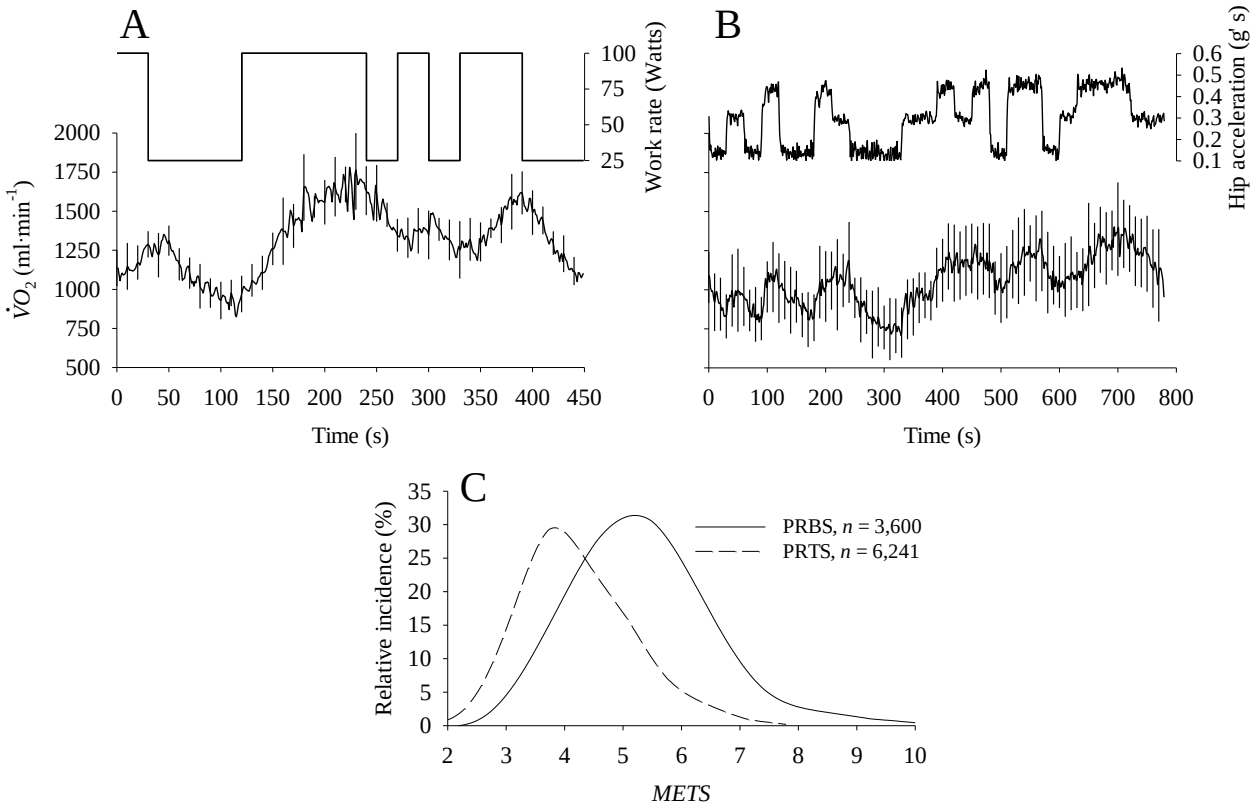

Figure 37. Oxygen uptake response during pseudorandom protocols.
Mean (—) ± SD (vertical bars at 10s intervals) of the oxygen uptake response ($\dot{V}O_2$) of all participants (n = 8) during pseudorandom binary sequence (A, PRBS) cycling protocol and pseudorandom ternary sequence (B, PRTS) over-ground walking protocol. The upper portion of each panel describe the work rate and hip acceleration of a representative participant during PRBS and PRTS protocols, respectively. C: distribution of the metabolic equivalents ($METS$) during PRBS and PRTS.

5.4.2 Frequency-domain

The system dynamics characterization by frequency-domain analysis was based on the study of the input-output relationship (gain) across different frequencies. Figure 38 shows the comparison of the interpolated normalized gain Amp obtained from PRBS and PRTS protocols across the range of 13 selected frequencies. The influence of the stimulus frequency over the aerobic system response was similar between protocols, indicating similar $\dot{V}O_2$ dynamics between these two exercise modalities (cycling *vs.* walking). As expected, the system gains in both protocols statistically (p < 0.001) decreased as the frequency increased. The strong linear correlation (r >

0.9 and $p < 0.001$) between PRBS and PRTS was not different whether the PRTS protocol used walking speed (Figure 38A) or ACC (Figure 38B) signal as system input.

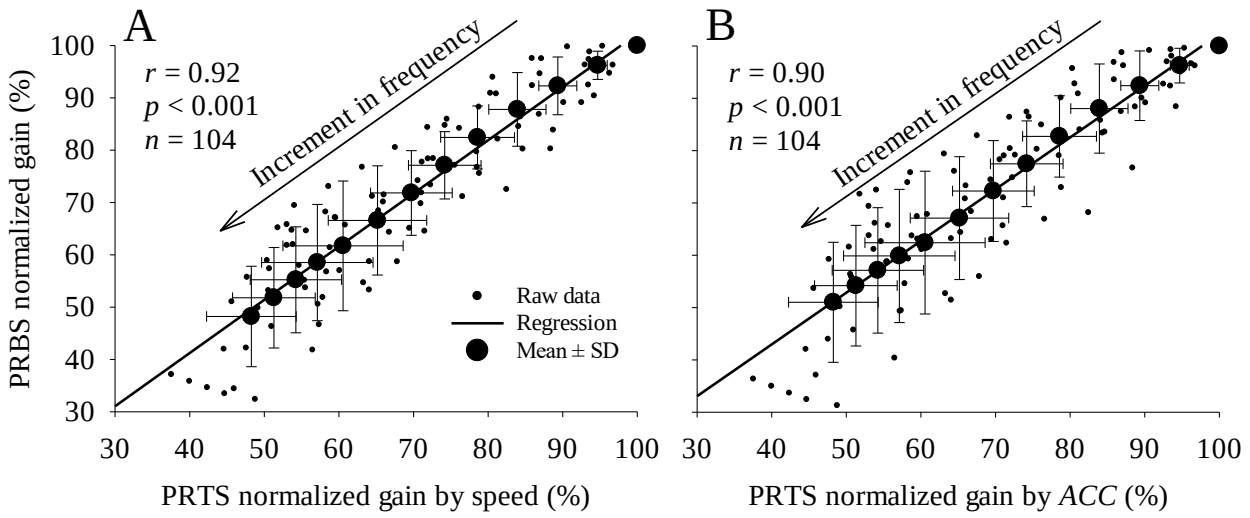

Figure 38. Normalized system gains during walking and cycling.
Correlation of the effect of the input frequency increment (arrow) over the normalized system gain between pseudorandom binary sequence (PRBS) and pseudorandom ternary sequence (PRTS) protocols. Graphs display the mean ± SD response of all participants (n = 8) at each frequency (n = 13) and the raw data for all participants and frequencies (n = 104). The Pearson correlation coefficient (r) and the statistical significance level (p) were calculated based on the raw data from all participants and frequencies. The aerobic system gain during PRTS was estimated using walking speed (A) or hip accelerometer (ACC) (B) as system input.

5.4.3 Mean Normalized Gain (MNG)

The MNG, as an index for the aerobic system dynamics evaluation, was estimated for each participant based on the average of the normalized gains. The MNG was statistically ($p > 0.05$) similar between PRBS and PRTS. During the PRTS protocol, the MNG estimated using walking speed as system input was strongly positively correlated (r = 0.99 and $p < 0.001$) with the MNG estimated from ACC (Figure 39A). The MNG during PRTS, from either walking speed or ACC, was statistically similar and strongly positively correlated to the MNG obtained from the PRBS protocol (Figure 39B).

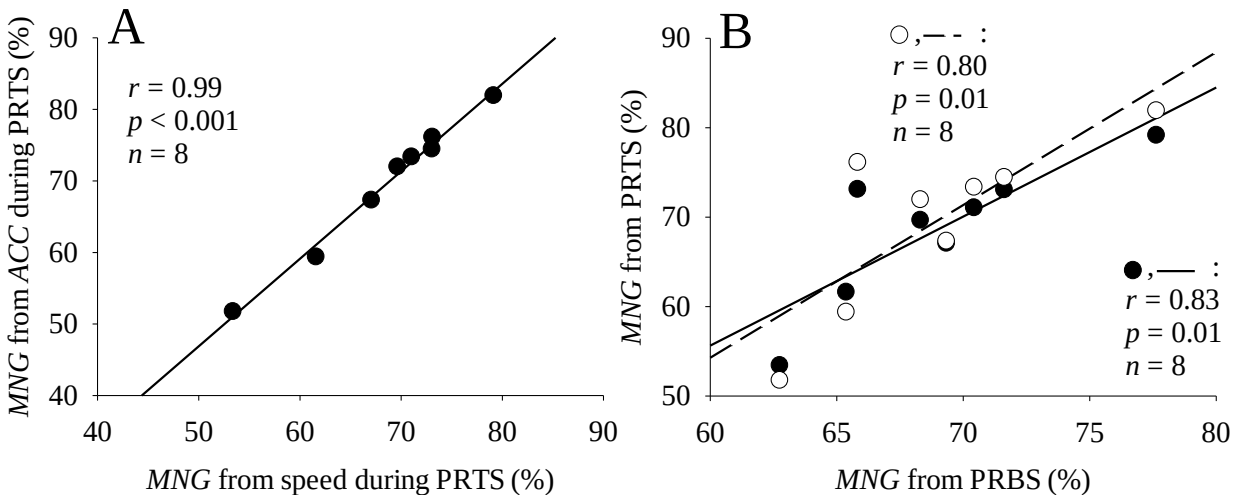

Figure 39. Mean normalized gain during pseudorandom ternary and binary sequences.
Mean normalized gain (MNG) obtained from the oxygen uptake response during pseudorandom ternary sequence (PRTS) and pseudorandom binary sequence (PRBS) protocols. A: Correlation between the MNG estimated based on hip acceleration (ACC, ○) and walking speed (●) as system inputs during PRTS. B: correlation between MNG estimated during PRBS and PRTS protocols. The MNG was estimated using ACC or walking speed as system inputs during PRTS. r: Pearson's correlation level, p: statistical significance level and n: sample size.

Figure 40 displays the correlation between the MNG estimated from PRBS (Figure 40A) and PRTS (Figure 40B) protocols with the maximal $\dot{V}O_2$ obtained during incremental cycling protocol. The MNG during PRBS protocol was strongly positive correlated (r = 0.79 and p = 0.01) with maximal $\dot{V}O_2$. The MNG and maximal $\dot{V}O_2$ were strongly positive correlated during PRTS when walking speed or ACC signals were used as system inputs.

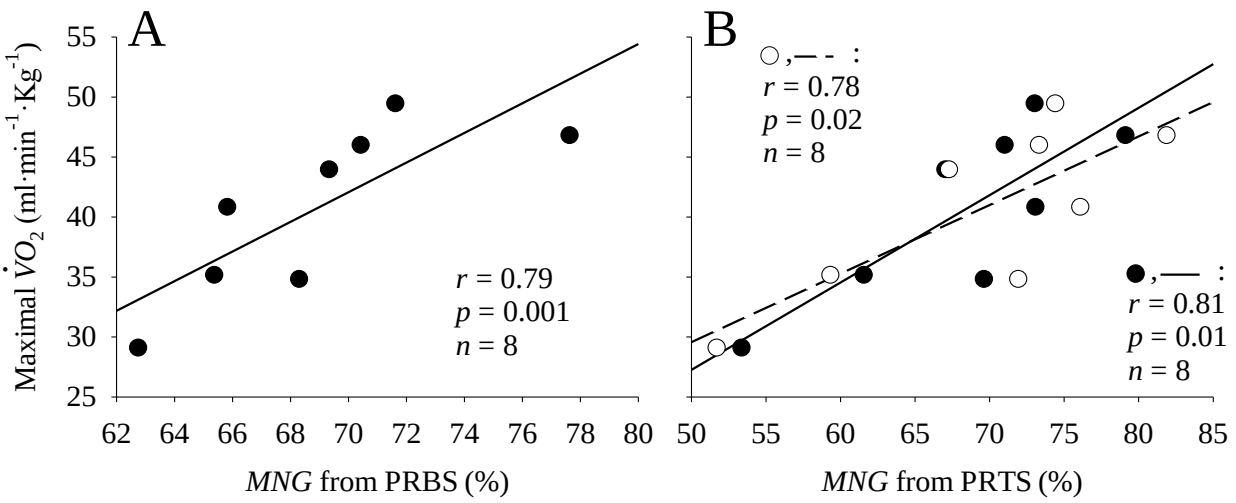

Figure 40. Maximal oxygen uptake and mean normalized gain.
A: correlation between maximal oxygen uptake ($\dot{V}O_2$) and mean normalized gain (MNG) obtained from the oxygen uptake response during pseudorandom binary sequence (PRBS). B: correlation between maximal $\dot{V}O_2$ and MNG obtained from the oxygen uptake response during pseudorandom ternary sequence (PRTS). The MNG was estimated using hip acceleration (ACC, ○) or walking speed (●) as system inputs during PRTS. r: Pearson's correlation level, p: statistical significance level and n: sample size.

5.5 Discussion

In alignment with our initial hypothesis, the aerobic system dynamics in response to a novel over-ground walking protocol correlated with the aerobic dynamics during cycle ergometry testing. The oxygen uptake kinetics assessed by the mean normalized gain during the pseudorandom ternary sequence walking test correlated with the traditionally determined time constant measured during cycling exercise. The current study has added to the understanding of $\dot{V}O_2$ kinetics during dynamic transitions in exercise and provided a foundation upon which $\dot{V}O_2$ kinetics could be studied during variations in the speed of over-ground walking such as might occur during normal activities of daily living. To our knowledge, this was the first time that a PRTS protocol was used to study $\dot{V}O_2$ kinetics. Our results showed that hip accelerometers can be used as a proxy of work rate during random activities and therefore as a system input for aerobic system dynamics investigation. In

addition, the $\dot{V}O_2$ dynamics, assessed by the MNG, were similar between PRTS and PRBS, and correlated with maximal $\dot{V}O_2$.

The advancements of low-cost and comfortable wearable sensors allowed the acquisition of intensive longitudinal biological data during unsupervised activities of daily living (Nakamura, Kiyono, Wendt, Abry, & Yamamoto, 2016; Walls & Schafer, 2012). Accelerometers are one of the most common wearable sensors used to infer the external work originating from spontaneous physical activity (Whitcher & Papadopoulos, 2014). Therefore, this sensor has the potential to be used as a system input for the study of the aerobic system dynamics during realistic activities, which might expand physical fitness evaluation far beyond the laboratory constraints. In this study, the hip accelerometer signals were successfully validated in comparison to walking speed data (Figure 36) that is correlated to metabolic demand (Holt, Hamill, & Andres, 1991; Tudor-Locke & Rowe, 2012). However, the detection algorithm used to estimate walking cadence, and therefore the walking speed, may fail to identify steps during complex body movements as expected during activities of daily living (Marschollek et al., 2008). Therefore, the metabolic cost and system input during activities of daily living might be better characterized by the hip accelerometer in comparison to walking speed or cadence since it is not necessary to detect cyclic events (steps). In addition, the accelerometer was located closer to the body center of mass (i.e., hip) with a higher correlation to the metabolic demand during physical activity (Chen et al., 2003).

Walking is considered a common activity of daily living that requires a high O_2 demand (and therefore, greatest increase in $\dot{V}O_2$) due to the high degree of muscle activation. This characteristic enables the clear differentiation of the $\dot{V}O_2$ response from the resting metabolic rate. During activities of daily living, the evaluation of the $\dot{V}O_2$ data during walking periods has the potential to be used to assess the aerobic system dynamics. To test this potential, the proposed

PRTS protocol was used to simulate the step cadence changes that are expected to occur during realistic activities of daily living, although not with the same pattern. The $\dot{V}O_2$ dynamics in response to the PRTS protocol was similar to the well-established PRBS protocol (Eßfeld et al., 1987; Hughson et al., 1990). However, the proposed PRTS protocol has more applicability for the general population since the work rate was delivered by over-ground walking.

Like PRBS, the $\dot{V}O_2$ adjustment during the PRTS protocol depends on the ability of the cardiorespiratory and muscular systems to provide and utilize O_2, respectively (Hughson, 2009). This ability modulates the rate in which the $\dot{V}O_2$ increases after the exercise stimulus and faster dynamics responses are associated with better aerobic fitness (Hagberg et al., 1980; Powers et al., 1985). Therefore, a better coupling between O_2 delivery and its utilization will directly influence the $\dot{V}O_2$ response during PRTS, allowing the identification of different aerobic responses in submaximal exercise (Hughson et al., 1990; Yoshida et al., 2008).

Despite the strong linear correlation between MNG and maximal $\dot{V}O_2$ (r = 0.80), the MNG was not able to account for all variation in maximal $\dot{V}O_2$ between participants. However, the maximal $\dot{V}O_2$ estimation, used as the gold standard method, also has an expected source of error (Howley et al., 1995). Nevertheless, a faster $\dot{V}O_2$ response (i.e., higher MNG) was observed in participants with higher maximal $\dot{V}O_2$ which indicates that MNG can be used, at least, as a complementary marker of the aerobic system integrity in association to maximal $\dot{V}O_2$.

Unlike a completely random protocol, PRTS protocols offer stimulus patterns optimized to study the physiological responses during exercise for a detectable and wide frequency range that is necessary for the precise $\dot{V}O_2$ kinetics analysis. The unit length for each PRTS stimulus was 30 s rather than 5 s (Figure 34B). In addition to be more reliable for walking and to maintain consistency between studies, the choice to use this work rate unit duration was based on previous

findings (Eßfeld et al., 1987; Hughson et al., 1990). These researchers studied the $\dot{V}O_2$ response during 30 s- and 5 s-unit PRBS protocols and found that the aerobic dynamics assessed through the $\dot{V}O_2$ data measured at the mouth level was less susceptible to hemodynamics confusing factors if a 30 s-unit was used rather 5 s-unit.

As demonstrated in Figure 35, the MNG index has the characteristic to isolate temporal dynamics of a linear system from variable static gains between participants and exercise modalities. The strong correlation between the MNG obtained from the $\dot{V}O_2$ response to cycling PRBS and walking PRTS protocols (Figure 39B) might suggest that the temporal characteristics of the aerobic system are controlled by the same fundamental mechanism(s) in these different exercises (Cerretelli, Pendergast, Paganelli, & Rennie, 1979). Participants who presented a faster $\dot{V}O_2$ adjustment (i.e., higher MNG values) during cycling also presented faster dynamics during walking, even with the expected difference in muscle contraction regimen and fiber recruitment between these exercise modalities. However, the metabolic demand between both protocols was alike (Figure 37C), differing only ~1.5 $METS$, indicating that further studies are necessary to evaluate how different absolute metabolic demands required by different exercise modalities might influence the $\dot{V}O_2$ dynamics in random physical activities.

5.6 Limitations

Some important limitations have to be considered from the evidence presented in this study. The range of maximal $\dot{V}O_2$ evaluated (29 to 49 $mL \cdot min^{-1} \cdot Kg^{-1}$) was smaller in comparison to previous literature (Eßfeld et al., 1987). Therefore, new studies are necessary to verify the association between the $\dot{V}O_2$ dynamics during submaximal dynamics exercise across a wider range of maximal aerobic power assessed by maximal $\dot{V}O_2$ (in athletes or disease state for example).

The frequency-domain $\dot{V}O_2$ kinetics analysis based on PRBS/PRTS stimuli might be "contaminated" by asymmetries between the temporal dynamics of the on- and off-transient phases (Paterson & Whipp, 1991). The MNG obtained from the Fourier transformation has the potential to identify different system dynamics based on random exercise protocols if the exercise is constrained to the moderate intensity domain, where the $\dot{V}O_2$ on- and off-kinetics are symmetrical (Ozyener et al., 2001) and the dynamic system linearity is preserved for the evaluated frequencies (Eßfeld et al., 1991; Hoffmann et al., 1992). Fortunately, the metabolic rate of the majority of activities of daily living fits into this range (Hendelman et al., 2000), so the current study was intentionally limited to light and moderate exercise (Figure 36C).

5.7 Conclusion, Applications, and Future Perspectives

In conclusion, our data suggest that pseudorandom ternary sequence protocols can be used to evaluate the aerobic system dynamics. As an over-ground walking protocol, the proposed methodology is more applicable for testing the aerobic response in the general population. In addition, the aerobic response dynamics from PRBS and PRTS were correlated to maximal $\dot{V}O_2$ (Figure 40), indicating a significant outcome of this study. Unlike cycling incremental protocols used to obtain maximal $\dot{V}O_2$, the proposed PRTS protocol is more functional, can be more broadly applied to normally sedentary or less healthy individuals, and reduces the risks associated with maximal exertion.

As a consequence of a slower energy supply by the aerobic system, a slower $\dot{V}O_2$ dynamics was previously associated with functional mobility impairments in older adults (Alexander et al., 2003). The early detection of subclinical aerobic response depletion might be an indication of a decreased physiological reserve, which contributes to frailty (Newman et al., 2001).

Therefore, indexes that describe “how fast” the energy demand is supplied by the aerobic system (such as the MNG) have the potential to be considered into models for the early detection of disease states. Additionally, wearable technologies (such as accelerometers and heart rate) are becoming more popular and less costly, allowing routine daily monitoring. The combination between wearables and new data processing techniques has direct applicability for disease prevention and for the evaluation of treatment progression. In addition, the MNG was obtained from an optimized exercise stimulus for frequency domain analysis. Further studies need to evaluate the consistency of the MNG to assess the aerobic system dynamics during completely random activities, such as unsupervised activities of daily living.

Chapter 6: Prediction of Oxygen Uptake Dynamics by Machine Learning Analysis of Wearable Sensors During Activities of Daily Living

This chapter was submitted as:

Beltrame T., Hughson R. L. Prediction of oxygen uptake dynamics by machine learning analysis of wearable sensors during activities of daily living. Submitted to Scientific Reports on September 27, 2016.

6.1 Overview

Currently, oxygen uptake ($\dot{V}O_2$) is the most precise means of investigating aerobic fitness and level of physical activity; however, $\dot{V}O_2$ can only be directly measured in supervised conditions. With the advancement of new wearable sensor technologies and data processing approaches, it is possible to accurately infer work rate and predict $\dot{V}O_2$ during activities of daily living (ADL). The main objective of this study was to develop and verify the methods required to predict and investigate the $\dot{V}O_2$ dynamics during ADL. The variables derived from the wearable sensors were used to create a $\dot{V}O_2$ predictor based on a random forest ensemble regression method. The $\dot{V}O_2$ temporal dynamics were assessed by the mean normalized gain amplitude (MNG) obtained from frequency domain analysis. The MNG provides a means to assess aerobic fitness. The predicted $\dot{V}O_2$ during ADL was strongly correlated (r=0.87, P<0.001) with the measured $\dot{V}O_2$ and the prediction bias was 0.2 ml·min^{-1}·kg^{-1}. The MNG calculated based on predicted $\dot{V}O_2$ was strongly correlated (r=0.71, P<0.001) with MNG calculated based on measured $\dot{V}O_2$ data. This new technology provides an important advance in ambulatory and continuous assessment of aerobic fitness with potential for future applications such as the early detection of deterioration of physical health.

6.2 Introduction

The measurement of oxygen uptake ($\dot{V}O_2$) responses in steady-state condition is commonly used to precisely estimate the individual energy expenditure of a given physical activity (Meijer, Westerterp, Koper, & Ten Hoor, 1989). Besides energy expenditure estimation, the evaluation of the temporal dynamics of the $\dot{V}O_2$ during physical activity transitions can provide valuable information about the aerobic system integrity (Borghi-Silva et al., 2012; Whipp & Ward, 1992). From a practical perspective, abnormal aerobic responses to exercise may precede the clinical detection of non-communicable diseases (Guazzi et al., 2012). Therefore, wearable technologies that continuously evaluate the aerobic response during non-supervised activities of daily living (ADL) have the potential to identify not only changes in physical fitness, but also disease states before the manifestation of clinical symptoms (Nakamura et al., 2016; Rudner, McDougall, Sailam, Smith, & Sacchetti, 2016).

In parallel with the advances in wearable devices, machine learning (ML) techniques are becoming popular to analyze the large quantities of longitudinal data streamed from these devices (Mannini & Sabatini, 2010). The ML algorithms may provide the technical basis to better identify non-trivial and complex patterns in long-term continuous biological signals (Witten & Frank, 2005). The data mining process by ML is often based on the relationship between known inputs and outputs (supervised learning) (Altini et al., 2016). The initial crude algorithms are feed with input and known output data (examples), and evolve according to the general structures that describe the input-output relationships. When the algorithm reaches a satisfactory generalization capacity, the output can be estimated by the inputs through a set of rules nested within the algorithm.

In this study ML will be used to build a $\dot{V}O_2$ predictor based on inputs provided by wearable sensors. The main objective of this study was to predict and evaluate the temporal dynamics of the aerobic response during realistic activities. Specifically, data acquired from wearable sensors fusion will be processed by ML algorithms to predict the $\dot{V}O_2$ data with subsequent aerobic system analysis. The hypothesis of this study is that the signals collected by wearable sensors contain latent features that allow the characterization of the aerobic system response to exercise.

6.3 Methods

6.3.1 Study Design

Sixteen healthy, active male adults enrolled in this study (27 ± 7 years old, 174 ± 7 cm and 78 ± 14 kg). A written, informed consent was obtained from all participants. The Office of Research Ethics at the University of Waterloo reviewed and approved the research procedures that were consistent with the Declaration of Helsinki.

As opposed to previous studies (Altini et al., 2016; Su et al., 2009; Su, Wang, Celler, & Savkin, 2007) that used treadmill ergometers, participants performed two pseudorandom ternary sequence (PRTS) over-ground walking protocols separated by simulated ADL. Considering a step duration of 30 s, the PRTS was generated according to previous literature (Kerlin, 1974; Peterka, 2002). The PRTS was composed by a warm-up period of 300 s of extra sequence followed by 13 min of protocol. The walking cadences alternated between three levels (75, 105 or 135 steps·min^{-1}). These levels corresponded to ≈ ±30% of the normal walking cadence (Tudor-Locke & Rowe, 2012). The simulated ADL protocol (≈ 20 min) was composed by sitting, organizing the shelf, carrying objects (≈ 4.5 Kg), stairs (four up and four down flights of stairs), self-paced walking and

sitting using the computer. Figure 41 exemplifies the behaviour of the hip acceleration (further explained) during these protocols.

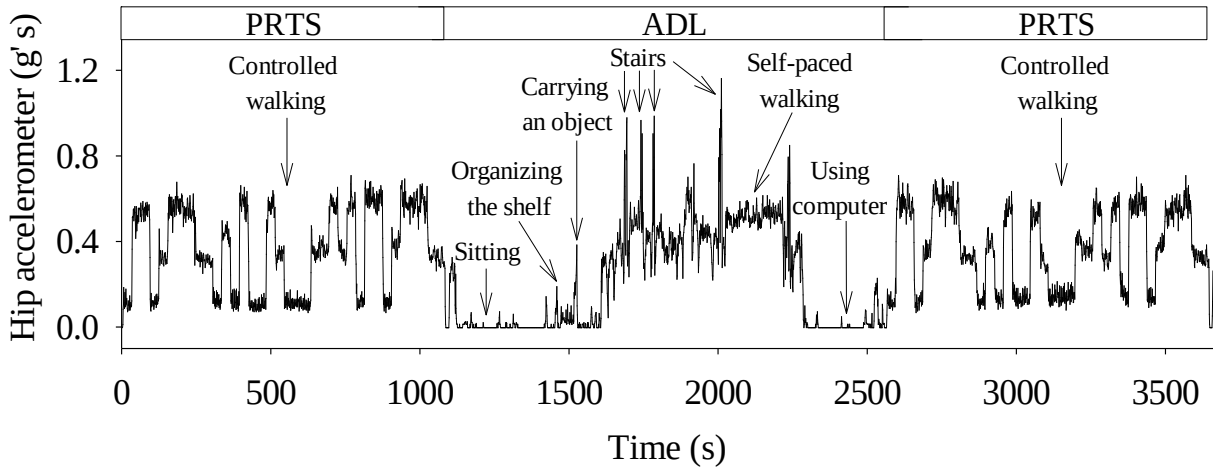

Figure 41. Hip acceleration during physical activity.
Representative hip acceleration response during pseudorandom ternary sequence (PRTS) walking protocol and simulated activities of daily living (ADL). The arrows point to each specific ADL (labels).

6.3.2 Data Acquisition

Throughout the PRTS and simulated ADL, the $\dot{V}O_2$ data were measured breath-by-breath by a portable metabolic system (K4b^2, COSMED, Italy). The gas concentrations and air volume/flow were calibrated following manufacturer's specifications before each visit. The wearable sensors hip accelerometer, ECG and respiration band were integrated into a smart shirt (Hexoskin®). The raw sensor signals were used to obtain heart rate (HR), minute ventilation ($\dot{V}E$), breathing frequency (BF), total hip acceleration (H_{acc}), and walking cadence (CAD) through previously validated proprietary algorithms (Villar et al., 2015). From the HR data, a new variable was derived. The ΔHR was composed by the difference between the current HR value and the previous value by a 1 s lag operator, capturing dynamic changes in cardiac activity. The combination of the accelerometer sample rate (64 Hz), resolution (0.004 g) and range (16 g's) was sufficient to capture

all expected ADL movements (Bouten et al., 1997). The data from the wearable sensors and the $\dot{V}O_2$ signal were synchronized, linearly interpolated and re-sampled at 1 Hz.

6.3.3 Machine Learning

As demonstrated in Figure 42, the $\dot{V}O_2$ predictor was based on a random forest machine learning method (Breiman, 2001). The re-sampled 1 Hz data for HR, ΔHR $\dot{V}E$, BF, H_{acc}, CAD and $\dot{V}O_2$ were low-pass filtered at 0.01 Hz. Frequencies higher than 0.01 Hz were filtered out to diminish the influences of non-linearities over the machine learning. Data mining was performed in Matlab R2016a (MathWorks, Natick, MS, US).

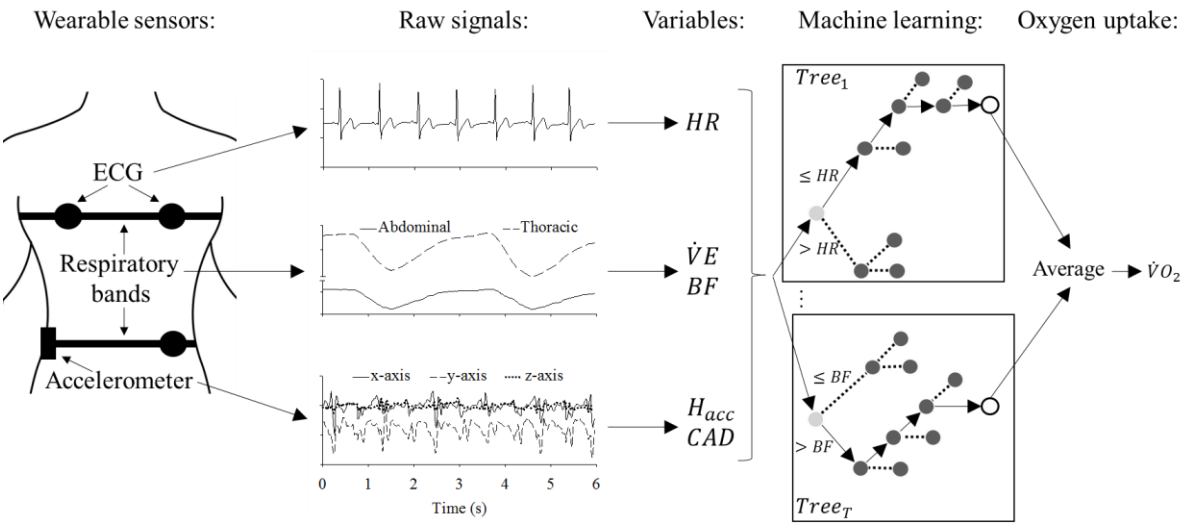

Figure 42. From wearable sensor signals into oxygen uptake.
Illustration of the transformation of wearable sensor signals into oxygen uptake ($\dot{V}O_2$) by a random forest regression model. This algorithm was created based on a machine learning approach (see text for details). The heart rate (HR) was estimated based on the ECG signal. The ΔHR variable consisted of the difference between the current HR value with the previous value. The ventilation minute ($\dot{V}E$) and breathing frequency (BF) were estimated based on two respiratory bands (abdominal and thoracic). The hip acceleration (H_{acc}) and walking cadence (CAD) were estimated based on tri-axis (x, y and z axis) accelerometer located at the hip. These variables were considered as inputs to a random forest algorithm consisting of a ruleset (regression trees, $Tree_T$) composed by thresholds that split the signal into two tree branches (light grey circles). The numerical output ($\dot{V}O_2$) was the average of all final selected tree leaves (open circles).

The tested algorithms were validated by leave-one-participant-out cross-validation (Ross et al., 2009). This validation was chosen to avoid data overlapping between training and testing datasets which might mislead the prediction accuracy evaluation (Witten & Frank, 2005). The mined algorithm accuracy was evaluated by the average of the Pearson's linear correlation coefficient (r) of all folds from the validation process. The time series data and the ability of the predictor to estimate the system temporal dynamics (further explained) were considered into this validation.

Ensemble models (i.e., "super" machine learning models that combine the output of individual models within) have gained popularity for outperforming singular models with large

complex data (Dietterich, 2000). The random forest model is a popular ensemble model that does not make any inherent assumptions about data distribution. It treats the feature space as clustered disjoint sets of target ($\dot{V}O_2$) values, which is helpful for aggregating many data points that may be similar but vary due to measurement noise. When building individual trees, the method actively seeks data that improve the fit. Finally, prediction is fast, only requiring fast tree traversals. These properties make it a good candidate for real-time $\dot{V}O_2$ prediction for future implementations in embedded systems.

The random forest model was implemented as an ensemble of bootstrap aggregate regression trees. Specifically, each tree is made up of nodes with up to two children nodes, starting with the root node and traversing down to the end. A node contains a splitting criterion (e.g., HR > 50 bpm). For each time point, the feature values were evaluated by traversing the nodes to the bottom of the tree based on their decision values. Each bottom node, the "leaf node", contains the tree's estimated output for the given feature values. Each regression tree was grown individually with a randomly sampled subset of the training data. The final estimated $\dot{V}O_2$ value for a given time point was computed as the average prediction across all the tree's leaves.

Mathematically, let $X = [\mathrm{x}_1, \ldots, \mathrm{x}_n]$ be a set of n feature vectors, and y be the (known) $\dot{V}O_2$ value corresponding to each feature set. The goal was to develop a random forest of T individual regression trees. Each individual regression tree was trained on a random data sample (in-bag selection) for generalizability. Each tree was grown node-by-node as follows. For each node, a random 1/3 subset of the features was selected as candidate splitting features. An optimal node split (into left and right subtrees) was sought such that it minimized the sum of squared residuals in the two prospective subsets:

Equation 10

$$\epsilon_i = \min_s \left\{ \underbrace{\sum_{i:x_i \le s} (y_i - \bar{c}_l)^2}_{left\ subregion} + \underbrace{\sum_{i:x_i > s} (y_i - \bar{c}_r)^2}_{right\ subregion} \right\};$$

where s is the splitting value, x_i is the candidate splitting feature, y_i, and $\bar{c}_l, \bar{c}_r$ are the mean responses from the prospective left and right subregion respectively. The feature that exhibited the smallest ϵ_j was chosen as this node's splitting criterion:

Equation 11

$$argmin_j \{\epsilon_j\}.$$

This process was repeated recursively for each node, until a full tree was grown. Thus, given a new feature vector x, each tree predicted the $\dot{V}O_2$ value $\hat{y}_t$ by following the binary splits according to the given feature vector and outputting the leaf node's prediction value where a leaf node (dark grey circles in Figure 42) is a node in the tree that doesn't have any split (light grey circles in Figure 42). The final predicted $\dot{V}O_2$ value was computed by the bag's weighted average of the individual tree predictions:

Equation 12

$$\widehat{\dot{V}O_2} = \frac{1}{T} \sum_{t=1}^{T} \hat{y}_t.$$

6.3.4 Oxygen Uptake Dynamics Evaluation

The data corresponding to the PRTS protocol, optimized for system identification (Kerlin, 1974), was used for the evaluation of the aerobic system dynamics. The H_{acc} data were considered as system inputs and the measured and predicted $\dot{V}O_2$ as outputs. To increase the signal-to-noise

ratio, input and output responses during each of the two PRTS were time aligned and averaged to obtain a single PRTS response per participant. Fast Fourier Transformations were used to convert the data from time to frequency domain. The frequency range was limited to 0.008 Hz to avoid the influence of system non-linearities (Hoffmann et al., 1992). As a characteristic of the PRTS protocol (Kerlin, 1974), the amplitudes for the even harmonics were excluded a priori due to the absence of system stimulus. As previously proposed (Eßfeld et al., 1991; Hoffmann et al., 1992), the system gains at the different frequencies (output/input ratio) were normalized by the gain at the first harmonic. This procedure eliminates the influence of the system static gain over the temporal characteristics of the system which ultimately are related to aerobic power (Chilibeck et al., 1995; Hagberg et al., 1980; Hughson, 2009; Powers et al., 1985). Finally, the mean of the normalized gains (MNG) was used as an index of the system temporal dynamics. Higher MNG values mean faster aerobic responses. Data analysis was performed by a certified (#100-314-4110) LabVIEW associated developer (National Instruments, Austin, TX, US).

6.3.5 Statistical Analysis

For each participant and considering the entire group response, the predicted $\dot{V}O_2$ data were validated during the PRBS and ADL using the raw measured $\dot{V}O_2$ data as reference (without 0.01 Hz high pass filtering). The MNG estimated from the predicted $\dot{V}O_2$ was also validated using the MNG estimated from the measured $\dot{V}O_2$ as reference. The r coefficient, Bland-Altman plot, confidence interval (CI_{95}) and Student t-test were used for data validation. The prediction bias (measured minus predicted) was also compared with the equality line (bias = 0) by Student t-test. To further explore the predictions during ADL, the sample was also clustered into three groups according to the metabolic equivalent ($METS$) estimated from the measured $\dot{V}O_2$ ($METS =$

$\dot{V}O_2/3.5$). The first cluster was composed by the resting metabolic rate (RMR) estimated from the 60 s average of the $\dot{V}O_2$ response during resting. Since the exercise protocol designed for this study was focused on realistic ADL that is in majority composed by light and moderate intensity (Hendelman et al., 2000), less than 2% of the experimental data were composed by $METS$ higher than 6.0. Therefore, the average of the samples within the intervals 2-3.9 (505 ± 137 samples per participant) and 4.0-5.9 (422 ± 67 samples per participant) were grouped as light and moderate activities, respectively (Jetté, Sidney, & Blümchen, 1990).

6.4 Results

Figure 43 displays the comparison of the measured and predicted $\dot{V}O_2$. The data obtained during ADL are displayed in Figure 43A, 3B and 3C and the data obtained during the PRTS protocol are displayed in Figure 43D, 43E and 43F. As demonstrated in Figure 43A, the quality of the prediction was verified by a strong and significant positive correlation (r = 0.87, P < 0.001 and n = 20,868) with the measured data during ADL. By individually analyzing the correlation level, all participants presented a strong and significant positive correlation (r = 0.88±0.05, P < 0.001±0.00 and n = ≈1200 per participant) between predicted and measured data with a bias of 0.331 ± 1.187 ml·min^{-1}·kg^{-1}. The Bland-Altman plot for the measured and predicted $\dot{V}O_2$ during ADL is shown in Figure 43B. Considering the entire sample for ADL, the bias (0.294 ml·min^{-1}·kg^{-1}, ≈ 2.2 % of the average response) was statistically (P < 0.05) higher than the equality line. The CI_{95} was 6.166 ml·min^{-1}·kg^{-1} around the bias. The relative distribution of the error is plotted in Figure 43C. The error distribution followed a Gaussian-like function with the majority of the error located close to the equality line (bias = 0).

Considering all data points from all participants during PRTS (Figure 43D), the correlation coefficient was strongly positively correlated (r = 0.69, P < 0.001 and n = 12,480). By individually analyzing the correlation level, all participants presented a strong and significant positive correlation (r = 0.77±0.09, P < 0.001±0.00 and n = 780 per participant) between predicted and measured data. The Bland-Altman plot for the measured and predicted $\dot{V}O_2$ during PRTS is shown in Figure 43E. The bias of the prediction, -0.259 ml·min^{-1}·Kg^{-1} was lower (P < 0.001) than the equality line representing only ≈ 1.7 % of the average response during the PRTS protocol. The CI_{95} was 4.250 ml·min^{-1}·kg^{-1}. The relative distribution of the error is plotted in Figure 43F. This distribution also followed a Gaussian-like function with the majority of the error located close to the equality line (bias=0).

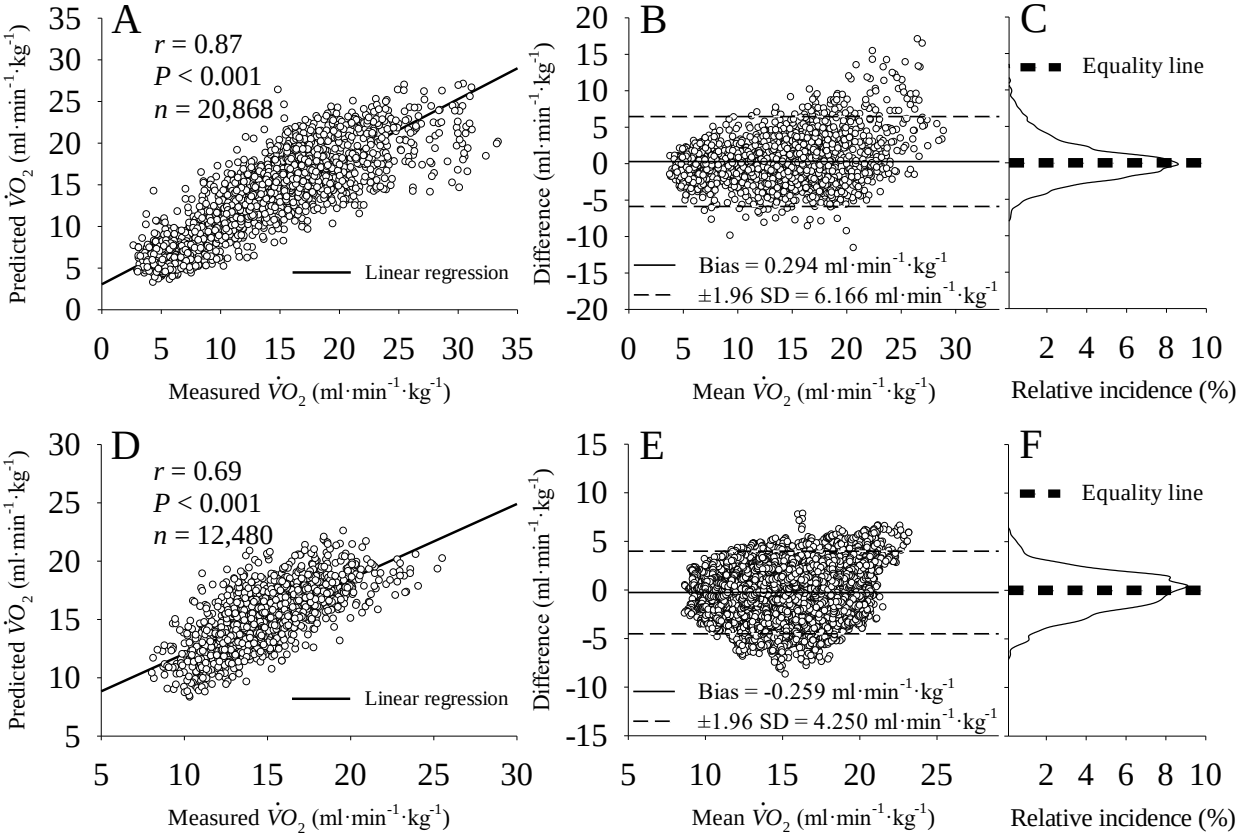

Figure 43. Predicted and measured oxygen uptake.
Data were down sampled to 0.1 Hz for a better data visualization. Graphs A, B and C are related to data obtained during activities of daily living (~1200 samples per participant) and graphs D, E and F are related to data obtained during pseudorandom walking protocol (1560 samples per participant). A and D: linear correlation of the measured and predicted oxygen uptake ($\dot{V}O_2$) between all participants. B and E: Bland-Altman plot of the predicted and measured $\dot{V}O_2$ data. C and F: distribution of the prediction error.

6.4.1 Metabolic Equivalent

The ability of the random forest algorithm in estimate different levels of metabolic equivalent at rest (resting metabolic rate, RMR) and during light and moderate ADL is depicted in Figure 44. These data were based on the same data displayed in Figure 43A but clustered into groups according to the metabolic demand during ADL (Jetté et al., 1990). Less than 2% of the experimental data were composed by intense activities (> 6 $METS$), therefore these data were excluded *a priori*. The proximity of the estimated $METS$ to the equality line demonstrates that the

random forest was able to dissociate between different metabolic demands. The proposed algorithm can be used to classify activity levels between light and moderate ADL.

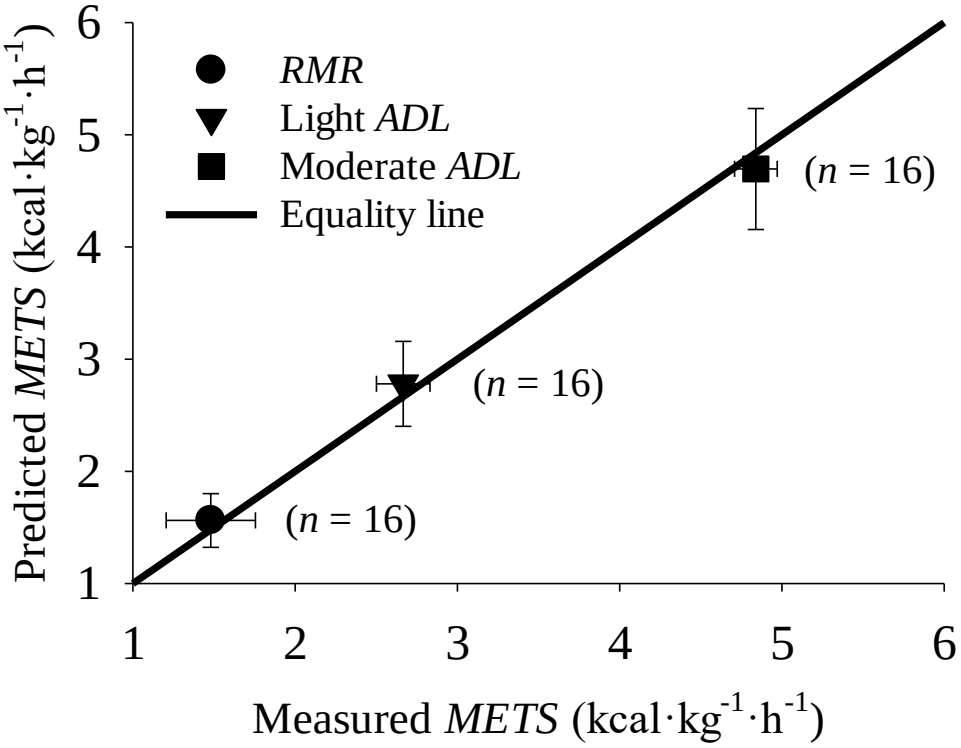

Figure 44. Predicted and measured metabolic equivalent.
Relationship between the measured and predicted metabolic equivalent ($METs$) during resting (defined as the resting metabolic rate, RMR, < 2 $METS$) and during light (2.0 – 3.9 $METS$) and moderate (4.0 – 5.9 $METS$) activities of daily living (ADL).

6.4.2 Aerobic System Temporal Dynamics

The group mean response for the second-by-second average $\dot{V}O_2$ during the PRTS protocol was computed and depicted in Figure 45.

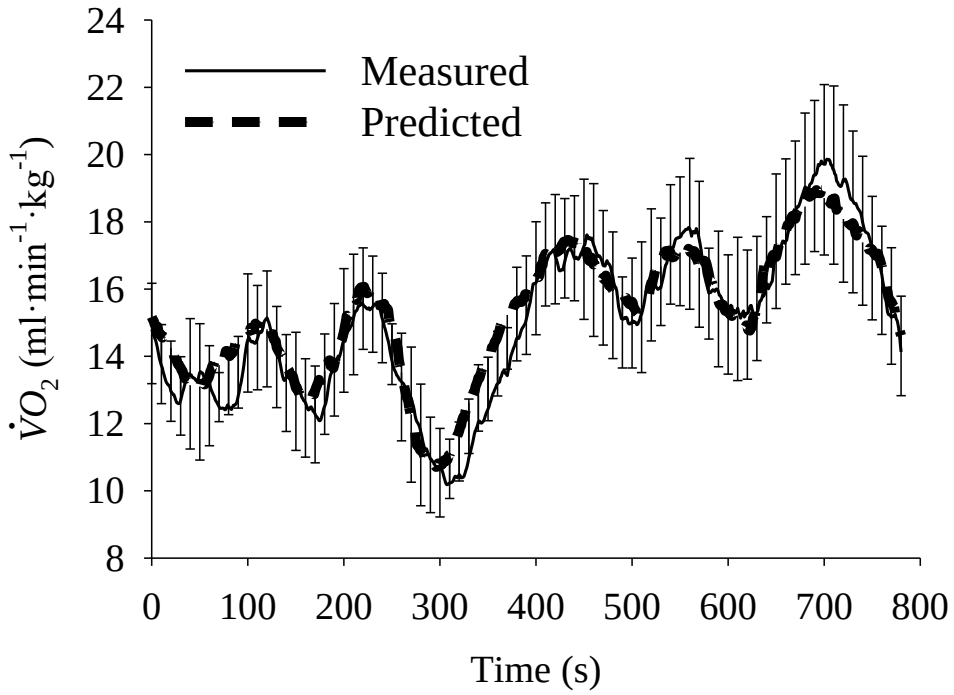

Figure 45. Measured and predicted oxygen uptake during pseudorandom ternary sequence. Second-by-second mean (lines, n =16 per point) of the measured and predicted oxygen uptake ($\dot{V}O_2$) during pseudorandom ternary sequence over-ground walking protocol. The SD (upward vertical bars for measured values, downward for predicted) are plotted at 10s intervals.

The comparison of the aerobic system temporal dynamics assessed by the MNG calculated from measured and predicted $\dot{V}O_2$ data during the PRTS protocol (Figure 45) is displayed in Figure 46. The MNG calculated from predicted $\dot{V}O_2$ data was statistically similar (P = 0.136) and strongly, positively correlated to the MNG calculated from measured $\dot{V}O_2$ data. The MNG calculated from predicted $\dot{V}O_2$ data presented a bias of -6.19 % which corresponds to 10% of the average MNG response. The bias was statistically (P = 0.012) lower than the equality line (bias = 0). The CI_{95} was 17.63 % around the bias (or 29% of the mean MNG response).

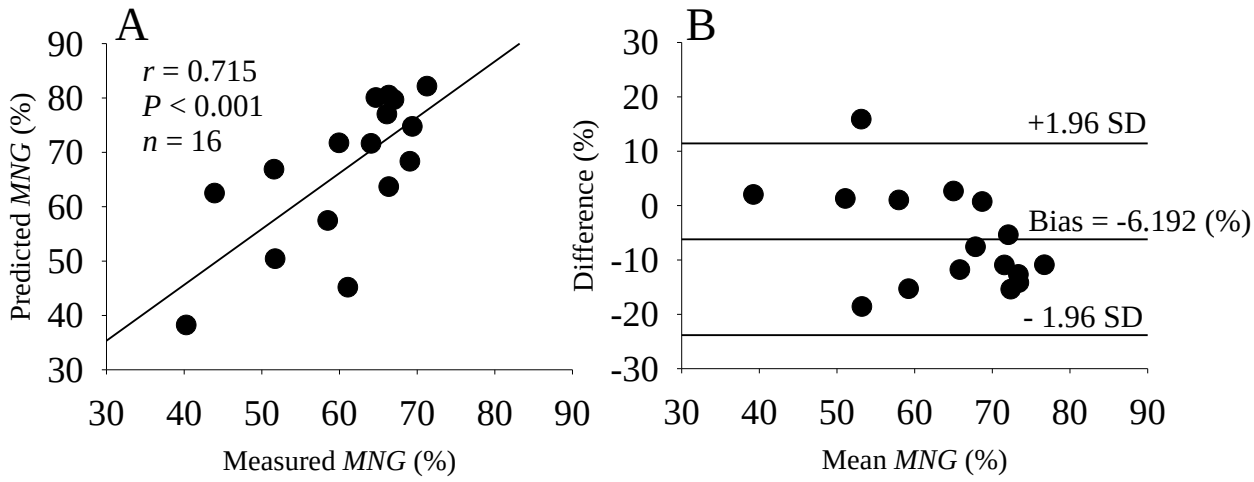

Figure 46. Measured and predicted mean normalized gain.
A: linear correlation between the mean normalized gain (MNG) calculated from predicted and measured oxygen uptake data. B: Bland-Altman plot of the data displayed in A.

6.5 Discussion

In agreement to the initial hypothesis, the signals obtained from the wearable sensors allowed the prediction of oxygen uptake during activities of daily living and random paced walking. Aerobic system temporal dynamics assessed by the MNG from the predicted oxygen uptake were similar to those of oxygen uptake measured by a portable metabolic device. In addition, the random forest algorithm was able to identify physical activity levels and the resting metabolic demand.

Estimating the correct measurement of physical activity level during realistic scenarios remains a challenge (Sallis & Saelens, 2000) and hence, new wearable technologies and data processing approaches are necessary. The quantification of the physical activity level usually involves the estimation of energy expenditure by indirect calorimetry. Indirect calorimetry has also been is used to calibrate wearable sensors for a wide range of activities during steady-state, allowing the energy expenditure estimation (i.e., steady-state $\dot{V}O_2$) without the need for the original calorimetry measurement (Staudenmayer et al., 2009). However, the complexity and diversity of ADL represent a challenge for the precise physical activity estimation in a realistic

scenario (Altini et al., 2016; Chen et al., 2004; Jacobi et al., 2007; Schrack et al., 2014; Tan et al., 2011).

During randomly varying exercise intensities, assessment of the rate at which $\dot{V}O_2$ adapts to the metabolic demands is indicative of aerobic fitness (Hagberg et al., 1980; Phillips et al., 1995; Powers et al., 1985). Thus, the ability to predict $\dot{V}O_2$ with an adequate time resolution provides an opportunity to obtain valuable information about cardiovascular health in addition to standard estimates of energy expenditure. Previous approaches to this problem have been restricted to studies conducted under controlled laboratory conditions (Su et al., 2009, 2007). In the present study, we investigated a simulated ADL protocol as well as an over-ground walking protocol (PRTS) that mimicked the dynamic changes in walking cadences expected during daily activities. The PRTS protocol offered an optimized stimulus for the aerobic system analysis through the study of the $\dot{V}O_2$ temporal dynamics and its prediction by a random forest machine learning regression model.

Recently, Altini et. al (Altini et al., 2016) used a novel approach for estimating $\dot{V}O_2$ during nonsteady-state phases. Their algorithm combined an activity classification method with a numerical prediction approach that predicted $\dot{V}O_2$ during dynamic phases of moderate ADL. However, the ability of the algorithm to correctly identify the $\dot{V}O_2$ dynamics was reported only as a lower error of the estimation during exercise transitions. No further validation of the modelling parameters was carried out to explore the characterization of the aerobic adjustment dynamics with eventual health-related outcome.

In addition to HR and accelerometer (Altini et al., 2016; Su et al., 2007), the acquisition of more biological data such as $\dot{V}E$ and BF improved the $\dot{V}O_2$ estimation during transitions and steady-state. When the MNG was calculated based on the predicted $\dot{V}O_2$ without considering $\dot{V}E$

and BF as inputs, the MNG accuracy decreased by 55 % (based on r value). Therefore, the integration of respiratory measurements for $\dot{V}O_2$ prediction seems to be indicated, evidencing some advantages of the smart-shirts over simpler wearable devices. As with the majority of the biological processes, $\dot{V}E$ and BF signals are also delayed during transitions and despite not having exactly the same dynamics as the $\dot{V}O_2$, they have predictable relationships (Xing, Cochrane, Yamamoto, & Hughson, 1991) which would contribute to a better understanding of the biological variability during transitions.

Studies that optimize the $\dot{V}O_2$ prediction during exercise transition with the intention to better estimate energy expenditure might be controversial. The O_2 deficit at the on-transition phase is counter-balanced by the excess of O_2 consumption during recovery (Ozyener et al., 2001) thus the calorie counts based on different predicted $\dot{V}O_2$ temporal dynamics should be almost similar. The energy expenditure estimation is independent on the $\dot{V}O_2$ temporal dynamics, being determined only by the correct system static gain estimation. Therefore, in terms of calories (i.e., energy expenditure) calculated after a period of time, algorithms that successfully predict steady-state $\dot{V}O_2$ might be enough to estimate energy expenditure and no further methods are necessary for the $\dot{V}O_2$ prediction during nonsteady-state phases. The justification for the correct $\dot{V}O_2$ estimation during exercise transition has to have a reason beyond a "better" physical activity level estimation as considered next.

The $\dot{V}O_2$ responses during transitions have been used to assess aerobic fitness in constrained settings (Eßfeld et al., 1987; Powers et al., 1985) and the expansion of these approaches outside of the laboratory environment represents the possibility to track changes in aerobic fitness and physical health on a daily basis. The assessment of aerobic fitness by wearable sensors during unsupervised daily living routine seems very promising. As demonstrated in Figure

46, our algorithm was able to characterize the temporal dynamics (MNG) of the aerobic system based on the predicted $\dot{V}O_2$ data. Therefore, the proposed algorithm can be used in the future for aerobic fitness assessment based on predicted $\dot{V}O_2$ data obtained from wearable sensors during transitions encountered during ADL for ordinary people or patient populations, or during prescribed variations in work rate, such as athletic training.

6.6 Study Limitations

The purpose of the current study was to predict $\dot{V}O_2$ during the most common ADL. Thus, the exercise protocols were limited to light and moderate activities with intensities lower than ~6 $METs$, and any attempt to extend this range should include extensive testing for reliability. Any studies that investigate the algorithm proposed in the current study for high intensity activities must recognize that $\dot{V}O_2$ dynamics become more complex under these conditions with the potential for nonlinear contributions. The $\dot{V}O_2$ predictor developed in this study can be applied to evaluate the aerobic system dynamics during ADL where intense activities are unlikely to occur (Hendelman et al., 2000).

The population tested in the current study (healthy men) had narrow weight and age ranges which might also restrict the use of the proposed algorithm. Further studies are necessary to verify the reliability of the $\dot{V}O_2$ predictions in different populations. It is recommended that any future study incorporate dynamic protocols (such as the PRTS) to evaluate the ability of the proposed algorithms to predict the $\dot{V}O_2$ dynamics during exercise transitions.

6.7 Conclusion

In conclusion, oxygen consumption dynamics can be predicted from the fusion of data from non-intrusive wearable sensors and machine learning prediction algorithms. Longitudinal predictions of oxygen uptake can be obtained from wearables based on the validation completed in the current study for activities of daily living and random over-ground walking. The proposed random forest ensemble predictor in conjunction with MNG can be used to investigate aerobic response during realistic activities with direct applicability for the general population. Developing the aforementioned predictive model will provide a unique opportunity for continued lifelong $\dot{V}O_2$ collections in unsupervised environments. This new technology provides a significant advance in ambulatory and continuous assessment of energy expenditure and aerobic fitness with potential for future applications such as the early detection of deterioration of physical health.

Chapter 7: Longitudinal Aerobic System Analysis During Unsupervised Activities of Daily Living Based on Wearable Sensors

7.1 Overview

Physical activity levels are related to the energetic demand throughout the day with no information regarding the integrity of the multiple physiological systems involved in the energetic supply. The longitudinal analysis of the oxygen uptake ($\dot{V}O_2$) data by wearable devices in realistic settings may permit development of a practical tool for the study of the aerobic system dynamics. The objective of this study was to evaluate the aerobic system dynamics based on predicted $\dot{V}O_2$ data obtained from wearable sensors during unsupervised activities of daily living ($uADL$). Thirteen healthy men (26 ± 5.6 years old, 179 ± 9 cm and 79 ± 13 kg) performed a laboratory controlled protocol and were monitored for ≈6 hrs per day, during four days ($uADL$ data). Variables derived from accelerometer, heart rate monitor and respiratory bands during $uADL$ were processed by a machine learning algorithm that predicted $\dot{V}O_2$ data. This algorithm was successfully validated (r = 0.86, p <0.001, n = 63,571) during the laboratory protocol by measuring the $\dot{V}O_2$ simultaneously by a metabolic analyzer. The predicted $\dot{V}O_2$ dynamics were evaluated by frequency domain analysis and compared with the measured $\dot{V}O_2$ during the laboratory visit. The temporal dynamics of the aerobic system based on predicted $\dot{V}O_2$ during $uADL$ was correlated to the aerobic system dynamics based on measured $\dot{V}O_2$ during laboratory controlled protocol (r = 0.82, p <0.001, n = 13). In conclusion, aerobic system dynamics can be investigated during unsupervised activities of daily living by wearable sensors. These algorithms have the potential to be incorporated into wearable systems for early detection of non-communicable diseases in realistic environments.

7.2 Introduction

The study of the oxygen uptake ($\dot{V}O_2$) dynamics during unsupervised activities of daily living ($uADL$) has never been attempted. Recent algorithms have used various strategies to predict $\dot{V}O_2$ or to assess cardiorespiratory fitness in the laboratory and during free-living conditions. One approach incorporated nonlinear multivariable modeling and achieved good prediction of $\dot{V}O_2$ during randomly varying treadmill walking (Su et al., 2009) but did not quantify dynamic responses, and did not apply the model to $uADL$. Another approach relied on context-specific categorization of $\dot{V}O_2$ responses during simulated ADL (Altini et al., 2016). These previous models enabled the precise evaluation of physical activity (PA) levels through prediction of $\dot{V}O_2$ ($\widehat{\dot{V}O_2}$) data (Altini et al., 2016; Su et al., 2009). However, PA levels were related to the energetic demand throughout the day with no information regarding the integrity of the multiple physiological systems involved in the energetic supply. The longitudinal study of the aerobic system dynamics through $\widehat{\dot{V}O_2}$ data analysis in realistic settings may permit development of a practical tool with direct physiological significance to clinical outcomes (Guazzi et al., 2012; Newman et al., 2006).

Wearable devices (e.g., accelerometers) are commonly used to estimate PA levels based on $\dot{V}O_2$ steady state response for each specific PA type (Staudenmayer et al., 2009). There is an association between the O_2 cost (steady state $\dot{V}O_2$) and energetic demand which allows the energy expenditure estimation based on wearable sensors. However, during PA transitions, the aerobic response and consequently the $\dot{V}O_2$ dynamic lags behind the energetic demand (Barstow et al., 1994). Nonetheless, it is during PA transitions, periods of high homeostatic perturbation, that the aerobic system demonstrates its integrity for the interactions with the external work. Classically, it is hypothesized that a faster aerobic adjustment to a new energetic demand is associated with a

better aerobic fitness (Norris & Petersen, 1998; Phillips et al., 1995; Powers et al., 1985), while slower adjustments are associated with disease prognosis (Borghi-Silva et al., 2012; Pessoa et al., 2013; Regensteiner et al., 1998). The energetic supply during PA transitions relies more on anaerobic high energy phosphate stores and glycolysis when the aerobic responses are slower (Koskolou et al., 1997) which might be associated with an impaired exercise perception with consequences on functional mobility and performance (Alexander et al., 2003). The early detection of abnormal aerobic system dynamics by wearable sensors might be used as a marker for primary prevention of non-communicable diseases (Guazzi et al., 2012).

The main objective of this study was to evaluate the aerobic system dynamics based on $\widehat{\dot{V}O_2}$ data obtained from wearable sensors during $uADL$. Specifically, data acquired from accelerometer, heart rate monitor and respiratory bands during $uADL$ were processed by a machine learning (ML) algorithm that predicts $\widehat{\dot{V}O_2}$ data. The aerobic system dynamics were characterized based on a parameter, mean normalized gain (MNG), derived from frequency domain analysis of $\widehat{\dot{V}O_2}$ and compared with the MNG calculated from laboratory testing with directly measured $\dot{V}O_2$. The hypothesis of this study was that it is possible to evaluate the aerobic system dynamics from wearables sensors during $uADL$.

7.3 Methods

7.3.1 Study Design

Thirteen healthy active men (26 ± 5.6 years old, 179 ± 9 cm and 79 ± 13 kg) participated in this study. A written, informed consent was obtained from all participants. The Office of Research Ethics at the University of Waterloo reviewed and approved the research procedures that were consistent with the Declaration of Helsinki. This longitudinal study was divided in two parts. The

first part comprised of data collection without supervision ($uADL$) where the participants wore wearable sensors during their normal daily routine for four consecutive days. One participant only wore the wearables for three days. The researchers briefly met with the participant twice a day, at 9:52 ± 1:17 am and 4:11 ± 1:21 pm, to administer and remove the wearable monitoring devices, respectively. Therefore, participants wore the sensors for 6.3 ± 1.4 hours a day. Three additional participants (26 ± 1.2 years old, 178 ± 4 cm and 89 ± 7 kg) started the protocol, but due to technical problems related to the respiratory bands and ECG electrodes, they were excluded from further analysis. From the 13 participants who completed the $uADL$ analysis, 1.16 billion samples for each variable were analyzed.

In the second part of this study, participants walked and performed prescribed, simulated ADL while wearing the wearable sensors and a portable metabolic measurement system. The test protocol included two identical pseudorandom ternary sequence (PRTS) (Kerlin, 1974) over-ground walking protocols. The PRTS consisted of units that were 30s duration and three levels of walking cadence: 75, 105 or 135 steps·min^{-1}. The selected cadences were within the range of normal walking expected during ADL (Tudor-Locke & Rowe, 2012). Between the two PRTS, participants performed simulated ADL composed by sitting (≈ 10 min), organizing the shelf (≈ 5 min), carrying an object (≈ 5 min), stairs (≈ 5 min) and self-paced over-ground walking in different environments (≈ 15 min). From the PRTS and simulated ADL, wearable sensor data and directly measured $\dot{V}O_2$ were used to build an algorithm to obtain $\widehat{\dot{V}O_2}$ with a ML algorithm as described further below. All 13 participants and three additional participants completed this part of the study.

7.3.2 Data Collection

For both study parts, participants wore the hip accelerometer, 3-lead ECG electrodes and two respiration bands that were integrated into a smart shirt (Hexoskin®, Carré Technologies Inc., Montréal, Canada). From the sensor raw signals, previously validated proprietary algorithms (Villar et al., 2015) were used to obtain second-by-second heart rate (HR), minute ventilation ($\dot{V}E$), breathing frequency (BF), total hip acceleration (ACC_{HIP}), and walking cadence (CAD) data. Data were recorded internally, and then uploaded to a PC for further analysis. These variables were considered features to obtain $\widehat{\dot{V}O_2}$. For the second part of this study, the $\dot{V}O_2$ data were acquired breath-by-breath by a portable metabolic system (K4b^2, COSMED, Italy) and expressed relative to each participant's body mass in kg. Before each test, the air volume/flow and gas concentrations of the metabolic system were calibrated following manufacturer's specifications.

7.3.3 Prediction Algorithm

Concurrently with the advances in wearable devices, ML methods are becoming popular to analyze the data generated by these devices. ML algorithms provide the technical basis to better identify non-trivial patterns in complex and intensive longitudinal data (Witten & Frank, 2005). The ML algorithm built to estimate $\widehat{\dot{V}O_2}$ was based on a random forest regression model (Breiman, 2001). All features (HR, $\dot{V}E$, BF, ACC_{HIP} and CAD) and the $\dot{V}O_2$ data collected during the second part of this study were time aligned, low-pass filtered at 0.01 Hz and processed in Matlab R2016a (MathWorks, Natick, MS, US). The predictor was validated by leave-one-participant-out cross-validation (Ross et al., 2009). Ensemble of random forest models were trained for optimal $\dot{V}O_2$ dynamics prediction. Each random forest contained a set of decision trees that predicted $\dot{V}O_2$ data based on an optimal split of the features. The output from these forests were ensemble averaged to

reduce system noise, resulting in a final $\widehat{\dot{V}O_2}$ predictor. The ML algorithm successfully predicted $\dot{V}O_2$ data during the PRTS and simulated ADL (part 2). The Pearson coefficient (r) indicated a strong linear correlation between measured and predicted data (r = 0.86, p <0.001, n = 63,571) with an error bias of only 0.02 $ml^{-1} \cdot min^{-1} \cdot kg^{-1}$. The generated algorithm was finally used to obtain $\widehat{\dot{V}O_2}$ based on the wearables-derived features during $uADL$.

7.3.4 Data Analysis

The BF, $\dot{V}E$, HR, and $\widehat{\dot{V}O_2}$ data obtained during the $uADL$ (part 1) were initially submitted to data distribution analysis. The data used in the histograms were clustered between "active" or "inactive" groups to allow a better identification of the PA influences over the variable tested. When the ACC_{HIP} was higher than 0.05 g, data were labeled as "active"; otherwise, "inactive". Since participants did not present exactly the same number of samples, the histograms were normalized to the total number of samples of each cluster for each participant.

When appropriate, the predicted metabolic equivalents ($\widehat{METS}$) were estimated by the ratio $\widehat{\dot{V}O_2}/3.5$. When active, PA levels were classified as light, moderate or vigorous intensity when $\widehat{METS}$ were < 3, between 3.1 - 6 or > 6.1, respectively (Crouter et al., 2011). The time spent in each PA level was also computed. Also, the duration of each walking bout and the time spent walking was obtained by a peak detection algorithm that extracted the feature CAD based on hip accelerometer data.

7.3.4.1 Aerobic System Analysis

Previous analyses of aerobic system dynamics under controlled laboratory conditions were based on the relationship between system input (i.e., PA) and the aerobic response inferred by $\dot{V}O_2$ data (i.e., system output) at different frequencies (Eßfeld et al., 1987; Hughson et al., 1990, 1991). Application of similar frequency domain methods to extract system dynamics during $uADL$ requires some modifications and application of specific criteria. Following previous literature (Hughson et al., 1990; Yoshida et al., 2008), the amplitude (Amp) of the ACC_{HIP} (system input) and the outputs ($\dot{V}O_2$ and $\widehat{\dot{V}O_2}$) were computed by fast Fourier transformation for a selected range of frequencies. The system gain was obtained by the (input Amp) / (output Amp) ratio. The selection of satisfactory energy delivered to the aerobic system was also based on ACC_{HIP} data. Since the focus of the frequency domain approach was aerobic system analysis, only ACC_{HIP} Amp responses higher than 0.05 g at a given frequency were classified as "satisfactory" for system analysis, otherwise, "unsatisfactory". Low energy stimulus does not allow the correct identification of the aerobic system gain since the observed output response cannot be discerned from non-exercise related factors which confound system analysis (Hughson et al., 1990).

The selection of the frequency range of interest was based on previous studies (Eßfeld et al., 1991; Hoffmann et al., 1992). To adhere to the linearity principle, the analyzed frequencies were limited to periods greater than 100s (i.e., ≤ 0.01 Hz). For frequencies higher than 0.01 Hz, the $\dot{V}O_2$ dynamics complexity/noise appears to increase considerably (Hoffmann et al., 1992), decreasing the physiological significance of the system responses. In addition to the detailed responses at different frequencies, the overall aerobic system temporal dynamics were assessed by the mean normalized gain (MNG). The MNG was calculated as the average of the gain Amp of all tested frequencies previously normalized by gain Amp of the very first frequency as previous

reported (Eßfeld et al., 1991). Like time constants obtained in time domain analysis (Henry, 1951; Hughson, 2009; Whipp & Ward, 1992), MNG is an indicator of the overall aerobic system temporal dynamics which seems to be related to aerobic power (Phillips et al., 1995; Powers et al., 1985).

The data window length (wl) selected for the frequency domain analysis will define the number of harmonics (h) included within the selected frequency range (<0.01 Hz) since the fundamental frequency (f_1) is the inverse of wl (Kerlin, 1974). Therefore, the frequency analyzed is defined by the product $h * f_1$. Higher wl means a better frequency domain resolution due to a lower f_1; therefore, more h can be included into the frequency interval. However, higher wl decreases the chance of having "satisfactory" samples for all tested frequencies (i.e., ACC_{HIP} < 0.05 g) since the input energy is dissipated between h (Kerlin, 1974) which compromise the aerobic system analysis (Hughson et al., 1990). The relationship between wl, h, f_1 and the number of "satisfactory" samples will be further explored.

The ACC_{HIP} response during PRTS (part 1) was initially investigated for the inspection of the stimulus signal in response to an optimized exercise protocol for frequency domain analysis (as the PRTS). For this optimized protocol, the wl was equal to the exercise protocol duration (i.e, 780s) thus the f_1 was 0.001 Hz. Figure 47 displays the ACC_{HIP} group response in frequency domain during the PRTS protocol. As a characteristic of the PRTS protocol and as expected to observe in completely random stimulus (e.g., $uADL$), some input Amp in the PRTS protocol were below the satisfactory amount of energy necessary for system analysis. In the case of PRTS, even h presented "unsatisfactory" energy for system analysis. In addition, PRTS protocols also stimulate the system with satisfactory energy in frequencies outside of the interval of interest (>

0.01 Hz). From the PRTS ACC_{HIP} responses in frequency domain, only the first four odd h could be labeled as "satisfactory" for system analysis between all participants.

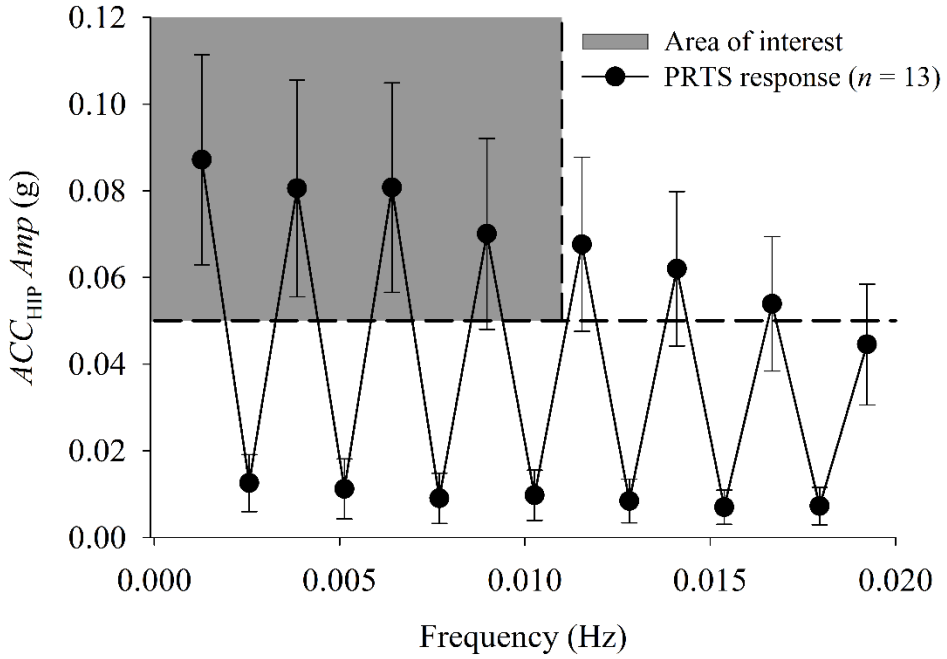

Figure 47. Frequency domain amplitude of the total hip acceleration.
Group response (mean ± SD) of frequency domain amplitude (Amp) of the total hip acceleration (ACC_{HIP}) during pseudorandom ternary sequence protocol. As a characteristic of this protocol, the stimulus energy decreases to values close to zero at even harmonics. For the correct system analysis, a range of frequencies and Amp was established (grey area). Amp lower than 0.05 g were considered as unsatisfactory for system analysis. Frequencies higher than 0.01 Hz were considered as non-linear and therefore excluded from further analysis (see text).

In contrast to the first four odd h in PRTS protocols, the system input during $uADL$ is not optimal for system analysis at these same frequencies. Therefore, further analysis was carried on to optimize the frequency domain analysis during $uADL$. With the minimal stimulus level (0.05 g) and frequency range (< 0.01 Hz) established, the only variable that can be arbitrarily altered to optimize system analysis was wl. The f_1 and h will change as consequence of wl variations. Accordingly, the search for an optimal wl aimed to fit as many h as possible (higher resolution)

within the frequency interval of interest but at the same time all tested h need to have "satisfactory" energy for system analysis.

A certified (#100-314-4110) LabVIEW associated developer (National Instruments, Austin, TX, US) programmed an iterative algorithm that continuously computed Amp from multiple fast Fourier transformations across the four days of ACC_{HIP} $uADL$ data for each arbitrarily selected wl of 200s to 1000s, incrementing 100s. The algorithm iteration stepwise was similar to the wl duration. The frequency range of interest was also maintained below 0.01 Hz. Samples composed by data from different days were discarded to avoid overlapping between days. This program classified the samples at each frequency ($h * f_1$) as "satisfactory" for system analysis when the ACC_{HIP} Amp was higher than 0.05 g. The $\widehat{VO_2}$ Amp was simultaneously computed. If more than one reliable Amp was computed for the same frequency between iterations, the final Amp value was taken as the average.

Figure 48A displays the mean group response (n = 13 for each data point) of the number of "satisfactory" samples (z-axis) at each tested frequency (x-axis) as a function of wl (y-axis). The plot was superimposed by a mesh plot for better pattern visualization. As the wl increases, the number of analyzed frequencies (i.e., resolution) increases (more data in x-axis); however, the number of samples with enough energy for system analysis decreases (z-axis). On the other hand, shorter wl presented more "satisfactory" samples for system analysis but at the same time less resolution (fewer frequencies analyzed). In addition, for all selected wl, more "satisfactory" samples are located at lower frequencies.

Figure 48B demonstrates the number of participants that did not present "satisfactory" Amp for system analysis in at least one tested frequency thus precluding a comparable aerobic system analysis. Below wl of 600s, all participants presented "satisfactory" ACC_{HIP} Amp for all

tested h. Therefore, based on ACC_{HIP} data, the wl of 600s was selected as optimal wl for system analysis during $uADL$. For the sake of data comparison between $uADL$ and PRTS stimulus, the final Amp responses were linearly interpolated to a common frequency bandwidth of 0.0022 to 0.0088 Hz with a stepwise of 0.0002 Hz, totaling 35 interpolated h for $uADL$ and PRTS. The MNG was also calculated during $uADL$ and PRTS considering this interval.

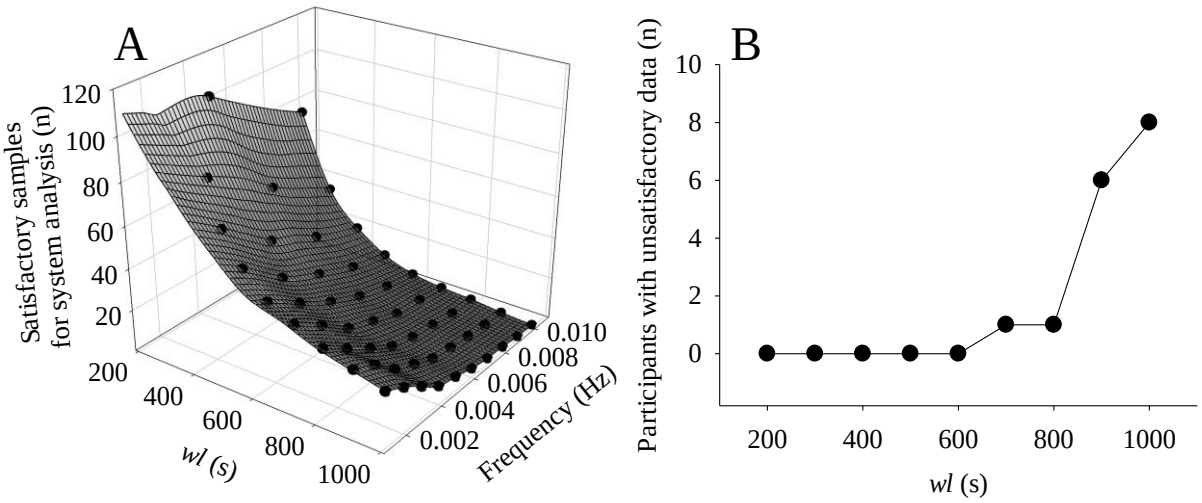

Figure 48. Satisfactory samples for frequency domain analysis.
A: mean group response (n = 13 for each data point) of the number of satisfactory samples for system analysis in frequency domain (z-axis) at each tested frequency (x-axis) as a function of data window length (wl, y-axis) during four days of unsupervised activities of daily living. B: Number of participants that did not present a satisfactory stimulus for system analysis in at least one tested frequencies as a function of wl.

7.3.5 Statistical Analysis

Student t-test was used to compare the frequency domain responses based on $\widehat{\dot{V}O_2}$ data obtained during the $uADL$ (part 1) with the responses based on $\dot{V}O_2$ data obtained during the PRTS protocol (part 2). When appropriate, r coefficient and Bland-Altman plot was used to compute the level of agreement between variables.

7.4 Results

The histograms for the relative distribution of incidence are displayed in Figure 49. The BF (Figure 49A) during resting was evenly distributed around 18 breath·min^{-1} while during ADL it increased ≈ 4 breaths·min^{-1}. The $\dot{V}E$ (Figure 49B) during rest has a peak of incidence at ≈ 7 L·min^{-1}. During PA, the $\dot{V}E$ reached a peak of incidence at ≈ 13 L·min^{-1} and then linearly decreased as the $\dot{V}E$ value increased. The HR (Figure 49C) during rest was normally distributed around a mean of ≈ 65 bpm and increased to ≈ 90 bpm during PA. The $\widehat{\dot{V}O_2}$ (Figure 49D) during resting was maintained at around 5 ml·min^{-1}·kg^{-1}. During PA, $\widehat{\dot{V}O_2}$ presented two peaks at ≈ 7.7 and ≈ 14 ml·min^{-1}·kg^{-1} (amplified in the smaller graph in Figure 49D) which corresponded to light and moderate intensities of PA, respectively.

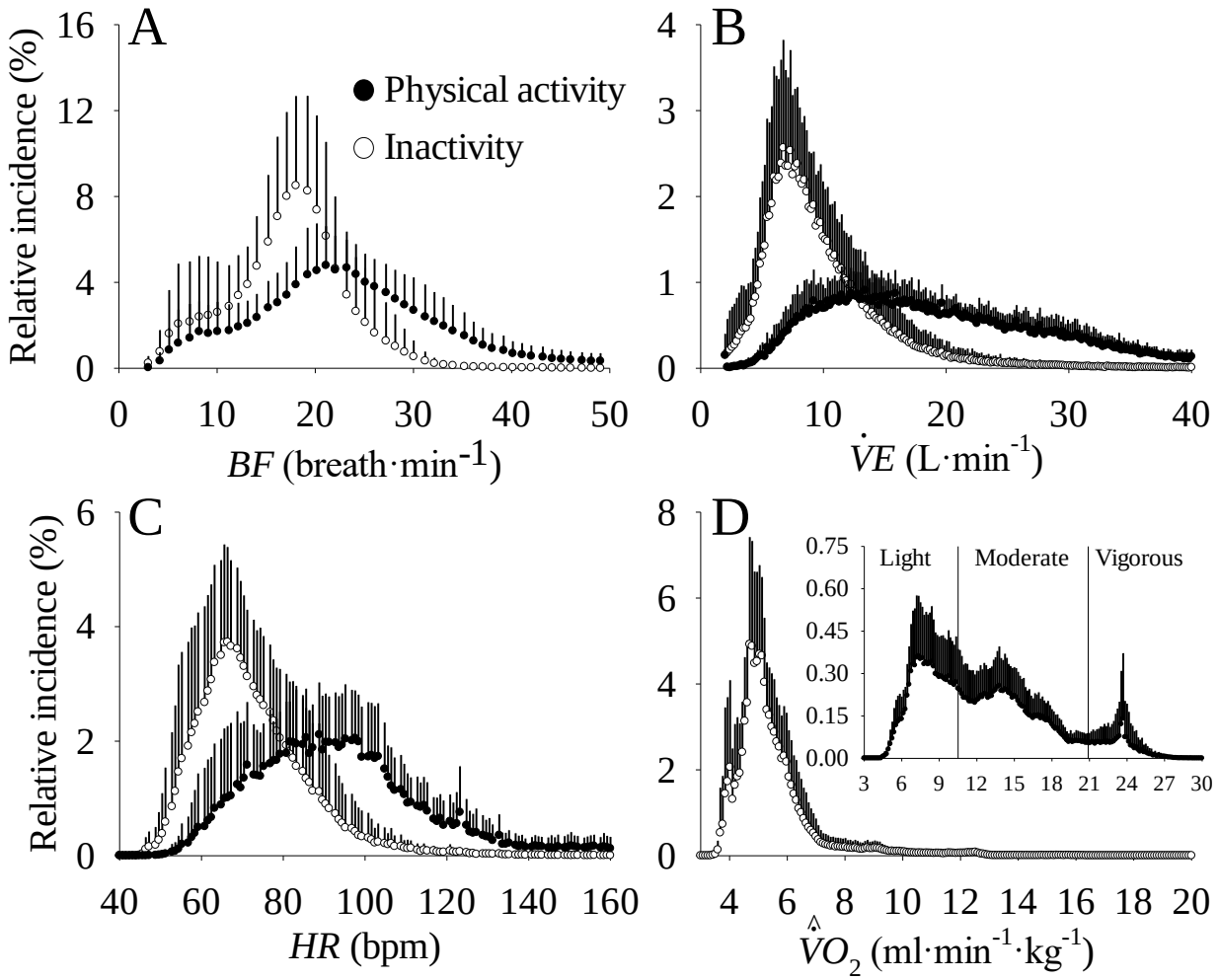

Figure 49. Histograms.
Normalized histograms of the incidence of breathing frequency (BF, A), ventilation minute ($\dot{V}E$, B), heart rate (HR, C) and predicted oxygen uptake ($\widehat{\dot{V}O_2}$, D) during four days of data collection of unsupervised activity of daily living. Data (mean ± SD) were clustered between active (solid circle) and inactive groups (filled circle) based on accelerometer values greater than or less than 0.05 g. The inset figure in D displays the incidence of $\widehat{\dot{V}O_2}$ data related to physical activity intensity domains.

The average walking bout duration was 24 ± 7 s. Participants spend ≈ 80 % of the time being inactive (Figure 50). When active, ≈ 90% of the $uADL$ was light or moderate intensity PA (< 6 $\widehat{METS}$). In 50% of the active time, participants were walking. The majority of the walking bouts (≈ 80 %) were contained in moderate intensity domain.

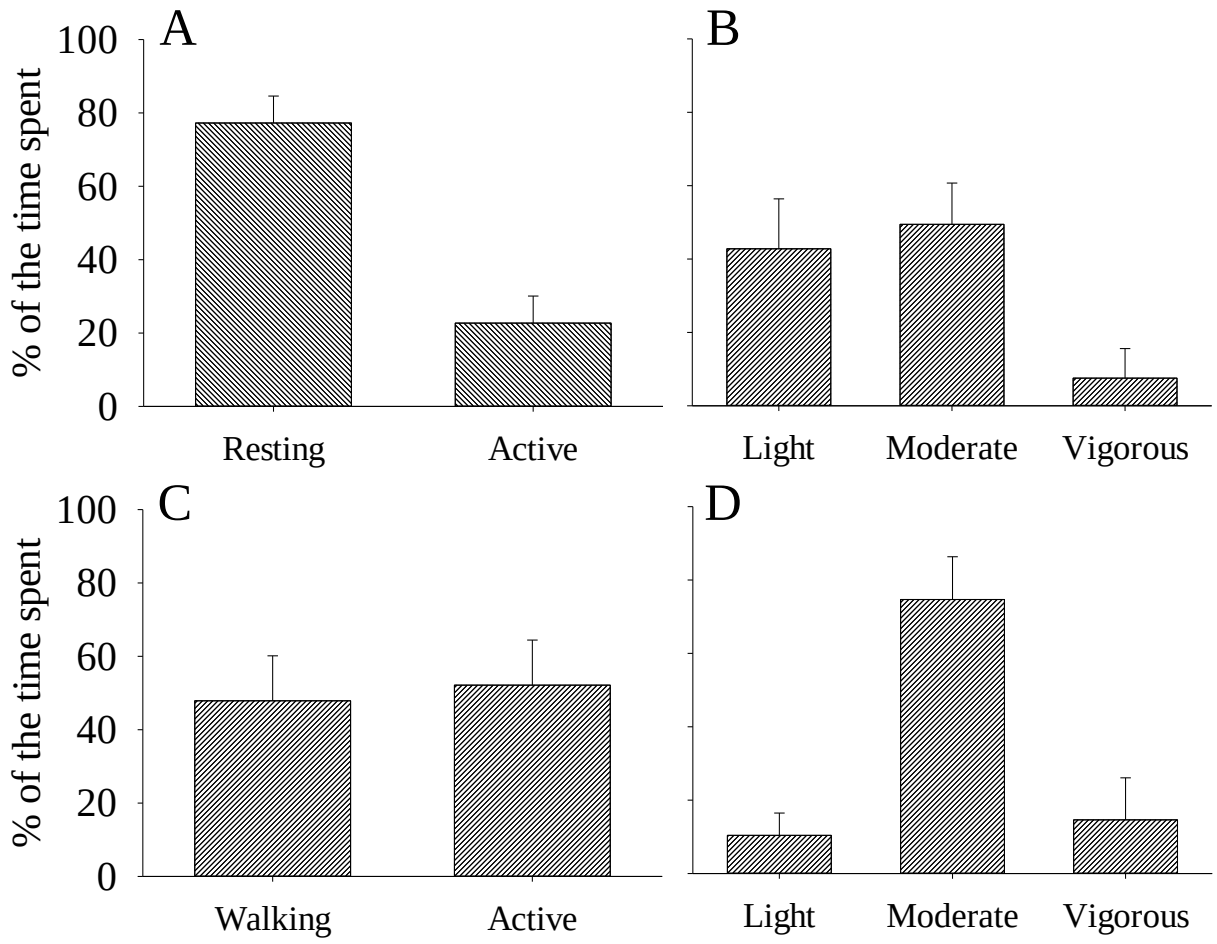

Figure 50. Physical activity patterns during unsupervised activities of daily living.
Identification of physical activity patterns during four days of unsupervised activities of daily living. A: percentage of time spent being active or inactive. B: when active, percentage of time spent within each physical activity intensity domain (light, moderate or vigorous). C: when active, percentage of time spent walking or performing another physical activity. D: when walking, percentage of time spent within each intensity domain.

The frequency domain analysis during $uADL$ considered a wl of 600s. For a better comparison between $uADL$ and PRTS, the responses from both inputs were interpolated at a common bandwidth of 0.0020 to 0.0088 Hz (period of 113 to 500 s). Figure 51A displays the system gain analyzed during $uADL$ and PRTS and the difference between them at each frequency (in mHz). After frequencies higher than 0.0036 Hz (or h = 9), the system gains were statistically

(p < 0.05) higher during $uADL$ in comparison to PRTS. When the system is normalized by the first analyzed frequency (h = 1 or 0.0020 Hz) which isolates the temporal dynamics of the system (Hoffmann et al., 1992), the normalized gains (Figure 51B in mHz) were statistically (p < 0.05) higher at frequencies higher than 0.004 Hz (h = 11). Notice that the difference between the system absolute or normalized gain during $uADL$ and PRTS linearly increases as the frequency increases.

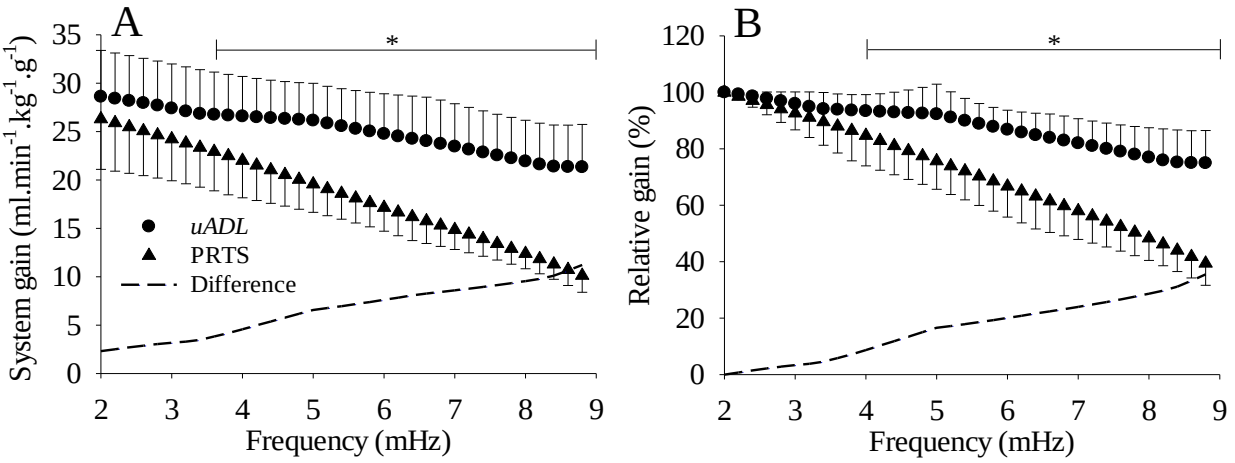

Figure 51. Aerobic system gain.
A: aerobic system gains per unit of hip acceleration at different frequencies based on predicted oxygen uptake during unsupervised activities of daily living ($uADL$) and based on measured oxygen uptake during pseudorandom ternary sequence (PRTS) walking protocol. The gain during $uADL$ was statistically (*, p < 0.05) higher than the gain during PRTS after 3.6 mHz. B: aerobic system normalized gain (see text). The normalized gain during $uADL$ was statistically (*, p < 0.05) higher than the gain during PRTS after 4 mHz.

Data presented in Figure 52B were used to obtain the MNG that indicate the overall aerobic system temporal dynamics. The MNG was obtained by the average between all Amp gains previously normalized by the Amp gain of the first frequency. The MNG was estimated from $\dot{V}O_2$ data during PRTS (ideal protocol) and from $\widehat{\dot{V}O_2}$ data obtain during PRTS and $uADL$. Higher MNG values are equivalent to a faster $\dot{V}O_2$ adjustment thus faster aerobic response. The MNG computed from $\dot{V}O_2$ during PRTS was statistically correlated (r = 0.68, p = 0.01 and n = 13) and

not statistically (p = 0.53) different in comparison to MNG estimated from $\widehat{\dot{V}O_2}$ during PRTS. In addition, the MNG computed from $\widehat{\dot{V}O_2}$ during PRTS was statistically correlated (r = 0.63, p = 0.01 and n = 13) and statistically (p < 0.001) faster (i.e., higher) than the MNG estimated from $\widehat{\dot{V}O_2}$ during $uADL$. Therefore, the MNG during $uADL$ was faster than the MNG during PRTS (considering both, $\dot{V}O_2$ or $\widehat{\dot{V}O_2}$). As depicted in Figure 52A, the MNG calculated from $\dot{V}O_2$ during PRTS and $\widehat{\dot{V}O_2}$ during $uADL$ were strongly correlated (r = 0.82, p < 0.001 and n = 13). However, the MNG obtained during $uADL$ was statistically (p < 0.001) faster in comparison to MNG during PRTS (Figure 52A). In addition, the linear regression between the MNG obtained from the $\dot{V}O_2$ data during PRTS and the MNG obtained from $\widehat{\dot{V}O_2}$ during $uADL$ had a slope of 45.1^0 which is similar to the expected slope of the equality line (45^0). Therefore, the MNG during $uADL$ can be biased by -16 % to match the equality line if further comparison with PRTS is desired. As depicted in Figure 52B, the difference between the MNG based on $\widehat{\dot{V}O_2}$ during $uADL$ and based on $\dot{V}O_2$ during PRTS (y-axis) seemed to be independent from MNG value (x-axis) with no significant (p > 0.05) statistical correlation between axis.

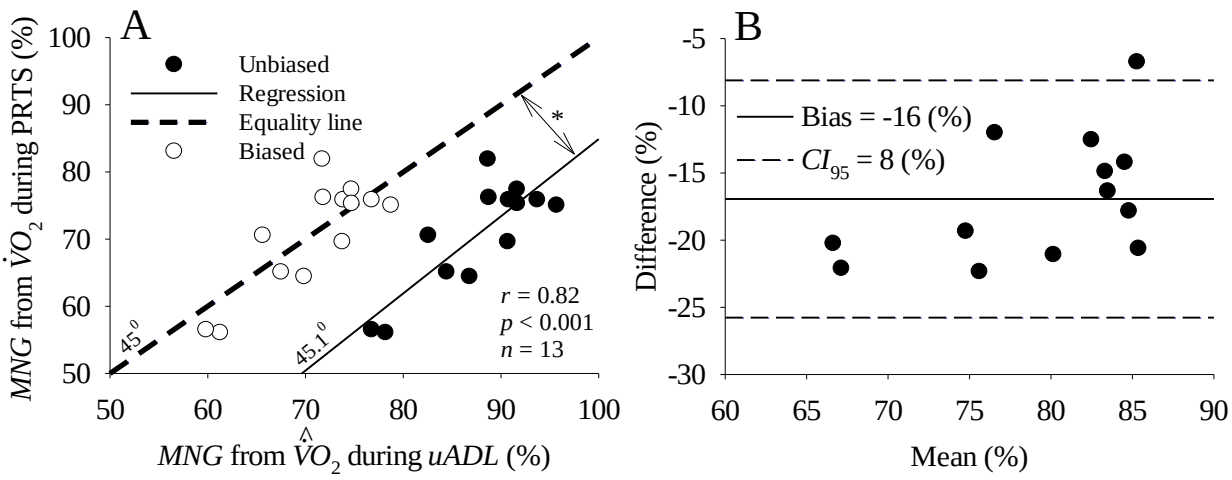

Figure 52. Predicted and measured mean normalized system gain.
A: linear correlation between the mean normalized gain (MNG) calculated from predicted oxygen uptake data ($\widehat{\dot{V}O_2}$) during unsupervised activities of daily living ($uADL$) and calculated from measured oxygen uptake ($\dot{V}O_2$) data during pseudorandom ternary sequence (PRTS) walking protocol. The MNG obtained from $\widehat{\dot{V}O_2}$ during $uADL$ was statistically (*, $p < 0.001$) higher than the MNG obtained from $\dot{V}O_2$ during PRTS. The difference between both MNG (16 %) was consistent across the participants characterized by a similar linear regression slope in comparison to the equality line. B: Bland-Altman plot of the data displayed in A with the bias and the confidence interval (CI_{95}) between the two methods used to estimate MNG.

7.5 Discussion

In agreement with our initial hypothesis, the aerobic system dynamics were successfully mined from wearable sensors during unsupervised activities of daily living. The temporal characteristics of the predicted oxygen uptake data during activities of daily living were correlated to the temporal characteristics of the measured oxygen uptake data during a controlled protocol. In addition, the predicted oxygen uptake can be used to study physical activity intensity during realistic environments.

In contrast to step-transition laboratory-based studies, the randomness characteristics of PA patterns during $uADL$ has complicated obtaining information with clinical significance. Time domain $\dot{V}O_2$ data modeling is not practical during $uADL$ due to the lack of steady state responses

which decreases the signal-to-noise ratio thus preventing calculation of the system temporal dynamics (Hughson, 2009). However, we demonstrated that frequency domain analysis can be used to infer about the aerobic system dynamics from random data during $uADL$. Our results showed that a data window of 600s can be used to extract information regarding the aerobic system temporal dynamics based on predicted $\widehat{\dot{V}O_2}$ data.

Since the system analysis quality also dependents on the number of analyzed frequencies, the data window size (wl) should be as large as possible. However, the larger the data window size, the greater the chance to present unreliable samples for system analysis. As depicted in Figure 48, a window size of 600s was found to be ideal for aerobic system analysis.

The MNG characterized overall system dynamics where a higher % as during $uADL$ is equivalent to faster kinetics than during the PRTS protocol. The linear increment of these differences between frequencies and consequently the MNG could originate from the prediction algorithm or from biological variability. There are a few observations that allow us to rule out the first possibility. First, the MNG computed from $\widehat{\dot{V}O_2}$ during PRTS was correlated and not statistically different from the MNG based on measured $\dot{V}O_2$ also during PRTS. In addition, the MNG computed from $\widehat{\dot{V}O_2}$ during PRTS was correlated with the MNG calculated from $\widehat{\dot{V}O_2}$ during $uADL$ but they were statistically different, suggesting that the observed difference did not originate from the predictor but from biological variability between PRTS and $uADL$.

The system analysis during $uADL$ has an elevated source of distortion. The rest-to-exercise transition is very common during $uADL$ and maybe this was the main cause of this faster response. However, the MNG during PRTS was used only as a reference to check if the MNG estimated from $uADL$ was also able to detect different aerobic system temporal dynamics, which was the case. Therefore, participants who presented a faster aerobic dynamics during PRTS also presented

a faster adjustment during $uADL$, demonstrating the effectiveness of our method to track future changes in aerobic fitness during $uADL$ by wearable sensors.

The MNG estimated during PRTS and *uADL* is an index composed of an amalgamated response of components with variable speeds (Chapter 2) that at the end translate the overall aerobic system temporal dynamic that has clinical relevance (Chapter 5). As it is possible to see in Figure 52A, the MNG calculated from $\widehat{\dot{V}O_2}$ during $uADL$ was strongly correlated to the MNG computed during PRTS indicating that a participant with a faster aerobic dynamic during an ideal protocol only composed by exercise-to-exercise transitions also presented a faster aerobic adjustment during a totally random stimulus as $uADL$. This observation demonstrates a certain degree of linearity of the aerobic response allowing us to obtain information with potential for clinical relevance during different stimulus patterns as expected during different exercise modalities. Regardless, even without practical applications, if future studies aim to compare the aerobic response during exercise-to-exercise controlled protocols with the aerobic response during $uADL$, the current results suggest that a simple linear bias of -16 % can adjust the MNG derived from $uADL$.

The MNG obtained during $uADL$ was calculated based on the mean $\widehat{\dot{V}O_2}$ of multiple "satisfactory" samples at each frequency while the MNG estimated from $\widehat{\dot{V}O_2}$ during PRTS was based only on a single sample for each frequency. In addition, the MNG calculated from $\widehat{\dot{V}O_2}$ data during $uADL$ was better correlated with the MNG estimated from $\dot{V}O_2$ during PRTS in comparison to the MNG estimated from $\widehat{\dot{V}O_2}$ during PRTS. Therefore, the MNG mined from $\widehat{\dot{V}O_2}$ data during $uADL$ seemed to be better to characterize the aerobic system temporal dynamics in comparison to the MNG estimated during PRTS based on $\widehat{\dot{V}O_2}$ data.

In agreement to previous study (Orendurff et al., 2008), the average of walking bout durations was 24 ± 7 s. However, it is peculiar, in $uADL$ context, that the hip was accelerating but the participant was not walking. Walking should be the major $uADL$ that changes the hip acceleration. We found that only 50% of the time participants were being active by moving their hip but at the same time not walking which is unlikely. Probably, the step detection algorithm of the smart shirt failed to detect low cadences walking due to the lower propagation of the acceleration generated at the heel to the hip during slow walking cadences. This demonstrated that ACC_{HIP} might be better for system analysis instead of CAD. As previously reported (Cleland et al., 2013), the total hip acceleration represents the total body movements and it can be used as a reliable proxy of energy expenditure (i.e., metabolic demand) during physical activity (A. Bauman et al., 2011; Ellis et al., 2014). However, further methods are necessary to optimize the metabolic demand prediction based on hip acceleration (Chen et al., 2003).

Our novel methodology is a combination of four main components.

1) Machine learning was used for $\dot{V}O_2$ data prediction based on wearable sensors to address the complexities of the $\dot{V}O_2$ response to ADL.

2) FFT was used for aerobic system analysis as it has intrinsic noise reduction characteristics and allows for a detailed investigation of the aerobic response during different stimulus periods.

3) The MNG calculation, that may have clinical relevance, was used to obtain the temporal dynamics of the aerobic system based on the FFT results.

4) An iterative algorithm was developed to search for the best data window for the investigation of the aerobic system dynamics during completed random physical activities.

Results from our work have suggested specific methods for the use of our model in evaluating aerobic system temporal dynamics during $uADL$. Standard algorithms need to be developed to transform the raw signals from wearable sensors into the initial model input variables (e.g. HR). These variables should feed our machine learning algorithm (random forests) that will generate the predicted $\dot{V}O_2$. The input (ACC_{HIP}) and the output (predicted $\dot{V}O_2$) can then be used to calculated the aerobic system gain based on FFT calculations. As shown in our study, the most appropriate data window length used for each FFT is 600s and gain should be computed and recorded only when the ACC_{HIP} is higher than 0.05 g. The frequency range should be limited to 0.01 Hz. The average is calculated if more than one reading is made for the same frequency. After four days, the MNG is computed based on the normalized system gain. This four-day data processing cycle can be repeated as often as necessary to account for changes in MNG.

Further epidemiologic studies are necessary to investigate the relationship between the aerobic system temporal dynamics with different PA patterns during realistic settings. These investigations would enable the identification of sedentary or active behaviors that are correlated with different aerobic system dynamics which might impact PA recommendations.

7.6 Conclusion

For the first time, this study has shown that aerobic system dynamics can be investigated during unsupervised activities of daily living by wearable sensors. The longitudinal frequency domain analysis of predicted oxygen uptake derived from wearables allowed the characterization of the temporal dynamics of the aerobic system during realistic activities. We identified reliable samples for aerobic system analysis based on 20% of the data when the participants were active during $uADL$.

Deployment of non-intrusive technologies in conjunction with the algorithms developed in the current study into large scale epidemiological investigations may offer the unique opportunity of investigating relationships between patterns of daily physical activity and health/fitness indicators.

Chapter 8: General Discussion

The accurate prediction of $p\dot{V}O_2$ data under randomly varying patterns of physical activity allows the precise estimation of EE and the investigation of the aerobic system dynamics. Specially, the $p\dot{V}O_2$ prediction during realistic ADL by wearable sensors is an innovative technology that can be used as tool to obtain health-related outcomes daily. The possibility to "mine" the temporal characteristics of the aerobic system based on predicted $p\dot{V}O_2$ data in realistic settings (Chapter 7) allows for inferences about the aerobic system integrity during ADL. This thesis provided a series of seven multiple-level studies that covered the prediction and evaluation of the $p\dot{V}O_2$ dynamic during controlled and free physical activities. The combination between new tools for the $p\dot{V}O_2$ prediction (such as machine learning) and innovative methods to characterize the aerobic response during random activities (such as MNG) evidenced the applicability of our finding. The proposed tools can be used, to characterize the temporal dynamics of the aerobic system allowing the development of personalized and "real-time" adjustable exercise programs. In the future, the algorithms presented in this thesis can be used to explore novel applications for wearable technologies to expand uses beyond sport-related activities into new user markets.

8.1 Summary of Findings

During moderate exercise, aerobic system linearity implies that the $p\dot{V}O_2$ response steady state amplitude is proportionally correlated to the magnitude of the $\dot{W}$ (static linearity) and that the $p\dot{V}O_2$ time course (i.e., τ) is independent of the $\dot{W}$ (dynamic linearity) (Hughson, 2009). However, results from Chapter 2 demonstrated, in agreement with previous studies (Brittain et al., 2001; Hughson & Morrissey, 1982), that the aerobic response followed a multiple-order system, thereby questioning the dynamic linearity assumption (Ozyener et al., 2001). Despite not being the first

time that aerobic system linearity was tested (Hughson & Morrissey, 1982), this study, for the first time, tested the linearity of the aerobic response simultaneously with HHb and $\dot{Q}$ responses during PRBS. Regardless, as demonstrated in Chapter 5, the presence of multiple components in $p\dot{V}O_2$ dynamics did not prevent the use of the overall system temporal dynamics as a tool to investigate health-related outcomes.

It is well accepted in the literature (Chilibeck et al., 1995; Eßfeld et al., 1987; Powers et al., 1985; Yoshida et al., 2008) that the overall $p\dot{V}O_2$ dynamic varies according to fitness status (Phillips et al., 1995; Powers et al., 1985) and has associations with clinical outcomes (Borghi-Silva et al., 2012) and functional mobility performance (Alexander et al., 2003). However, the time-domain characterization of $p\dot{V}O_2$ temporal dynamics, that assume dynamic linearity, presents data modeling limitations being restricted to controlled step protocols generally performed on the cycle ergometer. The pseudorandom protocols (PRBS and for the first time, over-ground PRTS) offered a unique possibility to test the aerobic response during realistic and dynamic changes in $\dot{W}$. Despite being a controlled stimulus, these protocols approximate the study of the $p\dot{V}O_2$ dynamics to what occurs during ADL where the variation of the metabolic demand is stochastic.

Chapters 5 and 7 demonstrated that the frequency domain responses of $p\dot{V}O_2$ datasets can be valuable to extract information with clinical relevance where time-domain approaches are inappropriate. So far, there was not an index able to translate the overall temporal dynamics of the aerobic system during random stimulus such as PRBS and PRTS protocols. As proposed in Chapter 3, the MNG was validated to characterize the aerobic system temporal dynamics. In addition, as described in Chapter 5, the MNG was correlated to the aerobic capacity estimated by maximal $p\dot{V}O_2$, demonstrating another clinical outcome of the MNG. Unlike incremental exercise

protocols used to obtain maximal $p\dot{V}O_2$, submaximal protocols such as $PRBS$ and $PRTS$ are more functional and involve less muscle aches, joint pain, discomfort, fatigue, muscle soreness, fainting and acute cardiovascular events associated with maximal exertion.

Interestingly, for the first time in literature and as described in Chapter 7, the MNG can be derived from predicted $p\dot{V}O_2$ data based on wearable sensors during unsupervised ADL.

Due to the complexity of the aerobic response, the prediction of the $p\dot{V}O_2$ dynamics is challenging and could explain why simple linear regressions fail to predict $p\dot{V}O_2$ data from wearable sensors during realistic activities (Ravussin, Lillioja, Anderson, Christin, & Bogardus, 1986). As described in Chapter 4 and 6, ML approaches could "understand" the complexity of the $\dot{V}O_2$ dynamics during transitions by predicting the aerobic responses based on variables obtained from wearable sensors.

Following Chapter 4, the subsequent chapters started moving beyond the laboratory environment. Chapter 5 focused on the development of a novel exercise protocol for over-ground walking that has similarities to the pattern of walking during ADL. In addition, the use of hip-placed accelerometer data to assess $\dot{W}$ during randomly varying stimulus was also investigated in Chapter 5. The results suggested that the proposed protocol (PRTS) can be used for aerobic system analysis during randomly varying walking cadences. Afterwards, as described in Chapter 6, accelerometer, HR and respiratory bands were used as inputs to predict the $\dot{V}O_2$ dynamics during PRTS and simulated ADL. It was successfully shown that the aerobic system dynamics can be predicted during PRTS protocol and simulated ADL.

Finally, Chapter 7 demonstrated some applications of the tools developed in this thesis. The algorithm developed in Chapter 6 was used to investigate the aerobic system dynamics during four days of unsupervised ADL. The predicted $p\dot{V}O_2$ data were used to investigate, among others,

PA levels and their occurrence, and the ambulatory monitoring of the aerobic system temporal dynamics. The MNG validated in Chapter 3 was used to investigate aerobic fitness during unsupervised ADL based on predicted $p\dot{V}O_2$ obtained from wearable sensors. A specific method was developed in Chapter 7 to investigate the optimal data window length for the ambulatory $p\dot{V}O_2$ frequency domain analysis.

8.2 Future Applications and Economic Impact

The early detection of subclinical aerobic system impairments (slower response for example) might be an indicative of impaired physiological reserve that impact physical activity capacity, which in turn can lead to frailty or illness (Newman et al., 2001). Therefore, indexes that describe "how fast" the energy demand is supplied by the aerobic system (such as the frequently used time domain indices τ and MRT, or the novel frequency domain index, proposed in this thesis, MNG) have the potential to be considered into models for the early detection of disease states. In addition, in a clinical practice, the new index MNG can be used in the future to track changes in aerobic fitness as a consequence of aging, training status, aerobic exercise programs effectiveness and disease prognosis, just to name a few.

Wearable technologies (e.g. Hexoskin®) are becoming more popular and less costly, allowing consumers to obtain personal data on a daily basis. The combination of wearable sensors and new data processing techniques has direct applicability for disease prevention, and for the evaluation of treatment progression. The investigation of $p\dot{V}O_2$ data during unsupervised ADL may allow us to search for potential associations between aerobic response and other variables like PA types, frequency of this PA throughout the day and the total energy expenditure, just to name a few. These associations could bring new insight about how to prescribe exercise and how a

specific activity pattern is stimulating the aerobic metabolism on a daily basis. The identification of loss in aerobic fitness could be also useful to investigate aging effects and the implementation of the proposed ready-to-use algorithms into wearable systems will make the benefits described in this thesis available for the general population. The temporal dynamics of the predicted $p\dot{V}O_2$ response might be investigated by MNG on a daily basis and impairments in the aerobic response might be identified before the clinical manifestation of chronic diseases.

As demonstrated in Chapters 4 and 6, the temporal characteristics of the aerobic system was predicted by the proposed algorithms that can be incorporated into wearable systems. For clinical practice, these algorithms in association with the methods described in Chapter 7 can be used to track changes in aerobic power during unsupervised activities of daily living.

Considering the price of the metabolic carts (≈ $ 30,000) and the cost associated with consumables such as calibration gases and masks, and the need for trained technicians, the prediction of $p\dot{V}O_2$ data by wearable sensors that cost ~ $ 400 has an evident economic impact. Even though this thesis did not validate the use of the proposed algorithm for all possible conditions and populations, it somehow offered a possible option to generate a reliable estimated $p\dot{V}O_2$ when metabolic carts are not easily accessible, as in new research groups in developing countries for example. In addition, the algorithms proposed in this thesis could be also used to monitor positive or negative aerobic adaptation to training, allowing a continuous assessment of aerobic fitness changes without the need of constant laboratory testing.

8.3 Thesis Limitations

Except for Chapter 4 that predicted the $p\dot{V}O_2$ for a metabolic demand higher than 6 $METS$, all the studies of this thesis dealt with light to moderate metabolic demands. Therefore, the applicability

of our findings is limited to light to moderate intensity activities. However, the general purpose of this thesis was to predict the aerobic response during ADL where the majority of the metabolic demand is constrained between light to moderate intensities (Hendelman et al., 2000). In fact, as described in Chapter 7, we showed that only ~10 % of data collected during four days of ADL in active young participants were related to vigorous metabolic demand (higher than 6 $METS$ or 21 $ml \cdot min^{-1} \cdot kg^{-1}$).

The population tested in this thesis was exclusively composed by healthy individuals and mainly by men with only small variations in weight and age. Therefore, more studies are necessary to verify the applicability of the described algorithm in different populations ranging from endurance athletes to younger or older participants, and to various disease states. In addition, the actual impact of this thesis over the clinical practice remains to be tested.

In this thesis, physical activity levels were based on the total vector magnitude of triaxial hip-worn accelerometers. As previously reported (Cleland et al., 2013), the total hip acceleration represents the total body movements and it can be used as a reliable proxy of energy expenditure (i.e., metabolic demand) during PA (Bassett et al., 2000; A. Bauman et al., 2011; Ellis et al., 2014). However, due to the direct link between $p\dot{V}O_2$ and energy expenditure, future work should optimize the feature extraction of triaxial hip-worn accelerometer data before training machine learning algorithms. In agreement with previous research (Bassett et al., 2000), our results supported the use of the total hip acceleration, considering vertical, anterior–posterior and medial–lateral planes, to predict energy expenditure during ADL. Our success might be attributed to the random forest approach developed in Chapter 6, which, in agreement with previous work (Ellis et al., 2014), has a better ability to understand highly complex data. However, some studies reported that total vector magnitude may overestimate (Hendelman et al., 2000) or underestimate

(Matthews & Freedson, 1995) energy expenditure predictions during ADL. Therefore, factors affecting movement patterns, and consequently the hip acceleration, can influence the prediction of energy expenditure (Ludlow & Weyand, 2016; Zarrugh, 1981) and more research is needed to define the best hip accelerometer planes for energy expenditure predictions during complex PA as ADL. In addition, identification of slow walking cadences may be compromised when hip, instead of ankle, accelerometers are used for step detection (Chapter 7). Further studies are necessary to optimize step detection algorithms based on hip accelerometer, which could improve energy expenditure predictions.

8.4 Thesis Conclusion

The conclusion of this thesis is that, despite the complexity of the oxygen uptake response to physical activity, the temporal dynamics of the aerobic system can be evaluated from an appropriate combination of wearable sensors processed by novel algorithms during unsupervised activities of daily living.

References

Ahuja, K. D. K., Robertson, I. K., & Ball, M. J. (2009). Acute effects of food on postprandial blood pressure and measures of arterial stiffness in healthy humans. *The American Journal of Clinical Nutrition*, *90*, 298–303.

Alexander, N. B., Dengel, D. R., Olson, R. J., & Krajewski, K. M. (2003). Oxygen-uptake (VO2) kinetics and functional mobility performance in impaired older adults. *The Journals of Gerontology*, *58*, 734–739.

Ali, H., Messina, E., & Bisiani, R. (2013). Subject-Dependent Physical Activity Recognition Model Framework with a Semi-supervised Clustering Approach. In *2013 European Modelling Symposium* (pp. 42–47). Manchester, LNH: IEEE.

Allart, E., Olivier, N., Hovart, H., Thevenon, A., & Tiffreau, V. (2012). Evaluation of muscle oxygenation by near-infrared spectroscopy in patients with Becker muscular dystrophy. *Neuromuscular Disorders*, *22*, 720–727.

Altini, M., Penders, J., & Amft, O. (2016). Estimating Oxygen Uptake During Nonsteady-State Activities and Transitions Using Wearable Sensors. *IEEE Journal of Biomedical and Health Informatics*, *20*, 469–475.

Altman, D. G., & Bland, J. M. (1983). Measurement in Medicine : the Analysis of Method Comparison Studies. *Statistician*, *32*, 307–317.

Åstrand, P. O. (2003). *Textbook of Work Physiology: Physiological Bases of Exercise*. Champaign, IL: Human Kinetics.

Astrand, P. O., & Saltin, B. (1961). Maximal oxygen uptake and heart rate in various types of muscular activity. *Journal of Applied Physiology*, *16*, 977–81.

Barker, G. A., Green, S., Green, A. A., & Walker, P. J. (2004). Walking performance, oxygen uptake kinetics and resting muscle pyruvate dehydrogenase complex activity in peripheral arterial disease. *Clinical Science*, *106*, 241–249.

Barstow, T. J., Buchthal, S., Zanconato, S., & Cooper, D. M. (1994). Muscle energetics and pulmonary oxygen uptake kinetics during moderate exercise. *Journal of Applied Physiology*, *77*, 1742–1749.

Barstow, T. J., Jones, A. M., Nguyen, P. H., & Casaburi, R. (1996). Influence of muscle fiber type and pedal frequency on oxygen uptake kinetics of heavy exercise. *Journal of Applied Physiology*, *81*, 1642–1650.

Barstow, T. J., Lamarra, N., & Whipp, B. J. (1990). Modulation of muscle and pulmonary O2 uptakes by circulatory dynamics during exercise. *Journal of Applied Physiology*, *68*, 979–989.

Bassett, D. R., Ainsworth, B. E., Swartz, a M., Strath, S. J., O'Brien, W. L., & King, G. A. (2000). Validity of four motion sensors in measuring moderate intensity physical activity. *Medicine and Science in Sports and Exercise*, *32*, S471-80.

Bauer, T. A., Brass, E. P., & Hiatt, W. R. (2004). Impaired muscle oxygen use at onset of exercise in peripheral arterial disease. *Journal of Vascular Surgery*, *40*, 488–493.

Bauer, T. A., Reusch, J. E. B., Levi, M., & Regensteiner, J. G. (2007). Skeletal muscle deoxygenation after the onset of moderate exercise suggests slowed microvascular blood flow kinetics in type 2 diabetes. *Diabetes Care*, *30*, 2880–2885.

Bauman, A., Ainsworth, B. E., Sallis, J. F., Hagströmer, M., Craig, C. L., Bull, F. C., … Tremblay, M. S. (2011). Physical Activity Assessments for Health-Related Research. *Med Sci Sports Exerc*, *40*, 296.

Bauman, A. E. (2004). Updating the evidence that physical activity is good for health: an epidemiological review 2000-2003. *Journal of Science and Medicine in Sport*, *7*, 6–19.

Beaver, W. L., Wasserman, K., & Whipp, B. J. (1986). A new method for detecting anaerobic threshold by gas exchange. *Journal of Applied Physiology*, *60*, 2020–2027.

Bell, C., Paterson, D. H., Kowalchuk, J. M., Padilla, J., & Cunningham, D. A. (2001). A comparison of modelling techniques used to characterise oxygen uptake kinetics during the on-transient of exercise. *Experimental Physiology*, *86*, 667–676.

Bennett, F. M., Reischl, P., Grodins, F. S., Yamashiro, S. M., & Fordyce, W. E. (1981). Dynamics of ventilatory response to exercise in humans. *Journal of Applied Physiology*, *51*, 194–203.

Borghi-Silva, A., Beltrame, T., Reis, M. S., Sampaio, L. M. M., Catai, A. M., Arena, R., & Costa, D. (2012). Relationship between oxygen consumption kinetics and BODE index in COPD patients. *International Journal of COPD*, *7*, 711–718.

Boushel, R., Langberg, H., Olesen, J., Gonzales-Alonzo, J., Bülow, J., Kjaer, M., & Boushel, R. (2001). Monitoring tissue oxygen availability with near infrared spectroscopy (NIRS) in health and disease. *Scandinavian Journal of Medicine & Science in Sports*, *11*, 213–222.

Bouten, C. V, Koekkoek, K. T., Verduin, M., Kodde, R., & Janssen, J. D. (1997). A triaxial accelerometer and portable data processing unit for the assessment of daily physical activity. *IEEE Transactions on Bio-Medical Engineering*, *44*, 136–147.

Bowen, T. S., Murgatroyd, S. R., Cannon, D. T., Cuff, T. J., Lainey, A. F., Marjerrison, A. D., … Rossiter, H. B. (2011). A raised metabolic rate slows pulmonary O2 uptake kinetics on transition to moderate-intensity exercise in humans independently of work rate. *Experimental Physiology*, *96*, 1049–1061.

Bowen, T. S., Rossiter, H. B., Benson, A. P., Amano, T., Kondo, N., Kowalchuk, J. M., & Koga, S. (2013). Slowed oxygen uptake kinetics in hypoxia correlate with the transient peak and reduced spatial distribution of absolute skeletal muscle deoxygenation. *Experimental Physiology*, *98*, 1585–96.

Breiman, L. (2001). Random forests. *Machine Learning*, *45*, 5–32.

Brittain, C. J., Rossiter, H. B., Kowalchuk, J. M., & Whipp, B. J. (2001). Effect of prior metabolic rate on the kinetics of oxygen uptake during moderate-intensity exercise. *European Journal of Applied Physiology*, *86*, 125–134.

Brunner-La Rocca, H. P., Weilenmann, D., Schalcher, C., Schlumpf, M., Follath, F., Candinas, R., & Kiowski, W. (1999). Prognostic significance of oxygen uptake kinetics during low level exercise in patients with heart failure. *The American Journal of Cardiology*, *84*, 741–744.

Buchheit, M., Laursen, P. B., & Ahmaidi, S. (2009). Effect of prior exercise on pulmonary O2 uptake and estimated muscle capillary blood flow kinetics during moderate-intensity field running in men. *Journal of Applied Physiology*, *107*, 460–70.

Carter, H., Jones, A. M., Barstow, T. J., Burnley, M., Williams, C., & Doust, J. H. (2000). Effect of endurance training on oxygen uptake kinetics during treadmill running. *Journal of Applied Physiology*, *89*, 1744–1752.

Casaburi, R., Weissman, M. L., Huntsman, D. J., Whipp, B. J., & Wasserman, K. (1979). Determinants of gas exchange kinetics during exercise in the dog. *Journal of Applied Physiology*, *46*, 1054–1060.

Casaburi, R., Whipp, B. J., Wasserman, K., Beaver, W. L., & Koyal, S. N. (1977). Ventilatory and gas exchange dynamics in response to sinusoidal work. *Journal of Applied Physiology*,

42, 300–301.

Cerretelli, P., Pendergast, D., Paganelli, W. C., & Rennie, D. W. (1979). Effects of specific muscle training on VO2 on-response and early blood lactate. *Journal of Applied Physiology*, *47*, 761–769.

Chen, K. Y., Acra, S. A., Donahue, C. L., Sun, M., & Buchowski, M. S. (2004). Efficiency of walking and stepping: relationship to body fatness. *Obesity Research*, *12*, 982–989.

Chen, K. Y., Acra, S. A., Majchrzak, K., Donahue, C. L., Baker, L., Clemens, L., … Buchowski, M. S. (2003). Predicting Energy Expenditure of Physical Activity Using Hip- and Wrist-Worn Accelerometers. *Diabetes Technology & Therapeutics*, *5*, 1023–1033.

Chiappa, G. R., Borghi-Silva, A., Ferreira, L. F., Carrascosa, C., Oliveira, C. C., Maia, J., … Neder, J. A. (2008). Kinetics of muscle deoxygenation are accelerated at the onset of heavy-intensity exercise in patients with COPD: relationship to central cardiovascular dynamics. *Journal of Applied Physiology*, *104*, 1341–1350.

Chilibeck, P. D., Paterson, D. H., Petrella, R. J., & Cunningham, D. A. (1995). The influence of age and cardiorespiratory fitness on kinetics of oxygen uptake. *Canadian Journal of Applied Physiology*, *21*, 185–196.

Christensen, P. M., Jacobs, R. A., Bonne, T., Fluck, D., Bangsbo, J., & Lundby, C. (2016). A short period of high-intensity interval training improves skeletal muscle mitochondrial function and pulmonary oxygen uptake kinetics. *Journal of Applied Physiology*, *120*, 1319–1327.

Clanton, T. L., Hogan, M. C., & Gladden, L. B. (2013). Regulation of cellular gas exchange, oxygen sensing, and metabolic control. *Comprehensive Physiology*, *3*, 1135–1190.

Cleland, I., Kikhia, B., Nugent, C., Boytsov, A., Hallberg, J., Synnes, K., … Finlay, D. (2013).

Optimal Placement of Accelerometers for the Detection of Everyday Activities. *Sensors*, *13*, 9183–9200.

Cochrane, J. E., & Hughson, R. L. (1992). Computer simulation of O2 transport and utilization mechanisms at the onset of exercise. *Journal of Applied Physiology*, *73*, 2382–2388.

Coggan, A. R., Spina, R. J., King, D. S., Rogers, M. A., Brown, M., Nemeth, P. M., & Holloszy, J. O. (1992). Histochemical and enzymatic comparison of the gastrocnemius muscle of young and elderly men and women. *Journal of Gerontology*, *47*, 71–76.

Collins, T. C., Lunos, S., Carlson, T., Henderson, K., Lightbourne, M., Nelson, B., & Hodges, J. S. (2011). Effects of a home-based walking intervention on mobility and quality of life in people with diabetes and peripheral arterial disease: A randomized controlled trial. *Diabetes Care*, *34*, 2174–2179.

Crouter, S. E., DellaValle, D. M., Horton, M., Haas, J. D., Frongillo, E. A., & Bassett, D. R. (2011). Validity of the Actical for estimating free-living physical activity. *European Journal of Applied Physiology*, *111*, 1381–1389.

Crow, M. T., & Kushmerick, M. J. (1982). Chemical energetics of slow- and fast-twitch muscles of the mouse. *The Journal of General Physiology*, *79*, 147–66.

Cureton, K., Bishop, P., Hutchinson, P., Newland, H., Vickery, S., & Zwiren, L. (1986). Sex difference in maximal oxygen uptake. *European Journal of Applied Physiology and Occupational Physiology*, *54*, 656–660.

Dart, A. M., Du, X., & Kingwell, B. a. (2002). Gender, sex hormones and autonomic nervous control of the cardiovascular system. *Cardiovascular Research*, *53*, 678–687.

DeLorey, D. S., Kowalchuk, J. M., & Paterson, D. H. (2003). Relationship between pulmonary O2 uptake kinetics and muscle deoxygenation during moderate-intensity exercise. *Journal*

of Applied Physiology, *95*, 113–120.

Dietterich, T. G. (2000). *Multiple Classifier Systems*. Berlin, BER: Springer.

DiMenna, F. J., Bailey, S. J., Vanhatalo, A., Chidnok, W., & Jones, A. M. (2010). Elevated baseline VO2 per se does not slow O2 uptake kinetics during work-to-work exercise transitions. *Journal of Applied Physiology*, *109*, 1148–1154.

Drake, V., Jones, G., Brown, J. R., & Shephard, R. J. (1968). Fitness performance tests and their relationship to the maximal oxygen uptake of adults. *Canadian Medical Association Journal*, *99*, 844–848.

Dumanoir, G. R., Delorey, D. S., Kowalchuk, J. M., & Paterson, D. H. (2010). Kinetics of VO2 limb blood flow and regional muscle deoxygenation in young adults during moderate intensity, knee-extension exercise. *European Journal of Applied Physiology*, *108*, 607–617.

Dyson, K. S., Shoemaker, J. K., Arbeille, P., & Hughson, R. L. (2010). Modelflow estimates of cardiac output compared with Doppler ultrasound during acute changes in vascular resistance in women. *Experimental Physiology*, *95*, 561–568.

Edwards, A. M., Challis, N. V, Chapman, J. H., Claxton, D. B., & Fysh, M. L. (2001). The test-retest reliability of gas exchange kinetics in humans using a pseudo random binary sequence exercise test. *European Journal of Applied Physiology*, *85*, 333–338.

Edwards, A. M., Claxton, D. B., & Fysh, M. L. (2003). A comparison of two time-domain analysis procedures in the determination of VO2 kinetics by pseudorandom binary sequence exercise testing. *European Journal of Applied Physiology*, *88*, 411–416.

Ekelund, U., Ward, H. A., Norat, T., Luan, J., May, A. M., Weiderpass, E., … Riboli, E. (2015). Physical activity and all-cause mortality across levels of overall and abdominal adiposity in European men and women: the European Prospective Investigation into Cancer and

Nutrition Study (EPIC). *American Journal of Clinical Nutrition*, *101*, 613–621.

Ellis, K., Kerr, J., Godbole, S., Lanckriet, G., Wing, D., & Marshall, S. (2014). A random forest classifier for the prediction of energy expenditure and type of physical activity from wrist and hip accelerometers. *Physiol Meas*, *35*, 2191–2203.

Endo, M. Y., Kobayakawa, M., Kinugasa, R., Kuno, S., Akima, H., Rossiter, H. B., … Fukuba, Y. (2007). Thigh muscle activation distribution and pulmonary VO2 kinetics during moderate, heavy, and very heavy intensity cycling exercise in humans. *American Journal of Physiology - Regulatory, Integrative and Comparative Physiology*, *293*, 812–820.

Eßfeld, D., Hoffmann, U., & Stegemann, J. (1987). VO2 kinetics in subjects differing in aerobic capacity: investigation by spectral analysis. *European Journal of Applied Physiology and Occupational Physiology*, *56*, 508–515.

Eßfeld, D., Hoffmann, U., & Stegemann, J. (1991). A model for studying the distortion of muscle oxygen uptake patterns by circulation parameters. *European Journal of Applied Physiology and Occupational Physiology*, *62*, 83–90.

Faisal, A., Beavers, K. R., & Hughson, R. L. (2010). O2 uptake and blood pressure regulation at the onset of exercise: interaction of circadian rhythm and priming exercise. *American Journal of Physiology - Heart and Circulatory Physiology*, *299*, 1832–1842.

Faisal, A., Beavers, K. R., Robertson, A. D., & Hughson, R. L. (2009). Prior moderate and heavy exercise accelerate oxygen uptake and cardiac output kinetics in endurance athletes. *Journal of Applied Physiology*, *106*, 1553–1563.

Fawkner, S. G., & Armstrong, N. (2004). Sex differences in the oxygen uptake kinetic response to heavy-intensity exercise in prepubertal children. *European Journal of Applied Physiology*, *93*, 210–216.

Fawkner, S. G., Armstrong, N., Potter, C. R., & Welsman, J. R. (2002). Oxygen uptake kinetics in children and adults after the onset of moderate-intensity exercise. *Journal of Sports Sciences*, *20*, 319–326.

Ferrari, M., Binzoni, T., & Quaresima, V. (1997). Oxidative metabolism in muscle. *Philosophical Transactions of the Royal Society of London*, *352*, 677–683.

Ferreira, L. F., Townsend, D. K., Lutjemeier, B. J., & Barstow, T. J. (2005). Muscle capillary blood flow kinetics estimated from pulmonary O2 uptake and near-infrared spectroscopy. *Journal of Applied Physiology*, *98*, 1820–1828.

Franco, R. L., Bowen, M. K., Arena, R., Privett, S. H., Acevedo, E. O., Wickham, E. P., & Evans, R. K. (2014). Sex differences in pulmonary oxygen uptake kinetics in obese adolescents. *The Journal of Pediatrics*, *165*, 1161–1165.

Grassi, B., Poole, D. C., Richardson, R. S., Knight, D. R., Erickson, B. K., & Wagner, P. D. (1996). Muscle O2 uptake kinetics in humans: implications for metabolic control. *Journal of Applied Physiology*, *80*, 988–998.

Guazzi, M., Adams, V., Conraads, V., Halle, M., Mezzani, A., Vanhees, L., … Myers, J. (2012). Clinical Recommendations for Cardiopulmonary Exercise Testing Data Assessment in Specific Patient Populations. *Circulation*, *126*, 2261–2274.

Guilbert, J. J. (2003). The world health report 2002 - reducing risks, promoting healthy life. *Education for Health*, *16*, 230.

Hagberg, J. M., Hickson, R. C., Ehsani, A. A., & Holloszy, J. O. (1980). Faster adjustment to and recovery from submaximal exercise in the trained state. *Journal of Applied Physiology*, *48*, 218–224.

Haizlip, K. M., Harrison, B. C., & Leinwand, L. a. (2015). Sex-based differences in skeletal

muscle kinetics and fiber-type composition. *Physiology*, *30*, 30–39.

Hall, M., National, H., Frank, E., Holmes, G., Pfahringer, B., Reutemann, P., & Witten, I. H. (2009). The WEKA Data Mining Software : An Update. *SIGKDD Explorations*, *11*, 10–18.

Hansen, J. E., Casaburi, R., Cooper, D. M., & Wasserman, K. (1988). Oxygen uptake as related to work rate increment during cycle ergometer exercise. *European Journal of Applied Physiology and Occupational Physiology*, *57*, 140–145.

Harms, C. A., & Rosenkranz, S. (2008). Sex Differences in Pulmonary Function during Exercise. *Medicine & Science in Sports & Exercise*, *40*, 664–668.

Harper, A. J., Ferreira, L. F., Lutjemeier, B. J., Townsend, D. K., & Barstow, T. J. (2006). Human femoral artery and estimated muscle capillary blood flow kinetics following the onset of exercise. *Experimental Physiology*, *91*, 661–671.

Hendelman, D., Miller, K., Baggett, C., Debold, E., & Freedson, P. (2000). Validity of accelerometry for the assessment of moderate intensity physical activity in the field. *Medicine & Science in Sports & Exercise*, *32*, 442–449.

Henry, F. M. (1951). Aerobic Oxygen Consumption and Alactic Debt in Muscular Work. *Journal of Applied Physiology*, *3*, 427–438.

Hickam, J., Cargill, W. H., & Golden, A. (1948). Cardiovascular reactions to emotional stimuli. Effects on the cardiac output, arteriovenout oxygen difference, arterial pressure, and peripheral resistance. *The Journal of Clinical Investigation*, *27*, 290–298.

Hickson, R. C., Bomze, H. A., & Hollozy, J. O. (1978). Faster adjustment of O2 uptake to the energy requirement of exercise in the trained state. *Journal of Applied Physiology: Respiratory, Environmental and Exercise Physiology*, *44*, 877–881.

Hill, A. V., & Long, C. N. H. (1925). Muscular exercise, lactic acid, and the supply and

utilisation of oxygen. *Ergebnisse Der Physiologie*, *24*, 43–51.

Hoffmann, U., Drescher, U., Benson, A. P., Rossiter, H. B., & Essfeld, D. (2013). Skeletal muscle V̇O2 kinetics from cardio-pulmonary measurements: Assessing distortions through O2 transport by means of stochastic work-rate signals and circulatory modelling. *European Journal of Applied Physiology*, *113*, 1745–1754.

Hoffmann, U., Eßfeld, D., Leyk, D., Wunderlich, H. G., & Stegemann, J. (1994). Prediction of individual oxygen uptake on-step transients from frequency responses. *European Journal of Applied Physiology and Occupational Physiology*, *69*, 93–97.

Hoffmann, U., Eßfeld, D., Wunderlich, H. G., & Stegemann, J. (1992). Dynamic linearity of VO2 responses during aerobic exercise. *European Journal of Applied Physiology and Occupational Physiology*, *64*, 139–144.

Holt, K. G., Hamill, J., & Andres, R. O. (1991). Predicting the minimal energy costs of human walking. *Medicine & Science in Sports & Exercise*, *23*, 491–498.

Howley, E. T., Bassett, D. R., & Welch, H. G. (1995). Criteria for maximal oxygen uptake. *Medicine & Science in Sports & Exercise*, *27*, 1292–1301.

Hughson, R. L. (1984). Alterations in the oxygen deficit-oxygen debt relationships with beta-adrenergic receptor blockade in man. *The Journal of Physiology*, *349*, 375–387.

Hughson, R. L. (1990). Exploring cardiorespiratory control mechanisms through gas exchange dynamics. *Medicine and Science in Sports and Exercise*, *22*, 72–79.

Hughson, R. L. (2009). Oxygen uptake kinetics: historical perspective and future directions. *Applied Physiology, Nutrition, and Metabolism*, *34*, 840–850.

Hughson, R. L., & Morrissey, M. (1982). Delayed kinetics of respiratory gas exchange in the transition from prior exercise. *Journal of Applied Physiology*, *52*, 921–929.

Hughson, R. L., & Morrissey, M. A. (1983). Delayed kinetics of VO2 in the transition from prior exercise. Evidence for O2 transport limitation of VO2 kinetics: a review. *International Journal of Sports Medicine*, *4*, 31–39.

Hughson, R. L., Sherrill, D. L., & Swanson, G. D. (1988). Kinetics of VO2 with impulse and step exercise in humans. *Journal of Applied Physiology*, *64*, 451–459.

Hughson, R. L., Shoemaker, J. K., Tschakovsky, M. E., Kowalchuk, J. M., Saltin, B., Gollnick, P. D., … Piehl, K. (1996). Dependence of muscle VO2 on blood flow dynamics at onset of forearm exercise. *Journal of Applied Physiology*, *81*, 1619–26.

Hughson, R. L., Tschakovsky, M. E., & Houston, M. E. (2001). Regulation of oxygen consumption at the onset of exercise. *Exercise and Sport Sciences Reviews*, *29*, 129–133.

Hughson, R. L., Winter, D. A., Patla, A. E., Swanson, G. D., & Cuervo, L. A. (1990). Investigation of VO2 kinetics in humans with pseudorandom binary sequence work rate change. *Journal of Applied Physiology*, *68*, 796–801.

Hughson, R. L., Xing, H. C., Borkhoff, C., & Butler, G. C. (1991). Kinetics of ventilation and gas exchange during supine and upright cycle exercise. *European Journal of Applied Physiology and Occupational Physiology*, *63*, 300–307.

Humphrey, R. (2006). Clinical Applications: The Exercise Caloric Challenge. *ACSM's Health & Fitness Journal*, *10*, 40–41.

Jacobi, D., Perrin, A.-E., Grosman, N., Doré, M.-F., Normand, S., Oppert, J.-M., & Simon, C. (2007). Physical Activity-Related Energy Expenditure With the RT3 and TriTrac Accelerometers in Overweight Adults. *Obesity*, *15*, 950–956.

Jetté, M., Sidney, K., & Blümchen, G. (1990). Metabolic equivalents (METS) in exercise testing, exercise prescription, and evaluation of functional capacity. *Clinical Cardiology*, *13*, 555–

565.

Jones, A. M., & Poole, D. C. (2005). *Oxygen Uptake Kinetics in Sport, Exercise and Medicine*. Abingdon, MD: Routledge.

Keir, D. A., Murias, J. M., Paterson, D. H., & Kowalchuk, J. M. (2014). Breath-by-breath pulmonary O2 uptake kinetics: effect of data processing on confidence in estimating model parameters. *Experimental Physiology*, *99*, 1511–22.

Keir, D. A., Nederveen, J. P., Paterson, D. H., & Kowalchuk, J. M. (2014). Pulmonary O2 uptake kinetics during moderate-intensity exercise transitions initiated from low versus elevated metabolic rates: insights from manipulations in cadence. *European Journal of Applied Physiology*, *114*, 2655–2665.

Keir, D. A., Robertson, T. C., Benson, A. P., Rossiter, H. B., & Kowalchuk, J. M. (2016). The influence of metabolic and circulatory heterogeneity on the expression of pulmonary VO2 kinetics in humans. *Experimental Physiology*, *101*, 176–192.

Kerlin, T. W. (1974). *Frequency Response Testing in Nuclear Reactors*. New York, NY: Academic Press.

Keytel, L. R., Goedecke, J. H., Noakes, T. D., Hiiloskorpi, H., Laukkanen, R., van der Merwe, L., & Lambert, E. V. (2005). Prediction of energy expenditure from heart rate monitoring during submaximal exercise. *Journal of Sports Sciences*, *23*, 289–297.

Kim, D.-Y., & Jung, S.-Y. (2014). Effect of Aerobic Exercise on Risk Factors of Cardiovascular Disease and the Apolipoprotein B / Apolipoprotein A-1 Ratio in Obese Woman. *Journal of Physical Therapy Science*, *26*, 1825–1829.

Kime, R., Fujioka, M., Osawa, T., Takagi, S., Niwayama, M., Kaneko, Y., … Katsumura, T. (2013). Which is the best indicator of muscle oxygen extraction during exercise using

NIRS?: Evidence that HHb is not the candidate. *Advances in Experimental Medicine and Biology*, *789*, 163–169.

Koga, S., Rossiter, H. B., Heinonen, I., Musch, T. I., & Poole, D. C. (2014). Dynamic heterogeneity of exercising muscle blood flow and O2 utilization. *Medicine and Science in Sports and Exercise*, *46*, 860–76.

Koskolou, M., Calbet, J., Rådegran, G., & Roach, R. (1997). Hypoxia and the cardiovascular response to dynamic knee-extensor exercise. *The American Journal of Physiology*, *272*, 2655–2663.

Kowalchuk, J. M., Rossiter, H. B., Ward, S. a, & Whipp, B. J. (2002). The effect of resistive breathing on leg muscle oxygenation using near-infrared spectroscopy during exercise in men. *Experimental Physiology*, *87*, 601–611.

Krogh, A., & Lindhard, J. (1913). The regulation of respiration and circulation during the initial stages of muscular work. *The Journal of Physiology*, *47*, 112–136.

Lamarra, N., Whipp, B. J., Ward, S. A., & Wasserman, K. (1987). Effect of interbreath fluctuations on characterizing exercise gas exchange kinetics. *Journal of Applied Physiology*, *62*, 2003–2012.

Lambrick, D., Faulkner, J., Westrupp, N., & McNarry, M. (2013). The influence of body weight on the pulmonary oxygen uptake kinetics in pre-pubertal children during moderate- and heavy intensity treadmill exercise. *European Journal of Applied Physiology*, *113*, 1947–1955.

Linnarsson, D. (1974). Dynamics of pulmonary gas exchange and heart rate changes at start and end of exercise. *Acta Physiologica Scandinavica. Supplementum*, *415*, 1–68.

Ludlow, L. W., & Weyand, P. G. (2016). Energy expenditure during level human walking:

seeking a simple and accurate predictive solution. *Journal of Applied Physiology*, *120*, 481–94.

Luenberger, D. G., & Ye, Y. (2015). *Linear and Nonlinear Programming*. New York, NY: Springer.

Lundsgaard, A.-M., & Kiens, B. (2014). Gender Differences in Skeletal Muscle Substrate Metabolism - Molecular Mechanisms and Insulin Sensitivity. *Frontiers in Endocrinology*, *5*, 195.

Macdonald, M., Pedersen, P. K., & Hughson, R. L. (1997). Acceleration of VO2 kinetics in heavy submaximal exercise by hyperoxia and prior high-intensity exercise. *Journal of Applied Physiology*, *83*, 1318–1325.

MacKey, D. C., Manini, T. M., Schoeller, D. A., Koster, A., Glynn, N. W., Goodpaster, B. H., … Cummings, S. R. (2011). Validation of an armband to measure daily energy expenditure in older adults. *Journals of Gerontology*, *66*, 1108–1113.

Mannini, A., & Sabatini, A. M. (2010). Machine learning methods for classifying human physical activity from on-body accelerometers. *Sensors*, *10*, 1154–1175.

Margaria, R., Manglli, F., Cuttica, F., & Cerretelli, P. (1965). The kinetics of the oxygen uptake consumption at the onset of muscular exercise in man. *Ergonomics*, *8*, 49–54.

Markovitz, G. H., Sayre, J. W., Storer, T. W., & Cooper, C. B. (2004). On issues of confidence in determining the time constant for oxygen uptake kinetics. *British Journal of Sports Medicine*, *38*, 553–560.

Marschollek, M., Goevercin, M., Wolf, K. H., Song, B., Gietzelt, M., Haux, R., & Steinhagen-Thiessen, E. (2008). A performance comparison of accelerometry-based step detection algorithms on a large, non-laboratory sample of healthy and mobility-impaired persons. In

2008 30th Annual International Conference of the IEEE Engineering in Medicine and Biology Society (pp. 1319–1322). Vancouver, BC: IEEE.

Matthews, C. E., & Freedson, P. S. (1995). Field trial of a three-dimensional activity monitor: Comparison with self report. *Medicine and Science in Sports and Exercise*, *27*, 1071–1078.

Meijer, G. A., Westerterp, K. R., Koper, H., & Ten Hoor, F. (1989). Assessment of energy expenditure by recording heart rate and body acceleration. *Medicine & Science in Sports & Exercise*, *21*, 343–347.

Molé, P. A., & Hoffmann, J. J. (1999). VO(2) kinetics of mild exercise are altered by RER. *Journal of Applied Physiology*, *87*, 2097–2106.

Montgomery, P. G., Green, D. J., Etxebarria, N., Pyne, D. B., Saunders, P. U., & Minahan, C. L. (2009). Validation of heart rate monitor-based predictions of oxygen uptake and energy expenditure. *Journal of Strength and Conditioning Research*, *23*, 1489–1495.

Mora, S., Lee, I.-M., Buring, J. E., & Ridker, P. M. (2006). Association of physical activity and body mass index with novel and traditional cardiovascular biomarkers in women. *JAMA : The Journal of the American Medical Association*, *295*, 1412–1419.

Motulsky, H. J., & Ransnas, L. A. (1987). Fitting curves to data using nonlinear regression: a practical and nonmathematical review. *The FASEB Journal : Official Publication of the Federation of American Societies for Experimental Biology*, *1*, 365–374.

Mukaka, M. M. (2012). Statistics corner: A guide to appropriate use of correlation coefficient in medical research. *Malawi Medical Journal : The Journal of Medical Association of Malawi*, *24*, 69–71.

Murias, J. M., Spencer, M. D., Kowalchuk, J. M., & Paterson, D. H. (2011a). Influence of phase I duration on phase II VO2 kinetics parameter estimates in older and young adults.

American Journal of Physiology - Regulatory, Integrative and Comparative Physiology, *301*, 218–224.

Murias, J. M., Spencer, M. D., Kowalchuk, J. M., & Paterson, D. H. (2011b). Muscle deoxygenation to VO2 relationship differs in young subjects with varying τVO2. *European Journal of Applied Physiology*, *111*, 3107–3118.

Murias, J. M., Spencer, M. D., & Paterson, D. H. (2014). The Critical Role of O2 Provision in the Dynamic Adjustment of Oxidative Phosphorylation. *Exercise and Sport Sciences Reviews*, *42*, 4–11.

Nakamura, T., Kiyono, K., Wendt, H., Abry, P., & Yamamoto, Y. (2016). Multiscale Analysis of Intensive Longitudinal Biomedical Signals and Its Clinical Applications. *Proceedings of the IEEE*, *104*, 242–261.

Nery, L. E., Wasserman, K., Andrews, J. D., Huntsman, D. J., Hansen, J. E., & Whipp, B. J. (1982). Ventilatory and gas exchange kinetics during exercise in chronic airways obstruction. *Journal of Applied Physiology: Respiratory, Environmental and Exercise Physiology*, *53*, 1594–1602.

Newman, A. B., Gottdiener, J. ., McBurnie, M. A., Hirsch, C. H., Kop, W. J., Tracy, R., … Fried, L. P. (2001). Associations of Subclinical Cardiovascular Disease With Frailty. *The Journals of Gerontology Series A: Biological Sciences and Medical Sciences*, *56*, M158–M166.

Newman, A. B., Simonsick, E. M., Naydeck, B. L., Boudreau, R. M., Kritchevsky, S. B., Nevitt, M. C., … Harris, T. B. (2006). Association of long-distance corridor walk performance with mortality, cardiovascular disease, mobility limitation, and disability. *JAMA : The Journal of the American Medical Association*, *295*, 2018–2026.

Norris, S. R., & Petersen, S. R. (1998). Effects of endurance training on transient oxygen uptake responses in cyclists. *Journal of Sports Sciences*, *16*, 733–738.

Nygaard, E. (1981). Skeletal muscle fibre characteristics in young women. *Acta Physiologica Scandinavica*, *112*, 299–304.

O'Connor, E., Kiely, C., O'Shea, D., Green, S., & Egaña, M. (2012). Similar level of impairment in exercise performance and oxygen uptake kinetics in middle-aged men and women with type 2 diabetes. *American Journal of Physiology - Regulatory, Integrative and Comparative Physiology*, *303*, 70–76.

Orendurff, M. S., Schoen, J. A., Bernatz, G. C., Segal, A. D., & Klute, G. K. (2008). How humans walk: bout duration, steps per bout, and rest duration. *Journal of Rehabilitation Research and Development*, *45*, 1077–1089.

Ozyener, F., Rossiter, H. B., Ward, S. A., & Whipp, B. J. (2001). Influence of exercise intensity on the on- and off-transient kinetics of pulmonary oxygen uptake in humans. *The Journal of Physiology*, *533*, 891–902.

Paterson, D. H., & Whipp, B. J. (1991). Asymmetries of oxygen uptake transients at the on- and offset of heavy exercise in humans. *The Journal of Physiology*, *443*, 575–586.

Pescatello, L. S. (2014). *ACSM's guidelines for exercise testing and prescription*. Philadelphia, PA: Wolters Kluwer.

Pessoa, B. V, Beltrame, T., Di Lorenzo, V. A. P., Catai, A. M., Borghi-Silva, A., & Jamami, M. (2013). COPD patients' oxygen uptake and heart rate on-kinetics at cycle-ergometer: correlation with their predictors of severity. *Brazilian Journal of Physical Therapy*, *17*, 152–162.

Peterka, R. J. (2002). Sensorimotor Integration in Human Postural Control. *Journal of*

Neurophysiology, *88*, 1097–1118.

Phillips, S. M., Green, H. J., MacDonald, M. J., & Hughson, R. L. (1995). Progressive effect of endurance training on VO2 kinetics at the onset of submaximal exercise. *Journal of Applied Physiology*, *79*, 1914–1920.

Pillonetto, G., Dinuzzo, F., Chen, T., De Nicolao, G., & Ljung, L. (2014). Kernel methods in system identification, machine learning and function estimation: A survey. *Automatica*, *50*, 657–682.

Pober, D. M., Staudenmayer, J., Raphael, C., & Freedson, P. S. (2006). Development of novel techniques to classify physical activity mode using accelerometers. *Medicine and Science in Sports and Exercise*, *38*, 1626–1634.

Powers, S. K., Dodd, S., & Beadle, R. E. (1985). Oxygen uptake kinetics in trained athletes differing in VO2max. *European Journal of Applied Physiology and Occupational Physiology*, *54*, 306–308.

Puyau, M. R., Adolph, A. L., Vohra, F. A., Zakeri, I., & Butte, N. F. (2004). Prediction of activity energy expenditure using accelerometers in children. *Medicine and Science in Sports and Exercise*, *36*, 1625–1631.

Raper, J. A., Love, L. K., Paterson, D. H., Peters, S. J., Heigenhauser, G. J. F., & Kowalchuk, J. M. (2014). Effect of high-fat and high-carbohydrate diets on pulmonary O2 uptake kinetics during the transition to moderate-intensity exercise. *Journal of Applied Physiology*, *117*, 1371–1379.

Ravussin, E., Lillioja, S., Anderson, T. E., Christin, L., & Bogardus, C. (1986). Determinants of 24-hour energy expenditure in man. Methods and results using a respiratory chamber. *Journal of Clinical Investigation*, *78*, 1568–1578.

Regensteiner, J. G., Bauer, T. A., Reusch, J. E., Brandenburg, S. L., Sippel, J. M., Vogelsong, A. M., … Hiatt, W. R. (1998). Abnormal oxygen uptake kinetic responses in women with type II diabetes mellitus. *Journal of Applied Physiology*, *85*, 310–317.

Robergs, R. A. (2014). A Critical Review of the History of Low- to Moderate-Intensity Steady-State VO2 Kinetics. *Sports Medicine*, *44*, 641–653.

Rodríguez, J., Goñi, A., & Illarramendi, A. (2005). Real-time classification of ECGs on a PDA. *IEEE Transactions on Information Technology in Biomedicine*, *9*, 23–34.

Roepstorff, C., Schjerling, P., Vistisen, B., Madsen, M., Steffensen, C. H., Rider, M. H., & Kiens, B. (2005). Regulation of oxidative enzyme activity and eukaryotic elongation factor 2 in human skeletal muscle: Influence of gender and exercise. *Acta Physiologica Scandinavica*, *184*, 215–224.

Ross, K. A., Jensen, C. S., Snodgrass, R., Dyreson, C. E., Jensen, C. S., Snodgrass, R., … Chen, L. (2009). *Cross-Validation*. *Encyclopedia of Database Systems*. Boston, MA: Springer.

Rossy, L. a, & Thayer, J. F. (1998). Fitness and gender-related differences in heart period variability. *Psychosomatic Medicine*, *60*, 773–781.

Rouleau, C. M., Santana, C. J., Jones, K. S., & Park, R. M. (1995). Dislocations in lattice-mismatched wide-gap II-VI/GaAs heterostructures as laser light scatterers: Experiment and theory. *Journal of Applied Physics*, *78*, 1203–1209.

Rudner, J., McDougall, C., Sailam, V., Smith, M., & Sacchetti, A. (2016). Interrogation of Patient Smartphone Activity Tracker to Assist Arrhythmia Management. *Annals of Emergency Medicine*, *68*, 292–294.

Sallis, J. F., & Saelens, B. E. (2000). Assessment of physical activity by self-report: Status, limitations, and future directions. *Research Quarterly for Exercise and Sport*, *71*, 1–14.

Schalcher, C., Rickli, H., Brehm, M., Weilenmann, D., Oechslin, E., Kiowski, W., & Brunner-La Rocca, H. P. (2003). Prolonged oxygen uptake kinetics during low-intensity exercise are related to poor prognosis in patients with mild-to-moderate congestive heart failure. *Chest*, *124*, 580–586.

Schmitz, K. H., Treuth, M., Hannan, P., Mcmurray, R., Ring, K. B., Catellier, D., & Pate, R. (2005). Predicting energy expenditure from accelerometry counts in adolescents girls. *Medicine and Science in Sports and Exercise*, *37*, 155–161.

Schrack, J. A., Zipunnikov, V., Goldsmith, J., Bandeen-Roche, K., Crainiceanu, C. M., & Ferrucci, L. (2014). Estimating Energy Expenditure from Heart Rate in Older Adults: A Case for Calibration. *PLoS ONE*, *9*, e93520.

Seals, D. R. (2013). Translational physiology: from molecules to public health. *The Journal of Physiology*, *591*, 3457–3469.

Selinger, J. C., & Donelan, J. M. (2014). Estimating instantaneous energetic cost during non-steady-state gait. *Journal of Applied Physiology*, *117*, 1406–1415.

Shmilovitz, D. (2005). On the definition of total harmonic distortion and its effect on measurement interpretation. *IEEE Transactions on Power Delivery*, *20*, 526–528.

Smolander, J., Juuti, T., Kinnunen, M. L., Laine, K., Louhevaara, V., Männikkö, K., & Rusko, H. (2008). A new heart rate variability-based method for the estimation of oxygen consumption without individual laboratory calibration: Application example on postal workers. *Applied Ergonomics*, *39*, 325–331.

Staron, R. S., Hagerman, F. C., Hikida, R. S., Murray, T. F., Hostler, D. P., Crill, M. T., … Toma, K. (2000). Fiber type composition of the vastus lateralis muscle of young men and women. *The Journal of Histochemistry and Cytochemistry : Official Journal of the*

Histochemistry Society, *48*, 623–629.

Staudenmayer, J., Pober, D., Crouter, S., Bassett, D., & Freedson, P. (2009). An artificial neural network to estimate physical activity energy expenditure and identify physical activity type from an accelerometer. *Journal of Applied Physiology*, *107*, 1300–1307.

Su, S. W., Celler, B. G., Savkin, A. V, Nguyen, H. T., Cheng, T. M., Guo, Y., & Wang, L. (2009). Transient and steady state estimation of human oxygen uptake based on noninvasive portable sensor measurements. *Medical & Biological Engineering & Computing*, *47*, 1111–1117.

Su, S. W., Wang, L., Celler, B. G., & Savkin, A. V. (2007). Oxygen uptake estimation in humans during exercise using a Hammerstein model. *Annals of Biomedical Engineering*, *35*, 1898–1906.

Sugawara, J., Tanabe, T., Miyachi, M., Yamamoto, K., Takahashi, K., Iemitsu, M., … Matsuda, M. (2003). Non-invasive assessment of cardiac output during exercise in healthy young humans: Comparison between Modelflow method and Doppler echocardiography method. *Acta Physiologica Scandinavica*, *179*, 361–366.

Sui, X., LaMonte, M. J., Laditka, J. N., Hardin, J. W., Chase, N., Hooker, S. P., & Blair, S. N. (2007). Cardiorespiratory fitness and adiposity as mortality predictors in older adults. *JAMA : The Journal of the American Medical Association*, *298*, 2507–2516.

Swanson, G. D. (1990). Assembling control models from pulmonary gas exchange dynamics. *Medicine & Science in Sports & Exercise*, *22*, 80–87.

Swartz, A. M., Strath, S. J., Bassett, D. R., Obrien, W. L., King, G. A., & Ainsworth, B. E. (2000). Estimation of energy expenditure using CSA accelerometers at hip and wrist sites. *Medicine & Science in Sports & Exercise*, *32*, 450–456.

Tan, S. Y., Batterham, M., & Tapsell, L. (2011). Activity counts from accelerometers do not add value to energy expenditure predictions in sedentary overweight individuals during weight loss interventions. *Journal of Physical Activity & Health*, *8*, 675–681.

Tanawongsuwan, R., & Bobick, A. (2003). Performance Analysis of Time-Distance Gait Parameters under Different Speeds. In *Audio- and Video-Based Biometric Person Authentication: 4th International Conference* (pp. 715–724). Berlin, BER: Springer.

Tarnopolsky, L. J., MacDougall, J. D., Atkinson, S. a, Tarnopolsky, M. A., & Sutton, J. R. (1990). Gender differences in substrate for endurance exercise. *Journal of Applied Physiology*, *68*, 302–308.

Tarnopolsky, M. A. (2008). Sex Differences in Exercise Metabolism and the Role of 17-Beta Estradiol. *Medicine & Science in Sports & Exercise*, *40*, 648–654.

Theodor, M., Fiala, J., Ruh, D., Förster, K., Heilmann, C., Beyersdorf, F., … Seifert, A. (2014). Implantable accelerometer system for the determination of blood pressure using reflected wave transit time. *Sensors and Actuators A: Physical*, *206*, 151–158.

Thompson, J. R., Swanson, S. a, Casale, G. P., Johanning, J. M., Papoutsi, E., Koutakis, P., … Pipinos, I. I. (2013). Gastrocnemius mitochondrial respiration: are there any differences between men and women? *Journal of Surgical Research*, *185*, 206–211.

Truijen, J., Kim, Y. S., Krediet, C. T. P., Stok, W. J., Kölgen, R. S., Colier, W. N., … van Lieshout, J. J. (2012). Orthostatic leg blood volume changes assessed by near-infrared spectroscopy. *Experimental Physiology*, *97*, 353–361.

Tschakovsky, M. E. (2014). Is it or isn't it oxygen delivery? The debate over what limits oxygen uptake kinetics continues. *Exercise and Sport Sciences Reviews*, *42*, 2–3.

Tschakovsky, M. E., & Hughson, R. L. (1999). Interaction of factors determining oxygen uptake

at the onset of exercise. *Journal of Applied Physiology*, *86*, 1101–1113.

Tschakovsky, M. E., Saunders, N. R., Webb, K. A., & O'donnell, D. E. (2006). Muscle Blood-Flow Dynamics at Exercise Onset. *Medicine & Science in Sports & Exercise*, *38*, 1811–1818.

Tudor-Locke, C., & Rowe, D. A. (2012). Using Cadence to Study Free-Living Ambulatory Behaviour. *Sports Medicine*, *42*, 381–398.

Vahlquist, B. O. (1950). The cause of the sexual differences in erythrocyte, hemoglobin and serum iron levels in human adults. *Blood*, *5*, 874–875.

Villar, R., Beltrame, T., & Hughson, R. L. (2015). Validation of the Hexoskin wearable vest during lying, sitting, standing, and walking activities. *Applied Physiology, Nutrition, and Metabolism*, *40*, 1019–1024.

Walls, T. A., & Schafer, J. L. (2012). *Models for Intensive Longitudinal Data*. New York, NY: Oxford University Press.

Wesseling, K. H., Jansen, J. R., Settels, J. J., & Schreuder, J. J. (1993). Computation of aortic flow from pressure in humans using a nonlinear, three-element model. *Journal of Applied Physiology*, *74*, 2566–2573.

Whipp, B. J., & Ward, S. A. (1982). Cardiopulmonary coupling during exercise. *The Journal of Experimental Biology*, *100*, 175–193.

Whipp, B. J., & Ward, S. A. (1990). Physiological determinants of pulmonary gas exchange kinetics during exercise. *Medicine & Science in Sports & Exercise*, *22*, 62–71.

Whipp, B. J., & Ward, S. A. (1992). Pulmonary gas exchange dynamics and the tolerance to muscular exercise: effects of fitness and training. *Annals of Physiological Anthropology*, *11*, 207–214.

Whipp, B. J., Ward, S. A., Lamarra, N., Davis, J. A., & Wasserman, K. (1982). Parameters of ventilatory and gas exchange dynamics during exercise. *Journal of Applied Physiology*, *52*, 1506–1513.

Whipp, B. J., & Wasserman, K. (1972). Oxygen uptake kinetics for various intensities of constant-load work. *Journal of Applied Physiology*, *33*, 351–356.

Whitcher, L., & Papadopoulos, C. (2014). Accelerometer Derived Activity Counts and Oxygen Consumption between Young and Older Individuals. *Journal of Aging Research*, *2014*, 1–8.

Wilcox, S. L., Broxterman, R. M., & Barstow, T. J. (2016). Constructing quasi-linear V̇O2 responses from nonlinear parameters. *Journal of Applied Physiology*, *120*, 121–129.

Witten, I. H., & Frank, E. (2005). *Data Mining: Practical machine learning tools and techniques*. San Francisco, CA: Elsevier.

Xing, H. C., Cochrane, J. E., Yamamoto, Y., & Hughson, R. L. (1991). Frequency domain analysis of ventilation and gas exchange kinetics in hypoxic exercise. *Journal of Applied Physiology*, *71*, 2394–2401.

Yoshida, T., Abe, D., Fukuoka, Y., & Hughson, R. L. (2008). System Analysis for Oxygen Uptake Kinetics with Step and Pseudorandom Binary Sequence Exercise in Endurance Athletes. *Measurement in Physical Education & Exercise Science*, *12*, 1–9.

Yoshida, T., Yamamoto, K., & Udo, M. (1993). Relationship between cardiac output and oxygen uptake at the onset of exercise. *European Journal of Applied Physiology and Occupational Physiology*, *66*, 155–160.

Zarrugh, M. Y. (1981). Power requirements and mechanical efficiency of treadmill walking. *Journal of Biomechanics*, *14*, 157–165.

Appendices

Appendix A: Sex Differences in the Oxygen Delivery, Extraction and Uptake During Moderate Walking Exercise Transition

This Appendix was submitted as:

Beltrame T, Villar R, Hughson RL. Sex differences in the oxygen delivery, extraction and uptake during moderate walking exercise transition. Submitted to Am J Physiol Regul Integr Comp Physiol since November 7, 2016

A.1 Overview

Due to known greater maximal aerobic power of men compared to women, it was hypothesized that men would have faster aerobic system dynamics in response to the onset of exercise challenge. This study investigated the interactions between oxygen supply and utilization by characterizing the dynamics of oxygen uptake ($\dot{V}O_2$), deoxyhemoglobin (HHb), tissue saturation index (TSI), cardiac output ($\dot{Q}$) and total arteriovenous O_2 difference ($a-vO_2diff$) in women and men. Eighteen healthy active young women and men (9 of each sex) with similar body mass index volunteered for this study. On the first day, participants performed an incremental cardiopulmonary treadmill exercise test. On the second day, three moderate intensity treadmill exercise tests (at 80 % $\dot{V}O_2$ of gas exchange threshold) were performed. Data related to the second visit were submitted to a exponential data modeling technique to obtain parameters related to the aerobic system dynamics. The time constants of the $\dot{V}O_2$, $a-vO_2diff$, HHb and TSI (30±6, 29±1, 16±1 and 15±2 s, respectively) in women were statistically (p<0.05) faster than the time constants in men (42±10, 49±21, 19±3 and 20±4 s, respectively). Although $\dot{Q}$ dynamics were not statistically different (p=0.06) between women and men, there was a trend to slower $\dot{Q}$ dynamics in men corresponding with the slower $\dot{V}O_2$ kinetics. These results indicated that the peripheral and central oxygen extraction dynamics were remarkably faster in women thus, contrary to the hypothesis, $\dot{V}O_2$ dynamics measured at the mouth at the onset of submaximal treadmill walking were faster in women compared to men.

A.2 New & Noteworthy

The regulation of the aerobic system response to moderate exercise seems to differ between women and men. However, the control mechanisms responsible for this hypothetical difference are not fully understood. We investigated the integrated aerobic response in both sexes by evaluating the oxygen delivery-utilization balance simultaneously with oxygen uptake response. Based on our results, women presented a faster aerobic adjustment during exercise transition in comparison to men due to an apparent faster peripheral oxygen extraction.

A.4 Introduction

The characterization of the oxygen uptake ($\dot{V}O_2$) dynamics during exercise transition can be used to investigate the adjustments of the aerobic response to supply a new energetic demand (Krogh & Lindhard, 1913). The rate at which the $\dot{V}O_2$ increases at the beginning of exercise seems to be determined by the integrative control of several mechanisms involving the O_2 transport by the circulation and its utilization by the myocyte (Grassi et al., 1996; Hughson & Morrissey, 1983; Keir et al., 2016; Macdonald et al., 1997).

The sex influences over the aerobic response dynamics during exercise transition are not fully understood. The greater maximal aerobic power of men compared to women is well recognized (Cureton et al., 1986), as well as sex differences in the autonomic nervous control (Dart, Du, & Kingwell, 2002; Rossy & Thayer, 1998) and muscle tissue composition (Nygaard, 1981). These differences are expected to influence the $\dot{V}O_2$ dynamics during exercise transition (Barstow, Jones, Nguyen, & Casaburi, 1996; Hughson, 1984; Powers et al., 1985). Nevertheless, some studies (Bauer, Reusch, Levi, & Regensteiner, 2007; Endo et al., 2007) investigated the $\dot{V}O_2$ dynamics in men and women as a single group.

Faster $\dot{V}O_2$ kinetics have been observed in pre-pubertal boys compared to girls (Fawkner & Armstrong, 2004), and in obese male compared to female adolescents (Franco et al., 2014). In older adults, sex explained some variation in $\dot{V}O_2$ kinetics (Chilibeck et al., 1995), but another study observed no difference between men and women in healthy or diabetic populations (O'Connor, Kiely, O'Shea, Green, & Egaña, 2012). However, none of these investigations performed measurements that allowed the simultaneous investigation of $\dot{V}O_2$ kinetics and the contributions of the O_2 delivery-utilization systems during exercise transition. Near infrared spectroscopy (NIRS) and cardiac output ($\dot{Q}$) measurements can be used to assess the O_2 delivery-utilization distortions *in vivo* (Faisal et al., 2010; Ferrari, Binzoni, & Quaresima, 1997; Murias et al., 2011b). These variables, when obtained simultaneously with $\dot{V}O_2$ data, offer the opportunity to study how the O_2 delivery-utilization balance differs between women and men, and how this might impact the rate at which the aerobic system supplies the energy demand.

Therefore, the purpose of this cross-sectional study was to further explore how sex influences the $\dot{V}O_2$ response during exercise transition with simultaneous measurement of NIRS and $\dot{Q}$. We hypothesized that men have a faster $\dot{V}O_2$ dynamics in comparison to women, and that this would be supported by a better peripheral O_2 delivery and extraction in men.

A.5 Methods

A.5.1 Participants

Eighteen healthy, recreationally active young adults (9 women and 9 men) of similar age and body mass index (women = age 23±3 years, height 164±7 cm, weight 62.9±5.9 kg, and BMI 23.2±1.2 kg/m^2 and men = age 29±6 years, height 181±8 cm, weight 81.1±11.1 kg, and BMI 24.6±2 kg/m^2) without any cardiovascular or orthopedic complications volunteered for this study. Participants

were evaluated during walking activities on a previously calibrated treadmill (error lower than 1% for speeds between 0.5 to 8 $km \cdot h^{-1}$) (Bodyguard, St-Georges, QB, Canada). Participants signed a written informed consent after receiving detailed information about the experimental procedures and potential risks involved. They were aware of their right to withdraw from the study at any time. The study procedures were reviewed and approved by the Office of Research Ethics at the University of Waterloo and in agreement with Declaration of Helsinki. It was requested of all participants to not consume a large meal within 2 h prior testing, not drink alcohol and caffeinated beverages as well as not perform high intensity exercise for 24 h prior testing.

A.5.2 Experimental Design

Data were collected on two separate visits. The first visit consisted of incremental cardiopulmonary exercise testing, while the second visit consisted of three moderate walking exercise tests. Following the measurement of height and weight, a 3-lead electrocardiogram (ECG) electrodes were applied over the participant's skin and an air cushion mask was fitted to the participant's face to allow measurement of gas exchange. Prior to testing, all individuals were trained to step on the treadmill in motion according to speed and inclination requirements and familiarized with the protocols. Experiments were performed in a quiet room with temperature and humidity relatively constant (22.4 ± 0.5 ºC, 23.4 ± 0.9% respectively) and barometric pressure of 728.7 ± 4.4 mmHg.

A.5.3 Experimental Protocols

The incremental cardiopulmonary exercise testing protocol consisted of 1-minute baseline, 6-minute warm-up at 4.5 $km \cdot h^{-1}$ no slope, followed by a new increment in speed (individual

maximum walking speed of ~6 km·h^{-1}) and then progressive increments in grade (1%·min^{-1}). The test was terminated when subjects reached 80% of their predicted maximal heart rate. This protocol was performed in order to obtain individual gas exchange threshold (GET) (Beaver et al., 1986) that was used to calculate the relative moderate work rate performed in the following laboratory visit. On the second visit, participants performed three identical walking exercises at a work rate corresponding to 80% of their $\dot{V}O_2$ at GET (Ozyener et al., 2001). This protocol included 1 minute of baseline standing at the treadmill edge followed by 6 min walking at individual selected speeds and grades and 6 minutes of recovery.

In order to minimize any carry over effect between exercise bouts, seated recovery periods between all constant work rate exercise tests lasted at least 20 min. The treadmill was operating at the target work rate even during baseline for at least 5 min to avoid anticipatory responses. To indicate when participants should start walking on the treadmill, a computer monitor was placed at the participant's eye level to control the transitions.

A.5.4 Data Acquisition

Breath-by-breath measurements of pulmonary $\dot{V}O_2$ and carbon dioxide output ($\dot{V}CO_2$) were taken during tests. A low dead space, bidirectional, low resistance turbine was used to measure inhale/exhale air volumes and flows (UVM-1725, Vacumed, Ventura, California, US) and it was attached to an air cushion mask (Vacumed, Ventura, California, US) for a total system dead space of 170 mL. A 3 L syringe using different flow rates (0.5 to 2 L·s^{-1}) was used to calibrate the turbine prior to each test bout. Air samples inside the mask were sent to a mass spectrometer (Amis 2000, Innovision, Odense, Denmark) by a short sample line (~1.5 m). The system gas concentration calibration was performed using gas tanks with known O_2, CO_2, N_2, and Ar concentrations. The

turbine and mass spectrometer signals were synchronized and utilized in the estimation of $\dot{V}O_2$ and $\dot{V}CO_2$ (First Breath, Waterloo, ON, Canada).

The heart rate beat-by-beat calculation was derived from the ECG signal (Pilot 9200, Colin Medical Instruments, San Antonio, TX, US) recorded with LabChart 7.3.7 (ADInstruments, Colorado Springs, CO, US). The finger arterial pressure signal (Finometer, Finapres Medical System, Arnhem, The Netherlands) was used to provide a beat-by-beat estimate of $\dot{Q}$ as previously validated for exercise (Faisal et al., 2009). The total arteriovenous O_2 difference ($a - vO_2diff$) was calculated by the ratio $\dot{V}O_2/\dot{Q}$ and it was used as a proxy of the total venous O_2 content during exercise transition (Barstow et al., 1990).

A multi-distance continuous-wave single channel near infrared spectroscopy (NIRS) (PortaLite, Artinis Medical Systems B.V., Elst, The Netherlands) evaluated changes in *Gastrocnemius Lateralis* muscle oxy- (O_2Hb) and deoxy-hemo/myoglobin (HHb) concentrations (expressed in $\Delta\mu M$) sampled at a rate of 10 Hz. The light emitting probe was composed by three light-emitting diodes operating at two wavelengths (λ_1=845 and λ_2=759 nm) resulting in six different light sources with different light in/out distances (~ 35 mm). The probe was placed in the target area and the device was warmed-up for at least 30 min before the data collection. In order to avoid any motion artifact and ambient light influences, the probe was fixed by tape and then a dark cloth was gently wrapped around the calf.

The tissue saturation index (TSI) expressed as the percent of O_2 for a given capillary blood volume was calculated in real time by the slope of the curve between the tissue optical density and the three light in/out distances. Any probe movement was checked in real-time by the correlation level (r^2) between the light in/out distance and the optical density. During the entire data collection, the r^2 was > 98% indicating appropriate signal quality. The adipose tissue thickness

(ATT) was determined by measurements of the *Gastrocnemius* lateral head skinfold thickness using a skinfold caliper. The ATT did not exceed the minimum penetration depth of the NIRS system. The average ATT was 7.06 ± 2.57 mm, or ~40% lower than the NIRS light penetration depth. The ATT was not correlated to any variable evaluated in this study. The selected HHb and O_2Hb signals were related to the deepest penetrating transmitter of the NIRS (i.e., highest light in/out distance).

A.5.5 Data Analysis

The data from the constant work rate protocols were linearly interpolated and re-sampled at 1 Hz. The signals for each of the three constant work rate exercise transitions were time-aligned with time zero matching the onset of walking exercise. The data from the three repetitions were ensemble-averaged generating a single exercise dataset per participant. Afterwards, a 5-s moving average was used for filtering to reduce the influence of the inter-breath oscillations (Lamarra et al., 1987), narrowing the confidence interval of the parameters to be estimated (Keir, Murias, et al., 2014). Finally, the kinetics of $\dot{V}O_2$, $\dot{Q}$, HR and $a-vO_2diff$ were analyzed by the bi-exponential model following previous literature (Hughson et al., 1988):

Equation 13 $$VO_2, \dot{Q}, HR \; or \; a-vO_2diff_{(t)} = a_0 + a_1 * \left(1 - e^{\left(-\frac{t-TD_1}{\tau_1}\right)}\right) + a_2 * \left(1 - e^{\left(-\frac{t-TD_2}{\tau_2}\right)}\right);$$

where: "t" is time (independent variable); "a_0" is the mean value during baseline; "a_1" and "a_2" are the steady-state amplitudes for the cardio-dynamic and fundamental phases, respectively;

"τ_1"and "τ_2" are time constants for each phase; "TD_1" and "TD_2" are time delays for each phase. For all variables, the steady-state of the cardio-dynamic phase (i.e., 4*[τ_1+TD_1]) coincided with the beginning of the fundamental phase (i.e., TD_2), so that phase 1 had minimal impact on fitting of phase 2. The mean response time (MRT) was calculated by the sum of TD_2 and τ_2. The quality of the fitting was assured by the analysis of residuals, degree of linear correlation between the experimental data and fitted function (r), 95% confidence interval band (CI_{95}) (Fawkner et al., 2002; Keir et al., 2016) and the significance level (p value) of the estimated parameters.

The NIRS signals were normalized by the average of the data during 30 s prior the onset of exercise for better data visualization. The HHb and TSI time constants were obtained following a previously described method (DeLorey et al., 2003; Murias et al., 2011b). Data not directly associated to the muscular $\dot{V}O_2$ dynamics (DeLorey et al., 2003) were excluded based on the detection of two nadir values for each individual exercise transition dataset. The first portion of excluded data was related to the muscle pump. The first nadir occurred at 11±0.6 and 11.6±1.3 s for women and men, respectively. This period was characterized by a sudden decrease in HHb signal (Figure 53A) with a simultaneous increase in TSI as a consequence of an elevated initial blood flow that surpasses the $\dot{V}O_2$ increase (Tschakovsky et al., 2006) decreasing the O_2 extraction (Murias et al., 2014). After this first nadir, the HHb increased and TSI decreased following an exponential-like function. It is believed that this behavior is a consequence of the $\dot{V}O_2$ dynamics characteristics during exercise transition, and therefore the phase of interest (Figure 53A) (Murias et al., 2011b).

Instead of studying the influence of data window selection over the parameters estimation by arbitrarily choosing different time intervals (Dumanoir et al., 2010; Keir et al., 2016; Murias et al., 2011b), the end of the data window was selected according to the identification of a second

nadir (Bauer, Brass, & Hiatt, 2004). Due to the late overshooting characteristics of the HHb signal (Bauer et al., 2007) usually more pronounced in women, the second nadir was set when a systematic increase in capillary blood volume assessed by the total hemoglobin ($tHb = HHb + O_2Hb$) was observed after a brief period of steady-state (—— in Figure 53B). This increment in the capillary blood volume (Truijen et al., 2012) might be occurring due to temperature increase that elevates skin blood flow and/or due to the local metabolites action over the capillary bed. The second nadir occurred after 37±8 and 41±11 s for women and men, respectively. To avoid misinterpretation of the HHb dynamics associated to non-steady capillary blood volume (Kime et al., 2013), both nadirs were used to select the optimized data widow to be fitted.

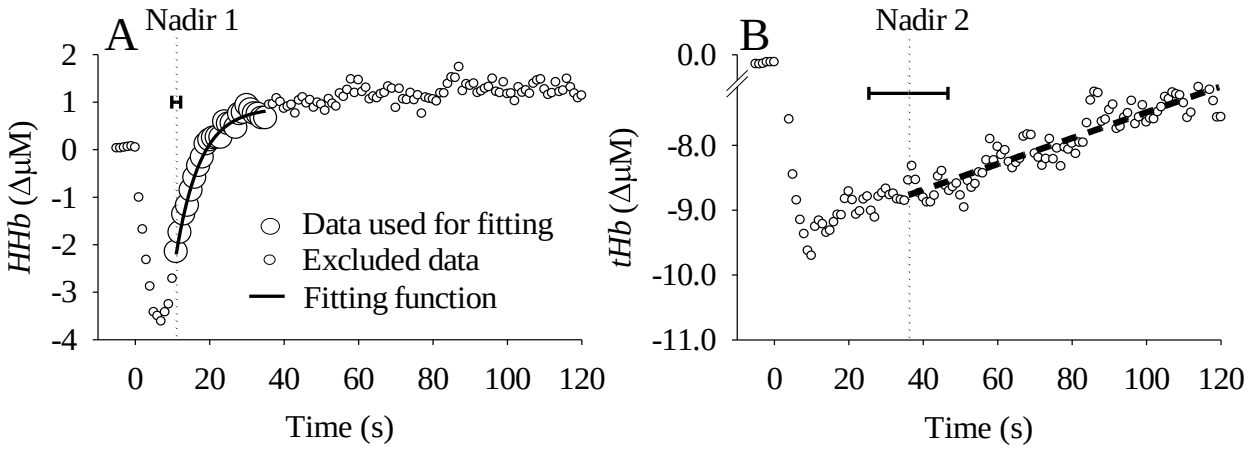

Figure 53. Near infrared spectroscopy signal dynamics evaluation during exercise transition.
Group mean response (n = 18) of the deoxyhemoglobin (A, HHb) and total hemoglobin (B, tHb) changes (in $\Delta\mu M$) during walking exercise transition. The method used to select the data to be fitted by an exponential function was based on the identification of two nadir values (see text).

To facilitate comparison with previous literature (Murias et al., 2011b, 2014), we implemented an exponential fitting procedure on the selected data. The HHb data contained between the two nadirs were fitted by the equation: $HHb_{(t)} = a_0 + a_1 * \left(1 - e^{\left(-\frac{t-TD_1}{\tau_1}\right)}\right)$, as depicted in Figure 53A. The equation parameters are the same as previously described. The selected TSI data were fitted by the same equation but instead of adding the exponential component to the a_0, it was decreased from the a_0. Since the response can be interpreted as a non-delayed local response, the MRT of the HHb and TSI (HHb-MRT and TSI-MRT, respectively) was also calculated by the sum of τ_1 and TD_1 and considered as the only time constant for these variables (Allart, Olivier, Hovart, Thevenon, & Tiffreau, 2012; Murias et al., 2011b). All data modeling parameters were calculated by a G-language computer program developed by a certified LabVIEW programmer (LabVIEW 2012, National Instruments, Austin, TX, US). This program fitted the data using a nonlinear curve fit function that finds the lowest sum of the squared errors by a standard Levenberg-Marquardt algorithm.

A.5.6 Statistical Analysis

Data were expressed as mean ± SD. The one-way repeated measures ANOVA was used to compare the $\dot{V}O_2$ baseline between the three bouts of moderate walking exercise to confirm no carryover effects prior to ensemble averaging to achieve a single exercise transition per participant. For comparison of the parameters obtained by the kinetics analysis between women and men, Shapiro-Wilk test was used to assess data distribution. The t-test or Mann-Whitney Rank Sum test was used for normal and non-normal data distribution, respectively. The established cut-off significance level was 5% ($p < 0.05$).

A.6 Results

The selected treadmill grade at 80% of GET was not statistically ($p > 0.05$) different between groups (6±1 % for women and 6±2 % for men). As statistically ($p < 0.05$) taller individuals, the treadmill speed at 80% of ET was statistically ($p < 0.05$) higher in men (3.4±0.0 km·h^{-1} for women and 3.9±0.2 km·h^{-1} for men). The $\dot{V}O_2$ at GET was not statistically ($p > 0.05$) different between groups (26±3 ml·min^{-1}·Kg^{-1} for women and 30±5 ml·min^{-1}·Kg^{-1} for men). One-way repeated-measures ANOVA indicated that there were no statistically significant differences between the $\dot{V}O_2$ baseline (initial condition) of three bouts of moderate walking exercise.

Figure 54 displays the normalized second-by-second group response of the $\dot{V}O_2$ (Figure 54A) and $\dot{Q}$ (Figure 54B) during exercise transitions. The $\dot{V}O_2$ -τ_2 was significantly faster in women in comparison to men (Figure 55A). The $\dot{Q}$-τ_2 was not different between women and men (Figure 54B), but the MRT approached statistical significance (p = 0.06), with men showing slower MRT than women.

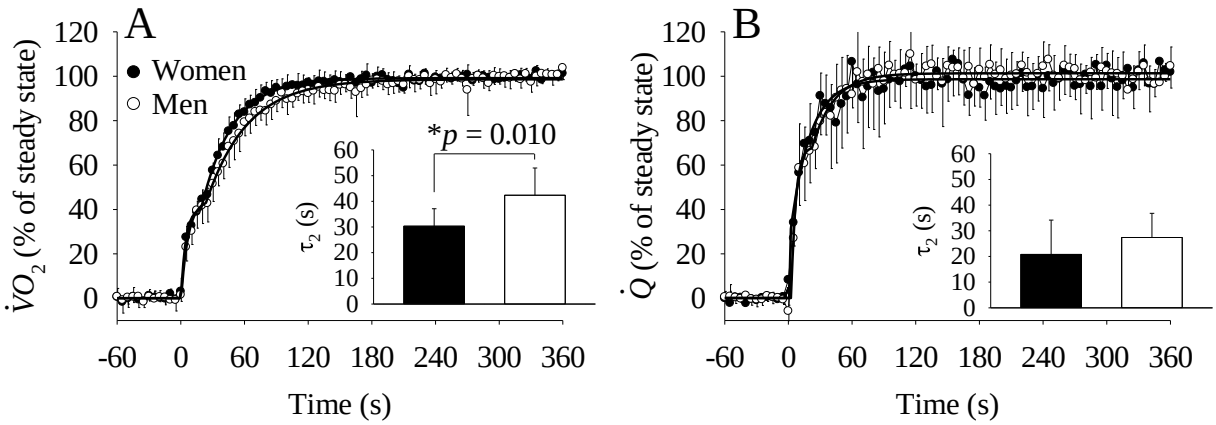

Figure 54. Oxygen uptake and cardiac output during exercise transition.

Mean ± SD of the normalized pulmonary oxygen uptake (A, $\dot{V}O_2$) and cardiac output (B, $\dot{Q}$) of women (n = 9) and men (n = 9) during moderate walking exercise transition. The smaller bar graphs show the speed of the signal adjustment (represented by "τ_2") of each variable. To display the function used for data fitting, the mean $\dot{V}O_2$ and $\dot{Q}$ responses were fitted by a bi-exponential model (**—**, see text for further details). *: statistically (p < 0.05) faster (i.e., lower τ_2) in women.

The second-by-second HHb and TSI data (Figures 55A and 55B, respectively) for the region of interest (selected as described in Figure 53) revealed a statistically (p < 0.05) faster adaptation in women. The exponential characteristics of the response were evident and the data modeling presented low residuals, as well as low CI_{95} and p values.

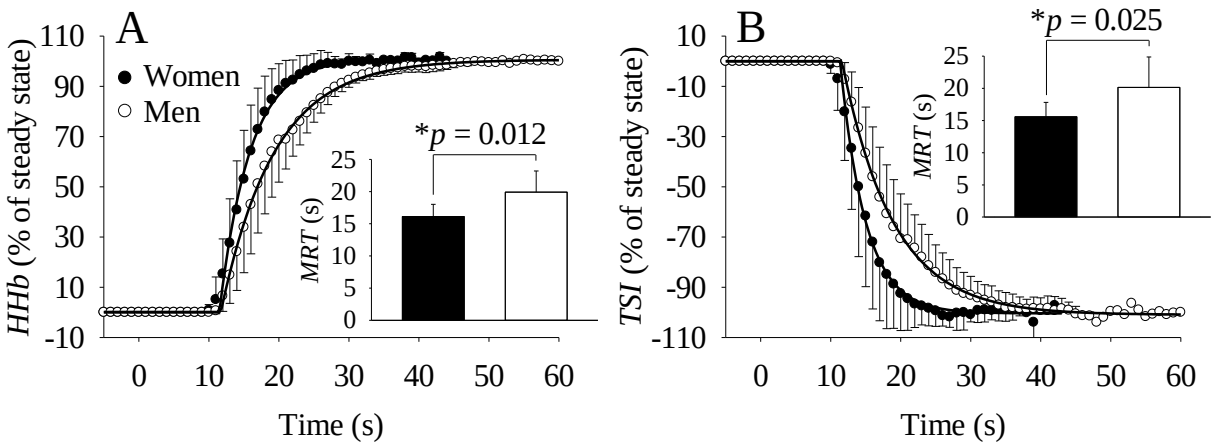

Figure 55. Deoxyhemoglobin and tissue saturation index during exercise transition.
Mean ± SD of the normalized deoxy-hemoglobin (A, HHb) and tissue saturation index (B, TSI) of women (n = 9) and men (n = 9) during moderate walking exercise. The smaller bar graphs show the speed of the signal adjustment (represented by the mean response time or "MRT") of each variable. *: statistically (p < 0.05) faster (i.e., lower MRT) in women.

Table 6 shows the comparison of the data fitting parameters between men and women. The statistical analysis indicated that women presented lower $\dot{V}O_2$-a_2 (p < 0.05) in comparison to men, but no differences for the parameters a_0, a_1, τ_1, TD_1 and TD_2. The $\dot{V}O_2$-MRT was statistically (p < 0.05) faster (i.e., lower) in women. The initial cardio-dynamic component of the $\dot{Q}$ response (i.e., $\dot{Q}$-a_1) was statistically (p < 0.05) more pronounced in men. No differences were found in $\dot{Q}$ for the parameters a_0, a_2, τ_1, τ_2 and TD_1; however, MRT for $\dot{Q}$ approached statistical significance (p = 0.06) with women having a faster response than men. The $\dot{Q}$ baseline amplitude (i.e., a_0) and the $\dot{Q}$-TD_2 also approached statistical significance between groups (p = 0.06) being both higher in men. In comparison to men, the faster local oxygen extraction (faster HHb-MRT) found in women was also associated to faster alveolar O_2 extraction investigated by $a - vO_2diff$-τ_2. The $a - vO_2diff$ parameters a_0, a_1, a_2, τ_1, TD_1 and TD_2 were not statistically different (p > 0.05) between groups. Like $\dot{Q}$, the MRT for $a - vO_2diff$ also approached statistical significance (p =

0.06) with women having a faster response than men. In addition, the HR-a_2 was higher in women in comparison to men ($p < 0.05$). However, the HR parameters a_0, a_1, τ_1, τ_2, TD_1 and TD_2 did not present statistical differences ($p > 0.05$) between groups.

Table 6. Parameters obtained from the kinetic analysis of the oxygen uptake ($\dot{V}O_2$), cardiac output ($\dot{Q}$), total arteriovenous O_2 difference ($a-vO_2diff$) and heart rate (HR) during moderate walking exercise transition in women and men.

		Women (n = 9)	**Men** (n = 9)
$\dot{V}O_2$	a_0 (ml·kg^{-1}·min^{-1})	4.75±0.48	4.38±0.53
	a_1 (ml·kg^{-1}·min^{-1})	7.62±1.31	8.79±1.93
	τ_1 (s)	4.04±2.56	3.98±2.28
	TD_1 (s)	0.55±0.59	1.21±1.56
	a_2 (ml·kg^{-1}·min^{-1})	11.97±1.19	14.99±2.46 *
	τ_2 (s)	30.30±6.42	42.40±10.00 *
	TD_2 (s)	18.26±4.70	16.98±6.24
	MRT (s)	48.56±3.99	59.38±8.33 *
$\dot{Q}$	a_0 (l·min^{-1})	4.22±0.72	5.18±1.17 #
	a_1 (l·min^{-1})	4.36±0.85	5.95±1.92 *
	τ_1 (s)	4.26±2.89	5.78±3.20
	TD_1 (s)	1.00±0.72	1.33±1.70
	a_2 (l·min^{-1})	3.06±0.77	5.07±2.80
	τ_2 (s)	20.78±12.59	27.37±8.88
	TD_2 (s)	14.91±7.21	20.32±2.84 #
	MRT (s)	35.69±14.96	47.69±8.87 #

$a - vO_2diff$	a_0 (mlO₂·(l·b)$^{-1}$)	71.80±10.18	72.77±30.72
	a_1 (mlO₂·(l·b)$^{-1}$)	24.62±11.33	34.90±19.73
	τ_1 (s)	4.90±7.83	0.67±0.88
	TD_1 (s)	3.90±8.28	1.32±1.60
	a_2 (mlO₂·(l·b)$^{-1}$)	40.47±12.61	65.35±67.93
	τ_2 (s)	29.22±12.5	49.94±21.96 *
	TD_2 (s)	28.49±11.23	24.45±2.52
	MRT (s)	57.71±12.16	74.39±21.37 #
HR	a_0 (bpm)	86.43±9.33	78.48±10.12
	a_1 (bpm)	24.65±13.63	27.50±7.32
	τ_1 (s)	6.65±8.49	7.36±4.18
	TD_1 (s)	0.44±0.77	1.38±3.44
	a_2 (bpm)	29.53±5.56	22.81±6.93 *
	τ_2 (s)	60.67±45.13	75.20±52.33
	TD_2 (s)	26.67±32.47	30.45±5.79
	MRT (s)	87.34±73.47	105.65±52.29

Abbreviation: a_0 is the baseline value; a_1 and a_2 are the steady state amplitude of the response above a_0 and a_1, respectively; τ_1 and τ_2 are time constants (i.e. speed of the adaptation) for each phase; TD_1 and TD_2 are time delays of each phase and MRT is the mean response time. Please see text for further details regarding the parameters. * means statistically different ($p < 0.05$) between women and men and # means statistical significance level of $p = 0.06$.

A.7 Discussion

Our hypothesis that men present faster $\dot{V}O_2$ dynamics in comparison to women was not supported by our findings. On the contrary, women had faster $\dot{V}O_2$ dynamics during walking exercise

transition than men. This contrasts with the normally greater maximal aerobic power in men (Cureton et al., 1986). In addition, there was a strong trend for faster central O_2 transport ($\dot{Q}$) while the peripheral and alveolar O_2 extraction dynamic were remarkably faster in women in comparison to men. To the best of our knowledge, this was the first time that the influence of sex on the adaptive dynamic and integrative cardiovascular and metabolic responses during moderate walking exercise was simultaneously explored in humans.

In contrast to previous studies that reported faster $\dot{V}O_2$ kinetics in younger boys compared to girls (Fawkner et al., 2002; Franco et al., 2014) and an investigation of 55-year-old men and women that reported no difference in $\dot{V}O_2$ kinetics between the sexes (O'Connor et al., 2012), we observed significantly faster responses in young, healthy women compared to men. The current study demonstrated that sex influenced the aerobic adaptation during moderate walking. From rest to exercise transition, women presented $\dot{V}O_2$ dynamics ~28 % faster in comparison to men as indicated by the faster τ_2 (Figure 54A) and MRT (Table 6). In addition, as depicted in Figure 55, the HHb and TSI adaptive responses (MRT) in women were 19 % and 22 % faster than men, indicating a faster peripheral O_2 extraction (HHb) and O_2 desaturation (TSI) dynamics, respectively. Despite the lack of statistical significance of the $\dot{Q}$ temporal dynamics (i.e., $\dot{Q}$-MRT) between groups, the mean effect size of ≈ 25% associated with a statistical significance level (p) of 0.06 cannot be overlooked. The observed faster $\dot{V}O_2$ dynamics in women might be also associated with faster $\dot{Q}$ dynamics reflecting O_2 transport in addition to the statistically significant faster O_2 extraction. Consequently, the blood with lower O_2 content might be reaching the lungs faster in women which would support the remarkable faster pulmonary $\dot{V}O_2$ observed in this group.

The faster $\dot{V}O_2$ dynamics for the same relative metabolic demand (80% GET) showed that women were able to utilize aerobic rather than anaerobic metabolism to supply the energetic demand during exercise transition. The mechanisms that underlie the more rapid increase in $\dot{V}O_2$ are complex. The capillary density of the gastrocnemius muscle seems to be similar between women and men (Coggan et al., 1992) but women have lower hemoglobin concentration (Vahlquist, 1950) and possibly different respiratory function (Harms & Rosenkranz, 2008) which contributes with $\dot{Q}$ dynamics to affect convective O_2 transport.

In order to diminish the influence of other variables beyond sex over the aerobic response (Lundsgaard & Kiens, 2014), women and men were similar in their age, BMI and GET. Differences between matched men and women in observed pulmonary $\dot{V}O_2$ might also reflect muscle metabolic potential. Women apparently have a higher slow-twitch muscle fiber composition which has a better oxidative capacity (Haizlip, Harrison, & Leinwand, 2015; Lundsgaard & Kiens, 2014; Staron et al., 2000). Different muscle type compositions has an impact over the $\dot{V}O_2$ measured at the mouth and as expected greater recruitment of slow-twitch fiber will speed up the aerobic system energy supply during an exercise transition (Barstow et al., 1996; Crow & Kushmerick, 1982). In addition, it was reported that women have similar citrate synthase (Roepstorff et al., 2005) and cytochrome c oxidase (Rouleau, Santana, Jones, & Park, 1995) activity in comparison to matched men. These enzymes have a direct effect over the electron transport chain which ultimately has the O_2 as the final electron receptor (Clanton, Hogan, & Gladden, 2013). In addition, the mitochondrial content and myocyte respiration was reported to be similar between women and men for the same muscle fiber type (Thompson et al., 2013). Therefore, the observed faster aerobic adjustment in the current study seems to be accounted for in part by a higher composition or recruitment of slow-twitch muscle in women.

Women have a greater reliance on fat oxidation in comparison to men during dynamic exercise (L. J. Tarnopolsky, MacDougall, Atkinson, Tarnopolsky, & Sutton, 1990; M. A. Tarnopolsky, 2008) which should also influence the $\dot{V}O_2$ dynamics during exercise transition (Molé & Hoffmann, 1999). However, $\dot{V}O_2$ dynamics were slowed during a high fat diet intervention (Raper et al., 2014), contrary to the observed faster $\dot{V}O_2$ adjustment in women of the current study. Nonetheless, despite the impossibility of exactly identifying the intracellular mechanisms that trigger a faster $\dot{V}O_2$ dynamics in women, the faster peripheral O_2 extraction in the capillary bed lead to a faster detachment of the O_2 from the O_2Hb, accelerating the dynamics of HHb concentration and the blood O_2 desaturation (i.e. TSI) (Figure 55). As previously described (Hughson, 2009), interactions of O_2 transport and O_2 delivery mechanisms establish the rate of increase in $\dot{V}O_2$ accounting for differences between men and women.

Regarding the quality of the parameters estimation, the data modeling presented elevated reliability which allowed us to infer about the aerobic system response profile based on the parameters estimated from the $\dot{V}O_2$ data measured at the mouth (Keir, Murias, et al., 2014; Lamarra et al., 1987). The CI_{95} of the $\dot{V}O_2$-τ_2 (main variable) was not statistically ($p > 0.05$) different between women (2.2±0.5 s) and men (2.6±0.5) and corresponded to ~7 and ~6 % of the women's and men's group mean response, respectively.

A.8 Conclusion

Women presented a faster $\dot{V}O_2$ dynamics during walking exercise transition, indicating a faster aerobic system adjustment to supply the energetic demand. Women also presented a remarkably faster O_2 extraction dynamics in comparison to men at both, peripheral and central compartments. The observed faster aerobic system adjustment in women during treadmill walking at a

submaximal intensity was a consequence of faster intracellular O_2 handling in combination with faster central O_2 delivery.

Appendix B: Common Procedures Between Studies

All participants came to the University of Waterloo where all studies were conducted. During each visit, a basic physical examination was performed (height, weight and self-reported medical history). Participants were advised to consume a light meal two hours before testing (Ahuja, Robertson, & Ball, 2009), and to refrain from consumption of caffeine and/or alcohol and any strenuous exercise 48 h before each of the laboratory visits.

At the beginning of the first visit for each study, participants completed a comprehensive questionnaire (PAR-Q & YOU, Figure 56), followed by an explanation of the procedures. A familiarization protocol (on cycling or treadmill depending on the study) with all the testing equipment was also performed to reduce anxiety that could affect the cardiovascular physiological response during exercise (Hickam, Cargill, & Golden, 1948). Room temperature, barometric pressure, and relative humidity were monitored to ensure similar environmental conditions between laboratory tests. Each laboratory visit had approximately three hours of duration.

All studies evaluated healthy young participants. The participants were recruited from the University of Waterloo campus and once they met the inclusion criteria, an initial interview was scheduled to explain the research study. During the interview, each participant had their medical history reviewed in order to search for any exclusion criteria that may restrict them to participate. The inclusion/exclusion criteria are described below.

Inclusion Criteria

- Male and female young healthy participants (age between 18-40 years old).

Exclusion Criteria

- Unstable medical condition
- Diabetes mellitus

- Uncontrolled hypertension (BP > 140/90)
- History of heart disease
- Resting heart rate >100
- Recent or past history of neurological disorder such as stroke or parkinsonism
- Medications that influence heart rate, or blood pressure, such as beta blockers;
- Medications that may influence cardiac and/or peripheral responses to exercise, such as anticoagulants or anticholinergics
- Hormone replacement therapy
- Chronic obstructive pulmonary disease
- Arthritis limiting mobility

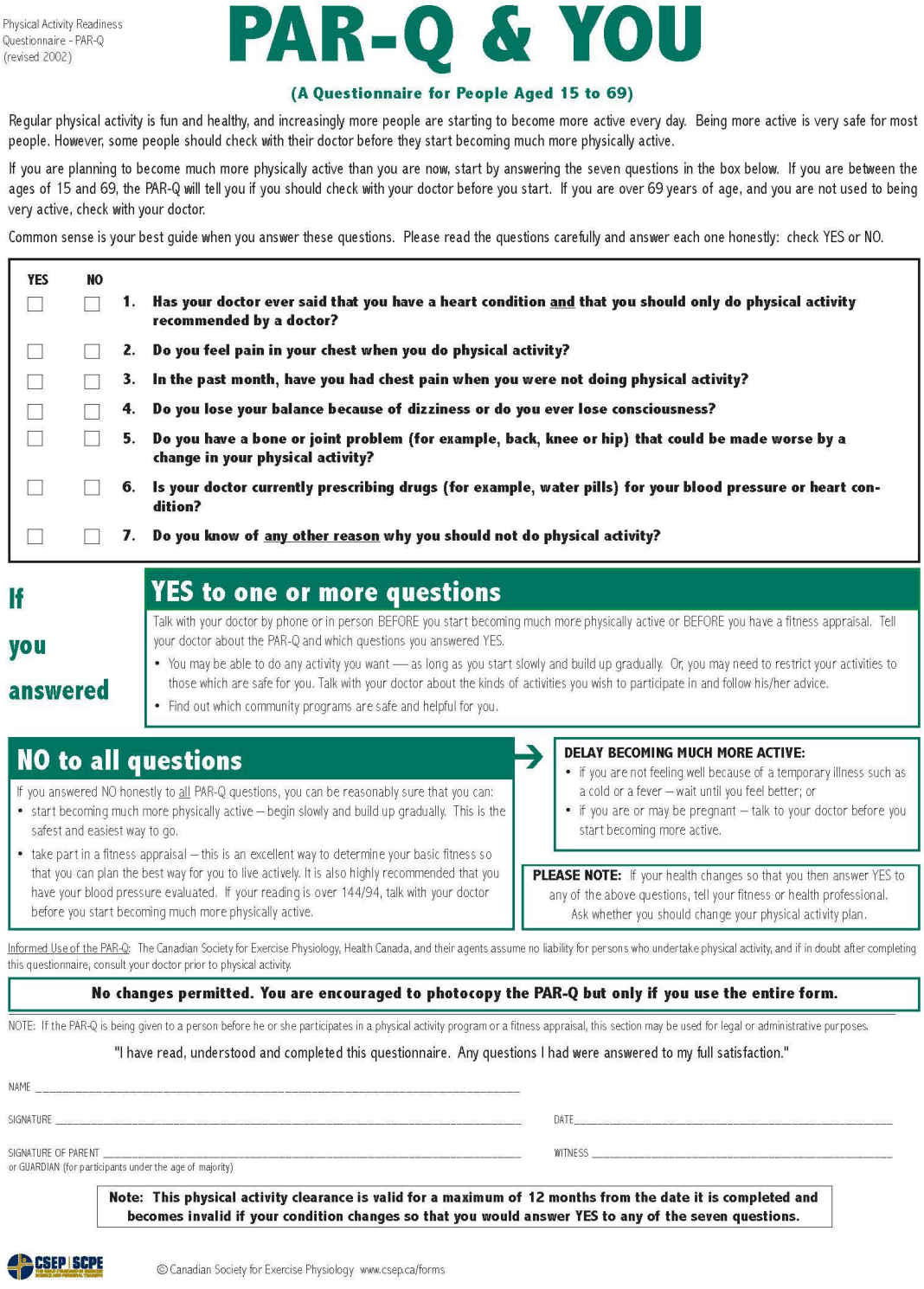

Physical Activity Readiness
Questionnaire - PAR-Q
(revised 2002)

PAR-Q & YOU

(A Questionnaire for People Aged 15 to 69)

Regular physical activity is fun and healthy, and increasingly more people are starting to become more active every day. Being more active is very safe for most people. However, some people should check with their doctor before they start becoming much more physically active.

If you are planning to become much more physically active than you are now, start by answering the seven questions in the box below. If you are between the ages of 15 and 69, the PAR-Q will tell you if you should check with your doctor before you start. If you are over 69 years of age, and you are not used to being very active, check with your doctor.

Common sense is your best guide when you answer these questions. Please read the questions carefully and answer each one honestly: check YES or NO.

YES	NO	
☐	☐	**1. Has your doctor ever said that you have a heart condition and that you should only do physical activity recommended by a doctor?**
☐	☐	**2. Do you feel pain in your chest when you do physical activity?**
☐	☐	**3. In the past month, have you had chest pain when you were not doing physical activity?**
☐	☐	**4. Do you lose your balance because of dizziness or do you ever lose consciousness?**
☐	☐	**5. Do you have a bone or joint problem (for example, back, knee or hip) that could be made worse by a change in your physical activity?**
☐	☐	**6. Is your doctor currently prescribing drugs (for example, water pills) for your blood pressure or heart condition?**
☐	☐	**7. Do you know of any other reason why you should not do physical activity?**

If you answered

YES to one or more questions

Talk with your doctor by phone or in person BEFORE you start becoming much more physically active or BEFORE you have a fitness appraisal. Tell your doctor about the PAR-Q and which questions you answered YES.

- You may be able to do any activity you want — as long as you start slowly and build up gradually. Or, you may need to restrict your activities to those which are safe for you. Talk with your doctor about the kinds of activities you wish to participate in and follow his/her advice.
- Find out which community programs are safe and helpful for you.

NO to all questions

If you answered NO honestly to all PAR-Q questions, you can be reasonably sure that you can:

- start becoming much more physically active – begin slowly and build up gradually. This is the safest and easiest way to go.
- take part in a fitness appraisal – this is an excellent way to determine your basic fitness so that you can plan the best way for you to live actively. It is also highly recommended that you have your blood pressure evaluated. If your reading is over 144/94, talk with your doctor before you start becoming much more physically active.

DELAY BECOMING MUCH MORE ACTIVE:

- If you are not feeling well because of a temporary illness such as a cold or a fever – wait until you feel better; or
- If you are or may be pregnant – talk to your doctor before you start becoming more active.

PLEASE NOTE: If your health changes so that you then answer YES to any of the above questions, tell your fitness or health professional. Ask whether you should change your physical activity plan.

Informed Use of the PAR-Q: The Canadian Society for Exercise Physiology, Health Canada, and their agents assume no liability for persons who undertake physical activity, and if in doubt after completing this questionnaire, consult your doctor prior to physical activity.

No changes permitted. You are encouraged to photocopy the PAR-Q but only if you use the entire form.

NOTE: If the PAR-Q is being given to a person before he or she participates in a physical activity program or a fitness appraisal, this section may be used for legal or administrative purposes.

"I have read, understood and completed this questionnaire. Any questions I had were answered to my full satisfaction."

NAME _____

SIGNATURE _____ DATE _____

SIGNATURE OF PARENT or GUARDIAN (for participants under the age of majority) _____ WITNESS _____

Note: This physical activity clearance is valid for a maximum of 12 months from the date it is completed and becomes invalid if your condition changes so that you would answer YES to any of the seven questions.

CSEP | SCPE

Figure 56. PAR-Q & YOU questionnaire for initial physical evaluation.